

**UNIVERSITE MONTPELLIER II**

**THESE**

pour obtenir le grade de

**DOCTEUR DE L'UNIVERSITE MONTPELLIER II**

Discipline : *Biologie des populations et écologie*

Ecole Doctorale : *Systèmes intégrés en Biologie, Agronomie, Géosciences, Hydrosciences et Environnement (SIBAGHE)*

présentée et soutenue publiquement

par

*Roberto Michael Ballón Soto*

le 11 mai 2010

Titre :

*Étude acoustique du macrozooplancton au Pérou: estimation de biomasse, distribution spatiale, impact du forçage physique, et conséquences sur la distribution des poissons fourrage*

Title :

*Acoustic study of macrozooplankton off Peru: biomass estimation, spatial patterns, impact of physical forcing and effect on forage fish distribution*

**JURY**

Mme. Catherine Aliaume	<i>Professeur, Université Montpellier II</i>	Présidente
M. Jacques Clavier	<i>Professeur, Université de Bretagne Occidentale</i>	Rapporteur
M. Xabier Irigoien	<i>Senior Scientist, AZTI</i>	Rapporteur
Mme. Anne Lebouges-Dhaussy	<i>Ingénieur de Recherche, IRD</i>	Examinateur
M. Frédéric Ménard	<i>Directeur de Recherche, IRD</i>	Examinateur
M. Arnaud Bertrand	<i>Chargé de Recherche, IRD</i>	Directeur de Thèse
M. François Gerlotto	<i>Directeur de Recherche, IRD</i>	Co-directeur de Thèse



## Résumé

La partie nord du Système du courant de Humboldt (NSCH) couvre moins de 0.1% de la surface océanique mondiale mais produit plus de poissons, en particulier d'anchois du Pérou (*Engraulis ringens*), par unité de surface que n'importe quelle autre région du monde. Bien que ce système produise suffisamment de macrozooplancton pour alimenter les populations de poisson fourrage, le manque d'informations sur ce compartiment limite nos capacités d'étude. L'objectif de cette thèse est d'étudier la dynamique de la distribution spatiotemporelle de la biomasse en macrozooplancton du NSCH en relation avec l'environnement physique et les poissons fourrage, à différentes échelles. Pour ce faire une méthode acoustique bi-fréquences a été développée et appliquée à des séries de données acoustiques historiques. Des informations à haute résolution ont ainsi pu être extraite sur la biomasse et les patrons de distribution du macrozooplancton, de la galathée pélagique 'munida', des poissons et des autres compartiments. Cette méthode nous a également permis d'estimer l'extension verticale de la communauté épipélagique ( $Z_{VEEC}$ ). Nous avons démontré que  $Z_{VEEC}$  coïncide avec la limite supérieure de la zone de minimum d'oxygène (ZMO), ce qui permet de produire des données spatialisées à haute résolution de la limite supérieure de la ZMO et d'estimer le volume d'habitat de l'anchois. Notre estimation de biomasse en macrozooplancton, environ quatre fois supérieures aux estimations antérieures, est en accord avec les découvertes récentes sur l'écologie trophique des poissons fourrage du NSCH et fournit des éléments étayant les théories actuelles sur l'origine de la haute productivité en poissons du NSCH. L'étude des impacts des structures physiques de submeso- et mesoéchelle sur la distribution du macrozooplancton supporte l'hypothèse d'une structuration de type 'bottom-up'. Nous avons également mis en évidence l'impact de la structuration spatiale du macrozooplancton sur la distribution des poissons fourrage. Les données physiques et biologiques à haute résolution obtenues grâce à cette étude ouvrent de nouvelles perspectives pour réaliser des études écologiques intégrées à échelles multiples et pour calibrer les modèles biogéochimiques, trophiques ou End-to-End.

**Mots clefs** Macrozooplancton, Euphausiacés, Système du Courant de Humboldt, Pérou, Acoustique, zone de minimum d'oxygène, communauté épipélagique, anchois *Engraulis ringens*, mesoéchelle, submesoéchelle, relations prédateurs-proies.



## *Abstract*

The Northern Humboldt Current system (NHCS) represents less than 0.1% of the world ocean surface but produces more fish, mainly Peruvian anchovy (*Engraulis ringens*), per unit area than any other region in the world. Although this system produces enough macrozooplankton to feed its high production of forage fish, the paucity of information on zooplankton hampers research in the system. The objective of this study was to investigate the multiscale dynamics of the spatiotemporal distribution of the macrozooplankton biomass off Peru in relation to the physical environment and their fish predators. For that a bi-frequency acoustic method was developed and applied to extract, from historical acoustic data, high-resolution information on the biomass and the patterns of distribution of macrozooplankton, the pelagic red squad 'munida', fish and other marine compartments. This method also allows estimating the vertical extension of this epipelagic community (ZVEEC). We demonstrated that ZVEEC coincide with the upper limit of the oxygen minimum zone (OMZ), which allowed both producing high-resolution spatial data of the upper limit of the OMZ and estimating the volume habitat of anchovy. The estimated macrozooplankton biomass was about four times higher than previously reported. This estimate is in agreement with the recent findings on forage fish trophic ecology and supports the current hypotheses explaining the NHCS high fish production. The study of the impacts of the submeso- and mesoscale physical structures on macrozooplankton provided evidence of the bottom-up physical effect on the distribution of macrozooplankton biomass. We also found further evidence of the structuring bottom-up effect that macrozooplankton exert on forage fish. The high-resolution biological and physical data obtained in this study opens new perspective to perform integrated multiscale ecological studies and to calibrate biogeochemical, trophic and End-to-End models.

**Key words** Macrozooplankton, Euphausiids, Northern Humboldt Current system, Acoustics, Oxygen minimum zone, Epipelagic community, Peruvian anchovy *Engraulis ringens*, Mesoscale, Submesocale, Predator-prey relationships.



## *Acknowledgments*

This study is a contribution to the cooperation agreement between the Instituto del Mar del Peru (IMARPE) and the Institut de Recherche pour le Developpement (IRD). The work was made possible by a PhD grant offered by the IRD “Department for training and capacity-building for research in developing countries” (DSF) and managed by Égide. Free access to Echoview was kindly provided by Myriax Software Pty. Ltd.

I would like to acknowledge the following people for their support throughout this project: First of all, Arnaud Bertrand, for all his enthusiasm and time dedicated to this project, for being not only an outstanding supervisor but also a good friend who supported me without hesitation when I needed it. I would like to thank François Gerlotto for all the entertaining and scientifically rich discussions and for his valuable comments and corrections. I also wish to thank Anne Lebourges-Dhaussy for introducing me to fisheries acoustics, for her support during my doctoral studies and for making my stay in Brest, France, a really nice experience. In part, it is her fault that I now consider Brest to be the nicest part of France. Speaking of Brest, I would like to thank Anne and Martin for their kindness and hospitality during my stay in Brest.

I want to thank Sophie Bertrand for her comments and valuable feed-back on the earlier versions of this thesis. My gratitude also goes to Alexis Chaigneau and Jeremie Habasque for their assistance with Matlab and their help in programming and making my data processing faster and more efficient. Speaking of efficiency, I would like to thank Daniel Grados for helping me process the acoustic data and for all those long hours discussing statistics. My thanks also goe to Mariano Gutierrez and Patricia Ayon for their enthusiasm and for giving me access to the acoustic and zooplankton data. I want to thank Juan Molineros, Yvan Simard and John Simmonds, members of my thesis committee, whose constructive criticism and comments guided my work during the first two years. I would particularly like to thank Ainhoa Lezama for her friendship and for helping before and after my dissertation defense.

Finally, I want to thank Johanna Holmgren, my wife, for putting up with me, far away from her country and her family, for making my life happy and, of course, for proofreading all versions of this thesis. This work is dedicated to her and to my children, Adriana and Michael.



# Contents

*Résumé*

*Abstract*

*Acknowledgments*

*Contents*

*List of figures*

*List of tables*

*Résumé exécutif en Français*

**1**

*General introduction*

**21**

**1 Insights on the Humboldt Current system**

**25**

1.1 Introduction.....	25
1.2 Physical oceanography.....	26
1.2.1 Atmospheric forcing.....	26
1.2.2 Oceanographic context.....	27
1.2.2.1 Oceanic circulation.....	27
1.2.2.2 Water masses.....	28
1.2.2.3 The oxygen minimum zone.....	29
1.2.2.4 Mesoscale physical activity.....	30
1.3 Productions of the NHCS.....	31
1.3.1 Primary production.....	31
1.3.2 Secondary production, zooplankton.....	32
1.3.2.1 Zooplankton horizontal distribution.....	32
1.3.2.2 Zooplankton vertical distribution.....	33
1.3.2.3 Macrozooplankton.....	33
1.3.3 Tertiary production.....	35
1.4 The dynamics of NHCS.....	36
1.4.1 Centennial variability.....	37
1.4.2 Decadal variability.....	37
1.4.3 Interannual variability.....	38
1.4.4 Seasonal Variability.....	39
1.5 Fisheries.....	40
1.5.1 Pelagic fisheries.....	40
1.5.2 Demersal fisheries.....	41
1.5.3 Fisheries management.....	41

**2 A bi-frequency acoustic method for zooplankton discrimination and biomass estimation** **43**

2.1 Introduction.....	43
2.1.1 Marine organisms as acoustic targets.....	44
2.1.2 Acoustic properties of fish and zooplankton.....	45
2.1.3 Organism discrimination based on acoustic properties.....	47
2.1.4 Bi-frequency organism discrimination .....	48
2.2 Materials and methods.....	48
2.2.1 Data.....	48
2.2.2 Pre-processing.....	49
2.2.3 Scatter discrimination and abundance estimation .....	51
2.2.4 Validation.....	56

2.3 Results.....	56
2.4 Discussion.....	61
<b>3 Acoustic observation of living organisms reveals the upper limit of the oxygen minimum zone</b>	<b>63</b>
3.1 Introduction.....	63
3.2 Materials and methods.....	64
3.3 Results.....	69
3.4 Discussion.....	75
<b>4 Is there enough macrozooplankton to feed the anchovy population?</b>	<b>77</b>
4.1 Introduction.....	77
4.1.1 Adding one more link to the anchovy food chain.....	77
4.1.2 Macrozooplankton biomass estimation in the NHCS.....	79
4.2 Materials and methods.....	81
4.2.1 Data.....	81
4.2.1.1 Diel patterns of macrozooplankton distribution.....	81
4.2.1.2 Across-shore macrozooplankton distribution.....	81
4.2.1.3 Along-shore macrozooplankton distribution.....	82
4.2.2 Data analysis.....	82
4.2.3 Mapping the horizontal distribution of macrozooplankton.....	84
4.3 Results.....	86
4.3.1 Diel variation in macrozooplankton biomass and size.....	86
4.3.2 Macrozooplankton biomass and size in relation to ecological domains.....	87
4.3.3 Across-shore distribution of macrozooplankton density, biomass and size.....	92
4.3.4 Along-shore macrozooplankton biomass distribution.....	93
4.3.5 Macrozooplankton horizontal distribution.....	95
4.4 Discussion.....	98
4.4.1. What are the main responsible organisms for the observed macrozooplankton acoustic pattern?.....	99
4.4.2 Macrozooplankton biomass in the NHCS: higher than assumed.....	101
4.4.3 What could be the reasons for such a high secondary production?.....	104
4.4.4 Conclusion.....	110
<b>5 Effects of the meso- and submesoscale physical forcing on the distribution of macrozooplankton and its further impact on the distribution of forage fish</b>	<b>111</b>
5.1 Introduction.....	111
5.2 Materials and methods.....	114
5.2.1 Data.....	114
5.2.2 Scale of description and sample unit.....	114
5.2.3 Exploratory analysis.....	115
5.2.4 Using Z <sub>VEEC</sub> to reveal small-scale physical structures.....	115

5.2.5 Statistical analysis.....	117
5.2.5.1 Dealing with autocorrelation.....	117
5.2.5.2 The effect of physical structuring on macrozooplankton distribution.....	121
5.2.5.3 Predator-prey relationships: fish vs. macrozooplankton	121
5.3 Results.....	122
5.3.1 The impact of satellite-resolved mesoscale structures on macrozooplankton distribution and $Z_{VEEC}$ .....	122
5.3.2 Mesoscale analysis.....	123
5.3.2.1 The impact of mesoscale physical structures on macrozooplankton.....	123
5.3.2.2 Mesoscale predator-prey relationships.....	124
5.3.3 Submesoscale analysis.....	127
5.3.3.1 The impact of submesoscale physical structures on macrozooplankton.....	127
5.3.3.2. Predator-prey relationships at submesoscale.....	128
5.4 Discussion.....	132
5.4.1 The impact of satellite-resolved mesoscale structures on macrozooplankton distribution and $Z_{VEEC}$ .....	132
5.4.2 The impact of mesoscale physical structures on macrozooplankton.....	133
5.4.3 The impact of submesoscale physical structures on macrozooplankton.....	133
5.4.4 Biological forcing - fish vs macrozooplankton.....	135
<i>General conclusions</i>	<b>137</b>
<i>References</i>	<b>141</b>
<i>Appendices</i>	<b>159</b>



## List of Figures

<p>1.1 <i>Chlorophyll-a concentration from SeaWifs for the period 1998-2007 and EBUS location arbitrarily delimited by the 200 nautical miles offshore limit and latitudinal extensions including seasonal upwelling zone (courtesy of H. Demarcq, IRD, France). Source: Fréon et al. (2009).....</i></p> <p>1.2 <i>Fish catch versus primary productivity for the four main eastern boundary coastal upwelling ecosystems for the years 1998-2005. Source: Chavez et al. (2008).....</i></p> <p>1.3 <i>(a) Climatological winter and summer winds triggered by the South-Eastern Pacific Subtropical Anticyclone. (b) Upwelling scheme along the Peruvian coast.....</i></p> <p>1.4 <i>Large oceanic circulation scheme with focus on the main surface and subsurface currents off Peru: the Chile-Peru Current (CPC), the Peruvian Coastal Current (PCC), the South Equatorial Current (SEC), the Peru-Chile Undercurrent (PCU) and the West Wind Drift (WWD). Adapted from Thiel et al. (2007).....</i></p> <p>1.5 <i>Distribution of the main water masses in the HCS: Cold coastal water (CCW), Surface subtropical water (SSW), Surface equatorial water (SEW), Surface tropical water (STW). Source: Ayón et al. (2008a).....</i></p> <p>1.6 <i>Oxygen minimum zone (OMZ), thickness is colour-coded according to the colour bar on the right-hand side of the figure; units are in m. The upper boundary of the OMZ is shown in black contour lines with 50 m intervals. Source: Fuenzalida et al. (2009).....</i></p> <p>1.7 <i>Distribution of Euphausia mucronata in the Northern Humboldt Current system during austral autumn 2008. Abundance is given in N° ind per 1000 m<sup>-3</sup> (courtesy of P. Ayón, MARPE).....</i></p> <p>1.8 <i>Proxies of primary production (a) and fish production (b) and (c) at a centennial time scale. All proxies are shown as a function of time: (a) bars: diatom accumulation rate (<math>10^6</math> valves <math>\text{cm}^{-2}\text{y}^{-1}</math>), white circles: flux of biogenic silica (<math>\text{mg cm}^{-2}\text{y}^{-1}</math>); (b) 3-term averages of anchovy scale deposition rates (<math>\text{Nr} \times 1000 \text{ cm}^{-2}\text{y}^{-1}</math>); (c) 3-term averages of sardine scale deposition rates and offshore pelagic (jack mackerel+mackerel) scale deposition rates (<math>\text{Nr} \times 1000 \text{ cm}^{-2}\text{y}^{-1}</math>). Source: Gutiérrez et al. (2009).....</i></p> <p>1.9 <i>Walker circulation during normal and El Niño conditions with their corresponding wind trade and effects on sea surface temperature and thermocline depth (source NOAA).....</i></p> <p>1.10 <i>Monthly average of the along-shore wind stress (1953-1989). Source: Bakun and Mendelssohn (1989). .....</i></p>	<p style="text-align: right;">25</p> <p style="text-align: right;">26</p> <p style="text-align: right;">27</p> <p style="text-align: right;">28</p> <p style="text-align: right;">29</p> <p style="text-align: right;">30</p> <p style="text-align: right;">35</p> <p style="text-align: right;">37</p> <p style="text-align: right;">39</p> <p style="text-align: right;">39</p>
---	---

1.11	<i>Mean seasonal zooplankton volumes (<math>mL.m^{-3}</math>) during the 1960s, 1970s, 1980s and 1990s. Source: Ayón et al. (2004) .....</i>	40
2.1	<i>Zooplankton from three anatomical categories: (a) fluid-like (e.g. euphausiids), (b) hard elastic-shelled (e.g. gastropod), and (c) gas-bearing (e.g. siphonophore). Near each animal is a diagram illustrating dominant scattering mechanisms. Source: Stanton et al. (1996) .....</i>	46
2.2	<i>Schematic description of the relative frequency response, <math>r(f)</math>. Horizontal lines indicate typical range positions of selected acoustic categories when measured at frequencies 18-200 kHz. Source: Korneliussen and Ona (2003) .....</i>	47
2.3	<i>Flow chart of the bi-frequency method for scatter discrimination.....</i>	50
2.4	<i>The relationship between <math>ka</math> and the difference in volume backscattering at 120 and 38 kHz. The overlaid shadow area indicates the range at which the high-pass model provides safe estimates of the spheres radius.....</i>	55
2.5	<i>Acoustic discrimination of fish, 'blue-noise', fluid-like and munida by the developed bi-frequency algorithm. The echograms of Fish and blue-noise correspond to the 38 kHz frequency. The Fluid-like and munida echograms correspond to the 120 kHz frequency. Data from Filamentos Survey 2008 .....</i>	57
2.6	<i>Regressions of log-transformed fish (a) and munida (b) acoustic nautical area scattering coefficients (NASC) with their respective log-transformed captures (biomass in kg) from pelagic trawl net sampling. Data from Cardumen 2004 survey.....</i>	58
2.7	<i>Day (a) and night (b) mean biovolume and confidence interval (horizontal segments) per stratum (<math>ml.m^{-3}</math>) estimated using multinet (open circle) and acoustic (plus symbol) samples. Data from Cardumen 2004 survey .....</i>	58
2.8	<i>Comparison of acoustic (in <math>mL.m^{-2}</math>) and multinet abundance (in <math>ind.m^{-2}</math>) of adult euphausiids (a), munida zoea (b), Eucalanus inermis (c) and euphausiids larvae and juveniles (d) integrated from 10 to 100 m. Data from Cardumen 2004 survey. ....</i>	59
2.9	<i>Comparison of fluid-like acoustic biovolume and multinet abundance estimation of euphausiids per depth strata during the Survey 'Filamentos 2008'. (a) fluid-like echogram with an overlaid dissolved oxygen profile corresponding to the vertical profile showed in (b). Day-time (b, c, and d) and night-time (e, f, g and h) vertical profiles of abundance of adults euphausiids (crosses) and euphausiids larvae-juveniles (asterisks) from multinet and fluid-like zooplankton biovolume from acoustic (open circles). Abundances/biovolume were standardized by dividing the abundance/biovolume of a stratum by the maximum abundance/biovolume of the profile. ....</i>	60
3.1	<i>Determination of the threshold to determine <math>Z_{VEEC}</math>. Examples of vertical</i>	

<i>profiles of the cumulated <math>S_v</math> (red solid lines) and its vertical gradient <math>\Delta S_v</math> (blue solid lines). The corresponding dissolved oxygen (DO) profile is also shown (black solid lines). Dotted black lines indicate the intersection with 98% of cumulated <math>S_v</math>.....</i>	66
<b>3.2 Oxycline definition. Example of vertical DO profile (thick black line, upper axis) and the corresponding DO vertical gradients (thick blue line, lower axis) acquired during the ‘Filamentos 2008’ survey. The shaded grey area corresponds to the oxycline separated into upper and lower oxycline as described in the text. The thin black line corresponds to the depth of the maximum DO vertical gradient and separates the upper and lower oxycline. The purple square corresponds to <math>Z_{VEEC}</math> whereas the red square indicates the depth of the <math>0.8 \text{ mL L}^{-1}</math> level (<math>Z_{0.8}</math>).....</b>	68
<b>3.3 Acoustic detection of the VEEC during the ‘Filamentos’ survey. A. Example of acoustic echogram showing a CTDO track and the VEEC. The superimposed black solid line is the corresponding DO vertical profile (<math>\text{mL L}^{-1}</math>, lower axis). B. Box plot of DO concentration at <math>Z_{VEEC}</math> according to the diel period. C. Relationship between <math>Z_{VEEC}</math> and <math>Z_{0.8}</math> for the 24 stations with detectable CTDO tracks on echograms (full red circles; the full red square in the upper right corner corresponds to the station presented in A) and the other 70 CTDO stations (full blue circles); Red and black solid lines correspond to the linear regression for the 24 stations with detectable CTDO tracks and for all the 94 stations, respectively. D. Vertical range of the lower oxycline (shaded area) for all 94 stations ranked toward increasing <math>Z_{0.8}</math> (black solid line); full dots represent <math>Z_{VEEC}</math> for the 24 stations with “visible” CTDO tracks (red) and the other 70 CTDO stations (blue).....</b>	70
<b>3.4 Correlation slope between <math>Z_{VEEC}</math> averaged over the 300 pings closest to the Niskin bottle profile and <math>Z_{0.8}</math> during the routine ‘Pelagic 2005’ acoustic survey (solid line). The dotted line indicates the 1/1 slope.....</b>	71
<b>3.5 Spatial distribution of the upper OMZ depth. Upper OMZ depth estimated from <math>Z_{0.8}</math> determined from CTDO measurements (A) and Niskin bottles profiles (D) and ZVEEC estimated from acoustic measurements (B, E). Black crosses indicate the position of hydrographic stations (A, D) whereas black lines indicate acoustic tracks (B, E). C and F differences between <math>Z_{0.8}</math> and ZVEEC; black contours correspond to a null difference; boxplots of the differences are displayed on the upper right part of (C) and (F). Upper panel (A, B, C) corresponds to the ‘Filamentos 2008’ survey; dotted lines indicate the depth of the 200 m bottom depth. Lower panel (D, E, F) corresponds to the ‘Pelagic 2005’ survey. Left colour-bars correspond to figures (A, B, D, E) while right colour-bars correspond to figures (C, F). G. Meridional variation of ZVEEC averaged between the coast and 200 km offshore during the ‘Pelagic 2005’ survey (black solid line) and corresponding <math>\pm</math> one standard deviation (grey shaded area).....</b>	72
<b>3.6 Volume of anchovy habitat along the Peruvian coast. A. Volume (red volume) estimated by integrating <math>Z_{VEEC}</math> over the area occupied by the cold</b>	

<i>coastal water and its mixing with adjacent water masses during ‘Pelagic 2005’ survey. The upper part of the volume shows anchovy distribution estimated during the same survey (see Supplementary Information). B. Zoom of the study area between 9°S and 15°S (black dotted rectangle) showing a region of shallower Z<sub>VEEC</sub>. This region corresponds to a mesoscale filament associated with strong westward geostrophic currents and high chlorophyll concentration as observed from geostrophic currents (black quivers) from satellite altimetry AVISO product and chlorophyll-a concentration (colours, in mg m<sup>-3</sup>) from satellite SeaWiFS data for the same time period (C). The black solid line south of Pisco in (A) corresponds to the transect presented in (D) showing the echogram and the Z<sub>VEEC</sub> (black solid line) along this transect. E. Wavelet power spectrum (in m<sup>2</sup>) of Z<sub>VEEC</sub> in this transect showing the presence of mesoscale (<math>\geq 10</math> km) and submesoscale (F) Features.....</i>	74
4.1 <i>(a) Two step anchovy trophic chain as suggested by Ryther (1969) and (b) actual anchovy trophic web (Konchnina, 1991; Espinoza and Bertrand, 2008). The arrows represent the main source of carbon for organisms.....</i>	79
4.2 <i>Experimental (dash line) and model (solid line) variograms and their main parameters.....</i>	85
4.3 <i>Box plot of day and night epipelagic macrozooplankton biomass (g.m<sup>-2</sup>) during austral summer (a) and spring (b) pelagic surveys 2005. The size of the box is determined by the upper and lower quartiles, median is indicated as a horizontal line inside the box. Weighted mean is represented as a black solid square point. The whiskers indicate the minimum and maximum values without considering outliers.....</i>	86
4.4 <i>Box plot of day and night epipelagic macrozooplankton equivalent spherical radius (mm) during Austral summer (a) and spring (b) pelagic surveys 2005 (for details on box plot see the caption of Figure 4.3).....</i>	87
4.5 <i>Day and night box plots of epipelagic macrozooplankton biomass (in g.m<sup>-2</sup>) according to the shelf, slope and the offshore ecological domains for both austral summer (a,b) and spring (c,d) 2005 (for details on box plot see the caption of Figure 4.3).....</i>	88
4.6 <i>Day and night box plots of epipelagic macrozooplankton equivalent spherical radius (in mm) according to the shelf, slope and the offshore ecological domains for both austral summer (a,b) and spring (c,d) 2005(for details on box plot see the caption of Figure 4.3).....</i>	89
4.7 <i>Day and night box plots of across-shore macrozooplankton density (g.m<sup>-3</sup>) and biomass (g.m<sup>-2</sup>) in relation to the shelf break for both austral summer (a,b,c and d) and spring (e,f,g and h) 2005 (for details on box plot see the caption of Figure 4.3).....</i>	91
4.8 <i>Day and night box plots of across-shore macrozooplankton equivalent</i>	

<i>spherical radius (in mm) in relation to the shelf break for both austral summer (a, b) and spring (c, d) 2005. Box plot was made for every 10 km interval (for details on box plot see the caption of Figure 4.3).....</i>	92
<b>4.9 Day and night box plots of along-shore macrozooplankton biomass distribution (<math>\text{g.m}^{-2}</math>) for both austral summer (a,b) and spring (c,d) pelagic surveys of 2005. Box plot were constructed by intervals of one degree of latitude (for details on box plot see the caption of Figure 4.3).....</b>	94
<b>4.10 Day and night box plots of along-shore macrozooplankton equivalent spherical radius distribution (mm) for both austral summer (a,b) and spring (c,d) pelagic surveys of 2005. Box plot were constructed by intervals of one degree of latitude (for details on box plot see the caption of Figure 4.3).....</b>	95
<b>4.11 Horizontal macrozooplankton biomass (<math>\text{g.m}^{-2}</math>) distribution during austral summer 2005. Acoustic macrozooplankton biomass during day (a) and night (c). Zooplankton biomass from Hansen nets towed vertically from 50 m to the surface during day (b) and during night (d). The black line shows the (continental shelf limit, 200 m bottom depth).....</b>	96
<b>4.12 Horizontal macrozooplankton biomass (<math>\text{g.m}^{-2}</math>) distribution during austral spring 2005. Acoustic macrozooplankton biomass during day (a) and night (c). Zooplankton biomass from Hansen nets towed vertically from 50 m to the surface during day (b) and during night (d). The black line shows the continental shelf limit (200 m bottom depth).....</b>	97
<b>4.13 Environmental conditions during the summer survey 2005. (a) Depth of the upper limit of the OMZ. (b) Water masses. (c) Satellite chlorophyll concentration. (d) Satellite sea surface temperature The black line shows the continental shelf limit (200 m bottom depth).....</b>	98
<b>5.1 Schematic representation of the concept of bottom-up transfer of behaviours and spatial structuring. The physical forcing structures the pelagic landscape by introducing turbulence in the water mass. The dissipation of this turbulence is fractal by nature and generates a hierarchical structuring of the water mass. The inert particles (nutriments) and part of living organisms (phytoplankton and most of the zooplankton) are passively organized in space by this physical forcing. Then, biological interactions such as predator-prey relationships transmit to a certain extent this spatial structuring along the trophic chain. Source: Bertrand et al. (2008b).....</b>	111
<b>5.2 Schematic representation of the meso- and submesoscale physical structuring and their expected impacts on organism distribution. A convergence/divergence structure leads to a locally deeper/shallower oxycline that should concentrate/disperse zooplankton at the center of the structure. It is thus assumed that any positive or negative deviation of the</b>	

<i>oxycline, regardless of its origin (e.g. eddies, ocean fronts), have a corresponding positive or negative effect on zooplankton. Then fish should concentrate where zooplankton are concentrated since predator-relationship transmits to a certain extent this spatial structuring to fish. This figure was constructed from, Frontier (1987), Russel et al.(1992), Bakun (1996), Siegel et al. (1999), Lennert-Cody and Frank, 1999 and Bertrand et al. (2008a, 2008b) .....</i>	113
5.3 <i>Synthesis of data process at meso- and submesoescale.....</i>	116
5.4 <i>Example of macrozooplankton biomass variability at three scales; mesoesacale, submesoscale and from raw data.....</i>	117
5.5 <i>Example of autocorrelograms from the detrended <math>Z_{VEEC}</math> (a), the normalized macrozooplankton biomass (b), and their autocorrelation product (c). Values within dotted lines are not significantly correlated. Each data point corresponds to a 2 km elementary sample unit.....</i>	120
5.6 <i>Macrozooplankton biomass (in <math>\text{g.m}^{-2}</math> normalized by cubic root) distribution and <math>Z_{VEEC}</math> (in m) along five selected transects in relation to chlorophyll, sea surface temperature and water masses. Satellite maps (left panels) correspond to the average chlorophyll and sea surface temperature conditions during 14 -18 March and 16 -18 Mar 2005, respectively. Water masses are represented as horizontal colour bar on the x-axis of <math>Z_{VEEC}</math> panels. Transects were carried out during the period 13 -19 Mar 2005 and are represented as black (night) and white (day) lines on the satellite maps. X-axis of the macrozooplankton biomass panels represent the distance to the shelf break (indicated as vertical red dotted lines).....</i>	123
5.7 <i>Linear relation, at mesoscale, between macrozooplankton biomass (a, c) and density (b, d) normalized by cubic root and the detrended <math>Z_{VEEC}</math> during the day (a, b) and during the night (c, d). Each solid line corresponds to one transect. The dotted line corresponds to the linear correlation considering all transects together. Black and grey colors indicate significant and not significant linear correlation, respectively.....</i>	124
5.8 <i>Cubic spline fits (solid lines) of GAMs based on fish presence-absence at mesoscale according to: macrozooplankton biomass (a, c) and density (b, d) during the day (a, b) and during the night (c, d). The transformed fish presence index is in relative scale and corresponds to the spline smoother that was fitted on the data so that a y-value of zero is the mean effect of the x variable on the transformed fish presence index. Positive and negative y-values indicate positive and negative effect on the transformed fish presence index. The dotted lines show the 95% confidence limits of GAMs.....</i>	125
5.9 <i>Linear correlation, at mesoscale, between log-transformed fish acoustic nautical area scattering coefficient (NASC+) and macrozooplankton biomass (a, c) and density (b, d) normalized by cubic root, during the day</i>	

<i>(a,b) and during the night (c, d). Each solid line correspond to one transect. The dotted line corresponds to the linear correlation considering all transects together. Black and grey colors indicate significant and not significant linear correlation, respectively.....</i>	126
<b>5.10 Linear correlations, at submesoscale, between detrended shelf macrozooplankton biomass (a, c) and density (b, d) normalized by cubic root and the detrended <math>Z_{VEEC}</math> during the day (a,b) and during the night (c, d). Each solid line correspond to one transect. The dotted line corresponds to the linear correlation considering all transects together. Black and grey colors indicate significant and not significant linear correlation, respectively.....</b>	127
<b>5.11 Linear correlations, at submesoscale, between detrended offshore macrozooplankton biomass (a, c) and density (b, d) normalized by cubic root and the detrended <math>Z_{VEEC}</math> during the day (a,b) and during the night (c, d). Each solid line correspond to one transect. The dotted line corresponds to the linear correlation considering all transects together. Black and grey colors indicate significant and not significant linear correlation, respectively.....</b>	128
<b>5.12 Cubic spline fits (solid lines) of GAMs based on fish presence-absence at submesoscale according to: macrozooplankton biomass (a, c) and density (b, d) during the day (a, b) and during the night (c, d). The transformed fish presence index is in relative scale and corresponds to the spline smoother that was fitted on the data so that a y-value of zero is the mean effect of the x variable on the transformed fish presence index. Positive and negative y-values indicate positive and negative effect on the transformed fish presence index. The dotted lines show the 95% confidence limits of GAMs...</b>	129
<b>5.13 Linear correlation, at submesoscale, between detrended log-transformed shelf fish acoustic nautical area scattering coefficient (NASC+) and macrozooplankton biomass (a, c) and density (b, d) normalized by cubic root, during the day (a,b) and during the night (c, d). Each solid line correspond to one transect. The dotted line corresponds to the linear correlation considering all transects together. Black and grey colors indicate significant and not significant linear correlation, respectively.....</b>	130
<b>5.14 Linear correlation, at submesoscale, between detrended log-transformed offshore fish acoustic nautical area scattering coefficient (NASC+) and macrozooplankton biomass (a, c) and density (b, d) normalized by cubic root, during the day (a,b) and during the night (c, d). Each solid line correspond to one transect. The dotted line corresponds to the linear correlation considering all transects together. Black and grey colors indicate significant and not significant linear correlation, respectively.....</b>	131



## *List of Tables*

1.1 <i>Main characteristics of the water masses presents in the Humboldt Current System.....</i>	28
2.1 <i>Acoustic survey: spatio-temporal extension, acoustic systems and ancillary data .....</i>	49
3.1 <i>Survey characteristics.....</i>	64
3.2 <i>Linear regressions summary.....</i>	71
4.1 <i>Summary of the main types of regular zooplankton sampling surveys off Peru. Source: Ayón et al. (2008a).....</i>	80
4.2 <i>Acoustic survey characteristics.....</i>	84
4.3 <i>Post hoc Turkey multicomparison test of mean macrozooplankton size (in mm) according to survey, diel period and ecological domain. Asterisks indicate significant difference (<math>p&lt;0.05</math>) .....</i>	90
4.4 <i>Synthesis of biomass estimations (in <math>\text{g.m}^{-2}</math>) of meso- and macrozooplankton in main upwelling systems, Antarctic and eastern Canada.....</i>	107
5.1 <i>ANOVA test between shelf and offshore macrozooplankton biomass from diurnal and nocturnal transects.....</i>	121



## Résumé exécutif en Français<sup>1</sup>

### A. Introduction

Le Nord du système du Courant de Humboldt (NSCH), au large du Pérou, est la région la plus productive de l'océan mondial en matière de poissons. Ainsi, avec moins de 0.1% de la surface des océans, les débarquements péruviens représentent environ 10% des débarquements mondiaux (Chavez et al., 2008). Si l'on compare le NSCH aux autres systèmes d'upwelling de bord Est (EBUS), l'importante productivité en poisson du NSCH ne peut pas être expliquée par productivité primaire supérieure (Chavez et al., 2008). Depuis les travaux séminaux de Ryther (1969), l'anchois du Pérou (*Engraulis ringens*) été considéré comme se nourrissant directement de phytoplancton, ce qui n'était pas le cas pour les autres espèces d'anchois des autres EBUS. Cette "chaîne alimentaire courte et efficace" (Ryther, 1969; Walsh, 1981) a été suggérée comme la raison permettant au NSCH de soutenir cette importante populations de poissons. Pourtant, cette hypothèse de "courte chaîne alimentaire" a été récemment remis en question par Espinoza et Bertrand (2008) et Espinoza et al. (2009) qui ont montré que l'anchois et la sardine (*Sardinops sagax*) obtiennent la grande majorité de leur énergie calorique du zooplancton comme dans d'autres EBUS, et que le macrozooplancton, en particulier les euphausiacés et les copépodes, sont leurs principales proies. L'anchois et la sardine ont donc un niveau trophique beaucoup plus élevé que ce qui était estimé antérieurement. Étant donné que ces espèces, en particulier, l'anchois, atteignent des biomasses très élevées, une modification de leur régime alimentaire devraient affecter tous les autres composants du système. Par conséquent il est important de réévaluer les flux de carbone dans les modèles conceptuels et trophiques du NSCH. Dans ce but il est nécessaire de d'obtenir des informations quantitatives sur l'abondance et la distribution du macrozooplancton. Ces informations sont indispensables pour valider les modèles biogéochimiques, ajuster les modèles trophiques et, plus généralement, comprendre comment l'écosystème fonctionne. Malheureusement, jusqu'à présent, l'absence de données précises sur le macrozooplancton limite notre compréhension du système.

Dans la plupart des cas, l'abondance en zooplancton et sa distribution sont évalués par échantillonnage au filet à plancton qui fournit des données ponctuelles dans l'espace et le temps. En outre, le zooplancton, en particulier le macrozooplancton, est connu pour éviter les filets (Fleminger et Clutter, 1965; Brinton, 1967; Debby et al., 2004; Lawson et al., 2008) en raison des perturbations visuelles et mécaniques (Fleminger et Clutter, 1965) ; cet évitement étant d'autant plus élevé que l'on utilise des filets de petite taille. Il en résulte une sous-estimation systématique de la biomasse de macrozooplancton.

Pourtant, de grandes quantités d'informations sur le zooplancton sont présentes (bien que rarement traitées) dans les données acoustiques recueillies en routine par la plupart des laboratoires du monde entier. En raison de son caractère non invasif, l'acoustique permet d'échantillonner des organismes qui, autrement, ne seraient pas observés par échantillonnage au filet. En effet l'acoustique permet de collecter simultanément des données qualitatives et quantitatives sur les différentes communautés d'un écosystème, du zooplancton aux grands prédateurs. Toutefois, dans la plupart des cas, les

---

<sup>1</sup> Les figures et tables référencées dans ce résumé correspondent à celles du texte principal de cette thèse.

informations acoustiques sur le zooplancton sont considérées comme du bruit et simplement éliminées (Bertrand et al., 2003).

Le zooplancton, ainsi comme n'importe quel objet acoustique, peut être distingué des autres organismes (par exemple les poissons) en utilisant ses propriétés acoustiques et sa dépendance de fréquence théorique (Kloser et al., 2002; Logerwell et Wilson, 2004; Mosteiro et al., 2004; Simmonds et MacLennan, 2005). La capacité de discrimination entre les groupes d'organismes s'améliore à mesure que le nombre et la gamme des fréquences utilisées augmente (Napp et al., 1993). Malheureusement, la plupart des données acoustiques actuelles et historiques a été enregistrée à deux fréquences seulement: 38 et 120 kHz. C'est le cas des données acoustiques historiques disponibles au Pérou, où l'Instituto del Mar del Peru (IMARPE) a régulièrement recours à ces deux fréquences pour évaluer les populations de poissons pélagiques. La différence du volume moyen de rétrodiffusion entre deux fréquences ( $\Delta MVBS$ ) est couramment utilisée pour discriminer les types d'organismes observés par acoustiques (voir Murase et al., 2009). Malheureusement, le pouvoir de discrimination entre échos est limité si l'on applique seulement  $\Delta MVBS$ . Une méthode récemment développée (Lebourges-Dhaussy et Fernandes, soumis), basée sur la somme du volume moyen de rétrodiffusion ( $+MVBS$ ) à partir de deux ou plusieurs fréquences, permet d'augmenter le contraste entre les poissons et le zooplancton et donc d'améliorer le pouvoir de discrimination.

En plus de la discrimination des différents types d'organismes en fonction de leurs propriétés acoustiques, la distribution spatiale des organismes telle qu'observée par acoustique peut être utilisée pour détecter les contraintes physiques de leur habitat épipélagique. C'est le cas de l'oxycline qui délimite la partie supérieure de la zone de minimum d'oxygène et forme une barrière infranchissable par les organismes intolérants à l'hypoxie (Diaz et al., 2008; Prince et Goodyear, 2008).

Dans ce travail, nous avons combiné les deux approches,  $\Delta MVBS$  et  $+MVBS$ , ainsi que la répartition spatiale des organismes épipélagiques afin de distinguer et quantifier l'abondance en crustacés zooplanctoniques dans la couche épipélagique. Nous avons appliqué cette méthode à deux campagnes acoustiques de routine effectuées le long de la côte péruvienne et montré que: (i) la méthode est efficace pour discriminer les différents types d'échos acoustiques, (ii) l'observation acoustique de la distribution verticale des organismes permet de déterminer la limite supérieure de la zone de minimum d'oxygène ZMO qui correspond également à la limite inférieure de l'extension verticale de la communauté épipélagique, (iii) la méthode permet de fournir des cartes à haute résolution de la distribution du macrozooplancton épipélagique, (iv) l'estimation de la biomasse en macrozooplancton nous permet d'obtenir une réponse à une question clef sur le fonctionnement du système: y a-t-il assez de zooplancton pour nourrir la population d'anchois du Pérou?, et enfin, (v) grâce aux données obtenues par cette approche nous pouvons étudier l'impact de la physique sur la distribution du macrozooplancton et celle de ce dernier sur les poissons fourrage, à submésos et à mésos échelles.

## **B. Matériel et méthodes**

### **B.1. Les données acoustiques**

Les données acoustiques ont été collectées à l'aide d'échosondes 'split-beam' Simrad

EK60 et EK500 (Kongsberg Simrad AS) à 38 et 120 kHz durant quatre campagnes acoustiques effectuées au large du Pérou à bord du N/O 'José Olaya' de l'IMARPE (41 m de long) (Tableau 2.1). Deux de ces campagnes («Cardumenes 2004» et «Filamentos 2008») étaient des campagnes spécifiques multidisciplinaires, tandis que les autres («Pelagic050203» et «Pelagic051112») étaient des campagnes acoustiques de routine effectuées par IMARPE pour l'évaluation de la biomasse des principales ressources (voir Simmonds et al., 2009). Le plan d'échantillonnage consistait en des transects perpendiculaires à la côte réalisés à une vitesse de 10 nœuds sauf lors de la campagne «Cardumenes 2004» où le navire a réalisé une prospection "en carré" de deux milles nautiques de côté à une vitesse de huit nœuds (voir Bertrand et al., 2008a).

Les échosondes ont été calibrés selon la procédure décrite par Foote et al. (1987). La colonne d'eau a été échantillonnée à une profondeur de 250 m et 500 m pour le 120 kHz et 38 kHz canaux, respectivement. En raison de la présence de bruit dans les échogrammes à 120 kHz, seuls les premiers 150 m ont été considérés, sauf dans le cas de la campagne «Filamentos de 2008» où l'échosondeur employé (EK60) était plus performant. Seules les périodes de jour et de nuit ont été considérées; les données des crépuscules du matin et du soir ont été retirées avant les analyses. De plus nous avons considéré uniquement les données, enregistrées au sud de 6°S afin de se concentrer sur le NSCH et non sur l'écosystème tropical qui s'étend au nord du Pérou. La sélection, la classification et l'analyse des données acoustiques ont été réalisées en utilisant les logiciels Echoview (SonarData Pty Ltd, Hobart, Tasmanie, Australie) et Matlab (MathWorksTM, Natick, Massachusetts, USA).

### **B.2. Échantillonnage au filet**

Durant les campagnes acoustiques de routine ("Pelagic050203" et "Pelagic051112") le zooplancton a été échantillonné par traits verticaux entre 50 et 0 m de profondeur à l'aide d'un filet Hensen de 0,33 m<sup>2</sup> de diamètre possédant une maille de 300 µm (voir Ayón et al., 2004 pour plus d'information).

Lors des campagnes spécifiques, le zooplancton a été collecté en utilisant un filet à plancton de type 'Multinet', avec une maille de 300 µm, dans les strates de profondeur suivantes: 0-10 m, 10-25 m, 25-50 m, 50-75 m, et 75-100 m lors de la campagne «Cardumenes 2004», et 0-10 m 10-20 m, 20-30 m, 30-50 m, 50-75 m 75-100 m, 100-200 m et 200-300 m lors de la campagne «Filamentos 2008».

Le biovolume du zooplancton (en mL) a été déterminée immédiatement après la collecte en utilisant la méthode de déplacement (Kramer et al., 1972). Les échantillons ont été fixés dans du formol à 2% tamponné avec du borax, puis examinés au laboratoire à l'aide d'un microscope stéréoscopique pour identifier et compter les éléments du zooplancton.

Les poissons et la galathée "munida" (*Pleuroncodes mondon*), un crustacé pélagique très abondant depuis les années 1990 (voir Gutiérrez et al., 2008), ont été collectés à l'aide d'un chalut pélagique de type 'Engel 124/1800" (maillage de 12 mm au cul du chalut) . Pour chaque trait de chalut, un sous-échantillon des captures a été recueilli et les individus identifiés et mesurés.

### B.3. Analyse des données acoustiques

Pour comparer les échogrammes provenant des deux fréquences, nous avons tout d'abord synchronisé le numéro et la position de chaque émission (ping) en utilisant l'algorithme correspondant d'Echoview ('ping number algorithm'). Nous avons ensuite éliminé le bruit présent en surface (5 m de profondeur à partir du transducteur) et les échos de fond. Nous avons séparé les échogrammes en définissant et en éliminant les zones contenant des bruits parasites. Pour éliminer le bruit associé à l'absorption acoustique, nous avons suivi la méthode proposée par Fernandes et al. (2006) et créé un nouveau champ acoustique pour chaque fréquence en utilisant un algorithme générateur de données basé sur une fonction de bruit du type:

$$20 \log(R) + 2 \alpha R + \text{offset} \quad \text{Eq. (1),}$$

où  $R$  est la portée (en m),  $\alpha$  est le coefficient d'absorption de fréquences (en  $\text{dB.m}^{-1}$ ) alors que l' $\text{offset}$  (en dB) est le bruit estimé au niveau du premier mètre. Pour générer le champ de bruit nous avons besoin d'indiquer des valeurs initiales de  $\alpha$  et de l' $\text{offset}$ . Ces valeurs ont été déterminées à partir des valeurs minimum de bruit par strate de profondeur telles qu'estimée à partir d'une section d'échogramme prise en dessous du fond (programme de Matlab développé par P. Fernandes, Marine Lab., Aberdeen, Royaume-Uni). Le champ de bruit généré par l'équation (1) est ensuite soustrait à l'échogramme dans le domaine linéaire. Enfin, nous avons ré-échantillonné les échogrammes à chaque fréquence en utilisant des cellules élémentaires d'une émission de long et 0,75 m de haut.

Pour augmenter le contraste entre les échos de poisson et de zooplancton, nous avons utilisé une méthode récemment développée (Lebourges-Dhaussy et Fernandes, soumis) et sommé le volume rétrodiffusé moyen provenant des deux fréquences (+MVBS<sub>120+38</sub>). Cette étape renforce le pouvoir de discrimination de la méthode basée sur la différence d'énergie rétrodiffusée entre chaque fréquence ( $\Delta\text{MVBS}_{120-38}$ ). Cette dernière méthode ne permet en effet pas de prendre en compte des situations qui peuvent être rencontrées en mer: par exemple, présence de pneumatophores qui peuvent avoir, en fonction de leur taille, une tendance à émettre un écho respectivement plus fort ou plus faible à 38 ou 120 kHz. En outre, si l'intervalle de fréquences 38-120 kHz correspond à la zone de transition où l'efficacité de rétrodiffusion oscille (Stanton et al., 1998),  $\Delta\text{MVBS}$  peut être positif ou négatif. Ainsi, quelle que soit la tendance de  $\Delta\text{MVBS}_{120-38}$  la différence de variabilité entre les poissons et le zooplancton a été utilisée pour améliorer le contraste entre les deux types d'organismes (Lebourges-Dhaussy et Fernandes, soumis). Enfin, à partir d'observations, nous avons choisi empiriquement une valeur seuil de -135 dB pour la somme des échogrammes (+MVBS<sub>120+38</sub>) et avons utilisé un masque Booléen (vrai pour les valeurs au dessus du seuil) pour créer des échogrammes "poisson" - "non-poisson" à chaque fréquence. A partir de maintenant, tous les processus seront également appliquées aux deux fréquences; dans le cas contraire une information spécifiques sera fournie.

Dans le NSCH, toutes les espèces de poissons exploités (anchois, sardine, maquereau, chincharde, etc.) et la plupart des poissons mésopélagiques ont une vessie natatoire gazeuse. Par conséquent, toute référence à «poisson» dans cette étude correspond à des poissons pourvus de vessie natatoire gazeuse. Les poissons à vessie natatoire ont un pouvoir de rétrodiffusion acoustique légèrement supérieur à 38 kHz qu'à 120 kHz

(Kloser et al., 2002). Cependant, dans quelques cas,  $\Delta\text{MVBS}_{120-38}$  peut être positif (jusqu'à environ +2 dB) dans le cas d'échos de poissons. Nous avons donc affiné les échogrammes de poissons en appliquant un second masque Booléen pour ne garder que les cibles pour lesquelles  $\Delta\text{MVBS}_{120-38} < +2$  dB.

Les organismes zooplanctoniques composés de tissus faiblement diffusant et possédant des propriétés acoustiques similaires au milieu sont habituellement nommés "fluide-like zooplankton" (Stanton et al., 1996). Le groupe "fluide-like" comprend les euphausiacés, les copépodes, les salpes, les siphonophores (sans inclusion de gaz) et les autres espèces de crustacés zooplanctoniques de grande taille (par exemple, les larves de squilles, et les larves de décapodes munidae). Ce groupe a été extrait des échogrammes "non poisson" en appliquant un masque booléen pour sélectionner les cibles pour lesquelles  $\Delta\text{MVBS}_{120-38}$  était positif. Les cibles pour lesquelles  $\Delta\text{MVBS}_{120-38}$  était négatif ont été désignés comme "bruit bleu". Ce groupe inclut toutes les cibles différentes des crustacés "fluide-like" et des poissons (principalement des larves de poissons, des organismes gélatineux et des siphonophores avec inclusion de gaz). Pour plus de détails sur l'algorithme acoustique se référer au Chapitre 2 de la thèse.

Nous avons ensuite différencié la munida des autres organismes de type "fluide-like" pour différentes raisons: (i) la munida est plus grande que les autres espèces de zooplancton "fluide-like" dans l'écosystème et ne joue pas le même rôle écologique (par exemple la munida adulte n'est pas une proie pour les poissons pélagiques de petite taille mais plutôt un compétiteur), (ii) la munida rétrodiffuse plus d'énergie que les autres organismes de type "fluide-like" présents, (iii) au large du Pérou la munida est épipélagique et effectue des migrations verticales limitées à la couche épipélagique (Gutiérrez et al., 2008). Pour extraire la munida des autres "fluide-like" nous avons appliqué les seuils suivants sur le  $\text{Sv}_{120}$  "fluid-like": -72 dB  $<\text{Sv}<-53$  dB. Ces limites ont été déterminées empiriquement à partir des échogrammes où la présence ou l'absence de munida a été confirmée par chalutage pélagique. L'échogramme résultant correspondant à la munida a été validé par les échantillonnages de munida le long des transects (la munida est régulièrement évaluée par IMARPE) et la position des échos dans la couche épipélagique.

#### **B.4. Estimation de la biomasse en "fluid-like"**

Bien que le groupe "fluide-like" comprenne euphausiacés, copépodes, salpes, siphonophores (sans inclusion de gaz) et certaines munida juvéniles, nous nous sommes concentrés sur le macrozooplancton, en particulier les euphausiacés et les gros copépodes. En effet, les petits crustacés "fluide-like" (par exemple les petits copépodes) ne peuvent pas être correctement détectés et quantifiés à 38 kHz (Mitson, 1996). Les salpes sont peu abondantes en dehors de la zone nord (au nord de 6°S, domaine non inclus dans cette étude) (Ayón et al., 2008a), les siphonophores sans inclusion de gaz ont une biomasse très faible (Ayón et al., 2008a) et la munida juvénile n'est présente en quantité significative que dans les zones proches du littoral (Fagetti et Campodonico, 1971). Par ailleurs, les euphausiacés et les grands copépodes, particulièrement *Eucalanus spp.*, sont les principaux constituants du macrozooplancton (Ayón et al., 2008a) et les principales proies des espèces de poissons les plus abondantes: l'anchois, la sardine, le maquereau, le chincharde, et les poissons mésopélagiques (Konchina, 1981; Espinoza et Bertrand, 2008; Espinoza et al., 2009). Selon Murase et al. (2009), pour être détectés à 38 kHz, les grands copépodes ont besoin d'être distribués sous forme

d'agrégation de forte densité. Puisque les euphausiacés atteignent une biomasse plus importante que celle des copépodes (Ayón et al., 2008b) et sont les proies préférentielles des poissons fourrage (ex. Espinoza et Bertrand, 2008), nous avons ajusté la procédure selon les propriétés acoustiques des euphausiacés lors de l'estimation de la biomasse en macrozooplankton.

Bien que les euphausiacés aient une forme plus cylindrique que sphérique, dans la pratique, le modèle de fluide sphérique bi-fréquence est approprié pour estimer le biovolume du zooplancton (Holliday et Pieper, 1995). En effet, la représentation imparfaite de la forme devient négligeable une fois moyennée sur de nombreux échos et lorsque l'orientation des animaux couvre une ample gamme d'angles autour de l'horizontal (Stanton et Chu, 2000).

Pour estimer la taille moyenne (rayon de la sphère), le nombre d'organismes insonifiés et le biovolume en "fluide-like" dans chaque cellule de l'échogramme, nous avons appliqué une méthode fondée sur la différence de Sv entre les fréquences (Greenlaw, 1979).

Détermination du rayon de la sphère ( $a$ ) l'aide du modèle "fluid sphere high-pass" (Johnson, 1977):

$$(ka)^4 = (2/3) \cdot [(r^4 - R)/(r^2(R-1))] \quad \text{Eq. (2)}$$

où  $k = 2\pi f_m / c$ ,  $a$  est le rayon de la sphère (en mm),  $c$  est la vitesse du son (en  $\text{m.s}^{-1}$ ),  $f_m = (f_{120} \cdot f_{38})^{0.5}$  (en kHz),  $r = f_{120}/f_{38}$ , et  $R = 10^{(Sv(120)-Sv(38))/10}$ . La vitesse du son a été estimée à  $1509 \text{ m.s}^{-1}$ , ce qui correspond à une température moyenne de  $15,5^\circ\text{C}$  et une salinité de 35 psu.

La détermination de la section rétrodiffusante  $\sigma_{bs}$  de la sphère peut être ensuite estimée en utilisant l'équation proposée par Greenlaw (1979):

$$\sigma_{bs} = [(1-gh^2)/(3gh^2) + (1-g)/(1+2g)]^2 \cdot a^2 \cdot [2(ka)^4/(2+3(ka)^4)], \quad \text{Eq. (3)}$$

où  $g$  est le contraste de densité entre la sphère et le milieu environnant, et  $h$  la vitesse de contraste. Aucune estimation de  $g$  et  $h$  ne sont disponibles pour *Euphausia mucronata*, l'espèce dominante d'euphausiacés dans le NSCH. Par conséquent, nous avons utilisé les paramètres estimés pour une espèce similaire, *Euphausia pacifica*, du système du Courant de Californie. Pour ce faire nous avons moyenné les résultats obtenus par Greenlaw et Johnson (1982) sur des *E. pacifica* fraîchement pêchées ( $g = 1,037$  et  $h = 1,0097$ ).

Le nombre d'individus par unité de volume ( $N_f$ , en nombre d'individus par  $\text{m}^{-3}$ ) peut alors être estimé comme suit:

$$N_f = 10^{(Sv(f)-TS)/10}, \quad \text{Eq. (4)}$$

où  $TS = 10 \log_{10}(\sigma_{bs})$ .

Le biovolume en fluide-like a été calculé en multipliant la densité en organismes (ind.m<sup>-3</sup>) par le volume (en cm<sup>3</sup>) de la sphère de rayon  $\alpha$ , c'est à dire le volume estimé de chaque individu "moyen".

Les  $s_v$  correspondants aux poissons, au bruit bleu et à la munida ont été convertis en coefficient de diffusion acoustique par mille nautique (NASC), un indice d'abondance selon MacLennan et al. (2002), en utilisant l'équation suivante:

$$\text{NASC (en } m^2 \text{ mi.n.}^2\text{)} = 4\pi (1852)^2 s_v T, \quad \text{Eq. (5)}$$

où  $T$  est la distance verticale intégrée des cellules élémentaires de 0,75 m.

### **B.5. Extension verticale de la communauté épipélagique**

Le NSCH se caractérise par la présence de la plus intense et superficielle zone de minimum d'oxygène (ZMO) de l'océan mondial (Helly et Levin, 2004; Chavez et al., 2009; Paulmier et Ruiz-Pino, 2009). Bien que certaines espèces de zooplancton, de poissons mésopélagiques, et de calmars aient adapté leur métabolisme et puissent se distribuer dans la ZMO de façon temporaire (migration verticale nyctémérale) ou permanente, l'extension verticale de la communauté du zooplancton épipélagique (VEEC) est généralement limitée par la présence de la ZMO (Criales et al., 2008; Ayón et al., 2008a; Bertrand et al., 2010), qui forme une barrière infranchissable par la plupart des espèces marines. Nous avons défini la profondeur de la VEEC ( $Z_{VEEC}$ ) comme correspondant à la profondeur où 98% de la somme cumulée des échos acoustiques de la communauté épipélagique était atteint (Bertrand et al., 2010). Cette profondeur a été corrigée pour tenir compte de la position du transducteur sur la coque du N/O (3,4 m sous la surface de la mer).

L'anchois, le poisson épipélagique dominant dans le système, a un écho individuel (~ -50 dB) beaucoup plus élevé qu'un euphausiacé (~ -85 dB). Cependant les poissons occupent un volume moins important que le zooplancton (le zooplancton comprend essentiellement les crustacés et les organismes gélatineux). Par conséquent, afin de mieux refléter la répartition réelle de la communauté globale épipélagique, nous avons considéré tous les échos mais réduit le poids des échos de poissons par un facteur de 10<sup>-3</sup> lors de l'estimation  $Z_{VEEC}$ . Il est important de noter que l'estimation de  $Z_{VEEC}$  est robuste aux changements de méthodologie (vis-à-vis par exemple d'un changement dans la pondération appliquée aux échos de poissons). Finalement nous avons montré que la concentration moyenne en oxygène dissous à  $Z_{VEEC}$  était de 0,80 mL L<sup>-1</sup>, indépendamment du cycle nyctéméral (Bertrand et al., 2010).

Dans le SCH les principales espèces d'euphausiacés et d'*Eucalanus* sont adaptées à l'hypoxie et se distribuent dans la ZMO durant la journée (Antezana, 2009; Escribano et al., 2009). Pendant la nuit, cependant, ils migrent vers la surface et deviennent partie intégrante de la communauté épipélagique affectant sa composition spécifique et sa biomasse (Antezana, 2009; Escribano et al., 2009). Par conséquent, les estimations de biomasse de zooplancton épipélagique ont été réalisées de façon indépendante, de jour et de nuit.

### **B.6. Biomasse en macrozooplancton dans la couche épipélagique**

Pour estimer la biomasse en macrozooplancton (en  $\text{gm}^{-2}$ ) intégrée dans la couche épipélagique nous avons procédé en suivant les étapes suivantes:

- (i) nous avons réduit les échogrammes (fluid-like, poisson et bruit bleu) en calculant la valeur médiane toutes les trois émissions;
- (ii) en utilisant ces "échogrammes réduits", nous avons estimé  $Z_{VEEC}$  selon la procédure décrite précédemment (voir Bertrand et al., 2010) et considéré que  $Z_{VEEC}$  délimitait verticalement la couche épipélagique.
- (iii) nous avons estimé le biovolume moyen en fluid-like et la taille du macrozooplancton contenu dans la couche épipélagique. Étant donné que chaque cellule élémentaire a été attribuée à un groupe unique de type de cible en fonction des propriétés des échos dominants qui la composent, les cibles ayant un écho faible peuvent être "cachées" lorsque des cibles à échos forts sont présentes dans la cellule élémentaire. Ainsi, si dans la même cellule des fluid-like et des poissons sont présents, les échos de poissons dominent et il n'est pas possible de détecter la présence de fluid-like (Korneliussen et Ona, 2003). Pour réduire ce biais, le biovolume de fluid-like, a été estimé sans inclure les cellules affectées à d'autres types de cibles acoustiques.
- (iv) la densité moyenne en fluid-like en poids humide ( $WW$ , en  $\text{g.m}^{-3}$ ) a été estimée selon l'équation de régression fonctionnelle suivante (Wiebe et al., 1975; Wiebe, 1988):

$$\text{Log}(BV) = 0.139 + 1.003 * \text{Log}(WW) \quad \text{Eq. (6)}$$

où  $BV$  est le biovolume moyen en fluid-like (en  $\text{cm}^3 \cdot \text{m}^{-3}$ ) dans la couche épipélagique.

- (v) la biomasse intégrée en macrozooplancton de la communauté épipélagique par unité d'échantillonnage élémentaire (longueur de 3 émissions et hauteur égale à  $Z_{VEEC}$ ) a ensuite été estimée en multipliant la densité moyenne par  $Z_{VEEC}$ .

Par la suite, les données de jour et de nuit ont été classées par domaine écologique (plateau continental, talus et zone océanique). La biomasse acoustique totale par campagne et par période diurne a été estimée comme étant la biomasse moyenne provenant de chaque domaine pondérée par la surface occupée par chaque domaine. Une procédure similaire a été réalisée pour estimer la biomasse totale en zooplancton telle qu'estimée par échantillonnage au filet à plancton.

### **B.7. Validation**

La validation de la méthode acoustique a été réalisée en trois étapes. Premièrement, nous avons comparé la biomasse acoustique (NASC) en poissons et munida estimée durant la campagne «Cardumen 2004» avec leurs captures respectives au chalut pélagique. Afin que les captures soient comparables, la vitesse (~ 2 nœuds) et la durée (20 min) ont été maintenues constantes au cours des traits de chalut. Les estimations acoustiques de NASC de poissons et de munida comprises dans les 10 minutes centrales de l'échantillonnage au chalut ont été utilisées pour cette comparaison.

Deuxièmement, nous avons comparé les profils verticaux de biovolume acoustiques de fluid-like avec ceux obtenus par échantillonnage avec le 'Multinet' à différentes strates de profondeur au cours de la campagne «Cardumen 2004». De plus, l'abondance des

principaux types de macrozooplancton (euphausiacés adultes, munida zoea, *Eucalanus inermis*, et juvéniles et larves d'euphausiacés) intégrée sur 10-100 m a été comparée avec le biovolume acoustique intégré de macrozooplancton de type fluid-like. Comme il n'y avait pas d'enregistrement acoustique au moment de l'échantillonnage au filet à plancton nous avons utilisé les 25 émissions enregistrées juste avant que le profil de Multinet ne soit réalisé.

Troisièmement, nous avons comparé les profils verticaux de biovolume acoustiques de fluid-like, avec l'abondance des adultes, juvéniles, et larves d'euphausiacés échantillonnés par Multinet durant la campagne «Filamentos 2008» où les données acoustiques bi-fréquence étaient disponibles jusqu'à 300 m de profondeur. Étant donné que durant cette campagne, les enregistrements acoustiques se sont poursuivis durant l'échantillonnage par Multinet, il a été possible de comparer directement les deux types d'estimations.

### ***B.8. Patrons de distribution de la biomasse en fluid-like***

Pour chaque période diurne, les grands patrons de distribution du macrozooplankton par domaine écologique et selon la distance au talus (intervalles de 10 km) ont été représentés en utilisant des 'box plot'.

Puisque des histogrammes préliminaires ont montré que les données de biomasse en macrozooplancton ne présentaient pas une distribution normale, ces données ont été normalisées par l'application d'une transformation racine cubique avant d'appliquer tout test statistique. Nous avons utilisé des ANOVA pour tester l'effet du cycle diurne au sein de chaque domaine écologique indépendamment. Nous avons également appliqué des ANOVA suivies par des tests post hoc (Turkey) pour déterminer si la biomasse/densité en macrozooplankton différait sensiblement entre les domaines écologiques.

Finalement nous avons construit des cartes (jour et nuit), interpolées par krigage, de la biomasse en macrozooplankton pour les campagnes de printemps et d'été 2005. La distribution spatiale de la biomasse en zooplancton étant anisotrope, avec plus d'autocorrelation dans le long de la côte que perpendiculairement, nous avons ajusté un variogramme directionnel sur les données. Ces cartes ont ensuite été comparées avec les cartes correspondantes réalisées à partir des échantillonnages au filet à plancton.

### ***B.9. Effet de la structuration physique sur la distribution du macrozooplankton et des niveaux trophiques supérieurs***

Pour explorer l'impact des structures physiques de méso et submeso échelles sur la distribution du macrozooplankton et des niveaux trophiques supérieurs, nous avons formé des hypothèses, sur la base des connaissances disponibles dans la littérature (Fig. 5.2).

Les tourbillons anticycloniques de mésoéchelle sont des structures convergentes qui transportent l'eau et le plancton vers leur centre où la pycnocline/oxycline tend à s'approfondir (Bakun 1996; Siegel et al., 1999). Ces structures sont donc sensées accumuler du zooplancton en leur centre (Yebra et al., 2005) et être attractives pour les prédateurs du zooplancton. A l'inverse, les tourbillons cycloniques de mésoéchelle sont

des structures divergentes qui pompent de l'eau depuis les couches plus profondes vers la surface ce qui fait remonter la pycnocline/oxycline (Bakun, 1996; Siegel et al., 1999). Dans ces structures le zooplancton doit être transporté du centre vers le bord de la structure et donc contenir relativement peu de zooplancton. En raison de la faible abondance en zooplancton dans ces structures, une faible abondance en prédateurs du zooplancton est également attendue. Les structures similaires de submésoséchelle, telles que des ondes internes ou les petits tourbillons, peuvent également avoir des caractéristiques convergentes ou divergentes avec des effets sur la distribution du zooplancton similaires aux modèles décrits pour les structures de mésoséchelle. Dans ce travail nous avons utilisé  $Z_{VEEC}$  comme approximation de la limite supérieure de la ZMO (qui correspond au bas de l'oxycline) pour discriminer les structures physiques de mésoséchelle et submésoséchelle présentes. La biomasse acoustique en macrozooplankton et en poissons a été estimée selon la méthode décrite précédemment. Seules les données acoustiques prélevées durant la campagne de l'été Austral 2005 ont été utilisées pour cette analyse.

#### *B.9.1. Échelles et unités d'échantillonnage*

En nous basant sur la littérature nous avons défini deux échelles basée sur la taille de structures spatiales physiques connues: (i) la submésoséchelle ( $100^{\text{aine}}$  de m à kms), et (ii) la mésoséchelle ( $10^{\text{aines}}$  de km). Pour travailler à ces deux échelles, deux valeurs d'ESU (Elementary Sampling Unit) ont été définies: 200 m et 2 km pour l'analyse à submésoséchelle et mésoséchelle, respectivement.

Pour décrire les principaux patrons spatiaux de  $Z_{VEEC}$  et de la biomasse en macrozooplankton à l'échelle d'un transect en présence de structures de mésoséchelle, nous avons superposé une sélection de transects aux cartes satellites de chlorophylle-a et de température superficielle de la mer. Les patrons spatiaux de  $Z_{VEEC}$  et de la biomasse en macrozooplankton le long des transects ont ensuite été comparés avec les principales structures physiques, les masses d'eau et la distance au bord du talus à l'échelle du transect.

#### *B.9.2. Processus de mésoséchelle et submésoséchelle*

La limite supérieure de la ZMO n'oscille pas seulement sous l'influence de structures physiques de mésoséchelle et submésoséchelle mais également en raison de forçages de plus grande échelle. Ainsi, la profondeur de la limite supérieure de la ZMO est connue pour présenter une tendance côte - large en s'approfondissant au fur et à mesure que l'on s'éloigne de la côte (Fuenzalida, 2008). Comme notre but n'est pas de se concentrer sur ces processus de grande échelle, mais sur l'activité de mésoséchelle et submésoséchelle, nous avons d'abord éliminé cette tendance en appliquant une régression de type "least trimmed square" (LTS) sur  $Z_{VEEC}$  le long de chaque transect (Fig. 5.3). Avec cette méthode de régression l'effet des valeurs aberrantes sur la tendance globale linéaire est réduit parce que seul un pourcentage donné des données, celles présentant les plus faibles résidus (90% dans cette étude) est utilisé; les données présentant les plus forts résidus étant éliminées (10% dans notre cas).

Pour travailler à mésoséchelle, nous avons utilisé les résidus de la régression LTS et agrégé les données par échantillons élémentaires de 2 km de long (Fig. 5.3). Pour

travailler à submésoséchelle nous avons agrégé les données par échantillons élémentaires de 200 m de long, éliminé les patrons de mésoséchelle et travaillé à partir des résidus de la régression LTS (Fig.5.3).

La même méthode a été appliquée à la série de la biomasse et de densité en macrozooplancton et à l'abondance en poissons. Dans ces cas la tendance à grande échelle présente dans  $Z_{VEEC}$  n'était pas présente et n'a donc pas été supprimée. La biomasse et la densité en macrozooplancton de la série ont été transformées par l'application d'une racine cubique, tandis que l'abondance en poissons a été transformée en prenant son logarithme.

#### *B.9.3. Relations prédateur-proies: poissons vs. macrozooplancton*

Les données acoustiques de poissons (par exemple le NASC par ESU) se caractérisent par une très forte proportion de zéros, ce qui limite l'utilisation des méthodes statistiques. Pour surmonter ce problème, nous avons travaillé en deux étapes pour les deux échelles. Tout d'abord, nous avons travaillé avec les données de présence-absence de poisson. Dans ce cas, nous avons utilisé des modèles additifs généralisés (GAM, Hastie et Tibshirani, 1990) pour modéliser la présence - absence en poissons en fonction de la biomasse/densité en macrozooplancton. Ces modèles ont été construits en utilisant une loi binomiale. Deuxièmement, nous avons seulement utilisé les données où les poissons étaient présents (NASC+). Dans ce cas, nous avons fait une exploration préliminaire entre la biomasse en poissons (NASC+) et la biomasse/densité en macrozooplancton. Comme la tendance était linéaire nous avons appliqué une corrélation linéaire. Pour contrebalancer l'effet potentiel de l'autocorrelation, nous avons utilisé un niveau de confiance de 0,99% dans les tests de corrélations.

## **C. Résultats**

### **C.1. Validation**

La première étape de la validation, la comparaison des estimations par acoustiques (NASC) et par chalutage pélagique des poissons et des munida, a montré que les corrélations étaient positives et significatives (poissons:  $p = 0,006$ ,  $r^2 = 0,62$ ; Munida:  $p = 0,008$ ,  $r^2 = 0,56$ ).

Bien que le biovolume moyen en macrozooplancton estimé par acoustique était d'un ordre de grandeur plus élevé que le biovolume estimé par échantillonnage au filet, les profils verticaux des deux sources présentaient des profils verticaux similaires de jour comme de nuit (Fig. 2.7)

La deuxième étape de la validation a consisté en la comparaison des profils de l'abondance intégrée verticalement (10 - 100 m) des euphausiacés adultes (Fig. 2.8a), des munida zoea (Fig. 2.8 b), d'*Eucalanus inermis* (Fig. 2.8 c) et des larves et juvéniles d'euphausiacés (Fig. 2.8d) avec le biovolume intégré de fluid-like acoustique. Les résultats ont montré que les euphausiacés adultes étaient le groupe présentant le patron le plus semblable à celui du biovolume de fluid-like acoustique.

L'importance des euphausiacés comme organismes principaux responsables de la

tendance acoustique observée a également été confirmé par la comparaison du biovolume de fluid-like acoustique avec l'abondance en euphausiacés estimée par Multinet par strate de profondeur au cours de la campagne "Filamentos 2008" (troisième étape). L'échantillonnage par Multinet a montré que les euphausiacés adultes, juvéniles et larvaires ont été abondants dans la couche épipélagique pendant la journée (Fig. 2.9 b,c,d). Une zone intermédiaire, presque sans euphausiacés, était située entre la couche épipélagique et la couche profonde d'euphausiacés. La couche plus profonde, distribuée entre 200 et 300 m (c.à.d. dans le cœur de la ZMO), était seulement composée d'euphausiacés adultes. Au cours de la nuit (Fig. 2.9 e,f,g), les euphausiacés étaient distribués uniquement dans la couche épipélagique, quel que soit leur stade ontogénique.

### ***C.2. Variation nycthémérale de la biomasse et la taille du macrozooplancton***

La biomasse acoustique totale (nocturne) en macrozooplancton épipélagique a été estimée à 114,6 et 112,4 g<sup>-2</sup> en été et printemps Austral 2005, respectivement (Fig. 4.3). Ces estimations de nuit étaient environ quatre fois plus élevées que la biomasse estimée durant le jour: 28,6 et 24,3 gm<sup>-2</sup> en été et printemps Austral 2005, respectivement. Les tailles estimées des organismes macrozooplanctoniques ont varié légèrement selon le cycle nycthéméral, mais étaient très similaires entre les deux campagnes (~ 4 mm pendant la journée et ~ 4,2 mm au cours de la nuit). La biomasse nocturne en zooplancton estimée par échantillonnage au filet a été estimée à 21,2 et 22,1 gm<sup>-2</sup> en été et printemps Austral 2005, respectivement. De jour cette biomasse était de 12,9 et 13,8 gm<sup>-2</sup> en été et printemps Austral 2005, respectivement.

### ***C.3. Biomasse et taille du macrozooplancton selon les domaines écologiques***

La biomasse en macrozooplancton épipélagique (transformée par la racine cubique) a varié de façon significative avec le domaine écologique et ce, de jour (ANOVA:  $F_{[2, 115020]} = 10758,1$ ,  $p = 0,0000$  pour la campagne d'été et  $F_{[2, 132416]} = 22699,5$ ,  $p = 0,0000$  pour la campagne de printemps) comme de nuit (ANOVA:  $F_{[2, 91995]} = 25249,8$ ,  $p = 0,0000$  pour la campagne d'été et  $F_{[2, 96455]} = 18912,5$ ,  $p = 0,0000$  pour la campagne de printemps). Dans tous les cas les tests post hoc de Turkey étaient significatifs ( $p < 0,05$ ). La biomasse en macrozooplancton augmentait depuis le plateau continental, vers la pente, et la zone océanique quel que soit la campagne et la période diurne considérée (sauf pendant la journée en été Austral 2005 lorsque la biomasse était légèrement inférieure au niveau du bord du talus comparé à la plateforme continentale). Les tailles du macrozooplancton ont présenté moins de variations en fonction du domaine écologique au cours de la journée que pendant la nuit (Fig. 4.6). Quelle que soit la campagne ou la période diurne, le macrozooplancton était significativement plus gros dans la zone océanique que sur le plateau continental (ANOVA et tests post hoc de Turkey non montrés).

### ***C.4. Distribution côte-large de la biomasse, densité et taille du macrozooplancton***

Les résultats précédents ont montré que la biomasse en macrozooplancton augmente de la côte vers le large. Une description plus détaillée de la distribution côte-large de la biomasse en zooplancton (Fig. 4.7) illustre l'importance de la rupture de plateforme continentale en tant que point de coupure avec les biomasses océaniques plus élevées,

en particulier durant la nuit. La forte variabilité de la taille du macrozooplancton, illustre sans doute la diversité en taille de la communauté du macrozooplancton épipélagique (Fig. 4.8). La tendance côte-large d'augmentation de la taille du macrozooplancton était claire durant la nuit alors que durant la journée aucun patron clair n'est apparu (Fig. 4.8).

### ***C.5. distribution horizontale du macrozooplancton***

Les cartes de répartition horizontale de la biomasse en zooplancton construites à partir des données acoustiques et des échantillonnages au filet Hensen (Fig. 4.11) montrent des structures spatiales globalement similaires. En particulier, l'augmentation côte-large de la biomasse en macrozooplancton est observée à partir de deux sources de données. Ce patron est particulièrement fort durant la nuit mais également observable de jour. Toutefois, la biomasse acoustique en macrozooplancton montre une plus forte différence jour-nuit que celle estimée par filet à plancton, en particulier dans la zone océanique. En outre, certaines zones riches en macrozooplancton (par exemple l'extrême nord de la zone d'étude en l'été austral 2005 et la partie océanique vers ~13°S au printemps Austral 2005) ont pu être détectées par les deux sources de données.

### ***C.6. Effet de la structuration physique sur la distribution du macrozooplancton et des niveaux trophiques supérieurs***

#### *C.6.1. Impact des structures de mésoéchelle observées par satellite sur Z<sub>VEEC</sub> et la distribution du macrozooplancton*

Au cours de la campagne de l'été Austral 2005, les cartes satellites de chlorophylle-a et de SST ont révélé la présence d'un filament d'upwelling caractérisé par un fort courant géostrophiques vers 12°S (Fig. 5.6). Ce filament, présent durant environ deux semaines, a advecté vers le large les eaux côtières augmentant la production primaire de la zone océanique. En outre, un intense front océanique était présent au sud du filament. Ces structures hydrographiques ont très clairement affecté la Z<sub>VEEC</sub> et la biomasse en macrozooplancton. En effet, le long du cœur du filament, Z<sub>VEEC</sub> et la biomasse en macrozooplancton étaient très faibles (Fig. 5.6 transect 2). Sur les côtés du filament, indépendamment de la période diurne, Z<sub>VEEC</sub> était également plus faible (Fig. 5.6 transects 1 et 3) que dans les régions situées hors du filament (Fig. 5.6 transects 4 et 5). Quelle que soit la période diurne considérée, la biomasse en macrozooplancton était beaucoup plus élevée sur les côtés du filament que dans son cœur. Au sud du filament et pendant la journée, un front océanique relativement stable a coïncidé avec un approfondissement de Z<sub>VEEC</sub> vers le large et une augmentation rapide de la biomasse en macrozooplancton (Fig. 5.6 transect 4). Dans la partie sud de la zone sélectionnée et pendant la nuit, Z<sub>VEEC</sub> et la biomasse en macrozooplancton augmentaient rapidement vers le large juste après le bord du talus (Fig. 5.6 transect 5).

#### *C.6.2. Impact des structures physiques sur le macrozooplancton*

Considérant tous les transects ensembles, la biomasse en macrozooplancton était significativement et positivement corrélée à Z<sub>VEEC</sub> de jour comme de nuit (Fig. C1). A submésoscale, sur le plateau continental, la biomasse en macrozooplancton était également significativement et positivement corrélée à Z<sub>VEEC</sub> de jour comme de nuit. Au

large, la biomasse en macrozooplancton était significativement et positivement corrélée à Z<sub>VEEC</sub> durant la journée (Fig. 5.11a, Annexe G), mais significativement et négativement corrélée de nuit. Dans la plupart des cas (indépendamment de l'échelle ou de la période nyctémérale) la densité en macrozooplancton n'était pas significativement corrélée à Z<sub>VEEC</sub>.

### C.6.3. Relations prédateur-proie

Considérant tous les transects ensembles, la biomasse en poissons était significativement corrélée à la biomasse et la densité en macrozooplancton pendant la nuit, indépendamment de l'échelle d'étude. De jour, une telle corrélation n'a été observée qu'à submesoéchelle.

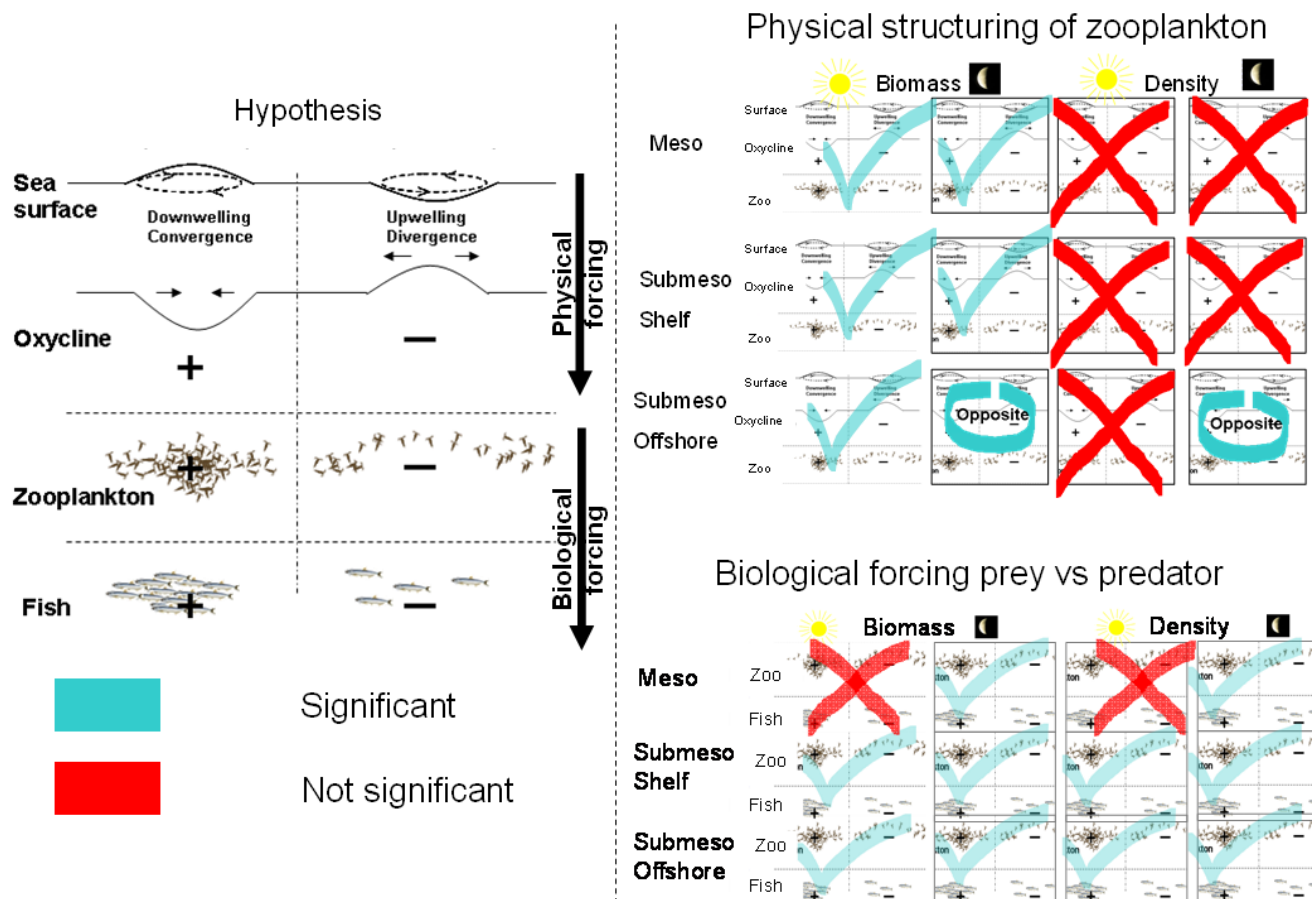


**Figure C.1** Synthesis of the overall results (all transects together) of the linear correlations between (a) macrozooplankton biomass/density and the detrended Z<sub>VEEC</sub>, as well as correlations between (b) fish acoustic nautical area scattering coefficient (NASC+) and macrozooplankton biomass/density. Blue and red colour represents significant and non-significant correlations respectively. Check symbol indicate if the significant correlation was in agreement with the proposed hypothesis while the circle indicate that the correlation was opposite to the proposed hypothesis.

## **D. Discussion**

### **D.1. Validation**

La principale difficulté pour valider les résultats acoustiques réside dans la disponibilité d'observations indépendantes. L'échantillonage au filet est la manière la plus commune pour échantillonner des organismes marins pélagiques. Malheureusement, le degré de confiance que l'on peut associer à ce type d'estimation est plus ou moins élevé selon le type de filet et l'espèce cible. En dépit de ces limitations, nos résultats démontrent que la discrimination entre les différents types d'organismes est correcte dans la mesure où les patrons de la distribution verticale et horizontale de la biomasse acoustique en poisson, munida, et zooplancton fluid-like sont en accord avec les observations indépendantes obtenues par échantillonnage au filet. Même si une méthode acoustique bi-fréquence a déjà été utilisée pour séparer l'anchois et le munida (Bertrand et al., 2008a), notre étude est la première à offrir une méthode acoustique détaillée et validée pour la séparation de ces deux organismes dans le SCH. En plus des résultats de l'échantillonnage au chalut, l'examen visuel des échogrammes a confirmé la robustesse de la discrimination.

Nos résultats montrent que les patrons verticaux et horizontaux de la distribution acoustique du macrozooplancton fluid-like sont très semblables à ceux des euphausiacés, le groupe dominant du macrozooplancton dans le système (Ayón et al., 2008; Espinoza et Bertrand, 2008). En dépit de cette similarité, il y a un ordre de magnitude de différence entre les biovolumes estimés par acoustique et par Multinet. Un tel écart peut être lié au fait bien connu que le macrozooplancton évite l'échantillonnage au filet (Fleminger et Clutter, 1965; Brinton 1967; Debby et al., 2004). Bien que la catégorie fluid-like comprenne une grande variété de crustacés du macrozooplancton, les euphausiacés sont le groupe dont les profils horizontaux et verticaux de biovolume sont les plus proches de ceux obtenus par acoustique.

#### *D.1.1. Différence jour-nuit*

La grande différence jour-nuit dans la biomasse en macrozooplancton épipélagique estimée par acoustique illustre le fait que la majeure partie de la biomasse épipélagique nocturne est composée de macrozooplancton migrant verticalement (migration nyctémérale avec distribution dans la ZMO durant la journée et dans la couche épipélagique durant la nuit). Par définition, les organismes migrateurs n'ont pas été inclus dans la biomasse épipélagique pendant la journée. L'estimation de la biomasse de ces organismes n'a pas été possible de jour, car ils migrent à une strate plus profonde que la portée réelle (150 m) du sondeur utilisé dans cette étude (Simrad EK500 à 120 kHz). Cependant nous avons pu estimer la biomasse en macrozooplancton migrant en soustrayant l'estimation diurne à l'estimation nocturne qui comprend à la fois les communautés migrantes et non-migrantes. Nous avons obtenu qu'environ 77% du zooplancton observé au cours de la nuit réalise des migrations verticales. Ce résultat est semblable aux estimations faites par Escribano et al. (2009) dans le Sud du SCH (75%) et Postel et al. (2007) dans le Nord du système du Benguela (71%). Dans cette étude, nous avons constaté que la taille du macrozooplancton augmente d'environ 5% au cours de la nuit, ce qui suggère que le zooplancton migrateur qui a une biomasse beaucoup plus élevée que la communauté des non-migrateurs, est composé par de plus grands individus.

#### *D.1.2. Distribution côte-large du zooplancton*

Dans cette étude, le macrozooplancton migrateur, composé d'organismes relativement grands, était plus abondants sur la pente et dans la région océanique. La limite entre faible et forte biomasse semble correspondre au bord du talus continental. Dans le NSCH il ya a un manque de connaissances sur la distribution euphausiacés (Ayón et al., 2008b), les informations en provenance d'autres régions d'upwelling ont cependant montré que la distribution des euphausiacés est fortement affectée par le bord de la plateforme continentale (Barange et al., 1992; Swartzman et al., 2005). Dans le système du Courant de Californie, les agrégations d'euphausiacés sont plus fréquemment observées le long du bord de la plateforme et sur la pente du talus (Swartzman et al., 2005). Dans le système de Benguela, le bord du talus semble séparer efficacement les populations côtières et océaniques d'euphausiacés qui complètent leurs cycles de vie au sein de chaque région (Barange et al., 1992). Dans le système du Courant des Canaries, l'abondance des euphausiacés est également plus importante au delà du plateau continental, dans la zone du talus (Blackburn, 1979). Ainsi, le patron côte-large de la biomasse en macrozooplancton observé dans cette étude, et les autres études ayant décrit ce mode de distribution des euphausiacés (Vinogradov et Shushkina, 1978), suggèrent que le bord du plateau pourrait également jouer un rôle important pour l'accumulation de macrozooplancton au niveau de la pente et des zones océaniques adjacentes dans le SCH.

#### *D.1.3. Identification des taxons du zooplancton ayant un patron de distribution spatial similaire à celui du macrozooplancton acoustique*

En dépit du manque de confiance dans les données de capture au filet à plancton pour identifier les taxons responsables de la forte biomasse observée par acoustique durant la nuit (les données de Multinet n'étaient disponibles que pendant les campagnes Cardumenes «2004» et «Filamentos 2008» et les données obtenues en utilisant le filet Hensen ne sont disponibles que sous forme de biovolume global sans détermination des groupes taxonomiques), seuls quelques organismes du zooplancton peuvent parvenir à de tels niveaux de biomasse et/ou s'ajuster aux patrons spatiaux décrits dans ce travail: la munida, les salpes, les copépodes et les euphausiacés. Toutefois, lorsque l'on prend en compte le comportement et l'habitat des organismes et qu'on le compare avec les variabilités spatiotemporelles observées dans le cas du macrozooplancton acoustique, il est possible de conclure que les euphausiacés sont probablement le groupe dominant le signal acoustique. D'autres organismes fluid-like, en particulier *Eucalanus spp.*, doivent cependant contribuer de façon non négligeable à la biomasse estimée par acoustique. La présence d'une forte biomasse d'euphausiacés est indirectement confirmée par le régime alimentaire de l'anchois, la sardine et du chinchard (Konchina, 1981, 1991; Espinoza et Bertrand, 2008; Espinoza et al., 2009).

### ***D.2. La biomasse en macrozooplancton dans le NSCH: supérieure aux prévisions***

Cette étude fournit la première estimation directe à haute résolution et à grande échelle de la biomasse en macrozooplancton dans le NSCH (et à notre connaissance dans un grand système d'upwelling). La biomasse totale estimée ( $\sim 112 \text{ gm}^{-2}$ ) est 5 fois supérieure aux estimations réalisées par échantillonnage au filet à plancton ( $\sim 21 \text{ gm}^{-2}$ ). Cette grande différence n'est pas surprenante puisque le macrozooplancton évite généralement les filets (Fleminger et Clutter, 1965; Debby et al., 2004). L'utilisation des

paramètres acoustiques de densité et de contraste de vitesse du son d'*Euphausia pacifica* au lieu d'*E. mucronata* a pu introduire un biais puisque le biovolume estimé est très sensible à de petites différences dans les paramètres de contraste (Stanton et Chu, 2000). Par conséquent, à ce stade il reste un doute quant à la précision de l'évaluation de biomasse par acoustique: notre estimation de la biomasse en macrozooplancton du NSCH est-elle réaliste?

Pour répondre à cette question, il faudrait idéalement pouvoir comparer nos résultats à des estimations acoustiques validées dans ce système ou dans un système comparable. Cependant, l'acoustique a été rarement utilisée dans les systèmes d'upwelling de bord est (EBUS) pour estimer la biomasse en zooplancton (Ressler et al., 2005; Postel et al., 2007) et seules des estimations obtenues par échantillonnage au filet et modèle trophique sont disponibles pour comparer nos résultats (Fig. D1).

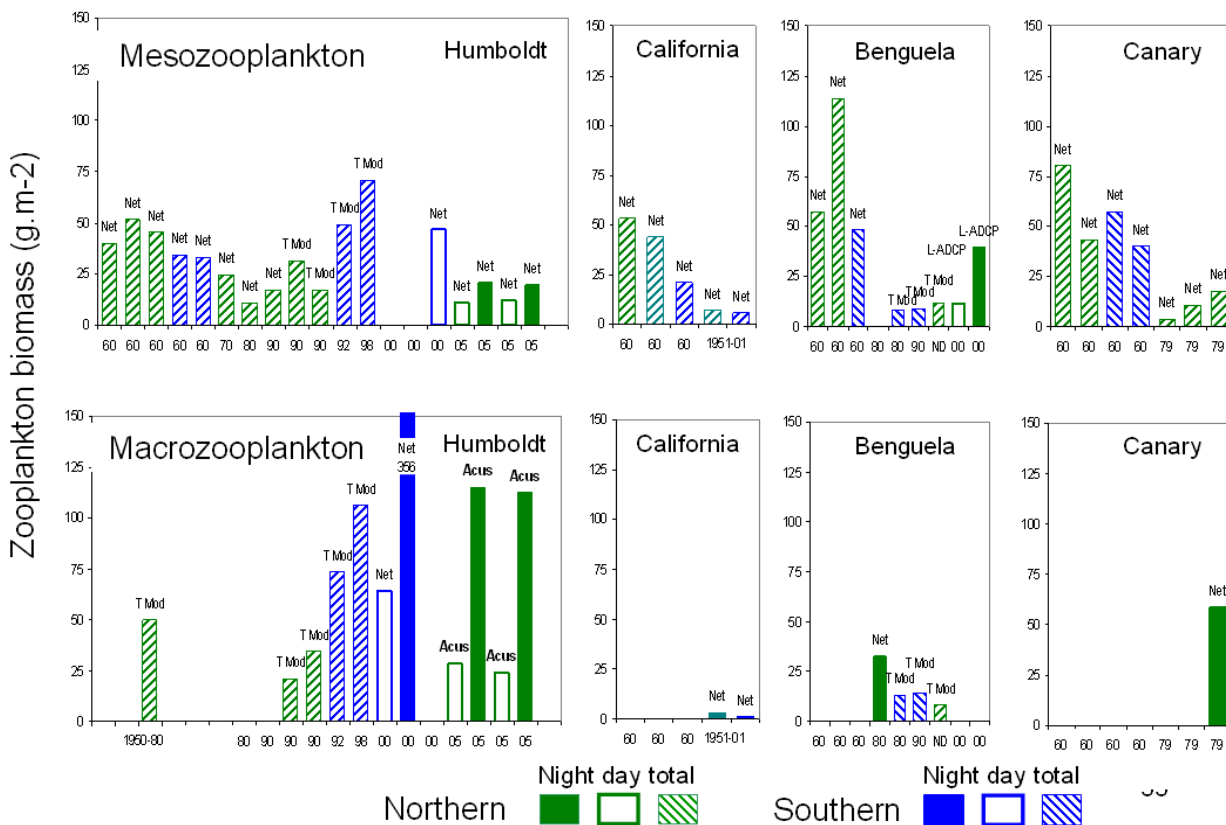


Figure D1 Synthesis of biomass estimations (in  $\text{g.m}^{-2}$ ) of meso- and macrozooplankton in main eastern boundary upwelling systems from net (Net), trophic models (T Mod) acoustic (Acus) and L-ADCP calibrated by multinet (L-ADCP)

#### D.2.1. Comparaison avec les données in situ (filet et acoustique)

Si l'on compare nos résultats avec toutes les estimations de biomasse en zooplancton provenant d'autres EBUS, nos estimations sont parmi les plus élevées et généralement plus de deux fois plus élevées que les autres (Fig. D1). Des estimations de biomasse comparables ou supérieures ont été cependant été reportées dans certains échantillons prélevés dans le Sud du SCH (Escribano et al., 2009: 4 échantillons prélevés au filet dans une structure de mésoéchelle), le Benguela Nord durant les années 1960 (Cushing

et al., 1971), le Canada (Cotté et Simard, 2005) et l'Antarctique. Le seul travail qui compare la biomasse en zooplancton (estimée à partir d'échantillons collectés au filet) entre systèmes d'upwelling est une synthèse réalisée par Cushing (1971). Selon Cushing (1971) la biomasse en zooplancton était d'environ  $40\text{-}50 \text{ gm}^{-2}$  dans tous les EBUS. Notre estimation se range parmi les valeurs les plus élevées proposées par Cushing (1971) mais est plus de deux fois supérieure dans la plupart des autres cas.

#### *D.2.2. Comparaison avec les modèles trophiques et ce que nous savons de trophodynamique*

L'abondance en macrozooplancton et/ou son taux de renouvellement (turn-over) peut être indirectement déterminé à l'aide de modèles trophiques. Jusqu'à présent, les modèles trophiques construits dans le NSCH ont considéré que les anchois se nourrissaient principalement de phytoplancton ou dans une même proportion de phytoplancton et de zooplancton (ex. Jarre-Teichmann, 1992; Tam et al., 2008). Comme nous savons maintenant que ce n'est pas le cas et que ces poissons tirent la majorité de leur énergie du macrozooplancton (Espinoza et Bertrand, 2008; Espinoza et al., 2009), on peut supposer que ces modèles trophiques sous-estiment fortement la biomasse en macrozooplancton. En effet, si on augmente l'apport en macrozooplancton dans le régime alimentaire de l'anchois il est nécessaire d'augmenter la biomasse en macrozooplancton pour équilibrer le modèle (Guénette et al., 2008). En plus des informations sur le régime alimentaire, un modèle trophique doit être documenté sur la vitesse à laquelle une population de proies produit sa propre biomasse dans un temps donné. En d'autres termes, elle exige de connaître le rapport production/biomasse (P/B) des proies. Pour construire leurs modèles trophiques du NSCH, Tam et al. (2008) et Guénette et al. (2008) ont utilisé un P/B de 20 pour le macrozooplancton (euphausiacés). Toutefois les expérimentations montrent que le rapport P/B d'euphausiacés d'environnements similaires oscille habituellement entre 9 et 15 (Taki, 2006). Ainsi, le rapport P/B, apparemment surestimé, utilisé dans la construction des modèles trophiques du NSCH conduit également à une sous-estimation de la biomasse en macrozooplancton dans ces modèles.

Dans le NSCH la biomasse d'anchois a été estimée à  $83 \text{ gm}^{-2}$  (période 1995-96, Tam et al., 2008), cette biomasse est 27% inférieure à notre estimation de biomasse en macrozooplancton ( $112 \text{ gm}^{-2}$ ). On peut se demander si cette biomasse en proies est suffisante pour nourrir la population d'anchois. Pour apporter une réponse nous avons besoin de déterminer si, lorsque l'on utilise notre estimation de la biomasse du macrozooplancton ( $112 \text{ gm}^{-2}$ ), on obtient un rapport P/B cohérent (de 9 à 15; Taki, 2006) et si cette biomasse permet théoriquement de nourrir les anchois et les autres principaux prédateurs du macrozooplancton. Nous avons obtenu qu'un rapport P/B de  $\sim 10$  permet de produire assez de macrozooplancton pour nourrir l'anchois ( $83 \text{ gm}^{-2}$ ) et d'autres prédateurs ( $\sim 27,6 \text{ gm}^{-2}$ ) tels que la sardine, le maquereau et le chinchar (Tam et al., 2008). Notre estimation de biomasse semble donc être cohérente.

#### *D.3. Effet de la structuration physique sur la distribution du macrozooplancton et des niveaux trophiques supérieurs*

Nos résultats ont montré que la présence d'un filament d'upwelling (Fig. 5.6) était caractérisée par l'advection vers le large d'eaux côtières froides et entraîne une remontée de ZVEEC. Cependant, c'est dans le cœur de ce filament que la biomasse en

macrozooplancton était la plus faible de la région. Ces résultats étaient attendus puisque notre méthode permet de détecter principalement le macrozooplancton et sous-estime fortement le petit zooplancton. Les filaments d'upwelling peuvent significativement étendre la distribution des communautés associées avec les eaux côtières froides vers le large (Keister et al., 2009). L'abondance en petit zooplancton non-migrant verticalement caractéristiques des eaux des côtes froides est donc généralement plus élevée dans un filament qu'à l'extérieur, dans les masses d'eaux plus chaudes (Keister et al., 2009).

Nous avons déjà montré que la biomasse en macrozooplancton était supérieure dans la zone océanique que sur le plateau continental. Toutefois, si l'on regarde les processus de plus près, il apparaît que l'augmentation rapide de la biomasse en macrozooplancton coïncide plus avec la zone frontale qu'avec la position du bord du plateau continental. Le comportement du zooplancton associé à la circulation frontale conduit à un fort gradient perpendiculaire au front dans la composition spécifique, la distribution verticale, et la biomasse du zooplancton (Olson et al., 1994). Nous suggérons donc que le comportement du zooplancton associé à la circulation frontale pourrait être responsable de l'accumulation macrozooplancton observée dans le bord océanique des fronts.

#### *D.3.1. Impact des structures physiques sur le macrozooplancton*

Nos résultats montrent que globalement l'impact des structures de méso et submeso échelles sur la répartition de la biomasse de macrozooplancton s'accorde avec les modèles théoriques. En effet, les zones où  $Z_{VEEC}$  est inférieure/supérieure à la moyenne locale, qui sont censées correspondre à des structures convergentes/divergentes, ont été caractérisées par une augmentation/diminution de la biomasse en macrozooplancton. Toutefois, aucun impact significatif n'a été observé lorsque l'on s'intéresse à la densité en macrozooplancton au lieu de sa biomasse. Dans cette étude, la plupart des corrélations entre la biomasse en macrozooplancton et  $Z_{VEEC}$  étaient faibles et on n'a pas observé d'effet significatif des structures physiques sur la distribution de la densité du macrozooplancton. Ces résultats reflètent la complexité des facteurs qui déterminent la distribution du zooplancton. Nous suggérons cependant que la densité en zooplancton répond à la physique d'une manière différente comparé à la biomasse. En outre, nos résultats fournissent une preuve d'une structuration spatiale bottom-up à méso et submeso échelles de la biomasse en macrozooplancton conformément à notre hypothèse.

#### *D.3.2. Forçage biologique: poissons vs. macrozooplancton*

Nos résultats indiquent qu'il y a plus de probabilités de trouver du poisson là où la biomasse/densité en macrozooplancton est élevée. Lorsqu'à la fois les prédateurs et les proies sont présents, nos résultats indiquent qu'une plus grande biomasse/densité de macrozooplancton attire une plus grande abondance en poissons. Cette tendance a été observée de nuit à mésoéchelle et de jour et de nuit à submesoéchelle. Nos résultats confirment ceux de Bertrand et al. (2008a), qui ont observé que les 'clusters' de poissons s'agréguaient dans les agrégations de macrozooplancton pendant la nuit. A ce moment du cycle nyctheméral, la majorité du macrozooplancton est distribué en surface (Chapitre 4) et est disponibles aux prédateurs. De nuit, les bancs de poissons se dispersent (Bertrand et al., 2008a), ce qui améliore la capacité d'alimentation individuelle (Fréon et al., 1996; Cardinale et al., 2003).

Dans la plupart des transects et indépendamment de l'échelle, nous avons également constaté que lorsque la biomasse en poissons était significativement corrélée à la biomasse en macrozooplancton, elle était également corrélée à la densité en macrozooplancton. La répartition des poissons semble donc structurée par des agrégations de macrozooplancton qui remplissent deux caractéristiques: haute densité et forte biomasse. D'autre part, nous avons montré un effet des structures physiques sur la répartition spatiale de la biomasse en macrozooplancton, mais pas sur la densité en macrozooplancton. Bien que nous ayons des preuves que la physique structure la distribution du zooplancton en formant des agrégations plus ou moins abondantes, d'autres études sont nécessaires pour comprendre les processus physiques qui font que certaines agrégations sont plus denses, et donc apparemment plus attrayantes pour les poissons, que d'autres. En outre, nos résultats sont en accord avec le concept classique de la plus grande abondance de poissons dans les zones riches en proies (Bertrand et al., 2002). Indépendamment de la façon dont le macrozooplancton était structuré, nos résultats indiquent que la biomasse/densité macrozooplancton exerce une structuration bottom-up sur ses prédateurs à meso et submésos-échelles.

## *General introduction*

In ecosystem-based fishery management (EBFM, Pikitch et al., 2004), target species must be managed within the understanding of the overall state of the system. There is thus an urgent need for broadening our view of exploited marine ecosystems, and including knowledge of non-exploited components of the marine ecosystems (Link, 2002; Pikitch et al., 2004; Smith et al., 2007) in the fishery management process. Unfortunately, up to now, data collection efforts have been much more driven by the commercial value of the species than by their importance in ecosystem functioning. As a consequence, while commercial species are usually quite well documented for consistent time series, there is still a dramatic lack of information on many ecosystem compartments; and it is particularly critical in the case of zooplankton (Carlotti and Poggiale, 2010).

Zooplankton consume primary producers, microzooplankton and detritus, producing dissolved and particulate organic matter, thereby actively contributing to the remineralisation of nutrients. Furthermore, zooplankton contributes to the export of matter to the ocean's interior with fast-sinking faecal pellets, and via vertical migration (Carlotti and Poggiale, 2010). Thus, zooplankton play a critical role in structuring higher and lower trophic levels, influencing the population dynamics of exploited species, and modifying the flux of organic materials to the deep ocean (Bertrand et al., 2008b; González et al., 2009; Carlotti and Poggiale, 2010). Information on zooplankton is also crucial for calibrating mathematical models. Zooplankton is generally the closure term of biogeochemical models and the opening term of trophic models. In end-to-end models, zooplankton is the interface between the primary producers (i.e. phytoplankton), which influence planetary biogeochemical cycling through carbon fixation and CO<sub>2</sub> sequestration, and the different fish communities (Carlotti and Poggiale, 2010; John et al., 2010; Mitra and Davis, 2010).

Although valuable information on zooplankton time series exists, such time series are mostly concerning the mesozooplankton (Mackas and Beaugrand, 2009), excluding other important groups such as macrozooplankton or gelatinous zooplankton, as they are difficult to capture quantitatively with plankton nets (Mackas and Beaugrand, 2009). Since zooplankton abundance and distribution are mainly assessed on the basis of net sampling and this method provides data which is discrete in space and time, zooplankton data is, in general, insufficient in quantity and quality for a mechanistic understanding of ecosystem dynamics (Mitra and Davis, 2010).

The lack of high-resolution zooplankton data and the paucity of information about some zooplankton groups (e.g. macrozooplankton) particularly hampers research in the most productive region in the world in terms of fish (Chavez et al., 2008), the Northern Humboldt Current system (NHCS), off Peru. Although the NHCS represents less than 0.1% of the world ocean surface, it produces more fish per unit area than any other region in the world; presently about 10% of the global fish catch (Chavez et al., 2008). This vast fish catch is primarily composed by a small pelagic clupeid, the Peruvian anchovy or anchoveta (*Engraulis ringens*); however, the sardine (*Sardinops sagax*) has made up an important share during certain

periods (Alheit and Niquen, 2004). While the primary production of the NHCS is not substantially higher than that of other eastern boundary upwelling systems (Carr, 2002; Patti et al., 2008), it probably supports a high enough macrozooplankton production (mainly euphausiids and large copepods) to feed the anchovy and sardine populations that forage on it (Espinoza and Bertrand, 2008; Espinoza et al., 2009). In the HCS, macrozooplankton (particularly euphausiids) consume primary production (Antezana, 2010) and are capable of exerting a local top-down pressure on primary producer biomass (González et al., 2009). They also play a major biogeochemical role in the system by promoting carbon flux into the subsurface oxygen minimum zone (OMZ) due to their vertical migration (Escribano et al., 2009) and their production of faecal pellets (González et al., 2009). Unfortunately, as in other systems, macrozooplankton have been inadequately studied in the NHCS (Ayón et al., 2008a), in part because of the difficulty to capture them with traditional plankton nets. The facts stated above highlight the urgent need to increase our knowledge of the zooplankton compartment, particularly of macrozooplankton, if we are to move toward an EBFM.

Fisheries acoustics has been recognized as a key tool for EBFM, because it allows a simultaneous collection of qualitative and quantitative data on various communities of an ecosystem, from zooplankton to large predators (Bertrand et al., 2003). Although information on zooplankton is available (albeit not processed) from routine acoustic surveys performed by laboratories all over the world, this information is rarely used to assess the abundance of organisms other than fish. However, in low-diversity Polar regions, in particular the Antarctic, acoustics is the main sampling tool for estimating the biomass of macrozooplankton (Watkins and Brierley, 2002). In these regions, the acoustic records from two frequencies, 38 kHz and 120 kHz, provide the basis for distinguishing macrozooplankton from other organisms and for estimating its biomass (Watkins and Brierley, 2002). These two frequencies also form most of the present-day and historical acoustic databases of the marine laboratories over the world. It is the case for the Instituto del Mar del Perú (IMARPE), which is in charge of the monitoring of the NHCS and of the associated scientific research. There is thus an opportunity to exploit this database to obtain quantitative and qualitative data on various organism communities and their habitats, particularly on the poorly known macrozooplankton compartment.

In this context, the objective of this study is to use acoustics to investigate the multiscale dynamics of the spatiotemporal distribution of the macrozooplankton biomass off Peru in relation to the physical environment and their predators. To achieve this objective, the study is organised into five chapters:

In Chapter 1, we provide a broad outline of the NHCS in order to facilitate the interpretation of the main findings of this study. We first describe the physical oceanography and the production of the system, with particular emphasis on the secondary production. We then describe how the system properties and its production are strongly affected by an intense multi-timescale physical variability. Finally, we briefly describe the fisheries and fisheries management, with particular emphasis on anchovy.

In Chapter 2, we propose an acoustic method using the 38 and 120 kHz frequencies for discriminating between crustacean macrozooplankton, the pelagic squat lobster *munida* (*Pleuroncodes monodon*), fish and other organisms, and quantifying their respective biomass. For this purpose, we first describe the acoustic properties of marine organisms, highlighting the difference between fish and zooplankton. We then exploit these distinct organisms' acoustic properties to separate them and estimate their biomass. Finally, we propose a first validation of the method by applying it to a set of acoustic records for which independent net sampling estimates of the organisms' abundance were also available.

In Chapter 3, using routine underwater acoustic observations of the vertical distribution of marine organisms, we propose a new method that allows for a precise determination of the upper limit of the OMZ. This original sample technique provides high-resolution information on the depth of the upper OMZ, allowing the documentation of mesoscale and submesoscale features (e.g., eddies and filaments) that structure the upper ocean and the marine ecosystems. We also use this information to estimate the habitable volume for anchovy. Our approach is a novel way of studying the impact of physical processes on marine life and extracting valid information about the pelagic habitat and its spatial structure, a crucial aspect of EBFM in the current context of climate change. Indeed, the OMZ are expanding in the World Ocean as a result of climate change and direct anthropogenic influence. OMZ expansion greatly affects biogeochemical processes and marine life, especially by increasing greenhouse gas production and constraining the vertical habitat of most marine organisms.

In Chapter 4, based on the recent finding on anchovy and sardine feeding ecology, we hypothesise that the macrozooplankton biomass in the NHCS must be substantially higher than previously reported. To test for that, we apply the acoustic method detailed in chapters 2 and 3 on two surveys performed by IMARPE in 2005 along the Peruvian coast and provide the first acoustic estimate of macrozooplankton biomass in the NHCS. The results, that seem to validate our hypothesis, are compared with estimates from the same and other upwelling and highly productive systems and discussed with regard to the unique properties of the NHCS.

Finally, in Chapter 5 we test the impact of meso- and submesoscale physical features on macrozooplankton distribution, and infer the further impact these structures have on the fish distribution by examining the relationship between macrozooplankton and fish. To do this, we take advantage of the high-resolution physical and biological data extracted from acoustic data from the survey performed by IMARPE in austral summer 2005, using the methods described in Chapters 2 and 3. We first focus on selected large mesoscale structures. Then, at both meso- and submeso scales, we examine the relationships physics-macrozooplankton and macrozooplankton-fish.



## *Chapter I*

### *Insights on the Humboldt Current system*

#### **1.1 Introduction**

Upwelling regions, in particular the Eastern Boundary Upwelling systems (EBUS), are among the most productive marine ecosystems in the world and provide one fifth of the global marine fish catch (Fréon et al., 2009). While all EBUS apparently share some similarities in rates of primary production (Hutching, 1992; Carr, 2002) and secondary production (Cushing, 1971; Huggett et al., 2009), the Northern Humboldt Current system (NHCS) stands out as being very different from the other EBUS in terms of fish yields (Fig. 1.2) (Hutching, 1992; Chavez et al., 2008). This system has other particularities; some of which have been suggested as being partially responsible for the system's high fish production (Bakun and Weeks, 2008; Chavez et al., 2008): (i) it is the closest system to the equator (Fig. 1.1), while being unusually cool for an ocean at these latitudes, (ii) it has the shallowest and most intense Oxygen Minimum Zone (OMZ), (iii) it has the most stable and least intense mesoscale physical variability compared with other EBUS, and (iv) it is intimately linked to equatorial Pacific dynamics and is subject to large interannual (e.g. El Niño Southern Oscillation, ENSO) and multidecadal fluctuations.

The aim of this chapter is to briefly describe the most important physical and biological features of the HCS, particularly of the NHCS, in order to facilitate the interpretation of this study.

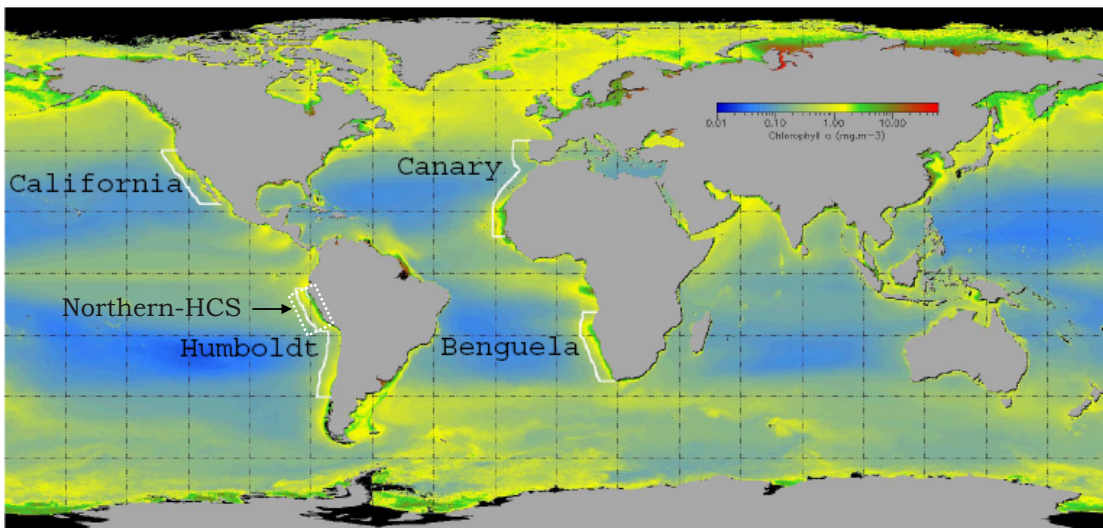


*Figure 1.1 Chlorophyll-a concentration from SeaWiFS for the 1998-2007 period and EBUS location arbitrarily delimited by the 200 nautical miles offshore limit and latitudinal extensions including seasonal upwelling zone (courtesy of H. Demarcq, IRD, France). Source: Fréon et al. (2009).*

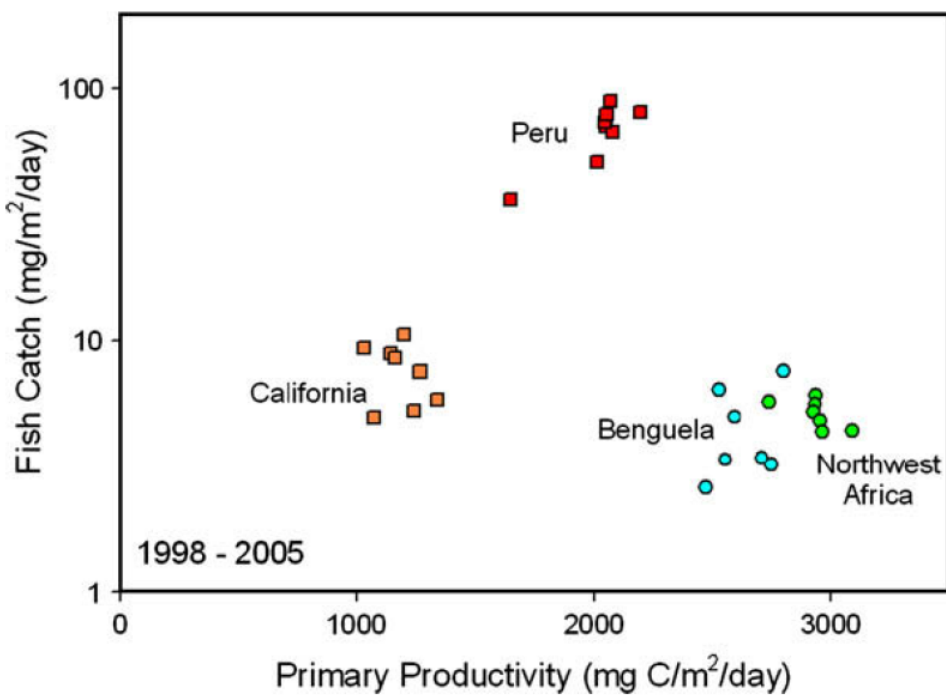
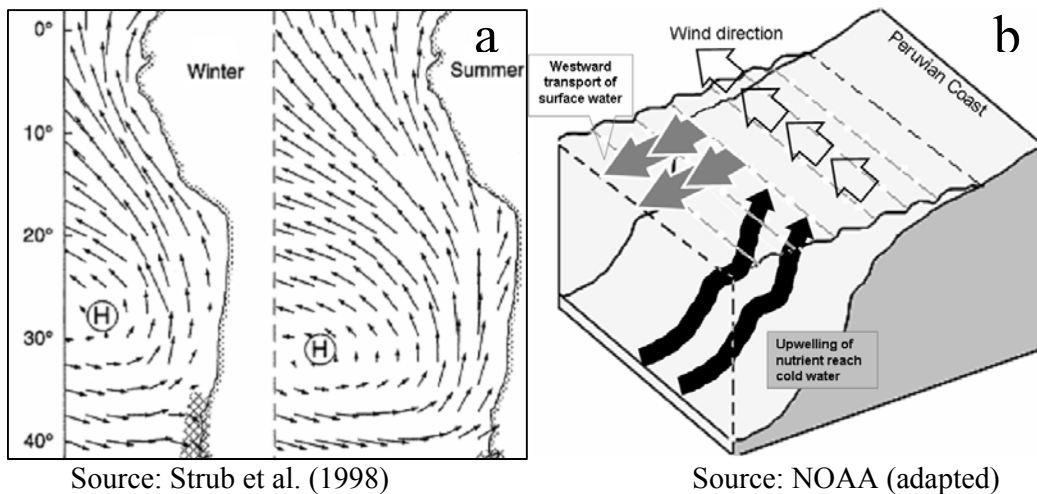


Figure 1.2 Fish catch versus primary productivity for the four main eastern boundary coastal upwelling ecosystems for the years 1998-2005. Source: Chavez et al. (2008).

## 1.2 Physical oceanography

### 1.2.1 Atmospheric forcing

The South-Eastern Pacific subtropical anticyclone is the main atmospheric system triggering equatorward winds along the coast of Chile and Peru (Strub et al., 1998). Off Peru, those equatorward winds blow all year round, with the seasonal maximum occurring in austral autumn and winter (Strub et al., 1998) (Fig. 1.3a). The combined effect of wind force and earth rotation (Coriolis force) creates a natural pump system, the Ekman transport, advecting coastal surface waters offshore; those are replaced close to coast by colder nutrient rich waters welling up from the bottom (Bakun, 1996) (Fig. 1.3b).



*Figure 1.3 (a) Climatological winter and summer winds triggered by the South-Eastern Pacific Subtropical Anticyclone. (b) Upwelling scheme along the Peruvian coast.*

### 1.2.2 Oceanographic context

#### 1.2.2.1 Oceanic circulation

The oceanic circulation of the HCS (Fig.1.4) is initiated by the atmosphere physical forcing of the subtropical anticyclone of the south eastern Pacific (Strub et al., 1998). At around 38/39°S and 75/76°W, the southern branch of the subtropical gyre, also known as the West Wind Drift (WWD) or South Pacific Current, reaches the South-American coast. At this point, this branch is deflected northward, forming the relatively wide (~1500 km), deep (700-1000 m) and weak ( $5-10 \text{ cm s}^{-1}$ ) Chile-Peru Current (CPC). The CPC flows northward from central Chile and feeds the northwestward South Equatorial Current (SEC) (Strub et al., 1998; Chaigneau and Pizarro, 2005a; Fuenzalida et al., 2008). At around 23°S the CPC also creates a more coastal branch, heading toward the coast of Peru, the Peruvian Coastal Current (PCC). The PCC is a relatively thin (100 km), shallow (0-100 m) and strong ( $20 \text{ cm s}^{-1}$ ) current that flows northward and separates the Cold Coastal Water (CCW) of the upwelling cells from the relatively warm Subtropical Surface Water (SSW) of the offshore ocean (Strub et al., 1998). At the subsurface and centered at 100-300 m depth, the Peru-Chile Undercurrent (PCU) is the main current of the HCS. The PCU flows poleward along the shelf break and transports salty and poorly oxygenated water from the Equatorial Subsurface Water (ESSW). This water mass, in turn, is thought to be the main origin of both the coastal upwelling off Peru (e.g. Huyer et al., 1987) and the oxygen minimum zone (OMZ) (Wyrtki, 1963).

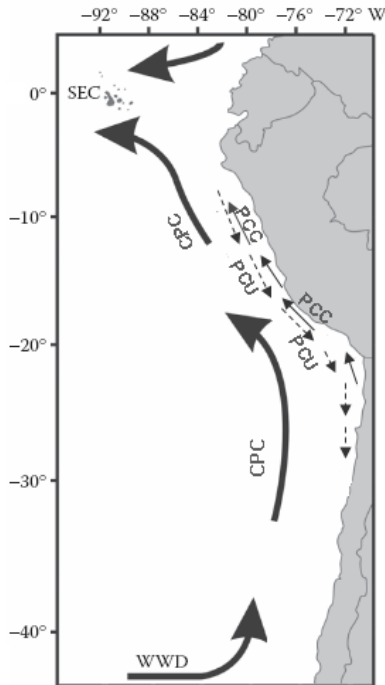


*Figure 1.4 Large oceanic circulation scheme with focus on the main surface and subsurface currents off Peru: the Chile-Peru Current (CPC), the Peruvian Coastal Current (PCC), the South Equatorial Current (SEC), the Peru-Chile Undercurrent (PCU) and the West Wind Drift (WWD). Adapted from Thiel et al. (2007).*

### 1.2.2.2 Water masses

Because of the constant upwelling of subsurface cold water, a wide region off the Peruvian coast is dominated by relatively cold, highly productive water mass, the Cold Coastal Water (CCW). The oligotrophic Subtropical Surface Water (SSW) is located offshore the CCW. The Surface Tropical Water (STW) is found north of the equator and characterized by higher temperatures and lower salinities than the other water masses present off Peru. The Surface Equatorial Water (SEW) is found between the CCW and the STW (Fig. 1.5). The main characteristics of the mater masses can be found in Table 1.1.

*Table 1.1- Main characteristics of the water masses presents in the Humboldt Current System.*

Water mass	Abbreviation	Main characteristics
Cold coastal water	CCW	Salinity: 34.80–35.05; superficial temperature: 15–17°C in winter and 15–19°C in summer. Influenced by upwelling, very productive
Surface subtropical water	SSW	Salinity >35.10; superficial temperature: 17–25°C in winter and 20–25°C in summer. Oceanic characteristics, oligotrophic water mass
Surface equatorial water	SEW	Salinity: 34.00–34.80; superficial temperature: 20–26°C in winter and 21–26°C in summer. Mesotrophic water mass
Surface tropical water	STW	Salinity <34.00; superficial temperature: >23°C in winter and >26°C in summer.

Source: Bertrand et al. (2004b)

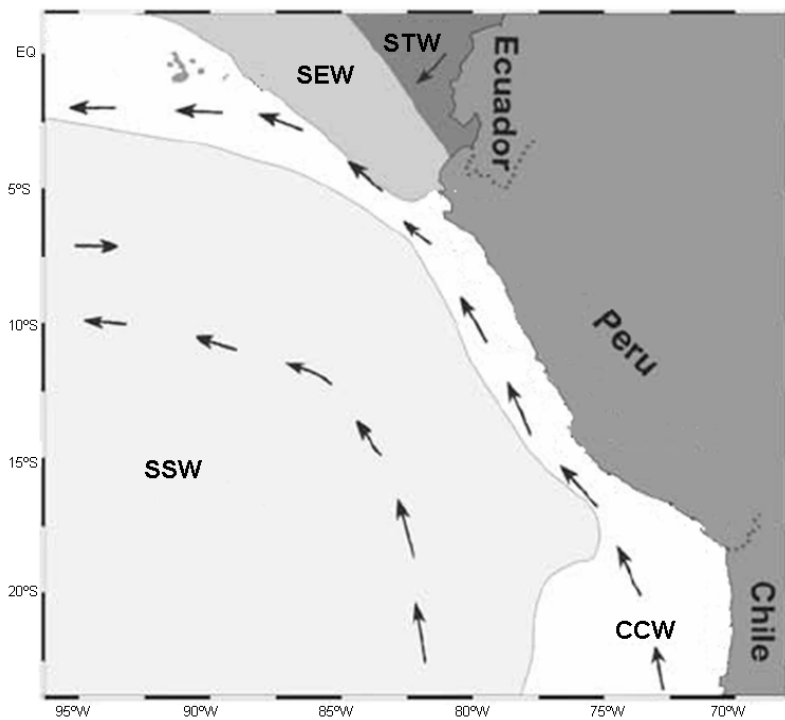


*Figure 1.5 Distribution of the main water masses in the HCS: Cold coastal water (CCW), Surface subtropical water (SSW), Surface equatorial water (SEW), Surface tropical water (STW). Source: Ayón et al. (2008a).*

### 1.2.2.3 The oxygen minimum zone

A prominent feature of a coastal upwelling system is the presence of a permanent oxygen minimum zone (OMZ, Fig. 1.6), resulting from the sinking and decay of surface-derived high primary production and poor ventilation. In the HCS, the OMZ is thickest (>600 m) off Peru between 5 and 13°S and to about 1 000 km offshore (Fuenzalida et al., 2009). Because of the coastal upwelling, which lifts the coastal hypoxic layer closer to the sea surface (Fuenzalida et al., 2009), the OMZ upper boundary is shallowest at the coast (25-50 m) off Peru and northern Chile (e.g., Morales et al., 1996; Strub et al., 1998). The shallow coastal upper boundary of the OMZ strongly influences the distribution of some organisms, as it concentrates living resources near the surface, or defines the limits of refuge for avoiding predation (Chavez et al., 2008). This is because the OMZ forms a sharp barrier for living organisms intolerant to hypoxia (e.g., anchovy) but a refuge for those physiologically adapted to low oxygen conditions (e.g., euphausiids).

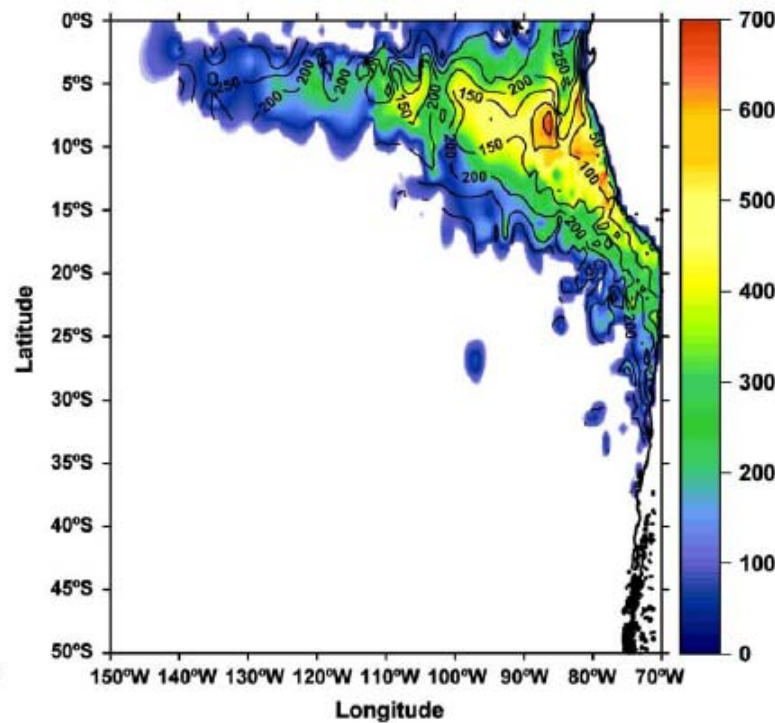


*Figure 1.6 Oxygen minimum zone (OMZ), thickness is colour-coded according to the colour bar on the right-hand side of the figure; units are in m. The upper boundary of the OMZ is shown in black contour lines with 50 m intervals. Source: Fuenzalida et al. (2009).*

#### 1.2.2.4 Mesoscale physical activity

Mesoscale physical features (e.g., filaments, eddies) can increase productivity (Siegel et al., 1999), structure zooplankton patterns of distribution (Goldthwait and Steinberg 2008) and, through a succession of predator-prey relationships, structure higher trophic levels (Bertrand et al., 2008b). In the HCS, most of the intense mesoscale activity is generated near the coast (Chaigneau et al., 2008). This is mainly due to interaction of the Peru-Chile Current system with the coastline, the presence of the strong upwelling front, and/or the high temporal variability of the coastal flow (Pizarro et al., 2002). According to Chaigneau et al. (2008), during the first 50 days, eddies formed near the coast are propagated offshore, remaining close to their latitude of birth. After this period, however, cyclonic eddies continue westward, whereas anticyclonic eddies tend to move northwestward. Although the number of coastal eddies and their sizes do not vary significantly according to season, they seem to be more intense during autumn (Chaigneau et al., 2008). These authors suggested that the intense activity during autumn may be related to the strength of the thermal front separating the cold upwelled coastal water from warmer offshore water.

In the NHCS, mesoscale physical processes are more stable and less intense than in other EBUS (Chaigneau et al., 2009), which may be important for increasing the transfer efficiency of primary production through the food web to fish (Chavez and Messie, 2009). Also submesoscale physical processes can enhance productivity (Klein and Lapeyre, 2009) and structure zooplankton and higher trophic levels (Bertrand et al., 2008a).

## 1.3 Production of the NHCS

### 1.3.1 Primary production

Because of constant nutrient fuelling, upwelling areas are characterized by a high primary production. When the upwelled nutrient-rich water reaches the surface, sunlight triggers the phytoplankton production. Thus, high primary production is a main characteristic of coastal upwelling. The primary production of the EBUS represents 2% of the global marine production, although their ocean area only account for 0.3% (Carr, 2002). The primary production of the HCS is comparable to the one from the Benguela and Canary systems, but apparently higher than the primary production of the California system (Chavez and Messié, 2009).

- **The phytoplankton cycle**

In the core of an active upwelling, nutrient-rich deep waters are brought to the surface at a rate exceeding phytoplankton growth. Phytoplankton increase offshore or downstream of the upwelling core and biological uptake eventually consumes the surface nutrients (Chavez et al., 2002).

According to Mac Isaac et al. (1985), the phytoplankton cycle can be schematised as follows: (i) at the core of the upwelling, phytoplankton grow and take up nutrients at rates considerably lower than their inherent maximal rates; (ii) as the water progresses outward it is stabilised by solar heating, and phytoplankton begin to adapt to both high nutrient concentrations and near-surface light intensities, increasing the rate of their physiological processes (nutrient uptake and photosynthesis, as well as synthesis of enzymes and macromolecules); (iii) the internal biochemical changes of the phytoplankton cells lead to an increased growth rate; nutrient concentrations are rapidly reduced by fast-growing ‘shifted-up’ phytoplankton and there is a rapid increase in biomass; the processes are all taking place at maximal rates and (iv) nutrient depletion occurs, in particular iron limitation (Hutching et al., 2002); the phytoplankton cells respond by undergoing ‘shift-down’ through a sequence of rate decreases of nutrient uptake, photosynthesis, and macromolecule synthesis. For Mac Isaac et al. (1985), the time and space range where this entire sequence occurs is relatively small; they found that in an upwelling plume off Peru (15°S), the cycle from initial upwelling to ‘shift-down’ was completed in 8 to 10 days within 30 to 60 km off the coast.

Phytoplankton species composition also changes during the primary production cycle; from small diatoms with a high reproduction rate (e.g., *Skeletonema costatum*, *Chaetoceros debilis*) to larger diatoms species (e.g. *Thalassionema nitzchioides* *Proboscia alata*) (Sanchez, 2000). This change in species composition is also influenced by the water masses. Thus, while diatoms dominate phytoplankton communities within the CCW, the dominant species in the STW is dinoflagellates (Sanchez, 2000).

### ***1.3.2 Secondary production, zooplankton***

As a consequence of the high primary production of the upwelling areas which fuel phytoplankton predators, particularly zooplankton, high secondary production is also a common attribute of upwelling areas. Among upwelling areas, the EBUS apparently show the greatest secondary production (Cushing, 1971). According to Huggett et al. (2009) mesozooplankton biomass is - on average - of the same order of magnitude in all four EBUS. It has to be noted, however, that methodological differences (e.g. in sample collection and analysis), effects of time (diel, event-scale, seasonal, annual and decadal variability and sampling frequency) and space (ranging from sampling at a single location to regional and basin-scale measurements) may have affected the comparison of zooplankton biomass performed by Cushing (1971) and Huggett et al. (2009).

Regardless of how the secondary production of the HCS ranks compared to the production from other EBUS, this system seems to have particular conditions that favour zooplankton production. According to Bakun and Weeks (2008) the low latitude situation of the NHCS permits a strong upwelling-based nutrient enrichment with low wind-induced turbulence generation. Additionally, the residence times (time within the Ekman layer) within this favourable near-coastal habitat dramatically increases at near equatorial latitude (Bakun and Weeks, 2008). While in other EBUS the zooplankton feeding efficiency and residence time are negatively affected by the intense turbulence and advection resulting from the intense upwelling condition, zooplankton from the NHCS may benefit from a longer residence time and a less turbulent and highly productive (primary production) habitat. According to Patti et al. (2008), the NHCS consistently show lower turbulence values compared to the other upwelling regions. This could make the NHCS an ideal upwelling system in terms of transferring the high primary production to higher producers.

In the NHCS, secondary production is mainly composed by the zooplankton groups copepods, euphausiids and chaetognaths (Gutiérrez et al., 2005; Ayón et al., 2008a). Based on the conversion of anchovy stomach content into carbon units, Espinoza and Bertrand (2008) have recently emphasized that euphausiids (66%) and copepods (28%) are the main prey of anchovy, an indirect confirmation of the high abundance of these groups in the system.

#### ***1.3.2.1 Zooplankton horizontal distribution***

At an oceanic scale, zooplankton biomass generally declines from east to west and is higher in upwelling and shallow thermocline areas (Fernandez-Alamo and Färber-Lorda, 2006). Within the CCW, however, higher biomass is found offshore, probably due to stronger predation nearshore and low zooplankton biomass in freshly upwelled water (Ayón et al., 2008a). The nearshore areas, however, support a highly diverse zooplanktonic community in which meroplanktonic larvae of benthic invertebrates (e.g. decapoda, cirripedia, mollusca and polychaeta) constitute an important fraction (Criales-Hernández et al., 2008). Off Peru, the along-shore distribution of zooplankton biomass seems to be inversely related to the width of the continental shelf, which is narrow in its northern and southern part (Ayón et al., 2008a).

### 1.3.2.2 Zooplankton vertical distribution

Most of marine and freshwater zooplankton species undergo diel vertical migration (Forward, 1988; Lampert, 1989; Heywood, 1996). In the HCS, many zooplankton species perform diel vertical migration with depth amplitudes ranging from 10s m to 100s m (Ayón et al., 2008a; Escribano et al., 2009). The usual pattern is ascent at dusk and descent at dawn, although ‘reversed’ migration patterns have also been described (Ayón et al., 2008a; Criales-Hernández et al., 2008). Most migrating zooplankton thus spend the day in deep waters but are distributed near the surface at night. The presence of a permanent OMZ in the HCS seems to be the most important environmental factor in structuring and modifying the diel vertical distribution of zooplankton (Criales-Hernández et al., 2008; Ayón et al., 2008a).

In general, the epipelagic zooplankton community is constrained to the near-surface layer due to their low tolerance to low oxygen (Ayón et al., 2008a). However, since different zooplankton have different life strategies and different physiological tolerances to low oxygen, there are distinct patterns of zooplankton vertical distribution according to zooplankton species and life stage (Criales-Hernández et al., 2008; Escribano et al., 2009). For instance, adults of *Euphausia mucronata*, the most important zooplankton species in terms of biomass (Antenzana, 2002), seems to have physiologically adapted to low oxygen conditions and inhabit the OMZ during the day but migrate to the surface during the night (Antenzana, 2002, 2010; Escribano et al., 2009). The juvenile and larvae of *Euphausia mucronata*, however, are mainly found in the surface layer (Antenzana, 2002; P. Ayón, IMARPE, pers. communication). The copepod *Acartia tonsa* provides an example of an inverse pattern in which adults remain in the surface layer while the early stages mostly occupy the deep anoxic zone (Criales-Hernández et al., 2008).

### 1.3.2.3 Macrozooplankton

- **Large copepods**

Large copepods, in particular *Eucalanus inermis*, are very abundant in the system (Ayón et al., 2008a) and are the second most important food item of anchovy and sardine (Espinoza and Bertrand, 2008; Espinoza et al., 2009). *E. inermis* is considered a typical zooplankton of the cold coastal water and used as indicator for the presence of this water mass (Ayón et al., 2008a). This species perform large diel vertical migration between the epipelagic layer and the OMZ (Ayón et al., 2008a; Escribano et al., 2009) and, together with euphausiids, comprise most of the biomass of the migratory community (Escribano et al., 2009)

- **Euphausiids**

Euphausiids seem to be the most abundant (in terms of biomass) zooplankton group in the Humboldt system (Antezana, 2002). They constitute up to 66% of the anchovy diet (Espinoza and Bertrand, 2008) and are the main prey of hake (Ballón, 2005); the most abundant pelagic and demersal fish species, respectively. The fact that these fish species are opportunistic feeders (Espinoza, 2001; Muck, 1989) indirectly indicates that euphausiids probably form a large part of the zooplankton biomass. Among the fifteen euphausiids species found in the system (Ayón et al., 2008a), *Euphausia mucronata*, an endemic species of the system (Briton, 1962), seems to be the most abundant (Fig. 1.7) and may constitute up to 50% of the zooplankton biomass (Antenzana, 2002). According

to Antenzana (2010) very dense euphausiid swarms are able to remove most of diatoms biomass, exerting a local top-down control on primary production. Euphausiids are therefore suggested to play a major role in channelling primary production to higher trophic levels (Antezana, 2010) and sinking organic carbon (González et al., 2009).

- ***Munida***

Since the mid-1990s and coinciding with the change of the HCS to colder conditions, Munida (*Pleuroncodes monodon*), a macrocrustacean species mainly distributed off Chile in a demersal habitat, has extended its distribution range from northern Chile to Peru, and has drastically increased its biomass off Peru (Gutiérrez et al., 2008). These changes have also been accompanied by a change in munida's ecology, towards a complete pelagic lifecycle. This change has been attributed to the intense and shallow OMZ off Peru, which restricts its demersal habitat (Gutiérrez et al., 2008). Because of its high biomass, between 0.6 and 3.4 million of tonnes from 1998 to 2005 (Gutiérrez et al., 2008), munida plays an important role in the system, either by competing for space and food with important pelagic fish stocks, or as a food source for apex predators (Gutiérrez et al., 2008).

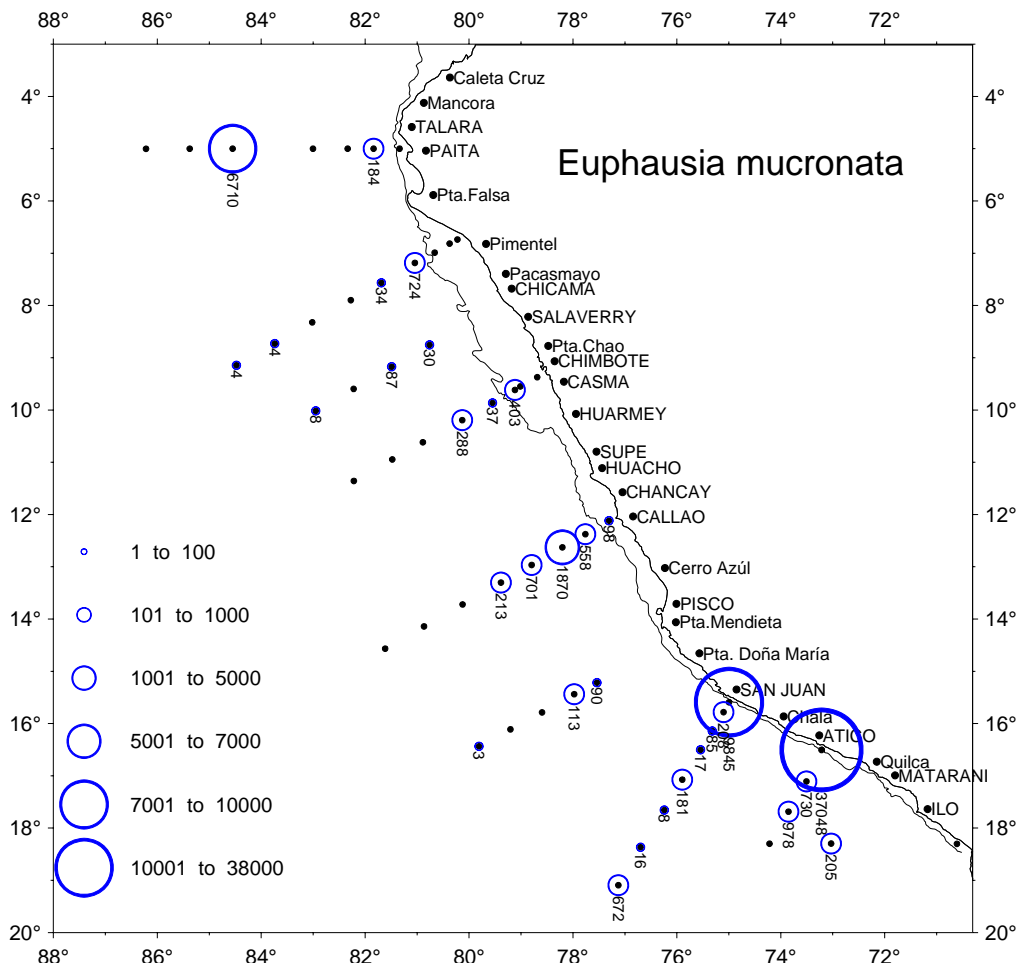


Figure 1.7 Distribution of *Euphausia mucronata* in the Northern Humboldt Current system during austral autumn 2008. Abundance is given in  $N^o$  ind per  $1000\text{ m}^{-3}$  (courtesy of P. Ayón, IMARPE).

### 1.3.3 Tertiary production

Although neither the primary production (Carr, 2002) nor the secondary production (Cushing, 1971; Huggett et al., 2009) of the HCS seem to be significantly higher than those of other EBUS, the fish production of this system is remarkably higher than that of other EBUS. The HCS has routinely produced more than 20 times the tonnage of fishery landings produced by other comparable EBUS (Chavez et al., 2008; Fig. 1.2.). The major portion of the entire system's fish production is often generated in the small near-equatorial sub-segment of the system, in the NHCS (Bakun and Weeks, 2008). Furthermore, most of the fish production consists of a single species, anchovy, which is restricted to the cold and highly productive water masses, in particular to the CCW (Bertrand et al., 2004b; Swartzman et al., 2008).

- ***Anchovy: a zooplankton predator***

The ability of anchovy to feed at low trophic levels (directly on primary producers) was suggested as the reason why such large populations, biomasses and fisheries could be sustained in the HCS (Ryther, 1969). However, neither the system has the highest primary production of the EBUS (Carr, 2002; Patti et al., 2008) nor phytoplankton is the main prey of anchovy. Indeed, Espinoza and Bertrand (2008) found that most of the anchovy food energy (98%) comes from zooplankton rather than phytoplankton, which agrees with the reported feeding behaviour of other anchovy species (van der Lingen et al., 2009). Although anchovy might prey on phytoplankton to get some nutrients, zooplankton is therefore its main food energy source. According to Espinoza and Bertrand (2008), anchovy is able to utilize food from several trophic levels, to choose energetically advantageous food types, and to adjust its foraging period and duration to prey availability. This high trophic plasticity is an evolved adaptive strategy of anchovy (Espinoza and Bertrand, 2008).

Additionally, anchovy has an extended spawning period of eight or nine months from July to March (Santander and De Castillo, 1973) and can change its reproductive behaviour to increase its chance to allocate offspring within better environmental conditions (Buitrón and Perea, 2000). Other strategies include the ability to track and concentrate in refuge areas when conditions are adverse (Bertrand et al., 2004b), and distribute its population over a rather large temperature range (Bertrand et al., 2004b; Gutiérrez et al., 2008).

In combination, these characteristics may explain the ‘anchoveta paradox’ (Espinoza and Bertrand, 2008), i.e., how a fish which (i) performs very small migrations and cannot escape adverse conditions, (ii) is mainly distributed in dense surface aggregations and is thus highly accessible to predators (fish, cephalopods, birds, mammals and fishers), and (iii) is very slow in its avoidance reactions to predators (Gerlotto et al., 2006), can achieve such enormous biomass in a relatively short time. To achieve this biomass, anchovy must encounter enough food to prey on, in particular a high biomass of macrozooplankton (Espinoza and Bertrand, 2008). Despites its significance as the most important prey of anchovy, macrozooplankton biomass has not yet been properly estimated in the NHCS (Ayón et al., 2008a). This is because macrozooplankton are capable of avoiding net sampling (Debby et al., 2004), so far the most common zooplankton sampling method in the NHCS (Ayón et al., 2008a).

Although the sardine is almost completely absent in the system since the early 2000s (Gutiérrez et al., 2007), this species has been very abundant and supported an important part of the pelagic fishery during the 1980s (Alheit and Niñuen, 2004). As occurred with anchovy, this species was thought to primarily prey on phytoplankton. However, recent studies have shown that sardine main preys are zooplankton; copepods and euphausiids in particular (Espinoza et al., 2009). This again emphasizes the important role of large zooplankton in the system.

## 1.4 The dynamics of the NHCS

The Peruvian upwelling system is subjected to bottom-up forcing at intraseasonal (Bertrand et al., 2008b) interannual (Barber and Chavez, 1983), multidecadal (Chavez et al., 2003; Alheit and Niñuen, 2004; Ayón et al., 2008b) and centennial time scales (Gutiérrez et al., 2009; Siffedine et al., 2008; Valdés et al., 2008).

### 1.4.1 Centennial variability

At centennial time scale, the system is experiencing a high production phase which started at about 1820 AD (Valdés et al., 2008; Gutiérrez et al., 2009). At this date the intertropical convergence zone and the South-Eastern Pacific subtropical anticyclone migrated northward to their current location. As a consequence, the upwelling was enhanced and the subsurface nutrient-rich OMZ rapidly expanded, resulting in a higher biological productivity, including pelagic fish (Fig. 1.8).

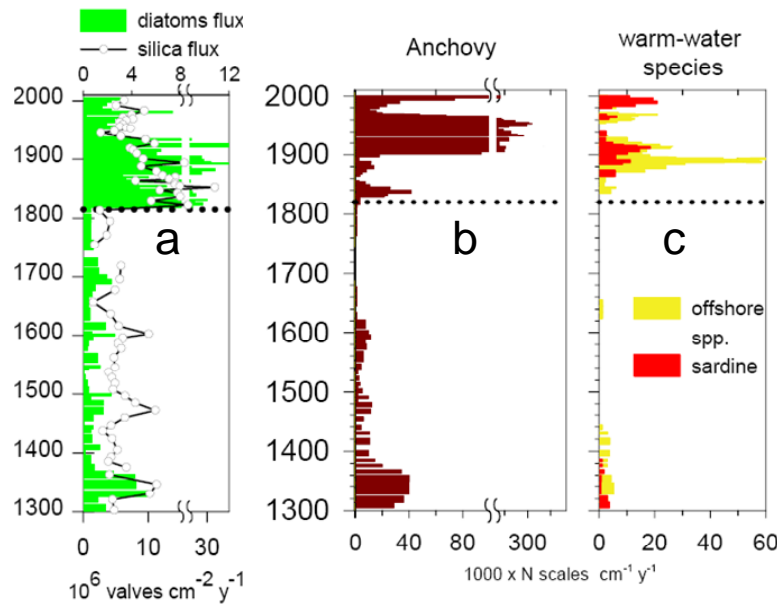


Figure 1.8 Proxies of primary production (a) and fish production (b) (c) at a centennial time scale. All proxies are shown as a function of time: (a) bars: diatom accumulation rate ( $10^6 \text{ valves cm}^{-2} \text{ y}^{-1}$ ), white circles: flux of biogenic silica ( $\text{mg cm}^{-2} \text{ y}^{-1}$ ); (b) 3-term averages of anchovy scale deposition rates ( $\text{Nr} \times 1000 \text{ cm}^{-2} \text{ y}^{-1}$ ); (c) 3-term averages of sardine scale deposition rates and offshore pelagic (jack mackerel+mackerel) scale deposition rates ( $\text{Nr} \times 1000 \text{ cm}^{-2} \text{ y}^{-1}$ ). Source: Gutiérrez et al. (2009).

### **1.4.2 Decadal variability**

Within the recent period of high production observed at centennial scale (Fig. 1.8), decadal fluctuations in the Ocean Pacific average climatic conditions have been reported (Mantua et al., 1997) and proposed as a cause for the alternation in the abundance of the main pelagic fish of the Peruvian upwelling system; anchovy and sardine (Chavez et al., 2003). During colder periods, the eastern Pacific exhibits a lower sea level slope and shallower thermocline, conditions which increase the nutrient supply and productivity. This in turn seems to favour the anchovy population (Chavez et al., 2003), probably as a result of the expansion of the CCW (Bertrand et al., 2004b, Swartzman et al., 2008). During warmer periods, however, the thermocline is deeper, the upwelling is weaker and productivity is lower, so that the range of habitat favourable to anchovy is dramatically reduced while the habitat favourable to sardine increases and spreads towards the continental shelf (Bertrand et al., 2004b). Warmer conditions thus seem to be related to an increase in the sardine population (Chavez et al., 2003). However, this alternation in the abundance of anchovy and sardine has only been observed in the fishing records, covering just one cycle. When looking at larger records, such as paleo-fish scales from sediments (Fig. 1.8 b,c), this alternation seems to occur only occasionally (Valdés et al., 2008; Gutiérrez et al., 2009).

### **1.4.3 Interannual variability**

At the basin scale, the Equatorial Pacific Ocean is characterized by a pressure gradient between the low pressure of the tropical warm and wet western Pacific and the high pressure of the cool and dry eastern Pacific. This creates a large convective circulation known as the Walker circulation. At the surface, the trade winds blow from east to west pushing ocean-surface water from eastern equatorial Pacific toward the western equatorial Pacific (Bakun, 1996). The ocean water is piled up in the west, increasing sea surface level and deepening the thermocline. Thus, under normal conditions, the East tends to have a shallower thermocline and, because of the upwelling of cooler water from the shallow thermocline, cooler waters than the West. However, the Walker circulation is not stable and may intensify or slow down depending on atmospheric pressure differences between the western and eastern Pacific (Bakun, 1996). This pressure difference, named the Southern Oscillation index, is therefore used to measure the state of the Equatorial Pacific.

- ***El Niño Southern Oscillation (ENSO)***

The most remarkable expressions of the interannual variability of the Humboldt Current system are the warm and cold phases of ENSO, El Niño and La Niña respectively. These conditions are derived from the passage of coastally trapped Kelvin waves (KWs), themselves originating in the western and central Pacific as oceanic equatorial KWs (Pizarro et al., 2001). The waves travel eastward along the equator and poleward until they reach the coast. According to the type of wind anomaly (easterlies or westerlies), an equatorial KW can raise (upwell) or deepen (downwell) the thermocline (often tens of metres) and the sea surface height (centimetres).

El Niño conditions are generated by downwelling KWs which deepen the thermocline (Fig. 1.9), and make the coastal upwelling ‘inefficient’ in terms of nutrient enrichment (brings oceanic warm water, low in nutrients to the surface ; Barber and Chavez, 1983). Conversely, La Niña conditions are generated by upwelling KWs which raise the

thermocline and allow coastal upwelling to bring cold and nutrient-rich water toward the surface. As a consequence, the cold coastal water (CCW) mass expands. These two sets of conditions also affect the spatial organization of living organisms by modifying the volume of the favourable pelagic habitat, or the surface of the oxygenated bottom areas, due to the along-coast propagation of the KWs (Bertrand et al., 2008b; Gutiérrez D et al., 2008). Although, in the short term, the changes in the physical and biological conditions (for example during El Niño) could have some negative effects, like reducing the abundance of anchovy and its predators (Arntz and Fahrbach, 1996), in the long term, it might contribute to maintaining the high fish production of the system by favouring fast-growing fish species like anchovy, which take advantage of the low predation pressure and rapidly increase their population and dominate the system (Bakun and Weeks, 2008).

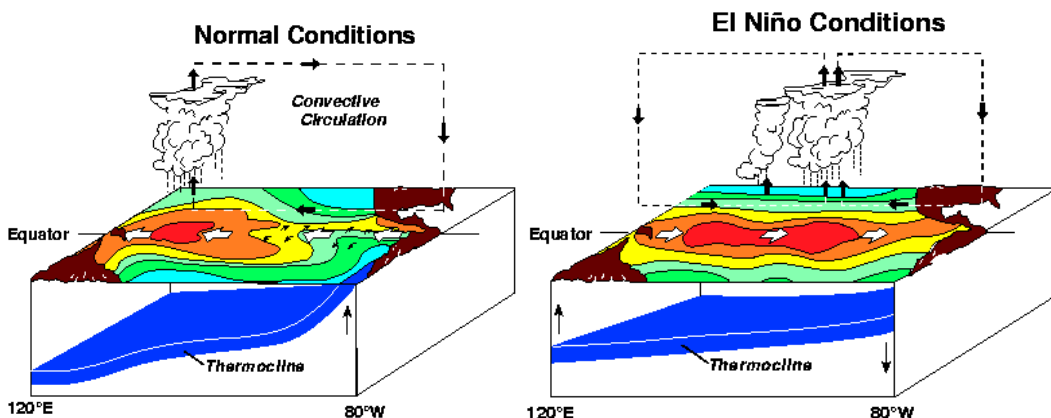


*Figure 1.9 Walker circulation during normal and El Niño conditions with their corresponding wind trade and effects on sea surface temperature and thermocline depth (source NOAA).*

#### 1.4.4 Seasonal variability

The NHCS does not present a strong upwelling seasonality as observed in other coastal upwelling systems. However, seasonal fluctuations can be observed in the physical environment (wind intensity, mixed layer depth, light, water masses, mesoscale activity, thermocline etc.) as well as in the biological production (chlorophyll, zooplankton, fish reproduction, etc.) of the system (Fig. 1.10 and 1.11). Although the highest upwelling intensity and nutrient supply occur during austral winter as a result of a higher wind intensity (Bakun and Mendelsohn, 1989), the system's maximum primary production occurs in spring (Thomas et al., 2001; Echevin et al., 2008) when a shallower mixed layer increases both the nutrient concentration and the light availability to phytoplankton (Echevin et al., 2008). As a result of the enhanced primary production during spring, zooplankton production (Ayón et al., 2008a) and fish reproduction activity (Santander and De Castillo, 1973, Mathisen, 1989) increase, showing a maximum during this season.

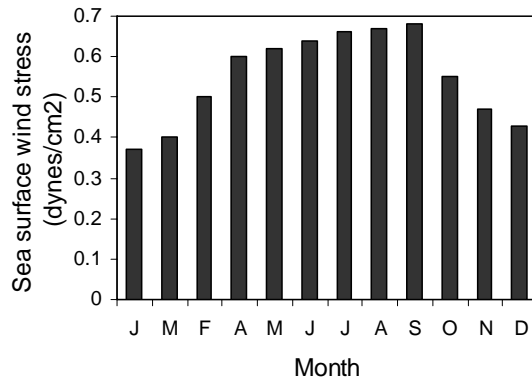


Figure 1.10 Monthly average of the along-shore wind stress (1953-1989). Source: Bakun and Mendelsohn (1989).

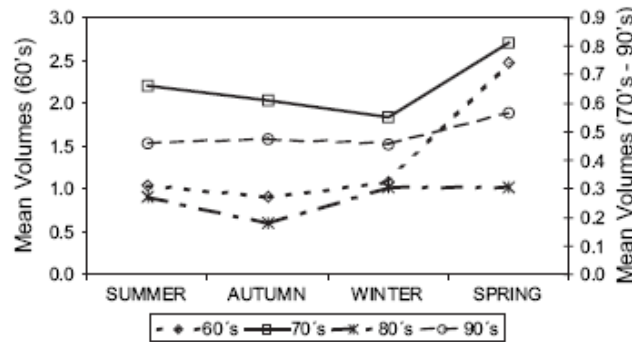


Figure 1.11 Mean seasonal zooplankton volumes ( $mL.m^{-3}$ ) during the 1960's, 1970's, 1980's and 1990's decades. Source: Ayón et al. (2004).

## 1.5 Fisheries

### 1.5.1 Pelagic fisheries

In a former period (~1850-1950), Man benefited from the biological richness of the Peruvian waters by exploiting guano (seabird excrement), used as fertiliser. This industry played an important role in the Peruvian economy during the 19th century (Chavez et al., 2008). The modern Peruvian fishery was developed during the 1940s and 1950s on species like bonito (*Sarda chilensis chilensis*) and tuna (primarily *Thunnus albacares*). It was driven by the high demand for the liver oil of these species in the US market during World War II and later the Korean War (Chavez et al., 2008). The anchovy fishery began in the 1950s and kept growing during the 1960s up to a peak of harvest of 12 million of tonnes per year in 1970, then accounting for 20% of the world catch.

While during El Niño 1972 and El Niño 1982-83 the anchovy fishery experienced strong collapses, the sardine population and exploitation increased to become the most important pelagic fishery during the 1980s (Alheit and Niquen, 2004). The favourable long-term environmental conditions (La Vieja) prevailing since the beginning of the

1990s, however, led to a significant increase in anchovy abundance and catches during the 1990s. In contrast, sardine abundance and catches gradually decreased during this period, maybe as a result of unfavourable conditions and overfishing (Bertrand et al., 2004b). The El Niño event of 1997-98 once again put the anchovy fishery at risk and in 1998 catches fell to 1 200 000 tonnes (IMARPE). These low catches, however, did not reflect the real anchovy abundance, but the quota imposed by the fisheries administration, which limited anchovy landings. According to Bertrand et al. (2004b), the presence of local coastal refuge areas with relatively ‘cold’ conditions together with a low fishing effort led to a sustained high abundance of anchovy during the 1997-98 El Niño. During this event, however, the already low sardine population became more available to fishing and was strongly affected by part of the anchovy fleet which shifted to fish sardine. While the 1997-98 El Niño marked an era (2000s) of full abundance of anchovy with relatively high catches ranging from 5 to 9 million of tonnes (source: IMARPE), this El Niño also marked the collapse of the sardine stock (Bertrand et al., 2004b; Gutiérrez et al., 2007) with no sign of recovery until now.

### ***1.5.2 Demersal fisheries***

The second most important industrial fishing activity is the trawl fishery, with hake being the main target species. This fishery began in the mid-sixties, with landings subsequently increasing mainly due to the use of factory vessels. Intense fishing pressure has been exerted on hake since the early 1970s. Fishing efforts increased from an average of 40 active vessels per year before the 1990s to 74 in the early 2000s (Guevara-Carrasco and Lleonart, 2008). Fishing caused radical declines in hake biomass leading to the change of fishery status from fully exploited to overfished and to the closure of the fishery for 20 months in 2002-2004 (Guevara-Carrasco, 2004). According to Ballón et al. (2008), fishing has diminished hake’s reproductive capacity, modified the sex ratio in favour of females and increased population vulnerability to environmental stress, in particular to El Niño.

### ***1.5.3 Fisheries management***

In 2008 the overcapacity of the anchovy fishery was estimated to 300% (Fréon et al., 2008), in other words, the fleet has the capacity to capture over 30 million tonnes per year even though current quotas have ranged from 5 to 8 million tonnes (Chavez et al., 2008). This overcapacity was economically driven by the classical ‘tragedy of the commons’ i.e., the race to catch a larger share of a global annual quota. Its roots can be traced to the inability of fisheries managers, under several administrations, to enforce laws controlling the expansion of the fleet and fish processing plants (Chavez et al., 2008). For management purpose, the fishing year is divided into two semesters (April-September and October-March) or fishing seasons, with long-established closures coinciding with the two main spawning periods in winter and summer (Chavez et al., 2008). The quota or total allowable catch (TAC) was assigned or adjusted by management at the beginning of each fishing period, formerly by season and over the last few years by month. When the TAC for a period is reached (or the period ends) the fishery is closed. Several periods make up the fishing season. Since there is a single quota for all there is a premium on skilled captains and high capacity. A new individual quota system, where the TAC is distributed among registered fishing vessels holding a valid fishing license, was implemented in 2009 removing the need to race to harvest as much as possible.

In the demersal fisheries, after a closing period of 20 months, the hake fishery was reopened and total allowable catches and individual nontransferable quotas were implemented to control the exploitation of hake. Although there has been a reduction in fishing effort, hake mean size and abundance remain low (Guevara-Carrasco and Leonart, 2008).



## Chapter 2

### *A bi-frequency method for macrozooplankton discrimination and biomass estimation*

#### **2.1 Introduction**

Information on zooplankton is available (albeit not processed) from routine acoustic surveys performed by most laboratories all over the world. Indeed, acoustics allows for a simultaneous collection of qualitative and quantitative data on various communities within an ecosystem, from zooplankton to large predators. Zooplankton acoustic data, however, are in most cases considered as noise and is usually eliminated from the data together with other non-target species (Bertrand et al., 2003).

Zooplankton, as any acoustic scattering object, can be discriminated from other organisms (i.e., fish) by using its acoustic properties and its frequency dependence (Simmonds and MacLennan, 2005; Kloser et al., 2002; Logerwell and Wilson, 2004; Mosteiro et al., 2004). The ability to distinguish between scatter groups improves as the number and range of frequencies increase (Napp et al., 1993). Unfortunately, most of present-day and historical routine acoustic surveys are performed using only two frequencies. It is the case of the historical acoustic records held by IMARPE, where the 38 and 120 kHz frequencies have been used to assess pelagic fish populations (note: in 2008 IMARPE began to equip its R/V with a third frequency, 200 kHz).

The aim of this chapter is to describe the development of an acoustic method that uses the 38 and 120 kHz frequencies for discriminating and quantifying mainly the abundance of crustacean macrozooplankton, but also of fish and ‘blue-noise’. The blue-noise encloses all targets that are not crustacean zooplankton and adult fish (mainly gas-bearing small organisms, such as fish larvae with small swimbladders or siphonophores with pneumatophores. Some gelatinous organisms may also belong to this group (Colombo et al., 2003). We place special emphasis on the crustacean zooplankton, in particular large copepods, euphausiids and munida (*Pleurocondes monodon*), because of their ecological importance in the NHCS (Ayón et al., 2008a; Espinoza and Bertrand, 2008; Espinoza et al., 2009; Gutiérrez et al., 2008). The proposed method is derived from the acoustic approaches of Fernandes et al. (2006), Lebourges-Dhaussy and Fernandes (submitted) and Korneliussen and Ona (2003) for discriminating marine scatter groups. To estimate the abundance of macrozooplankton we estimate its biovolume, based on the difference in volume backscattering strength ( $S_v$ , see MacLennan et al., 2002 for the definition of acoustic symbols) between the two frequencies (Greenlaw, 1979, Mitson et al., 1996). The precise settings we propose are adapted to the main living communities present in the NHCS but the method can be easily adapted to other systems<sup>2</sup>.

<sup>2</sup> The method is currently adapted to and applied in the Bay of Biscay in the framework of the PhD thesis of Ainhoa Lezama from AZTI.

### 2.1.1 Marine organisms as acoustic targets

Unlike optical or electromagnetic waves, sound waves travel over long distances through water with reduced attenuation and absorption. Thus, acoustic instruments which transmit and receive sound waves can be used to detect fish or other objects far beyond the range of vision. Over the years, acoustic techniques have therefore become increasingly sophisticated and useful in fishery research (Simmonds and MacLennan, 2005). Using sonar systems it became possible to record simultaneously and continuously the echoes from zooplankton and fish communities from large volumes of water in a really short time.

When acoustic waves encounter a target, and particularly an organism, part of the incident energy is scattered, generating a secondary wave, which propagates in all directions away from the organism. The energy reflected back toward the sound source is said to be ‘backscattered’ (Urick 1975; Simmonds and MacLennan, 2005). The intensity of the backscattered energy is a complex function of organism size, shape, orientation and materials properties, as well as acoustic frequency or wavelength (Stanton and Chu, 2000). Due to the linearity of fisheries acoustics (Foote, 1983), if the proportion of the incident energy which is backscattered by a single organism is known, it is possible to estimate the abundance of a patch of organisms with similar characteristics (size, shape, orientation and material properties). The proportion of backscattered energy for a given frequency depends on the backscattering cross-section ( $\sigma_{bs}$ , in  $\text{m}^2$ ) which is defined as follow:

$$\sigma_{bs} = R^2 I_b/I_i \quad \text{Eq. (2.1)}$$

where

$R$  is the distance (in m) from the target at which the intensity is measured,  $I_b$  is this backscattered intensity (energy per time unit and area unit), and  $I_i$  is the intensity of the incident sound energy at the target.

The backscattering cross-section expressed in decibels is named target strength ( $TS$ ) and both parameters are related according to the formula (see MacLennan et al., 2002 for definition of acoustic terms):

$$TS = 10 \log_{10} (\sigma_{bs}) \quad \text{Eq. (2.2)}$$

When the backscatter involves more than one organism, the basic acoustic measurement is the volume backscattering coefficient,  $s_v$  (in  $\text{m}^{-1}$ )

$$s_v = \sum \sigma_{bs} / V_0 \quad \text{Eq. (2.3)}$$

where  $\sigma_{bs}$  is the backscattering cross-section of each discrete target present in the volume (in  $\text{m}^2$ ),  $V_0$  is the sampled volume (in  $\text{m}^3$ ) of a ping given a distance from the transducer, its equivalent angle, and the pulse length.

The logarithmic equivalent is the volume back scattering strength  $Sv$  (dB re  $1 \text{ m}^{-1}$ )

$$Sv = 10 \log (s_v) \quad \text{Eq. (2.4)}$$

An average of  $s_v$  is often calculated over a given distance unit and over a depth range, involving several pings and a set of depth samples; the logarithmic equivalent of the result is called the mean volume backscattering strength (MVBS).

### ***2.1.2 Acoustic properties of fish and zooplankton***

Acoustically, fish can be easily separated into fish with and without swimbladder. Indeed, the swimbladder reflects 90% or more of the backscattered energy of a fish (Foote, 1980). Apart from differences due to presence or absence of swimbladder, fish as acoustic scatterers are relatively similar, varying principally with size which is not the case of zooplankton. Aggregations of zooplankton typically contain a number of species with vastly different acoustic properties varying with both species and size (Foote and Stanton, 2000, Lavery et al., 2007).

Stanton et al. (1996) categorized zooplankton organisms in a few broad scatter groups according to their material properties, which determine their acoustic response (Fig. 2.1):

- (i) ‘Fluid-like’ (e.g. euphausiids, copepods): the body is made of weakly scattering tissue with acoustic properties similar to those of the medium, not supporting shear waves. The shapes may be spherical, spheroidal or cylindrical; the contributing waves are the reflections on the interfaces with a penetration of the wave inside the material (Fig. 2.1a);
- (ii) ‘Hard elastic-shelled’ (e.g. gastropods): soft tissue surrounded by a hard shell, except for the opercular opening, in which superficial waves can propagate. The echo comes primarily from the shell interface, the wave do not penetrate inside (Fig. 2.1b);
- (iii) ‘Gas-bearing’ (e.g. siphonophores): a soft body together with a gas bubble; the gas provides a strong echo but the body contribution can be important if the gas tissue volume ratio is small (Fig. 2.1c).

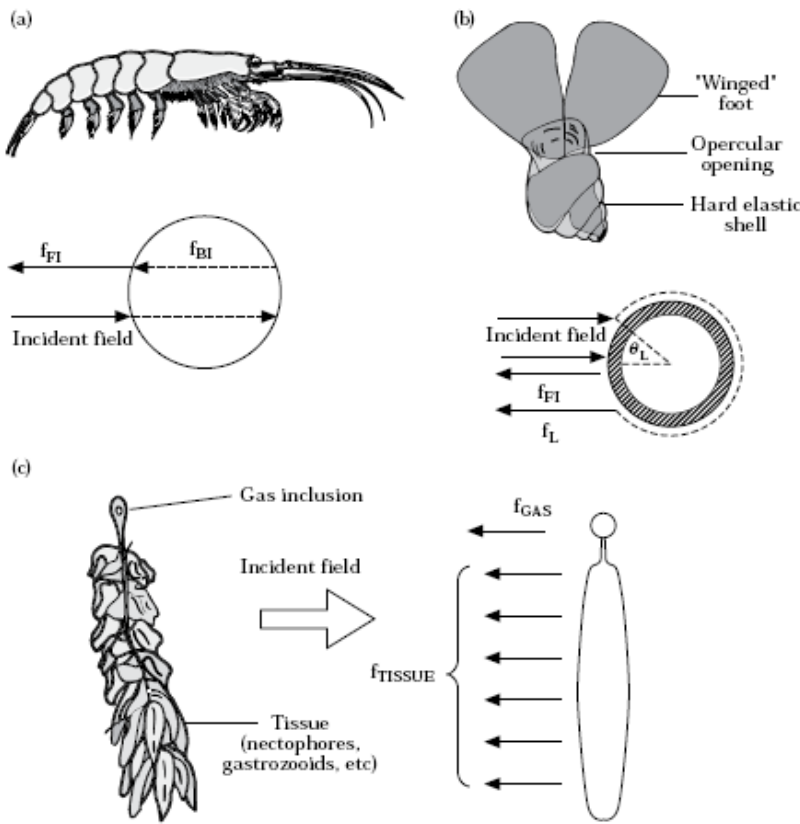


*Figure 2.1* Zooplankton from three anatomical categories: (a) fluid-like (e.g. euphausiids), (b) hard elastic-shelled (e.g. gastropod), and (c) gas-bearing (e.g. siphonophore). Near each animal is a diagram illustrating dominant scattering mechanisms. Source: Stanton et al. (1996).

### Fluid-like backscattering models

Fluid-like organisms include copepods, salps, siphonophores (without gas inclusion) euphausiids and other large crustaceans zooplankton (e.g. squilla larvae, munida and other decapods larvae). Various theoretical scattering models have been developed for describing the acoustic properties of fluid-like, mainly euphausiids and copepods, over a wide range of frequencies and organism sizes. Models vary from assuming fluid-like shapes as simple as a sphere (Greenlaw, 1977, 1979; Johnson, 1977; Stanton et al., 1987; Holliday et al., 1989; Holliday and Pieper, 1995) or a cylinder, to more realistic and complex morphology by increasing the resolution of the models (Stanton and Chu, 2000). In general, these models present two defined regions: (i) the low-frequency or Rayleigh zone, in which the backscattering efficiency increases over the frequencies, and (ii) the high-frequency or geometric zone, in which the backscattering efficiency is assumed to remain quite constant (Greenlaw, 1977, 1979; Johnson, 1977; Holliday et al., 1989; Holliday and Pieper, 1995; Stanton and Chu, 2000). In between these two regions, there is the transition zone that presents many fluctuations over the sizes/frequencies (see Fig. 2.2), and that is full of information about the organisms' signatures. To be able to take advantage of this information for a given model, a range of frequencies that extends from the Rayleigh zone to the geometric zone, is required to accurately identify and estimate the organism size-abundance structure. If the number of frequencies is high enough (at least 3), the numerical density can be estimated by means

of mathematical inversion in combination with assumed backscattering models of the organisms present (Simmonds and MacLennan, 2005). With 2 frequencies, a more simple method, in more restrictive conditions, can be used (Holliday and Pieper, 1995).

### 2.1.3 Organism discrimination based on acoustic properties

Independently of the size, shape or orientation of the target, backscattering occurs whenever there is a spatial change between (i) the sound velocity within the sea water and within the organism, and (ii) the density of sea water and that of the organism (Simmonds and MacLennan, 2005). The product of sound velocity and density is known as the impedance. Thus the greater the impedance differences between the medium (sea water) and the organism, the higher the backscatter.

When plotting the target strength of each scatter category versus frequency, each scatter type has a distinctive pattern and scattering efficiency (Stanton et al., 1996). Based on these patterns and their respective theoretical scattering models, it is possible to discriminate these scatter categories from multifrequency acoustic data.

Korneliussen and Ona (2003) characterized fish and zooplankton according to the relative response measure  $r_{\phi}$  ( $r_{\phi} = S_v \phi / S_v (38 \text{ kHz})$ ) at four acoustic frequencies, (18, 38, 120, and 200 kHz). According to the Korneliussen and Ona (2003) scheme, fluid-like objects are characterized by fluctuations between the low-frequency (Rayleigh) and high-frequency (geometric) scattering regions (Fig. 2.2). All gas-filled objects, such as siphonophores and swimbladder-bearing fish, display resonant scattering at a frequency that depends on the size of the gas inclusion. Backscatter from elastic-shelled zooplankton is characterized by a smooth transition between low-frequency and high-frequency regions.

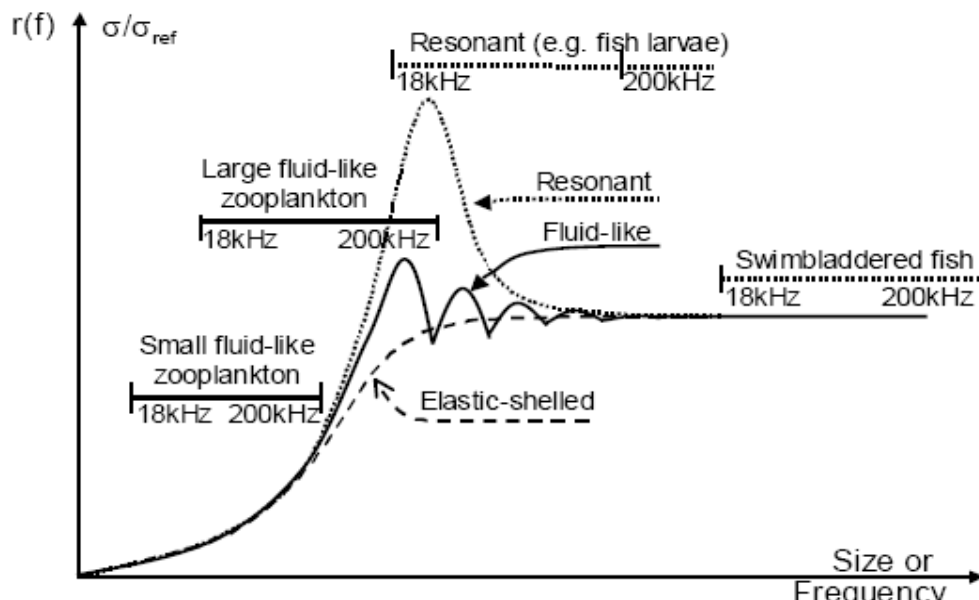


Figure 2.2 Schematic description of the relative frequency response,  $r(f)$ . Horizontal lines indicate typical range positions of selected acoustic categories when measured at frequencies 18-200 kHz. Source: Korneliussen and Ona (2003).

As observed in Figure 2.2, the backscatter of swimbladder-bearing fish remains relatively constant over the usual frequencies. For that reason, single frequency echosounders can be used for fish biomass estimation. However, zooplankton backscattering varies with both size and frequency and an increase in size/frequency could lead to an increase, decrease or no change at all, in the backscatter energy.

### **2.1.4 Bi-frequency organisms' discrimination**

The 38 and 120 kHz frequencies have traditionally been used in IMARPE for assessing pelagic fish stocks off Peru. Although data from these two frequencies have been recorded and saved, biomass estimates have been based on one frequency (mostly 120 kHz) and only a few studies have combined these two frequencies to assess other organisms (zooplankton e.g. Bertrand et al., 2008a; Gutiérrez et al., 2008).

As seen in the Korneliussen and Ona (2003) scheme (Fig. 2.2), the backscatter of fluid-like and elastic-shelled organisms increases with the size/frequency between 38 and 120 kHz. In contrast, the backscatter of larvae and adult swimbladder-bearing fish decreases or remains relatively constant between 38 and 120 kHz. This different frequency response makes it possible to use the 38 and 120 kHz frequencies to extract the fluid-like organisms from acoustic data in which other organisms (fish, other zooplanktons) or scattering objects (bubbles) are also present (Madureira et al., 1993; Kang et al., 2002; Watkins and Brierley, 2002). These studies have used the difference between the mean volume backscattering strengths at 38 kHz and 120 kHz ( $\Delta\text{MVBS}_{120-38}$ ) for discriminating krill (*Euphausia superba*) mainly, but the method is valid for other small euphausiids (Ressler et al., 2005) species and copepods (Fernandes et al., 2006). Furthermore, swimbladder-bearing fish have stronger backscattering response at 38 and 120 kHz frequencies, compared with zooplankton (Foote, 1990; Simmonds and MacLennan, 2005). At this frequency range, fish backscatter has a relatively low variation when compared to zooplankton backscatter, which substantially increases with the increase of frequency (Fig. 2.2). Although the use of  $\Delta\text{MVBS}$  has been applied successfully (Mitson et al., 1996) to discriminate zooplankton from fish, this method does not account for all possible situations that may be encountered in the ocean. For instance, the presence of pneumatophores that may have, depending on their size, an increasing or decreasing trend between 38 and 120 kHz, or the presence of large organisms with 'fluid-like' type response. If the range 38 to 120 kHz falls within the transition zone,  $\Delta\text{MVBS}$  may be positive or negative. So instead of basing the fish-zooplankton discrimination on the  $\Delta\text{MVBS}_{120-38}$  alone, the difference in variability between fish and zooplankton can be used to enhance the contrast between both types of organisms, regardless of the trend of the  $\Delta\text{MVBS}_{120-38}$ . We applied a recently developed methodology (Lebourges-Dhaussy and Fernandes, submitted) based on the sum of backscattering strength from two or more frequencies and the application of a 'multifrequency threshold' to build a Boolean mask (+MVBS).

## **2.2 Materials and Method**

### **2.2.1 Data**

Acoustic data were collected using hull-mounted Simrad EK500 (until 2007) and EK60 (since 2008) (Kongsberg Simrad AS) split-beam scientific echo-sounders at 38 and 120

kHz during the ‘*Cardumenes 2004*’ and ‘*Filamentos*’ surveys performed in November 2004 and February 2008 (Table 2.1) respectively. Echosounder calibration was performed according to Foote et al. (1987). Selection, classification, and analysis of the acoustic data were conducted using Echoview (SonarData Pty. Ltd., Hobart, Tasmania, Australia) and Matlab (MathWorks™, Natick, Massachusetts, USA) softwares.

Survey tracks consisted of parallel cross-shore transects with a target vessel speed of 10 knots except during the survey ‘*Cardumenes 2004*’ when the ship steamed at 8 knots around two, 2 nautical mile side square boxes repeatedly (see Bertrand et al., 2008a). During the *Filamentos* survey the water column was sampled down to depths of 300 m and 500 m for the 120 kHz and 38 kHz channels respectively. In the *Cardumen 2004* survey only the first 100 m of the water column was recorded for both frequencies.

Zooplankton were collected using a vertically profiling plankton net (multinet) with a 300 µm mesh size in the following depth strata: 0-10 m, 10-25 m, 25-50 m, 50-75 m, and 75- 100 m depths during the *Cardumenes 2004* survey, and 0-10 m 10-20 m, 20-30 m, 30-50 m, 50-75 m 75-100 m, 100-200 m and 200-300 m during the *Filamentos 2008* survey.

Zooplankton settled volume (mL) was determined immediately after collection using the displacement method (Kramer et al., 1972). Samples were fixed in 2% formaldehyde buffered with borax, then examined in the laboratory using a stereoscopic microscope to identify and count zooplankton items.

Fish and munida were collected by pelagic trawl ‘Engel 124/1800’ (12 mm codend mesh) (Table 2.1). For each trawl, a subsample of the catch was collected randomly and anchoveta size was measured to the nearest 0.5 cm.

*Table 2.1 Acoustic surveys characteristics: spatio-temporal extension, acoustic systems and ancillary data.*

Survey	Cardumen 2004	Filamentos 2008
Initial End	Nov. 17, 2004–Nov. 24, 2004	Feb. 05, 2008–Feb. 20, 2008
Covered area	12°34'S - 13°40' S	06°30'S - 08°02'S
Sampled hours	112	264
Echosounder system	Simrad EK500 split-beam	Simrad EK 60 split-beam
Frequencies	38 and 120 kHz	38 and 120 kHz
Plankton multinet sampling	17 profiles	6 profiles
Pelagic trawls with simultaneaus acoustic records	10 trawls with anchovy and 11 with munida	

## 2.2.2 Pre-processing

Acoustic data pre-processing and processing consisted of a series of steps synthesised in figure 2.3.

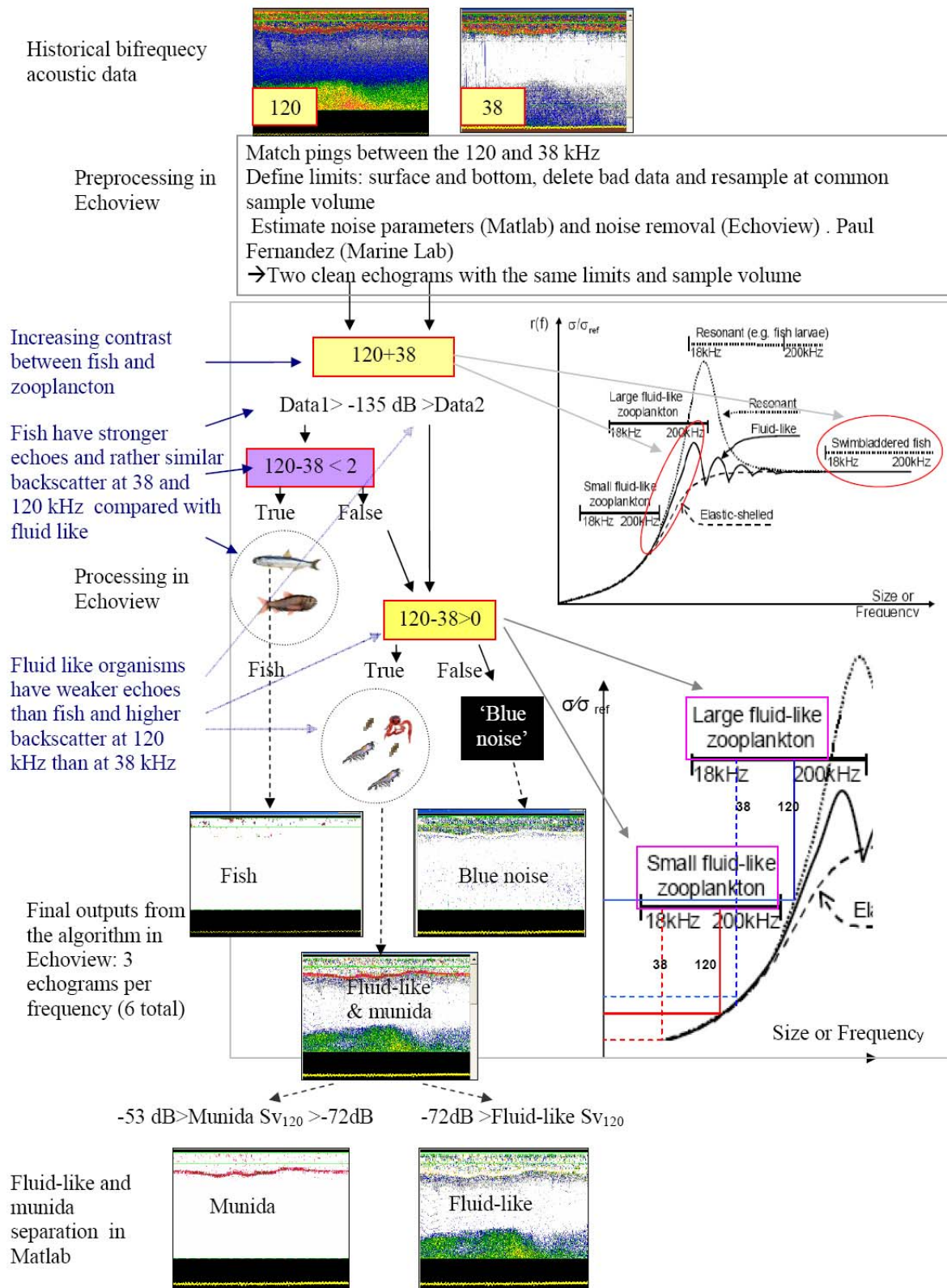


Figure 2.3 Flow chart of the bi-frequency method for scatter discrimination.

To compare two or more echograms from different frequencies, the ping number has to be synchronised (number and position) between echograms. For that we used the matching ping number algorithm from Echoview. We excluded the noise from the surface (5 m depth from the transducer) and the bottom echo. Similarly, we cleaned the echograms by defining and eliminating ‘bad regions’ containing parasite noise or a ‘school tail’. To eliminate the noise associated with the acoustic absorption, we followed the method proposed by Fernandes et al. (2006) and created a new acoustic field for each frequency using a data generator algorithm based on a noise function with the form:

$$20 * \log(R) + 2 * \alpha * R + \text{offset} \quad \text{Eq. (2.5),}$$

where  $R$  is the range (in m),  $\alpha$  is the frequency absorption coefficient (in dB.m<sup>-1</sup>) and the *offset* value (in dB) is the assumed initial noise at the first metre. For generating the noise field, the Echoview software needs initial inputs values of  $\alpha$  and the *offset*. These values were determined using a program written in Matlab (developed by P. Fernandes, Marine Lab., Scotland, U.K.). This program uses the minimum noise values per depth from an echogram section below the bottom and calculates the parameters of a TVG noise curve that better fits this curve. The noise field generated from Equation (2.5) was then subtracted from the echogram in the linear domain using the linear minus algorithm from Echoview. Finally, we used the ‘resample by number of ping’ algorithm from Echoview to resample the bi-frequency echograms in common elementary cells of 1 ping length and 0.75 m height.

### 2.2.3 Scatter discrimination and abundance estimation

- ***Enhancing the contrast between fish and zooplankton backscatter***

As a first step to separate fish from other organisms, we summed up the backscatter responses at 38 and 120 kHz frequencies (+MVBS<sub>120+38</sub>) (Lebourges-Dhaussy and Fernandes, submitted; Fernandes et al., 2006). Then, based on observations, we empirically chose a threshold value of -135 dB for this sum echogram and used a Boolean mask (true for values above threshold) to extract fish data from other scatters and create ‘fish’ and ‘no fish’ echograms at each frequency. From now on, all processes will be equally applied to both frequencies, unless specific information is provided.

- ***Separating fish scatters***

In the HCS, all the exploited fish (anchovy, sardine, jack mackerel and mackerel) and most mesopelagic fish are swimbladder-bearing. Therefore, any reference to ‘fish’ in this study pertains to swimbladder-bearing fish. Swimbladder-bearing fish have slightly higher backscatter at 38 than 120 kHz (Kloser et al., 2002), but weakly positive  $\Delta\text{MVBS}_{120-38}$  can be observed in the fish data, with a value of +2 dB that seems appropriate as a limit for extreme values. We thus refined the fish data from the fish echograms by applying a second Boolean mask to keep only the targets for which  $\Delta\text{MVBS}_{120-38} < +2$  dB.

- ***Separating Fluid-like and blue-noise***

Although fluid-like organisms can be separated because of their higher backscatter at 120 than at 38 kHz (Korneliussen and Ona, 2003), it is not possible to differentiate fluid-like from elastic-shelled zooplankton when using the 38 and 120 frequencies only.

Fluid-like zooplankton has lower backscatter efficiency than elastic-shelled zooplankton (Stanton et al., 1996) but both have a similar pattern at the used frequencies, i.e. lower backscatter at 38 than at 120 kHz (Korneliussen and Ona, 2003). Thus, in our case the so-called fluid-like group also includes the elastic-shelled zooplankton. The inability to discriminate between fluid-like and elastic-shelled zooplankton has limited consequences for this studies , because: (i) fluid-like zooplankton is by far the most abundant zooplankton in the system according to both net sampling (Ayón et al., 2008a) and pelagic fish stomach content (Espinoza and Bertrand, 2008; Espinoza et al., 2009) (ii) elastic-shelled zooplankton (i.e. ostracods or gastropods) are poorly adapted to live in low oxygen water (less than 2-3 mL.L<sup>-1</sup>) that are characteristic of the water column below the first few tens of metres in the HCS (except during the El Niño period), due to its permanent oxygen minimum zone (OMZ) (Castillo et al., 2007). For simplification purpose then after we refer to 'fluid-like' the field composed by fluid-like and elastic-shelled zooplankton.

We extracted the fluid-like organisms from the 'no fish' echograms by applying a Boolean mask selecting the targets with higher/lower backscatter at 120/38 kHz respectively. As a result the 'no fish' echograms were separated into 'fluid-like' echograms and 'blue-noise' echograms. A preliminary examination of the fluid-like echograms revealed that some targets located inside or at the edge of fish schools were inaccurately selected as fluid-like organisms. To correct this problem, we developed a 4-step procedure to extract the remaining fish backscatters from the fluid-like echograms and include them in the fish echograms:

- A copy of the fish echograms were 'expanded' by expanding the value of a cell (containing fish) to its immediate eight 'neighbour' cells (3x3 convolution matrix from Echoview);
- The expanded fish echograms were used to create a Boolean mask, with false values where fish are present;
- We applied this mask to the non-expanded echograms to create new no-fish echograms;
- We applied the Boolean mask again to select the targets with positive  $\Delta MVBS_{120-38}$  to create new fluid-like echograms.

- ***Refining the discrimination***

Although the new fluid-like echograms were almost free from fish echoes, some of the fluid-like targets were eliminated too. These gaps were filled in the final fluid-like echogram by using the 'select' operator from Echoview. This operator combines each fluid-like echogram and an expanded version of it (by applying a 3x3 convolution matrix) according to a logical bitmap. This bitmap has true values for all the cells where the original fluid-like echogram has a correspondence value in the new fluid-like echogram and false otherwise. If there was a true value in the bitmap then the corresponding data value from the new fluid-like echogram was used, otherwise the corresponding data from its expanded version was used. A similar procedure was used to include the fish echoes extracted from the fluid-like echograms into the final fish echograms.

- ***Exporting data to Matlab***

Virtual echograms of major scatter groups: fish (38 kHz), blue-noise (38 kHz), fluid-like (38 kHz and 120 kHz) were exported to Matlab. These data consisted of volume backscattering strength (Sv) by elementary cells of one ping length and 0.75 cm height, together with positional coordinates (latitude and longitude), time and bottom depth. To eliminate potential high noise echoes, we applied the following upper thresholds on these data: -21 dB for fish, -56 dB for blue-noise, and - 53 dB for fluid-like (120 kHz). Also, fish and blue-noise echoes below a lower threshold of -100 dB were excluded from the analysis. All scatter fields were also converted from  $s_v$  (by elementary cell) into an acoustic nautical area scattering coefficient (NASC), an index of abundance, according to the formula from MacLennan et al. (2002):

$$\text{NASC (in } m^2 \text{ n.mi.}^2\text{)} = 4\pi (1852)^2 * s_v * T, \quad \text{Eq. (2.6)}$$

where T is the integrated vertical distance of 0.75 m.

- ***Extracting munida from the fluid-like scatters***

As a final step, we separated munida from other fluid-like organisms for several reasons: (i) its abundance dramatically increased in the system since mid-1996 and occupies a specific ecological niche (Gutiérrez et al., 2008), (ii) munida are larger than any other fluid-like zooplankton in the ecosystem and do not play the same ecological role (e.g. adult munida are not foraged by small pelagic fish), (iii) munida have stronger backscatter than other fluid-like organisms present, (iv) munida are always epipelagic and perform reduced vertical migrations inside the epipelagic layer (Gutiérrez et al., 2008).

To extract munida from other fluid-like scatters we applied the following thresholds on the fluid-like  $Sv_{120}$ :  $-72 \text{ dB} < Sv < -53 \text{ dB}$ . The threshold limits were determined empirically using echograms where the presence or absence of munida was confirmed in pelagic trawls. The resulting munida echogram was validated by both ground-trusted munida records along transects (munida is routinely assessed by IMARPE) and the vertical position and shape of echotraces within the epipelagic layer.

- ***Fluid-like biovolume***

Although the fluid-like group includes euphausiids, copepods, salps, siphonophores (without gas inclusion) and munida, we focused on large macrozooplankton; mainly euphausiids, but also large copepods. This is because small copepods cannot be properly detected and quantified by the 38 kHz (Mitson et al., 1996), salps are not common outside the northern area (further north than 6°S, not included in this study) (Ayón et al., 2008a) and siphonophores without gas inclusion have a very low biomass (Ayón et al., 2008a). Furthermore, due to the larger size of munida and, consequentially, its stronger backscatter, it is possible to separate it. Although munida larvae cannot be discriminated from the fluid-like group, its abundance would only be important in near-coastal areas (Fagetti and Campodonico, 1971). On the other hand, euphausiids and large copepods are the most abundant zooplankton groups in the system (Ayón et al., 2008a) and the main prey of the most abundant fish species; anchovy, sardine, mackerel, jack mackerel and mesopelagic fish (Konchina, 1991; Espinoza and Bertrand, 2008; Espinoza et al., 2009). Euphausiids, however, attain larger biomass than copepods (Ayón et al., 2008a) and their acoustic detection is less biased (Murase et al., 2009).

According to Murase et al. (2009), large copepods need to occur in high densities to be detected by the 38 kHz frequency. For that reason, we set the method according to euphausiids acoustic properties when estimating the abundance of macrozooplankton (see below).

From now on, given the limitation to sample small zooplankton with the used frequencies, we will refer as macrozooplankton to the acoustic fluid-like zooplankton group obtained from the developed bi-frequency acoustic method.

While the euphausiid shape is cylindrical rather than spherical, in practice the fluid sphere model based on two frequencies seems to be appropriate for estimating zooplankton biovolumes (Holliday and Pieper, 1995). Indeed, the imperfect representation of the shape may become negligible once averaged with many echoes and when the range of orientation of the animals includes broadside incident (Stanton and Chu, 2000). According to Lawson et al. (2006), who measured *in situ* krill orientation angles, euphausiids orient themselves mostly horizontally, during both day and night. Since we have not included data from migratory periods, the effect of organism orientation is assumed to be minimal. For Stanton and Chu (2000) a zooplankton aggregation includes different sizes and orientations and the fluid sphere model might resemble the analytical average of the complex model of each individual within the aggregation.

To estimate fluid-like biovolume per cell in the echogram, we applied a method based on the  $Sv$  difference between frequencies (Greenlaw, 1979). This difference was used to estimate both the mean size and the number of the insonified organism. We assumed that the backscatter energy of a fluid-like organism is similar to the one produced by a fluid sphere and we used the fluid sphere high-pass model (Johnson, 1977; eq. 2.7) to estimate the sphere radius.

Determination of the sphere radius:

$$(ka)^4 = (2/3) \cdot [(r^4 - R)/(r^2(R-1))] \quad \text{Eq. (2.7)}$$

where  $k = 2\pi f_m / c$ ,  $a$  = the radius of the sphere (in mm),  $c$  = speed of sound (in  $\text{m.s}^{-1}$ ),  $f_m = (f_{120}f_{38})^{0.5}$  (in kHz),  $r = f_{120}/f_{38}$ , and  $R = 10^{(Sv(120)-Sv(38))/10}$ . The speed of sound was assumed to be: 1 509  $\text{m.s}^{-1}$  that correspond to mean temperature of 15.5°C and salinity of 35 ppm

Then, the determination of the backscattering cross-section  $\sigma_{bs}$  of the sphere can be estimated according to Greenlaw (1979):

$$\sigma_{bs} = [(1-gh^2)/(3gh^2) + (1-g)/(1+2g)]^2 \cdot a^2 \cdot [2(ka)^4/(2+3(ka)^4)], \quad \text{Eq. (2.8)}$$

where  $g$  is the density contrast between the sphere and the surrounding medium, and  $h$  is the speed contrast. Slight changes in density ( $g$ ) and sound speed ( $h$ ) contrasts result in an order of magnitude error in the acoustic scattering level estimation (Stanton and Chu, 2000). Since  $h$  and  $g$  contrasts depend on organism composition, in particular lipids storage, these parameters vary according to season and maturity. Estimation of these parameters can bring great uncertainty in this study. Indeed there is no estimation of  $g$  and  $h$  contrasts for *Euphausia mucronata* or any other euphausiid from the HCS. To reduce the uncertainty we applied the contrast parameters from a similar species, *Euphausia pacifica*, which belongs to a comparable ecosystem, the California Current.

We assume that the acoustic properties of *E. pacifica* are similar to *E. mucronata* because they have similar sizes and shapes and both live in upwelling systems characterized by high habitat variability (Knight, 1984). The g (1.037) and h (1.0097) parameters were calculated by averaging the contrast parameters, based on freshly caught individuals of *E. pacifica*, reported by Greenlaw and Johnson (1982). We selected the parameters obtained from freshly caught animals because they do not differ significantly from the ones obtained from living animals (Chu and Wiebe, 2005).

The number of individuals ( $N_f$ ) per unit volume can be estimated as follows

$$N_f = 10^{(Sv(f)-TS)/10} \quad \text{Eq. (2.9)}$$

where  $TS = 10\log_{10}(\sigma_{bs})$ , c.f. (Eq.2.10).

According to Mitson et al. (1996), the ratio of 120 to 38 kHz allows safe estimates of length over a  $ka$  range of 0.4 to 1.6. As seen in Figure 2.4, when the  $Sv$  difference is too small (<2 dB) or too large (>19 dB), the radius of the sphere  $a$  tends to be overestimated or underestimated, respectively. For that reason only the differences comprised between 2 and 19 dB were used for the biovolume estimation. Although this could underestimate the biovolume, in practice most of the observed  $Sv$  differences for fluid-like lay within this range.

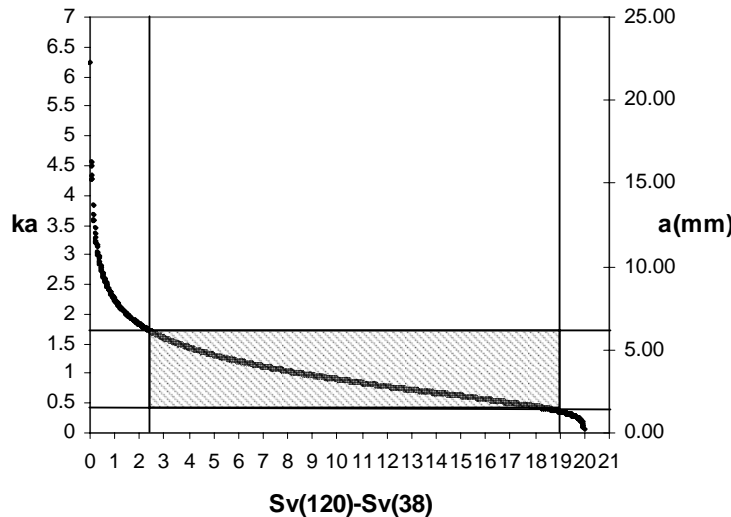


*Figure 2.4 The relationship between  $ka$  and the difference in volume backscattering at 120 and 38 kHz. The overlaid shadow area indicates the range at which high-pass model provides safe estimates of the spheres radius.*

Fluid-like biovolume was calculated by multiplying the densities of the organism ( $\text{ind.m}^{-3}$ ) by the volume ( $\text{in cm}^3$ ) of the sphere of radius  $a$ , i.e. the estimated volume of each ‘average’ individual.

### 2.2.4 Validation

The validation of the acoustic methodology was performed in three steps. First, we compared the acoustic biomass (NASC) of fish and munida from the Cardumen 2004 survey with their respective catches from pelagic trawl net sampling. To ensure comparable catches, the velocity (~2 knots) and duration (20 min) were kept constant when trawling. The acoustic fish and munida NASC comprised within the 10 central minutes of trawl net sampling were used for this comparison.

Second, we compared the vertical profiles of fluid-like acoustic biovolume with the zooplankton biovolume estimated using depth strata from multinet samples during the Cardumen 2004 survey. Also the integrated abundance (10-100 m) of the most important macrozooplankton (adult euphausiids, munida zoea, *Eucalanus inermis* and euphausiid larvae and juveniles<sup>3</sup>) was compared with the integrated acoustic biovolume of fluid-like macrozooplankton. As there were no acoustic records during the net sampling, we used the 25 pings recorded just before the multinet profile took place.

Third, we used data acquired during the Filamentos 2008 survey, where bi-frequency acoustic data are available until 300 m depth, to compare the vertical profiles of fluid-like acoustic biovolume with the abundance of adults, juveniles, and larvae of euphausiids sampled with the multinet. Since in this survey there were simultaneous acoustic records and multinet sampling, the acoustic records obtained within the time of multinet sampling were used to estimate fluid-like biovolume.

## 2.3 Results

An example of the scatter groups discriminated with the developed algorithm is presented in figure 2.5.

---

<sup>3</sup> In absence of a strict definition of macrozooplankton range size, in this study we define macrozooplankton as any zooplankton larger than 2 mm, a definition which theoretically includes all the organisms that can be observed with the applied bi-frequency method.

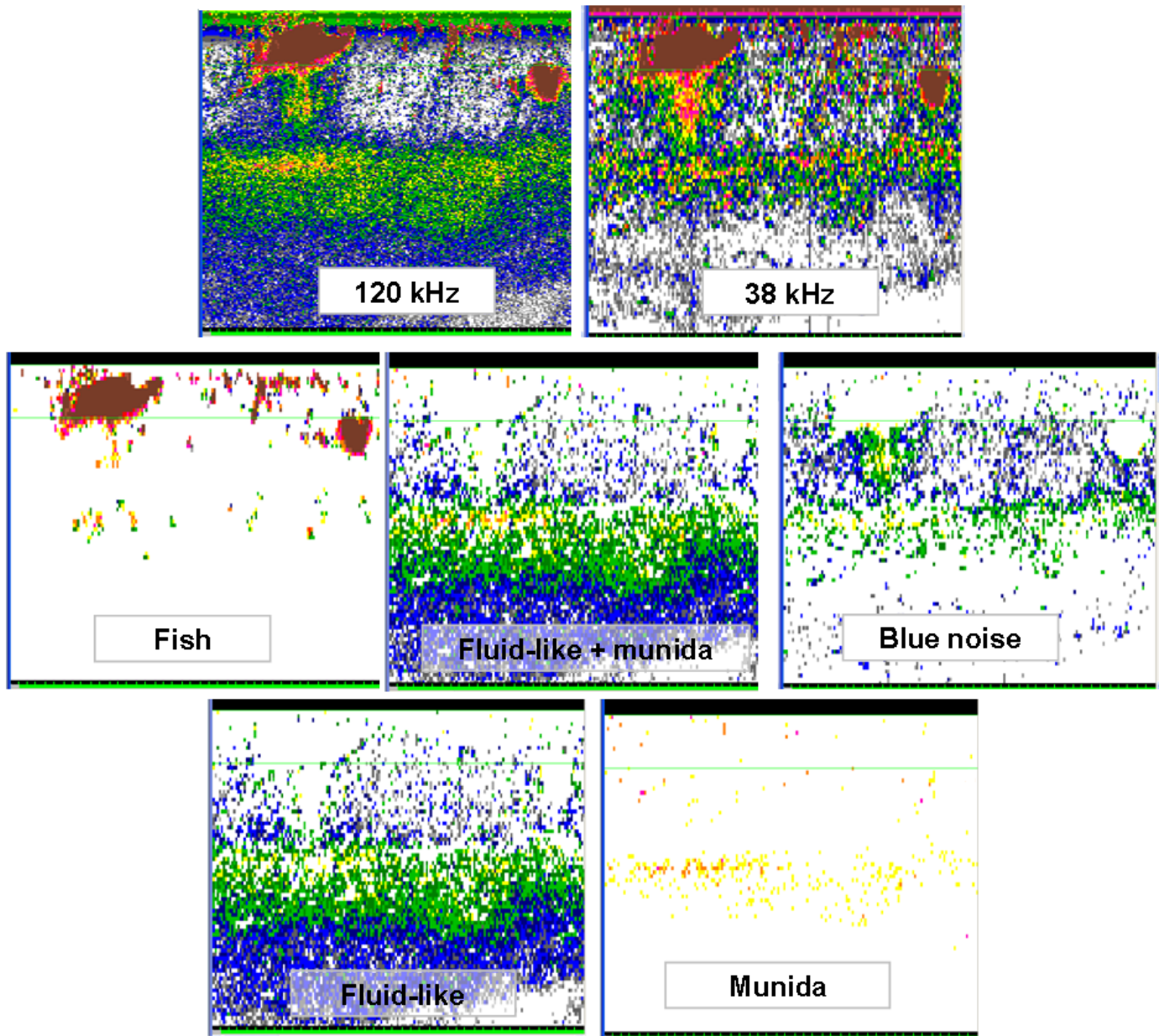


Figure 2.5 Acoustic discrimination of fish, 'blue-noise', fluid-like and munida by the developed bi-frequency algorithm. The echograms of Fish and blue-noise correspond to the 38 kHz frequency. The Fluid-like and munida echograms correspond to the 120 kHz frequency. Data from Filamentos Survey 2008.

The first step, the comparison of acoustic (NASC) and net sampling captures of fish and munida, showed that fish and munida from these two sources were significantly positively correlated (fish:  $p=0.006$ ,  $r^2=0.62$ ; munida:  $p=0.008$ ,  $r^2=0.56$  (Fig. 2.6).

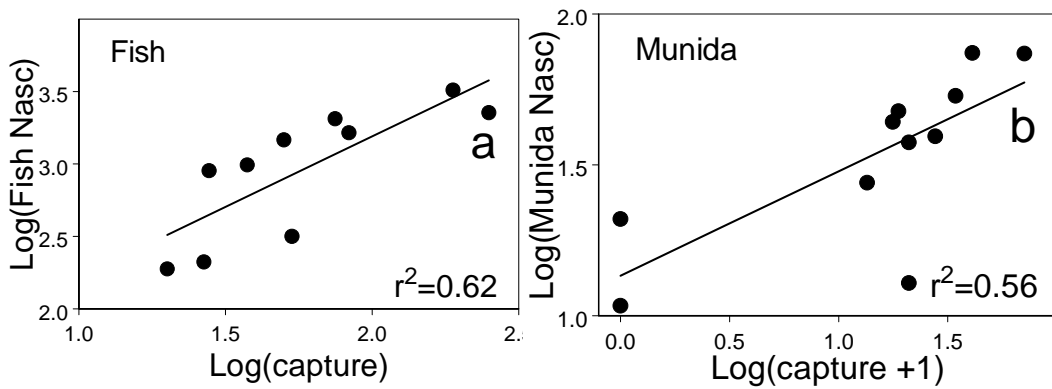


Figure 2.6 Regressions of log-transformed fish (a) and munida (b) acoustic nautical area scattering coefficient (NASC) with their respective log-transformed captures (biomass in kg) from pelagic trawl net sampling. Data from Cardumen 2004 survey.

Although the macrozooplankton mean biovolume from the acoustic method was 1 order of magnitude higher than the biovolume from net samples, there was an agreement between the vertical profiles of fluid-like biovolume from acoustic and net sampling during both day and night (Fig. 2.7), which was the second step in our validation process. Disregarding the sampling method, zooplankton biovolume was lower during the day than during the night (Fig. 2.7).

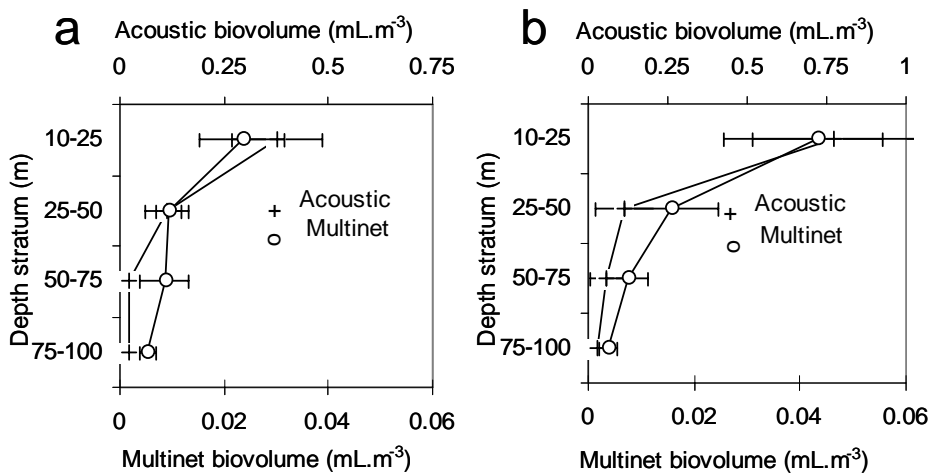


Figure 2.7 Day (a) and night (b) mean biovolume and confident interval (horizontal segments) per stratum ( $\text{ml.m}^{-3}$ ) estimated by multinet (open circle) and acoustic (plus symbol) samples. Data from Cardumen 2004 survey.

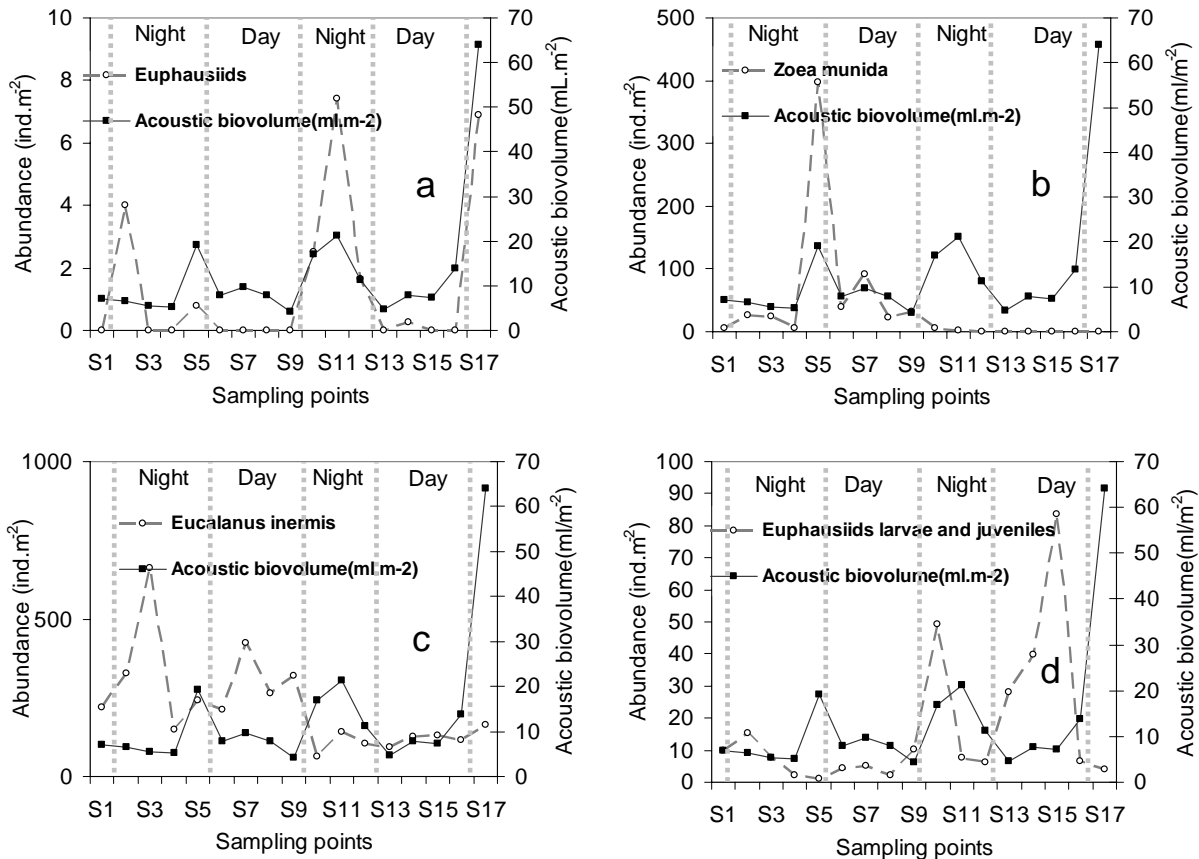
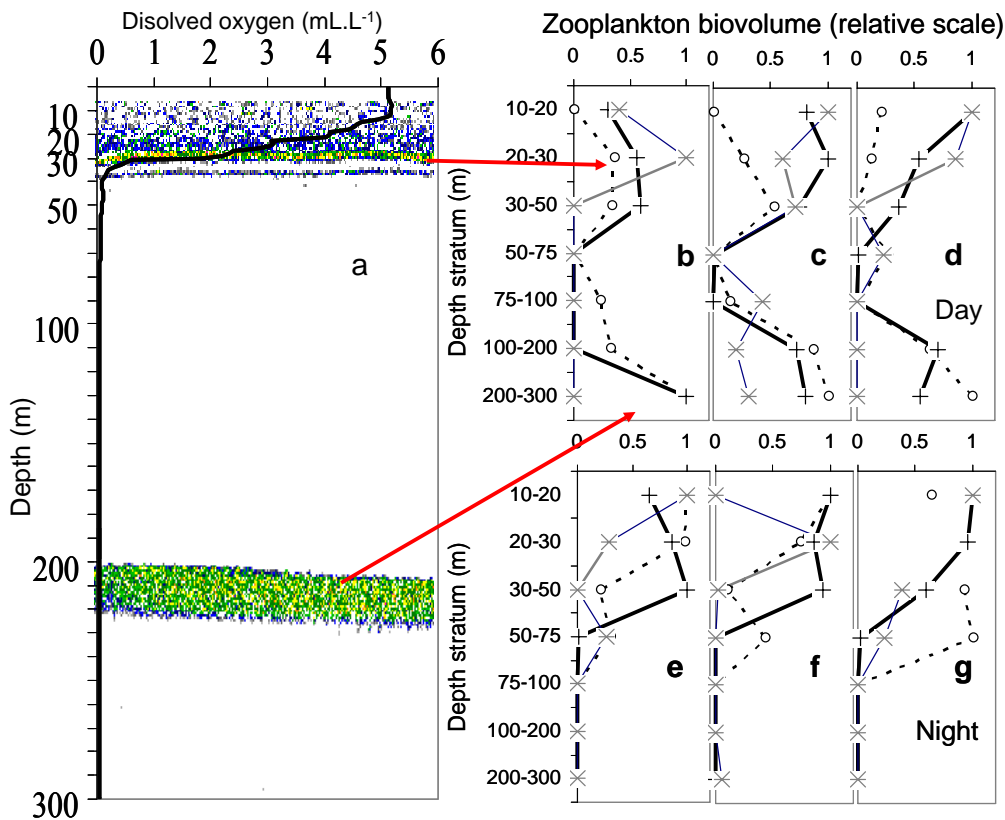


Figure 2.8 Comparison of acoustic (in  $\text{mL} \cdot \text{m}^{-2}$ ) and multinet abundance (in  $\text{ind} \cdot \text{m}^{-2}$ ) of adult euphausiids (a), zoea of munida (b), *Eucalanus inermis* (c) and euphausiids larvae and juveniles (d) integrated from 10 to 100 m. Data from Cardumen 2004 survey.

The additional comparison of the patterns of integrated abundance (10- 100 m) of adult euphausiids (Fig. 2.8a), zoea of munida (Fig. 2.8b), *Eucalanus inermis* (Fig. 2.8c) and euphausiids larvae and juvenile (Fig. 2.8d) with the integrated fluid-like acoustic biovolume showed that adult euphausiids was the group with the most similar pattern to the pattern of the integrated fluid-like acoustic biovolume. It is worth mentioning that biovolume not only depends on the organism's abundance but also on its size and shape. However, when working with a relatively homogenous group (e.g., zoea of munida, adult euphausiids) the effects of different sizes or shapes are assumed to be minimal when compared with the effect of organism abundance.



*Figure 2.9 Comparison of fluid-like acoustic biovolume and multinet abundance estimation of euphausiids per depth strata during the Survey Filamentos 2008. (a) fluid-like echogram with an overlaid dissolved oxygen profile corresponding to the vertical profile showed in (b). Day-time (b, c, and d) and night-time (e, f, g and h) vertical profiles of abundance of adults euphausiids (crosses) and euphausiids larvae-juveniles (asterisks) from multinet and fluid-like macrozooplankton biovolume from acoustic (open circles). Abundances/biovolume were standardized by dividing the abundance/biovolume of a stratum by the maximum abundance/biovolume of the profile.*

The importance of euphausiids as the main responsible organism for the observed acoustic pattern was also confirmed by the comparison of fluid-like acoustic biovolume and multinet abundance estimates of euphausiids during the Survey Filamentos 2008 (third step). Multinet samples showed that euphausiid adults, juveniles and larvae were abundant in the epipelagic layer during the day (Fig. 2.9b,c,d). An intermediate zone, almost free of euphausiids, was located between the upper and deeper euphausiid layers. The deeper layer, which was observed between 200 and 300 m (i.e. in the core of the OMZ), consisted of adult euphausiids only. During the night (Fig. 2.9e,f,g), euphausiids were distributed only in the epipelagic layer, whatever their ontogenetic stage. Acoustic vertical profiles of fluid-like biovolume presented very similar patterns of vertical distribution. Note the two diurnal dense scattering layers, one epipelagic, the other bathypelagic, observed in the acoustic echogram (Fig. 2.9a) that corresponded to two picks of euphausiid catches (Fig. 2.9b).

## 2.4 Discussion

In this section, our main objective was to develop a method to separate acoustic echoes into four broad categories: fish, fluid-like, munida and blue-noise. The main difficulty in validating the results resides in the availability of independent observations. Net is the most common tool used to sample marine pelagic organisms. Unfortunately, the confidence in this biomass estimation can be low or high depending on the type of net and the target species. We faced this difficulty when validating our data with net data known to be biased. Beside these limitations, our results demonstrate that the method is correct as the discrimination and the patterns of distribution of acoustic abundance of fish, munida and fluid-like macrozooplankton agreed with the independent observation from net sampling. In this study, we did not intend to validate the blue-noise scatter as it is a kind of ‘black box’ supposed to be made up of a heterogeneous mix of organisms other than fish, munida and fluid-like (e.g gelatinous, fish larvae).

Fish discrimination was not a challenge since IMARPE is performing accurate acoustic fish biomass estimation (from a single frequency) validated with ground-trusted catch data for decades (Simmonds et al., 2009). Also munida, with some limitation, is routinely assessed by IMARPE (since 1998, Gutiérrez et al., 2008) using a single frequency. The difficulty arises when munida and anchovy scatter in the same vertical layer (Bertrand et al., 2008a; Gutiérrez et al., 2008) particularly during the night. Our method has successfully separated fish from munida and may facilitate the study of both species during the night. Although a bi-frequency method has been previously used to separate anchovy and munida (Bertrand et al., 2008a), our study is very likely the first one that provides a detailed and validated acoustic method for separating these two organisms in the HCS.

The challenge we faced concerned the fluid-like category. Our results showed that acoustic fluid-like vertical and horizontal patterns of biomass distribution were very similar to the one of the euphausiids, the main macrozooplankton group in the system (Ayón et al., 2008a; Espinoza and Bertrand, 2008). Still, there was a one order of magnitude difference between fluid-like acoustic and multinet biovolumes. However, it is well known that macrozooplankton avoid net sampling (Debby et al., 2004), particularly vertical tows that are not appropriate for macrozooplankton. This avoidance is attributed to both visual and mechanical disturbances and usually increases when smaller nets are used (Fleminger and Clutter, 1965). The effect can be exacerbated by using nets that have not been designed for catching macrozooplankton, as in the case of the multinet with its small mesh size (300 $\mu$ ). According to Brinton (1967), euphausiids display a stronger avoidance at the surface as the higher illumination might allow them to detect the net. Although the fluid-like category includes other macrozooplankton crustaceans, euphausiids was the group that better fitted both the horizontal and vertical profiles of fluid-like acoustic biovolume. The simultaneous observation of superficial and deep layers of euphausiids also suggests the presence of subgroups of euphausiids (different species, sex or maturity stage) with distinct environmental preferences. This further suggests that, when combined with intensive net sampling and environmental information, more knowledge could be obtained on the patterns of distribution and behaviour of specific fluid-like groups.

Since the method separates the organisms into broad categories, there is still a large scope for working on further categorisation within each scatter group either using

ground-trusted catch data, which is usually available with the acoustic data, or performing further categorisation using the organism acoustic properties. For instance, it is possible to further distinguish between large and small swimbladder-bearing fish on the basis of their small and larger frequency Sv difference respectively (Kloser et al., 2002), this difference can also be used to separate distinct fish species (Logerwell and Wilson, 2004, Fernandes, 2009). However, since anchovy is the main fish species of the system in terms of biomass and it is constricted within the cold coastal water and mixed water (Swartzman et al., 2008) in many cases (i.e. during the day), the fish scatter group can be directly linked to anchovy.

The inclusion of more frequencies would definitely improve species recognition (Holliday and Pieper, 1995); however, there are still large bi-frequency databases (i.e IMARPE) which, ecologically speaking, have not been fully exploited. Our method enhances the exploitation of historical bi-frequency acoustic data in a more ecological approach in which each category can maintain the link to other scatters groups through a common spatiotemporal location. This may allow the analysis of large- and fine-scale organism distribution, in relation to physical forcing (see Chapters 4 and 5) and biological processes such as prey vs. predator behavior (Bertrand et al., 2004a).

The large difference between acoustic and multinet biovolume suggests that there is still an important methodological work to be done in zooplankton sampling strategies. Acoustics requires ground-trust catch data to effectively allocate the acoustic records to specific taxa, and better net sampling can be achieved by including the real time spatial distribution observed from the organisms' acoustic scatter records. Acoustic data can be employed as a spatial and temporal bridge between the isolated in situ samples, while the strength of the in situ samples is clearly the ability to identify species and quantify size (Trevorrow et al., 2005). Once this statement is accepted, research into the best sampling strategy to be designed using net and acoustics should be suggested. One conclusion could be that a plankton sampling strategy should be similar to trawl sampling for fish in acoustic surveys, i.e., not necessarily related to any a priori grid, but more likely to total biomass of 'acoustic macrozooplankton'.

The use of the density and sound speed contrast parameters from *Euphausia pacifica* instead of from *E. mucronata* may also introduce some bias, since biovolume estimates are quite sensitive to even small differences in the contrast parameters (Stanton and Chu, 2000). Also, since macrozooplankton (particularly euphausiids) are rather cylindrical than spherical, as assumed in our backscattering model, additional uncertainty in the biomass estimates could have been introduced because of this assumption. Although this bias maybe reduced in this study because we (i) restricted inference to zooplankton biovolume (Holliday and Pieper, 1995), (ii) we worked with averaged echoes, thus smoothing individual behaviour, and (iii) we restricted analysis to truly day and night time data, excluding migratory periods and thus increasing the chance to include broadside incidence in the range of animal orientation (Stanton and Chu, 2000), further studies are needed to unveil and quantify these effects in our biomass estimates. This is, however, our best guess from the available information. It is therefore necessary to test if the outcome macrozooplankton biomass and distribution pattern agree with the current knowledge about the macrozooplankton of the NHCS, which is the objective of the next chapters.

## *Chapter 3*

### *Acoustic observation of living organisms reveals the upper limit of the oxygen minimum zone*

#### **3.1 Introduction<sup>4</sup>**

Oceans include vast areas called oxygen minimum zones (OMZs) where subsurface layers are depleted in dissolved oxygen (DO) (Helly and Levin, 2004). OMZs are separated from the well-oxygenated surface mixed layer by strong vertical DO gradients forming the oxycline. These OMZs contribute to 25-75% of oceanic N<sub>2</sub>O production (Nevinson et al., 2004), a potent greenhouse gas, which influences the Earth's heat budget and depletes stratospheric ozone (Prather et al., 1995). OMZs are generally the site of intense denitrification (Naqvi et al., 2000) and have notable effects on the distribution and mortality of marine organisms. Although a few species of zooplankton, mesopelagic fish, and squids have adapted their metabolism to temporarily (through diel vertical migration) or permanently inhabit OMZs, most marine species limit their distribution to the surface oxygenated layer (Diaz et al., 2008; Prince and Goodyear, 2006). In response to global warming and direct anthropogenic influence, OMZs of the World Ocean are expanding (Diaz et al., 2008; Stramma et al., 2008; Chan et al., 2008; Oschlies et al., 2008). The upper limit of OMZs is rising and consequently, the vertical extent of the well-oxygenated surface layer shrinks, constraining the vertical habitat of epipelagic organisms. Intensification of oxygen-poor and acidic conditions could severely affect marine communities e.g. by (i) shrinking the available habitat, (ii) diminishing the capacity of plankton to develop calcium carbonate skeletons, (iii) eliminating species from metazoans to fish predators or (iv) hampering the spawning success of fish resources (Diaz et al., 2008; Levin, 2003; Orr et al., 2005; Feely et al., 2008; Vaquer-Sunyer and Duarte, 2008; Brewer and Peltzer, 2009; Walsh et al., 2009; Hazen et al., 2009). Upwelling regions are particularly vulnerable, given that they encompass the largest OMZs (Helly and Levin, 2004) and sustain ~20% of worldwide fish captures (Fréon et al., 2009).

The oxycline, which delimits the top of the OMZ, forms a sharp barrier for living organisms intolerant to hypoxia. It is also the site of the most intense particulate matter remineralization, a process which contributes to maintaining the underlying OMZ (Paulmier et al., 2006). Monitoring the spatial extension of the harshly acidic OMZ is crucial for assessing the effects of climate change on physical, chemical and biological mechanisms of marine ecosystems (Stramma et al., 2008; Walsh et al., 2009; Garcia et al., 2006; Bertrand et al., 2008b). However, since DO direct measurements require the

---

<sup>4</sup> This chapter corresponds to the following publication: Bertrand, A., Ballón, M. and Chaigneau, A. Acoustic observation of living organisms reveals the upper limit of the oxygen minimum zone. PLoS ONE 5(4): e10330.

deployment of oxygen sensors at discrete stations, the amount of available DO observations is relatively low (Stramma et al., 2008; Garcia et al., 2006). High-resolution observation of the spatiotemporal variability of oxycline cannot be achieved on a regional scale with conventional methods (including ARGO profilers or underwater autonomous vehicles).

Here we propose a new and alternative method for estimating the lower oxycline depth at very high spatiotemporal resolution using the vertical distribution of epipelagic organisms (mainly zooplankton and small pelagic fish). Acoustic instruments are widely used to detect fish, zooplankton and other objects far beyond the optical range (Simmonds and MacLennan, 2005). We exploited this capability to determine the lower vertical extension of the epipelagic community (VEEC), constrained by the OMZ, using bi-frequency acoustic data collected continuously along survey track

The method is applied in the highly productive region of the eastern South Pacific off Peru, which supports the world's largest monospecific fisheries (Chavez et al., 2008) and encompasses one of the most intense and shallow OMZ (Helly and Levin, 2004; Chavez et al., 2008; Paulmier and Ruiz-Pino, 2009; Karstensen et al., 2008). In this region, the intense upwelling cells leads to a coastal oxycline depth of usually less than 25 m, which strongly impacts marine life (Bertrand et al., 2008a). We use this information to estimate the habitable volume of anchovy.

### **3.2 Materials and methods**

#### **Data collection**

Field data were collected on board the 41 m long *R/V 'Olaya'* from the Instituto del Mar del Perú (IMARPE) during two scientific surveys: a multidisciplinary specific survey '*Filamentos 2008*' performed in February 2008 and a routine acoustic survey '*Pelagic 2005*' performed in February-April 2005 (Table 3.1).

*Table 3.1. Survey characteristics.*

Survey	'Filamentos 2008'	'Pelagic 2005'
Vessel	R/V Olaya from IMARPE	R/V Olaya from IMARPE
Start and End dates	Feb. 05, 2008 - Feb. 20, 2008	Feb. 20, 2005 - Apr. 04, 2005
Covered area	06°30'S - 08°02'S	3°29'S - 18° 03'S
Sampled hours	264	600
Echosounder	Simrad EK 60	Simrad EK500
Frequencies	38 and 120 kHz	38 and 120 kHz
DO measurement	CTD Sea Bird Electronic 911	Niskin bottle
Nº DO profiles	113	33
Nº of DO profiles visible on the echogram	24	0
Nº of DO profiles with $\geq$ 300 acoustic data available within a 5 km range	70	19

#### **Acoustic data**

Acoustic data were collected using hull-mounted Simrad split-beams bi-frequency (38 and 120 kHz) scientific echo-sounders EK500 and EK60 (Kongsberg

Simrad AS) during the ‘*Filamentos 2008*’ and ‘*Pelagic 2005*’ surveys, respectively. Survey tracks consisted of parallel cross-shore transects with a target vessel speed of 10 knots. Echosounder calibration was performed according to Foote et al. (1987). The water column was sampled down to depths of 250 m and 500 m for the 120 kHz and 38 kHz channels respectively. Due to the presence of noise in the echograms at 120 kHz, only the first 150 m were considered in the case of the ‘*Pelagic 2005*’ survey. Only day and night periods were considered; data from twilights were removed prior to analyses since it is not possible to determine  $Z_{VEEC}$  when mesopelagic organisms migrate through the upper limit of the OMZ.

Anchovy distribution was obtained from IMARPE routine acoustic biomass evaluation (Gutiérrez et al., 1999; Gutiérrez et al., 2007; Simmonds et al., 2009). Nautical-area-backscattering coefficients (NASC or  $s_A$ ; see MacLennan et al., 2002 for acoustic units) were recorded along survey tracks at each one nautical mile long georeferenced elementary distance sampling unit (EDSU) (Simmonds and MacLennan, 2005). During the ‘*Pelagic 2005*’ survey, anchovy biomass was estimated to 16.4 million tonnes (Simmonds et al., 2009). The interpolated map of anchovy NASC distribution was obtained by ordinary kriging fitted with an omnidirectional variogram based on robust estimator from (Cressie and Hawkins, 1980).

### **Oceanographic data**

During the *Filamentos* survey, 113 Conductivity-Temperature-Depth (CTD) casts were realized along 11 cross-shore oceanographic sections using a Seabird (SBE) CTD profiler composed of an underwater unit with conductivity, temperature and pressure sensors and a SBE911plus V2 deck unit. This CTD-SBE911plus model was also equipped with a SBE43 oxygen sensor calibrated one month before the cruise by the manufacturer, who ensures a precision of 0.03 mL L<sup>-1</sup>. The CTD was horizontally mounted on a SBE32 carousel water sampler including 12 1.7-liter Niskin bottles. Only downward CTD casts were retained for the analysis. During the ‘*Pelagic 2005*’ survey, water samples were collected using only Niskin bottles at 0, 10, 25, 50, 75, 100, and 150 m and DO concentrations were determined using the modified Winkler method (Carritt and Carpenter 1966) with a precision higher than 0.1 mL L<sup>-1</sup>. Oxygen profiles from both the ‘*Filamentos*’ and ‘*Pelagic 2005*’ surveys were linearly interpolated to determine the depth of the 0.8 mL L<sup>-1</sup> DO level ( $Z_{0.8}$ ). Oceanographic profile data were classified according to the diel period (day-night) and their spatial distribution: inshore-offshore.

### **Acoustic data processing**

The epipelagic community includes mainly zooplankton, gelatinous organisms and fish. Where OMZ is present, the vertical extension of most of this community is restricted to the oxygenated surface waters (see Vaquer-Sunyer and Duarte, 2008 for thresholds of hypoxia for marine organisms and Wishner et al., 1995). Below, the upper part of the OMZ is generally almost free of organisms. At dusk the mesopelagic community migrates towards the surface and mixes with the epipelagic community. At dawn they migrate vertically and take refuge in the OMZ. We defined the VEEC depth ( $Z_{VEEC}$ ) to be the depth where 98% of the cumulated sum of acoustic echoes ( $S_v$ , Volume backscattering strength, in dB re 1 m<sup>-1</sup>) from the epipelagic community was reached (the

cumulated sum is integrated downward from the surface). To determine the 98% threshold we used two different methods. First we tested different thresholds by 1% lag between 95 and 99% and visually scrutinized the patterns of  $Z_{VEEC}$  for each threshold in different conditions (day-night, offshore-inshore). Lower thresholds underestimated the main limit of organisms vertical distribution, while with a too high threshold (99%) the pattern of  $Z_{VEEC}$  was erratic in some cases (i.e. when few strong scatters were distributed below the main boundary); 98% appearing as the best compromise in any condition. Second, we plotted the vertical gradients of cumulated  $S_v$  ( $\Delta S_v$ ) and observed a higher gradient (or a pick, i.e. an accumulation of organisms) in the lower part of the distribution of epipelagic community when about 98% of the cumulated  $S_v$  was reached (Fig. 3.1.  $Z_{VEEC}$  was corrected to take into account the transducer position on the R/V hull (3.4 m below the sea surface).

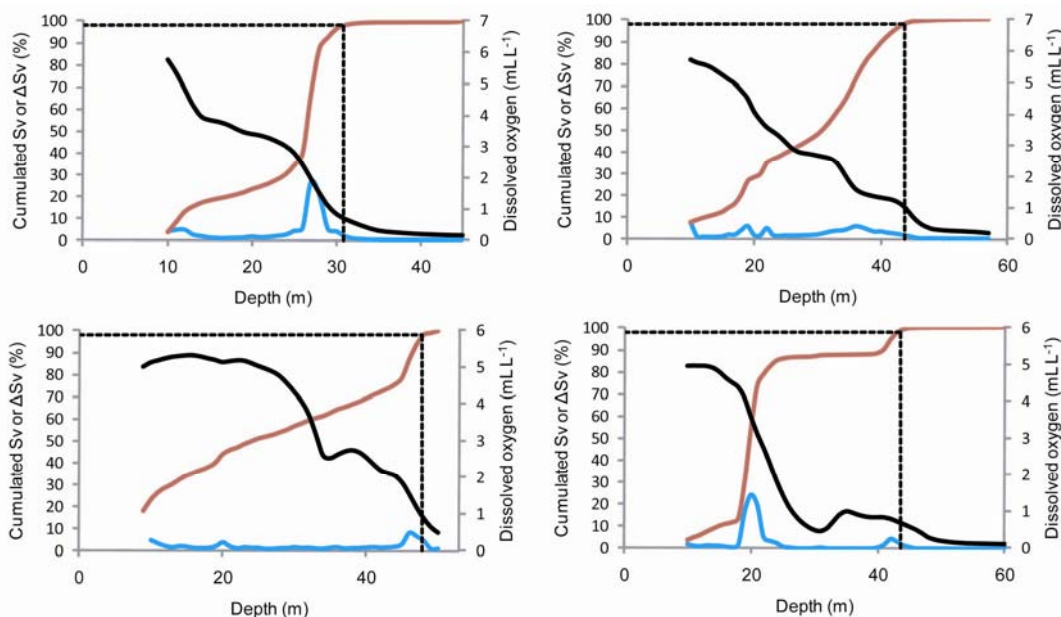


*Figure 3.1 Determination of the threshold to determine  $Z_{VEEC}$ . Examples of vertical profiles of the cumulated  $S_v$  (red solid lines) and its vertical gradient  $\Delta S_v$  (blue solid lines). The corresponding dissolved oxygen (DO) profile is also shown (black solid lines). Dotted black lines indicate the intersection with 98% of cumulated  $S_v$ .*

Anchovy, the dominant epipelagic fish in the system, have much higher target strength (~ -50 dB) than euphausiids (~ -85 dB), but fish generally occupy only a small part of the epipelagic habitat while zooplankton fills most of the space (zooplankton includes mainly crustaceans and gelatinous). Therefore, to better reflect the actual distribution of the overall epipelagic community, we considered all echoes but minimized the weight of fish echoes by a factor  $10^{-3}$  when estimating  $Z_{VEEC}$ .

To discriminate between fish and other scatters, we applied the developed bi-frequency method in Chapter 2. It is important to mention that the estimation of  $Z_{VEEC}$  was robust (<1 m except in some cases when very dense fish aggregation where present) to changes in methodology (for instance, the change in the weight of  $10^{-3}$  which we applied to fish echoes). Generally, with the exception of situations where a high

number of dense fish schools are present,  $Z_{VEEC}$  can be estimated directly from one frequency (120 kHz and probably 200 kHz) with no imperative need for multifrequency analysis.

### Comparing $Z_{VEEC}$ with DO profiles

The vertical distribution of the epipelagic community is not only affected by the oxycline but also by the vertical gradients of temperature, salinity or density (Graham et al., 2001; Ekau et al., 2009). However, since a exploratory linear correlation analysis revealed that only the oxcline ,in comparison with termocline and pycnocline, was highly correlated to the VEEC ( $r^2>80$ ), in this study we focused research effort on the effect of DO and leave out other parameters for further studies.

To determine the DO concentration at  $Z_{VEEC}$  for each profile two distinct methods were used. Firstly, when the CTDO track was visible on the concomitant echogram (e.g. Fig. 3.3 A) we precisely determined (in both the horizontal and vertical planes) the DO concentration at the depth where the CTDO cast crossed the epipelagic boundary ( $Z_{VEEC}$ ). Secondly, when the CTDO track was not visible on the concomitant echogram or when the considered profile was acquired from discrete Niskin bottles ('Pelagic 2005' survey) instead of CTDO ('Filamentos 2008' survey), such precision was not possible. In these cases, since  $Z_{VEEC}$  is affected by sub-mesoscale oceanographic dynamics such as internal waves and can exhibit vertical displacements of tenths of meters within typical horizontal range of ~100 m (Figs. 3.3 A, 3.6F; García et al., 2006), the small scale and high-frequency variability was filtered by averaging  $Z_{VEEC}$  over the closest 300 acoustic pings recorded within a maximum radius of 5 km from the oceanographic stations.

### Oxycline definition

The oxycline separates the well-oxygenated mixed-layer from the underlying OMZ. It can be divided into an upper and a lower oxycline. The upper oxycline extends from the base of the mixed-layer where oxygen values (around 5.5 mL L<sup>-1</sup>) start to decline to the depth where DO vertical gradients reach their maximum value (Fig. 3.2). In contrast, the lower oxycline extends from this latter level down to the bottom oxycline or the top of the OMZ defined either by the depth where DO concentrations drop below 0.5 mL L<sup>-1</sup> (Farías et al., 2007) or by the maximum depth where vertical DO gradients are weaker than -0.9 µMol kg<sup>-1</sup> m<sup>-1</sup> equivalent to -0.02 mL L<sup>-1</sup> m<sup>-1</sup> (Paulmier et al., 2006; Paulmier and Ruiz-Pino, 2009). In this study, the base of the lower oxycline was defined as the maximum depth between these two above criteria. In the particular case shown in Figure 3.2, the base of the lower oxycline corresponds to the definition given by Paulmier et al. (2006) and Paulmier and Ruiz-Pino (2009).

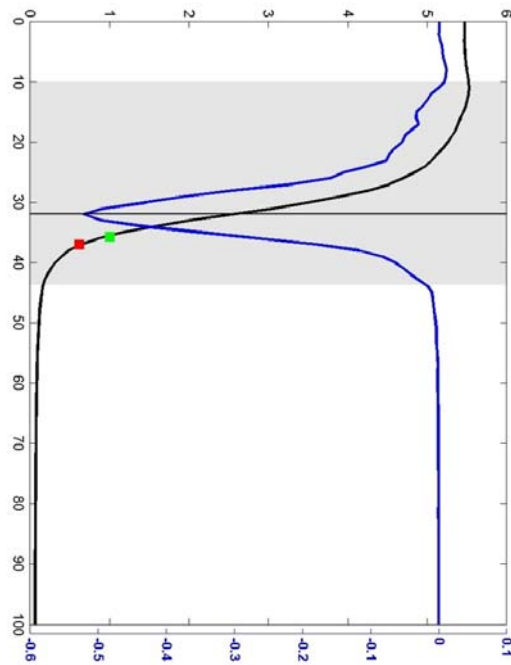


*Figure 3.2 Oxycline definition. Example of vertical DO profile (thick black line, upper axis) and the corresponding DO vertical gradients (thick blue line, lower axis) acquired during the ‘Filamentos 2008’ cruise. Shaded grey area corresponds to the oxycline separated into upper and lower oxycline as described in the text. The thin black line, corresponds to the depth of the maximum DO vertical gradient, and separates the upper and lower oxycline. The purple square corresponds to  $Z_{VEEC}$  whereas the red square indicates the depth of the  $0.8 \text{ mL L}^{-1}$  level ( $Z_{0.8}$ ).*

### Wavelet analysis

The cross-shore variation and periodicity of  $Z_{VEEC}$  was investigated using continuous wavelet analysis which is well suited to the study of multicycle, non-stationary phenomena, occurring over finite spatial and temporal domains (Lau and Weng, 1995). The continuous wavelet transform (CWT) of space series is its convolution with the local basis functions, or wavelets, which can be stretched and translated with flexible resolution in both wavelength and space. The CWT of the space series  $d$  with respect to the wavelet  $\psi$ , chosen here as the Morlet wavelet, is defined as

$$W_{d,\psi}(s,d) = (d(x) \times \psi_s(x)), \quad \text{Eq. (3.1)}$$

where  $x$  is space and  $\psi_s$  is the wavelet at the scale  $s$  (which is linearly related to the characteristic wavelength of the wavelet). The CWT decomposes the space series into a space-wavelength space, enabling the identification of both the dominant modes of variability and how those modes vary with space. Thus, the wavelet coefficients represent the correlation between the wavelet at a certain scale and the data array at a particular location. Larger positive amplitude implies a higher positive correlation, while large negative amplitude implies a high negative correlation.

A useful way to determine the distribution of energy within the data array is to compute the wavelet power spectrum defined as  $|W_{d,\psi}|^2$ , i.e., the squared transform coefficient. The power spectrum can be referred to as a graphical representation of cumulative information variation at each scale of decomposition. However, as mentioned by Liu et al. (2007), a physically consistent definition of energy for the wavelet power spectrum is the transform coefficient squared and divided by the scale it associates. Such an adjusted wavelet power spectrum is used in this study and results in a substantial improvement in the spectral estimate, allowing for a comparison of the spectral peaks across scales. Following Torrence and Compo (1998), a cone of influence (COI) is defined to remove the data  $d(x)$  whose wavelet transform is affected by edge effects.

### 3.3 Results

The lower limit of the VEEC ( $Z_{VEEC}$ ), was defined as the depth at which 98% of accumulated acoustic echoes occurs (Fig. 3.3 A, see Material and Methods). We first worked on acoustic data from the ‘Filamentos 2008’ survey realized off Peru in February 2008 (Fig. 3.5B, Table 3.1). During this survey, 113 hydrographic stations were sampled (Fig. 3.5A) to acquire vertical profiles of physical-biogeochemical parameters using a conductivity-temperature-depth probe equipped with a dissolved oxygen sensor (CTDO). Among these 113 stations, 96 included parallel acoustic measurements for which 25 showed visible CTDO tracks within the acoustic echograms such as the one displayed in Figure 3.3A. Those 25 reference casts allowed highly precise measurement of the DO concentration at  $Z_{VEEC}$ .

Based on these reference DO profiles and the concomitant echograms, we determined that the mean DO concentration at  $Z_{VEEC}$  was  $0.80 \text{ mL L}^{-1}$ , regardless of the diel period (Fig. 3.3B; ANOVA day-night effect:  $F_{[1,23]}=0.0005$ ,  $p=0.98$ ) or the distance from the coast (ANOVA offshore-inshore effect:  $F_{[1,23]}=0.3518$ ,  $p=0.56$ ). The linear relationship between  $Z_{VEEC}$  and the depth of the DO isovalue of  $0.80 \text{ mL L}^{-1}$  ( $Z_{0.8}$ ) was highly significant (Table 3.2; Fig. 3.3C). We extended the analysis to the remaining 71 CTDO profiles for which CTDO casts were not visible on the concomitant echograms and obtained similar results (Table 3.2; Fig. 3.3C).

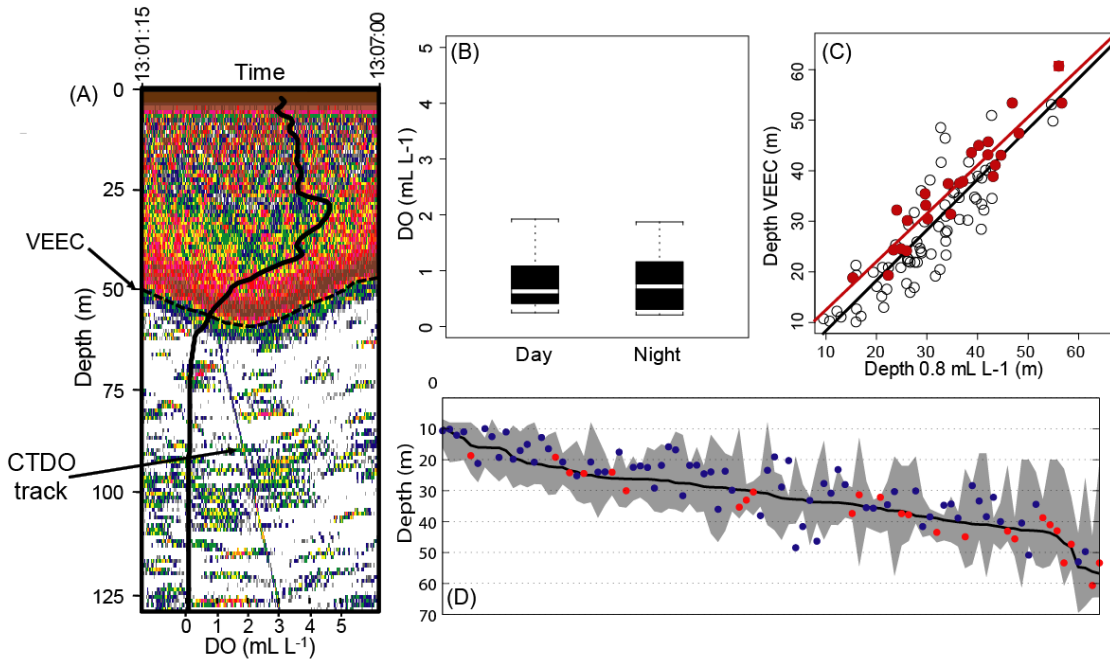


*Figure 3.3 Acoustic detection of the VEEC during the ‘Filamentos’ survey. A. Example of acoustic echogram showing a CTDO track and the VEEC. The superimposed black solid line is the corresponding DO vertical profile ( $\text{mL L}^{-1}$ , lower axis). B. Box plot of DO concentration at  $Z_{\text{VEEC}}$  according to the diel period. C. Relationship between  $Z_{\text{VEEC}}$  and  $Z_{0.8}$  for the 24 stations with detectable CTDO tracks on echograms (full red circles; the full red square in the upper right corner corresponds to the station presented in A) and the other 70 CTDO stations (white circles); Red and black solid lines correspond to the linear regression for the 24 stations with detectable CTDO tracks and for all the 94 stations, respectively. D. Vertical range of the lower oxycline (shaded area) for all 94 stations ranked toward increasing  $Z_{0.8}$  (black solid line); full dots represent  $Z_{\text{VEEC}}$  for the 24 stations with “visible” CTDO tracks (red) and the other 70 CTDO stations (blue).*

We defined the lower oxycline as the vertical region comprised between the depth of the maximum DO vertical gradient and the deepest level where vertical DO gradient value was weaker than  $-0.2 \text{ mL L}^{-1} \text{ m}^{-1}$  (bottom oxycline). The  $Z_{0.8}$  and most  $Z_{\text{VEEC}}$  were included in the lower oxycline region (Fig. 3.3D) and  $Z_{\text{VEEC}}$  was highly significantly correlated with the bottom oxycline (Table 3.2). To test for the robustness of  $Z_{\text{VEEC}}$  as a proxy of the upper OMZ we repeated the analysis with echograms and *in situ* DO profiles collected during the routine acoustic survey ‘Pelagic 2005’ performed in February-April 2005 along the entire Peruvian coast (Fig. 3.5E, Table 3.1). During this survey, 20 DO profiles were acquired from Niskin bottles (Fig. 3.5D), while acoustic data were also recorded. The linear correlation between  $Z_{\text{VEEC}}$  and  $Z_{0.8}$  estimated from Niskin bottle casts was again highly significant (Table 3.2, Fig. 3.4).

Table 3.2 Linear regressions summary

Survey	Case	<i>y</i>	<i>x</i>	Slope	Intercept	<i>n</i>	<i>F</i>	<i>p</i>	<i>R</i> <sup>2</sup>
Filamentos 2008	CTDO visible on echogram	$Z_{VEEC}$	$Z_{0.8}$	0.95	2.96	25	203.5	<0.0000	0.90
Filamentos 2008	CTDO not visible on echogram	$Z_{VEEC}$	$Z_{0.8}$	0.95	-1.19	71	177.1	<0.0000	0.72
Filamentos 2008	All CTDO with echogram	$Z_{VEEC}$	$Z_{0.8}$	1.00	-1.68	96	324.4	<0.0000	0.78
Filamentos 2008	CTDO visible on echogram	$Z_{VEEC}$	$Z_{bot.oxy.}$	0.87	2.59	25	108.5	<0.0000	0.83
Filamentos 2008	CTDO not visible on echogram	$Z_{VEEC}$	$Z_{bot.oxy.}$	0.88	-1.94	70*	154.6	<0.0000	0.70
Filamentos 2008	All CTDO with echogram	$Z_{VEEC}$	$Z_{bot.oxy.}$	0.93	-2.39	95*	272.5	<0.0000	0.75
Pelagic 2005	Use of Niskin bottles	$Z_{VEEC}$	$Z_{0.8}$	0.90	7.0	20	101.1	<0.0000	0.85

\*note that it was not possible to estimate  $Z_{bot.oxy.}$  for one coastal station since the corresponding CTDO profile did not reach the base of the oxycline.

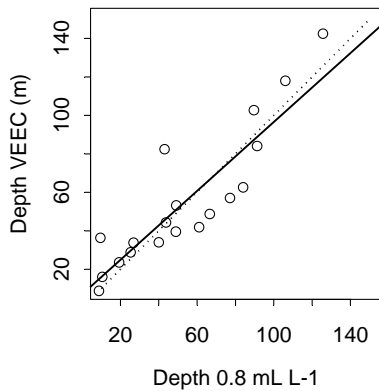
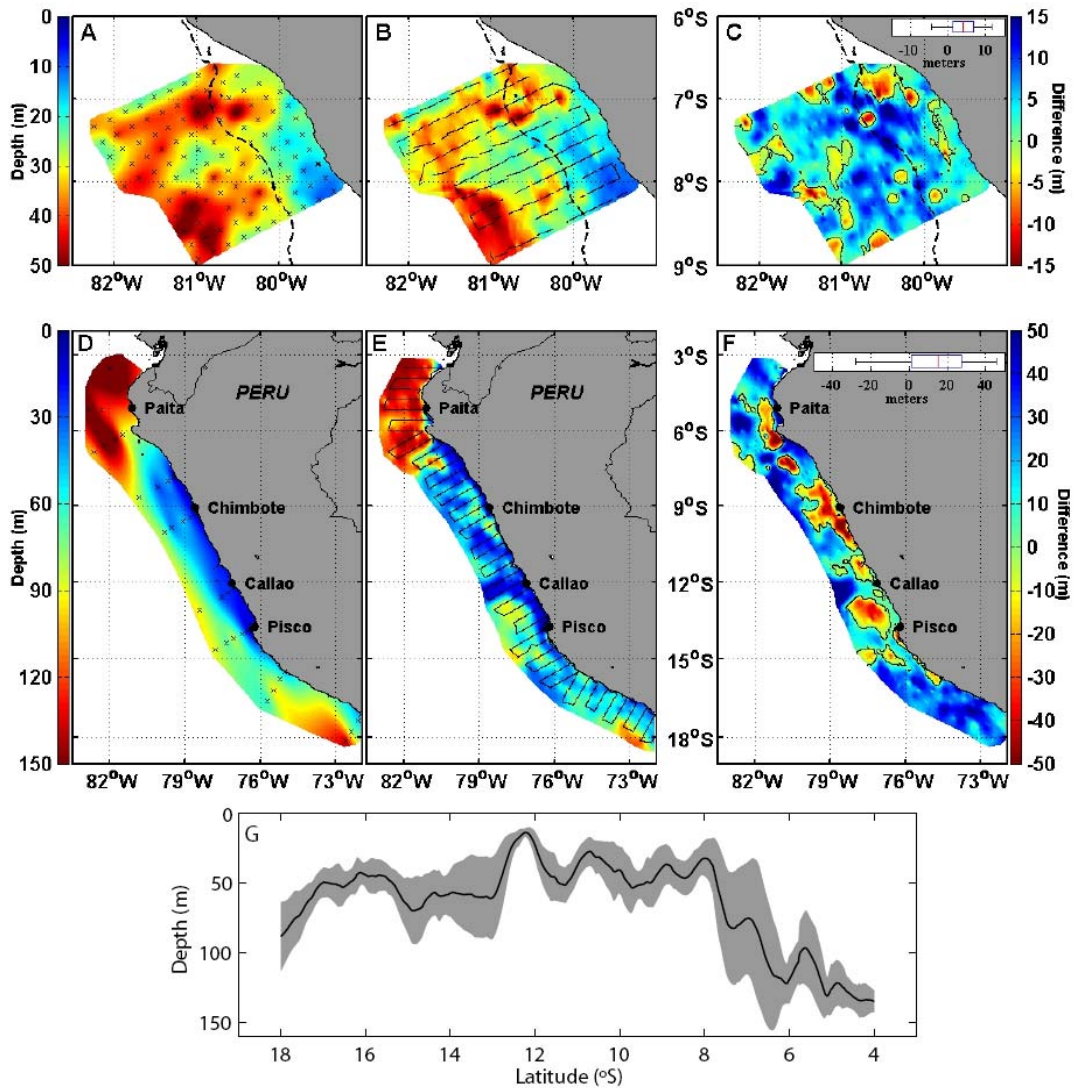


Figure 3.4 Correlation slope between  $Z_{VEEC}$  averaged over the 300 pings closest to the Niskin bottle profile and  $Z_{0.8}$  during the routine ‘Pelagic 2005’ acoustic survey (solid line). The dotted line indicates the 1/1 slope.



*Figure 3.5 Spatial distribution of the upper OMZ depth. Upper OMZ depth estimated from  $Z_{0.8}$  determined from CTDO measurements (A) and Niskin bottles profiles (D) and ZVEEC estimated from acoustic measurements (B, E). Black crosses indicate the position of hydrographic stations (A, D) whereas black lines indicate acoustic tracks (B, E). C and F differences between  $Z_{0.8}$  and ZVEEC; black contours correspond to a null difference; boxplots of the differences are displayed on the upper right part of (C) and (F). Upper panel (A, B, C) corresponds to the ‘Filamentos 2008’ survey; dotted lines indicate the depth of the 200 m bottom depth. Lower panel (D, E, F) corresponds to the ‘Pelagic 2005’ survey. Left colour-bars correspond to figures (A, B, D, E) while right colour-bars correspond to figures (C, F). G. Meridional variation of ZVEEC averaged between the coast and 200 km offshore during the ‘Pelagic 2005’ survey (black solid line) and corresponding  $\pm$  one standard deviation (grey shaded area).*

These results show that  $Z_{VEEC}$  estimated from acoustic data is a robust proxy of the lower oxycline depth - upper limit of the OMZ. Spatially interpolated maps of the upper OMZ as estimated from  $Z_{VEEC}$  are very consistent with those obtained from DO profiles (Fig. 3.5) with a mean difference lower than 5 m for the ‘Filamentos 2008’ survey (Fig. 3.5C). Again, since the use of Niskin bottles (7 discrete levels on the first 150 m of the

water column) only provides a rough estimation of  $Z_{0.8}$ , this mean difference is increased for the '*Pelagic 2005*' survey.

Our method provides high resolution spatial maps of the vertical limit of the oxygenated habitat (Figs. 3.5B, 3.5E) which allow estimating the available volume for organism habitat. We applied this to the Peruvian anchovy (*Engraulis ringens*) whose horizontal distribution is limited by the offshore extension of the upwelled cold coastal water and its mixing with adjacent water masses (Bertrand et al., 2004b; Swarzman et al., 2008). Anchovy volume of habitat can thus be estimated by integrating  $Z_{VEEC}$  over the horizontal area occupied by these water masses, and determined accordingly to Swarzman et al. (2008). Using this approach we estimated the available volume of anchovy habitat to be 9187 km<sup>3</sup> along the Peruvian coast during the '*Pelagic 2005*' survey (Fig. 3.6A). Thus, by applying this methodology to any acoustic survey, we are now able to describe the patterns of variability of this volume of habitat at different spatial scales.

During the '*Pelagic 2005*' survey, the upper limit of the OMZ exhibited large-scale meridional fluctuations varying from a local maximum of ~70-80 m south of 17°S, to an average value of ~50 m between 16°S and 8°S, and progressively deepened northward to reach 140 m at 4°S (Figs. 3.5E,G, 3.6A). These patterns agree well with previous estimates based on historical CTD casts (Fuenzalida et al., 2009). Cross-shore large-scale variations are also observed, with minimum  $Z_{VEEC}$  values in coastal regions where upwelling takes place and deeper ZMO in the offshore ocean (Figs. 3.5B, 3.5E), in agreement with Fuenzalida et al. (2009).

Superimposed to these large-scale patterns, mesoscale features of few tens of kilometres can be easily identified from  $Z_{VEEC}$  measurements. For instance, during '*Pelagic 2005*' survey eddy-like mesoscale structures were centred at 18°S-73°W and 14°S-77°W (Figs. 3.5E, 3.6A). Mesoscale structures observed from  $Z_{VEEC}$  fit well with those observed from satellite data. For instance, during the '*Pelagic 2005*' survey, the region of shallower  $Z_{VEEC}$  values (~15 m depth) perpendicular to the coast at 12°S-13°S (Fig. 3.5E,G) corresponds to a filament associated with strong westward geostrophic currents and high chlorophyll-a concentration (Fig. 3.6B,C).

Furthermore, the upper limit of the OMZ shows typical high-frequency variations of a few kilometres such as around 7°S (Figs. 3.5B, 3.5E). These submesoscale features are clearly observed along cross-shore acoustic transects (Fig. 3.6D,F) and this high-frequency and small-scale variability was confirmed using wavelet analyses. As an illustration, the wavelet analysis of  $Z_{VEEC}$  along a cross-shore transect realized south of Pisco during '*Pelagic 2005*' survey showed significant scales of 3 km very close to the coast and between ~60-70 km from the coast and a dominant ~10 km scale is observed all along this particular transect (Fig. 3.6E).

Thus, compared with conventional methods, the spatial resolution of the upper limit of the OMZ is drastically increased using acoustic data. For example,  $Z_{VEEC}$  acquired at a frequency of one ping per second corresponds to a ~5 m resolution along the vessel track for a cruising speed of 10 knots. Ground truth measurements from DO sensors however will always be needed to validate acoustic estimation and access to the whole DO vertical structure.

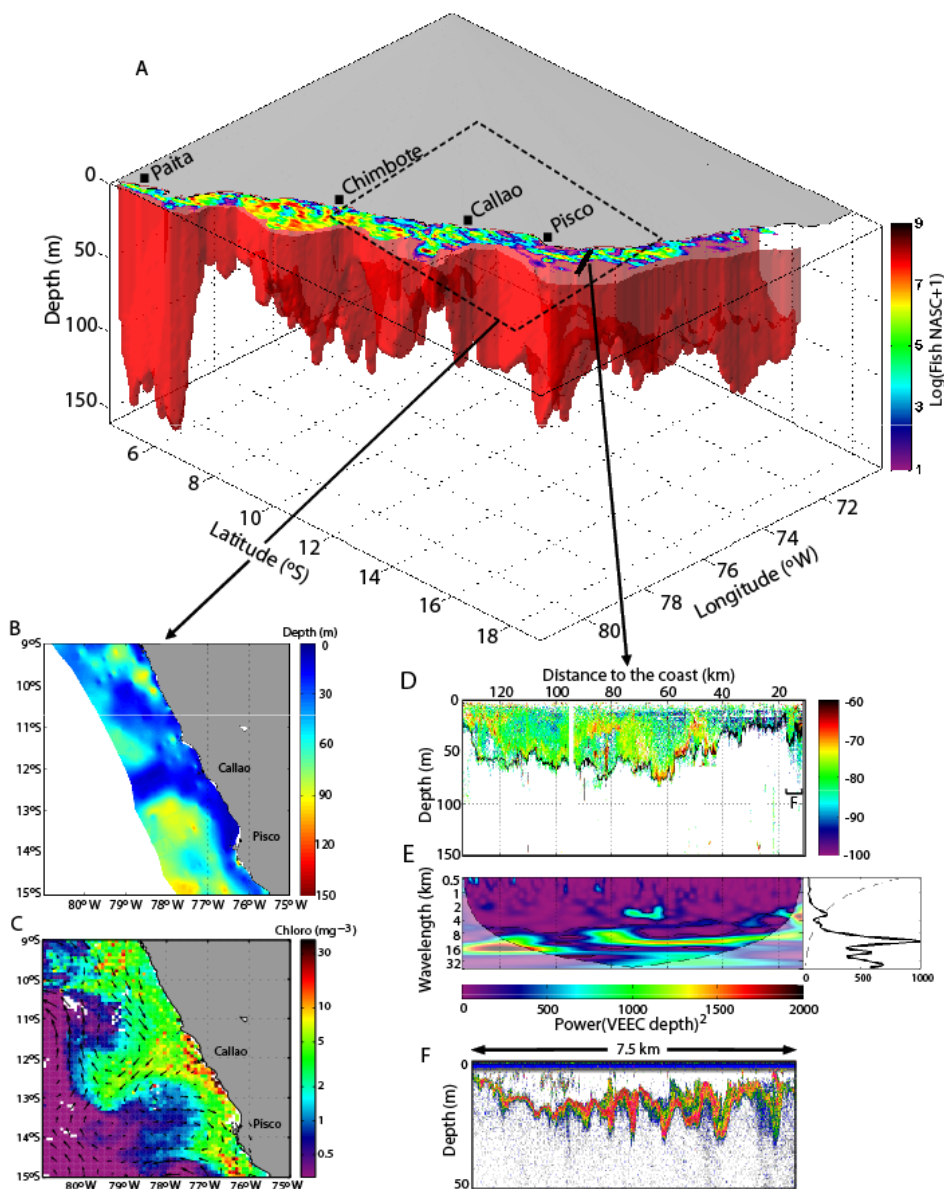


*Figure 3.6 Volume of anchovy habitat along the Peruvian coast. A. Volume (red volume) estimated by integrating ZVEEC over the area occupied by the cold coastal water and its mixing with adjacent water masses during 'Pelagic 2005' survey. The upper part of the volume shows anchovy distribution estimated during the same survey (see Supplementary Information). B. Zoom of the study area between 9°S and 15°S (black dotted rectangle) showing a region of shallower ZVEEC. This region corresponds to a mesoscale filament associated with strong westward geostrophic currents and high chlorophyll concentration as observed from geostrophic currents (black quivers) from satellite altimetry AVISO product and chlorophyll-a concentration (colours, in  $\text{mg m}^{-3}$ ) from satellite SeaWiFS data for the same time period (C). The black solid line south of Pisco in (A) corresponds to the transect presented in (D) showing the echogram and the ZVEEC (black solid line) along this transect. E. Wavelet power spectrum (in  $\text{m}^2$ ) of ZVEEC in this transect showing the presence of mesoscale ( $\geq 10 \text{ km}$ ) and submesoscale (F) Features.*

### 3.4 Discussion

Based on acoustic observations, our method allows for a precise determination of the upper limit of the OMZ with high spatiotemporal resolution. This estimated boundary ( $0.8 \text{ mL L}^{-1}$ ) was not affected by the diel changes in the species composition of the epipelagic community (nocturnal addition of migratory, adapted to hypoxia, organisms). Furthermore, this boundary did not seem to be affected by the distinct species composition of the inshore and offshore community (Bertrand et al., 2004b; Ayón et al., 2008a). These results suggest that when migratory and non-migratory species are distributed in the shallow near-surface layer (night situation); they share the same vertical range. They further suggest that the  $Z_{VEEC}$  can be defined regardless of the changes on species composition of the community.

The information provided by this study can be used for various scientific applications. For instance, according to the habitat-based hypothesis (Bertrand et al., 2008a; Bertrand et al., 2003), variations in the range of habitats constrain the extension-contraction of fish distribution and determine their abundance if favourable or unfavourable conditions last long enough to influence their population dynamics. A decrease in the vertical range of habitats can exclude species from a region and/or dramatically modify predator-prey relationships (Prince and Goodyear, 2006; Vaquer-Sunyer and Duarte, 2008; Keister et al., 2000; Taylor and Rand, 2003). Organisms intolerant to anoxia could form dense aggregations above the oxycline, while resistant species would have access to an extended refuge area. Monitoring the volume and characteristics of the 3D habitat of pelagic resources is thus crucial to better understand their population dynamics. We applied our method to the world most exploited fish species, the Peruvian anchovy and estimated its available volume of anchovy habitat for a specific survey (Fig. 3.6A). One might notice that the biomass of anchovy is not necessarily correlated with  $Z_{VEEC}$ , possibly because a deepened OMZ does not necessarily mean improved foraging efficiency. Rather, a shallow OMZ would concentrate plankton for foraging fish (Manriquez et al., 2009). Applying this method to historical and future acoustic surveys will allow reconstruct time series of volume of habitat and studying the impact of habitat volume dynamics on anchovy patterns of abundance and distribution at multiple scales.

This method allows performing integrated studies since acoustic data also provides information on most ecosystem components (see Fig. 3.6A for anchovy distribution) within and outside this volume, to which we can add ancillary information (satellite data, vessel monitoring system, top predator tagging, etc.). Such integrated approaches are crucial to implement the ecosystem approach to fisheries (Pikitch et al., 2004). Our methodology can also be applied to other ecosystems, e.g. oceanic dead zones<sup>2</sup>, and opens new perspectives for comprehensive multiscale studies on the impact of physical forcing on organisms.

Physical forcing at meso- and submesoscales is increasingly suspected to play a fundamental role in the structuring and functioning of marine ecosystems (Bertrand et al., 2008b; Thomas et al., 2008). However, instrumental sampling and present computational resolution limit the degree to which the impact of physical dynamics on living marine resources can be studied at these scales. The proposed method based on acoustic data allows for the resolving of a large range of meso- and submesoscale structures such as eddies, fronts, filaments and internal waves (Fig. 3.6 B,D,F). Scale

patterns described in high-resolution local models of eastern boundary currents (Capet et al., 2008; McWilliams et al., 2009) can now be documented from acoustic measurements.

In conclusion, the proposed method (i) allows for high-resolution spatial monitoring of the upper limit of the OMZ, a parameter especially relevant for physical, biogeochemical and biological processes and interactions in the context of climate change; (ii) can be easily implemented on any vessel equipped with acoustic echosounders (ICES, 2007; Gutiérrez TASa, pers. com<sup>5</sup>) and (iii) allows revisiting historical acoustic data for the reconstruction of spatiotemporal dynamics of the upper limit of the OMZ. This method should be applied not only in areas already known to encompass an OMZ (e.g. Eastern tropical North Pacific, Arabian Sea) but also, before fish kills were noted, in systems where hypoxia/anoxia has been apparently increasing and affecting organisms (e.g. Oregon, Chan et al., 2008).

---

<sup>5</sup> Main Peruvian commercial fishing companies are testing this method to monitor continuously the vertical extent of the epipelagic habitat (M. Gutiérrez, Tecnología de Alimentos, S.A., Peru, pers. com.)

## *Chapter 4*

### *Is there enough macrozooplankton to feed the anchovy population?*

#### **4.1 Introduction**

In ecosystem-based fishery management, target species must be managed in the context of the overall state of the system. There is thus a need to go beyond the target species and include other components of the marine environment (Pikitch et al., 2004), e.g. zooplankton. The lack of information on zooplankton limits our system understanding. Zooplankton play a key role as consumers of primary production and as prey. Indeed, zooplankton is the main prey of mesopelagic and forage fishes. In most cases, zooplankton abundance and distribution are assessed by net sampling<sup>6</sup>, which provides data discrete in space and time. Thus, due to zooplankton patchiness (Haury et al., 1978), no reliable estimation of zooplankton biomass is available at a high spatial resolution in both the horizontal and vertical plane. This drawback may be critical, as this information is required to validate biogeochemical models, adjust trophic models, study predator-prey relationships, and, more generally, to understand how the ecosystem functions. This lack of data particularly hampers research in the most productive region in the world in terms of fish (Chavez et al., 2008), the Northern Humboldt Current System (NHCS), off Peru. This system apparently produces enough macrozooplankton (mainly euphausiids and copepods) to feed the vast anchoveta or sardine populations (Espinoza and Bertrand, 2008; Espinoza et al., 2009). Yet surprisingly, the NHCS does not have a substantially higher primary production than that of other upwelling systems (Carr, 2002; Patti et al., 2008). Most zooplankton species in the NHCS are affected by the presence of the oxygen minimum zone (OMZ) which limits the range of vertical migration of organisms intolerant to anoxia (Crales-Hernandez et al., 2008). However, in the NHCS the bulk of zooplankton biomass has the ability to migrate vertically across the oxycline (Escribano et al., 2009). This behaviour affects biomass estimation because organisms can migrate far deeper than the classic range of vertical net samples. It is therefore critical to increase knowledge on zooplankton patterns of abundance and distribution taking into account the OMZ.

##### **4.1.1 Adding one more link to the anchovy food chain**

The first trophodynamic studies on anchoveta in Peru concluded that anchovy's main prey was phytoplankton (Rojas, 1953; Rojas de Mendiola, 1969). In upwelling areas, phytoplankters are larger than in oceanic region and can form colonies that increase their size as a food particle (Ryther, 1969). It was suggested that anchovy and sardine have gill rakers adapted for removing efficiently the larger species of phytoplankton (Ryther, 1969). The ability of clupeoids to feed at low trophic levels (directly on primary producers) was suggested as the reason why such large populations, biomasses

<sup>6</sup> Zooplankton can be assessed using a continuous plankton recorder providing a 1D data on patterns of zooplankton distribution (e.g. John et al., 2001).

and fisheries could be sustained in upwelling systems (Ryther, 1969). Later studies suggested that in addition to filter-feeding on phytoplankton, anchovy could also particulate feed on zooplankton (Rojas de Mendiola, 1989; Alamo, 1989), and zooplankton was sometimes considered as important as phytoplankton in anchovy diets (Alamo, 1989; Pauly et al., 1989; Jahncke et al., 2004). With the exception of Konchina (1991), who suggested that anchovy preferentially consume zooplankton, all other studies, carried out during the 1990s and early 2000s, concluded that anchovy depends mainly on phytoplankton (Alamo et al., 1996a,b, 1997a,b; Alamo and Espinoza, 1998; Espinoza et al., 1998a,b, 1999, 2000).

Recently, however, Espinoza and Bertrand (2008) have drawn attention to the fact that the apparent dominance of phytoplankton in anchovy diet is an artefact of the method employed, which is based on counts of anchovy prey. This method is considered inadequate for estimating dietary importance (James, 1987; Konchina and Pavlov, 1995). In contrast, methods based on prey weight (e.g. gravimetric) or on nutritional value (e.g. carbon content, caloric or energetic value) may be more ecologically relevant (Hyslop, 1980; Koslow, 1981; James, 1987; Konchina and Pavlov, 1995; van der Lingen et al., 2009).

According to Espinoza and Bertrand (2008), when counting anchovy prey, phytoplankton dominates anchovy diet and represents 99.5% of all ingested prey. When prey carbon content is considered, however, zooplankton becomes the dominant prey and contributes 98% of dietary carbon, whilst phytoplankton contributes only 2% (Espinoza and Bertrand, 2008). These authors also found that among zooplankters, macrozooplankton, particularly euphausiids (67.5%) and copepods (26.3%), were the dominant preys. In other upwelling systems, zooplankton, rather than phytoplankton, is also the main prey of clupeoid populations (e.g. Koslow, 1981; James, 1987; James and Chiappa-Carrara, 1990; Chiappa-Carrara and Gallardo-Cabello, 1993; van der Lingen et al., 2006, 2009).

These new findings on the diet of anchovy and sardine are in agreement with the apparent bottom-up control of zooplankton on anchovy (Ayón et al., 2008b) and highlight the importance of estimating the zooplankton biomass in the NHCS, in particular that of macrozooplankton. However, they call in question the current knowledge on macrozooplankton abundance and give rise to this crucial question: *Is there enough zooplankton to feed the anchovy population?*

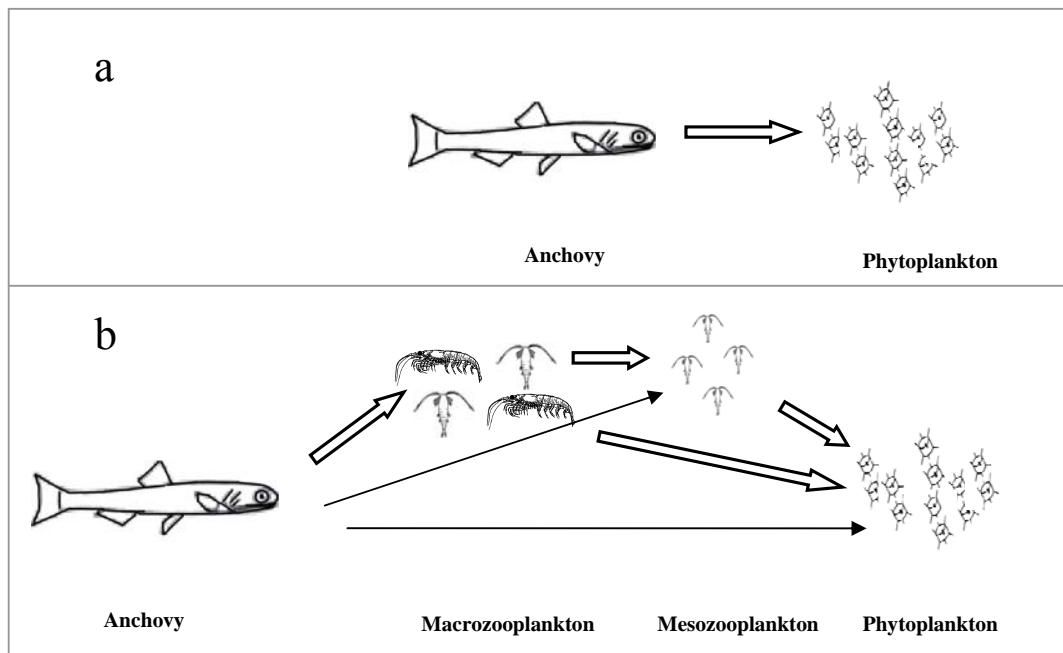


Figure 4.1 (a) Two step anchovy trophic chain as suggested by Ryther (1969) and (b) actual anchovy trophic web (Konchna, 1991; Espinoza and Bertrand, 2008). The arrows represent the main source of carbon for organisms.

#### 4.1.2 Macrozooplankton biomass estimation in the NHCS

In the NHCS, net sampling has been the primary tool for collecting zooplankton (Ayón et al., 2008a), with the exception of Gutiérrez et al. (2008) and Bertrand et al. (2008a), who used acoustics to study the interaction between anchovy, munida and macrozooplankton. In the HCS, net samplings have allowed studying a wide range of basic zooplankton biological aspects that would not be possible with other sampling techniques. Some examples are: taxonomic description (Santander et al., 1981), species composition (Castillo et al., 2007), species vertical migration (Escribano et al., 2009) and ontogenetic distribution (Escribano et al., 2009; Criales-Hernández et al., 2008). Also, because of a continuous net sampling program, which began in 1964 (Table 4.1), long-term zooplankton series have allowed the study of both short- and long-term zooplankton variability in relation to predation (Ayón et al., 2008b), El Niño (Arones et al., 2009) or anchovy-sardine regime shift (Alheit and Ñiquen, 2004).

However, because of zooplankton net avoidance (Debby et al., 2004; Fleminger and Clutter, 1965; Lawson et al., 2008; Brinton, 1967), net sampling presents great shortcomings when estimating abundance, especially of macrozooplankton such as euphausiids. Although underestimated by net sampling, euphausiids have been ranked as the second most abundant (in number) species of the system, after copepods (Ayón et al., 2008a). Since fish feeding does not depend on prey number but on prey biomass (Espinoza and Bertrand, 2008), on account of their larger size, euphausiids are probably the most important (in terms of biomass) zooplankton group of the system. According to Antezana (2002) the most abundant euphausiid species, *Euphausia mucronata*, could make up 50% of the total zooplankton biomass in the HCS.

*Table. 4.1 Summary of the main types of regular zooplankton sampling surveys off Peru. Source: Ayón et al. (2008a).*

Program	Method	Comment
Hensen Net Program	Hensen net (330 µm mesh, 60 cm diameter), towed vertically from 50 m depth to the surface. Determination of zooplankton settlement volume. → Additional oblique bongo hauls (330 µm mesh, 60 cm diameter) from 200 m depth to surface.	Several times per year since 1964, hundreds of stations located over the whole marine area off Peru.
Fixed Coastal Stations Program	WP2 net (330 µm mesh, 50 cm diameter), horizontal subsurface tows. → Since 2004, oblique bongo net samples have been regularly taken at the Fixed Coastal Stations (330 µm mesh, 60 cm diameter for the Callao transect, 330 µm mesh and 22 cm diameter for Paita and San José transects) from 200 m to the surface or from the bottom to the surface.	Bimonthly since 1994. Stations located on three transects perpendicular to the coast off Paita, San José, and Callao.
Intensive Cruises Program (CRIOS)	Experiments for secondary production and grazing, Multinet (330 µm mesh), WP2 net (330 µm mesh) oblique bongo net sampling, laser optical plankton counter.	Twice a year since 2005. Stations located on three transects off Callao and inside Bahía de Independencia. Started in the context of the CENSOR project.

Because of its non-invasive character, acoustics can sample organisms that would be missed by net sampling. Since the 1980s, acoustics has become the main sampling technique for estimating the abundance of euphausiids in the Antarctic (Watkins and Brierley, 2002). In standard protocols, acoustics is used to discriminate Antarctic krill from other targets and to estimate its density and biomass (Watkins and Brierley, 2002). Once the question of target identification is resolved, acoustic sampling does not only provide biomass estimation but it also allows describing its spatiotemporal patterns of distribution and other aspects of zooplankton natural history that would be difficult or impossible to investigate with direct sampling techniques. For instance, predator-prey relationships, changes in swarm dimensions, shape and density can be informed by acoustics (Mathisen and Macaulay, 1983). Also, the presence of high density patches near the bottom or in submarine canyons might be missed by net sampling but not by acoustics (Greene et al., 1988). Nevertheless, despite its advantages, acoustics has rarely been used in the upwelling systems to study zooplankton patterns of distribution or estimate zooplankton biomass.

We hypothesize that, in the NHCS, macrozooplankton biomass must be substantially higher than previously reported. To test for that we applied the acoustic method detailed in Chapters 2 and 3 for estimating macrozooplankton biomass of the epipelagic community. The results will be compared with estimates from the same and other upwelling and highly productive systems and discussed with regard to the unique properties of the NHCS.

## 4.2 Materials and Method

### 4.2.1 Data

Acoustic data were obtained from two pelagic surveys performed along the Peruvian coast onboard the R/V Olaya from IMARPE in austral summer and spring 2005 (Table 4.2). Only data recorded southern than 6° S were considered in this study (to focus on the NHCS and not on the tropical ecosystem that extends from Northern Peru). Acoustic data were collected with a 38 and 120 kHz Simrad EK500 split-beam, scientific echosounder system (Kongsberg Simrad AS, Kongsberg, Norway). Echosounder calibration was performed according to Foote et al. (1987). Zooplankton samples were taken with Hensen nets of 0.33 m<sup>2</sup> mouth area and 300 µm mesh, by vertical hauls between 50 and 0 m (see Ayón et al., 2004 for more information).

Data were classified according to diel period, ecological domain, distance to the shelf break and latitudinal location.

#### 4.2.1.1 Diel patterns of macrozooplankton distribution

Diel vertical migration is a common trait of zooplankton and nekton and its effects can be perceived at almost all spatial scales (see Strommel diagram in Haury et al., 1978). The diel vertical migration of macrozooplankton affects biomass, density and size estimation because some species can migrate beyond the range of the acoustic sample. Thus day and night data were processed independently. To focus only on day and night periods, data belonging to the twilights were eliminated. The selection of the twilight period was made according to the position and the ephemerides. To ensure working with actual day or night data (and avoid any possibility to mix twilight periods with day or night periods) ephemerides' twilight periods were extended of about 15 minutes in each side.

#### 4.2.1.2 Across-shore macrozooplankton distribution

##### *Ecological domain*

Zooplankton species composition and biomass change with distance to the shore (see Samaeto, 1981 and Ayón et al., 2008a for the NHCS). Different zooplankton communities have been related to three main ecological domains: the shelf, the slope and the oceanic domain (Santander, 1981). We used these three ecological domains as a first attend to take into account the across-shore macrozooplankton distribution. The shelf break, the steepening of the gradient between the continental shelf and the continental slope, was visually determined from the bottom profiles of each acoustic transect. The shelf domain was then defined as the sea bed region comprised between the coast line and the shelf break. The slope was defined as the sea bed region comprised between the shelf break and the 2000 m isobaths, while offshore domain was defined as the region beyond the 2000 m isobaths.

##### *Macrozooplankton distribution in regards with the shelf break*

The coast line is usually used as reference line to assess the across-shore organism distribution. Higher abundance in a close/far location to the coast could indirectly indicate habitat preference (i.e., munida and anchovy in Gutiérrez et al., 2008). However, zooplankton patchiness is mainly the result from the interaction of water

circulation, bathymetric features and zooplankton diel vertical migration (Lavoie et al., 2000; Lu et al., 2003; Cotté and Simard, 2005). The distribution of many macrozooplankton species, in particular euphausiids, is closely related with the shelf break (Lu et al., 2003; Cotté and Simard, 2005; Nicol, 2006). The shelf break also influences the ontogenetic horizontal distribution of many euphausiids (Lu et al., 2003; Nicol, 2006). Thus it seems better to use the shelf break as a reference line to assess the across-shore distribution of zooplankton, in particular if there is a high variation of the shelf extension, as is the case of the Peruvian shelf.

#### **4.2.1.3 Along-shore macrozooplankton distribution**

It has been reported that zooplankton community differs in relation to latitude; higher abundances in the northern and southern parts of NHCS have been reported as a common pattern of zooplankton distribution (Ayón et al., 2008a). To take into account the along-shore distribution of zooplankton we classified the acoustic data by latitudinal degree.

#### **4.2.2 Data analysis**

- ***Acoustic estimation of macrozooplankton mean size density and biomass***

The estimation of macrozooplankton biomass was performed as follow:

- (i) we reduced the echograms (fluid-like, fish and blue noise) by calculating the median value for every three pings;
- (ii) using these “reduced echograms” we estimated ZVEEC according to the procedure described before (see Chapter 3) and used it to delimit the epipelagic layer;
- (iii) we estimated the mean fluid-like biovolume and size of the macrozooplankton contained within the epipelagic layer. From this step, an elementary acoustic cell is 3 pings long and has a height equal to ZVEEC. Since each elementary acoustic cell of an echogram was assigned to a sole scatter group according to the properties of the dominant echoes composing it, weak scatters would be ‘hidden’ when strong scatters were present in the same elementary acoustic unit. Thus, if fluid-like was present together with fish, the later would dominate and it would not be possible to detect the presence of fluid-like (Korneliussen and Ona, 2003). To reduce this bias, the mean fluid-like biovolume and size were estimated without including the cells assigned to other scatters groups;
- (iv) fluid-like mean density in wet weight ( $WW$ , in  $\text{g} \cdot \text{m}^{-3}$ ) was estimated according to functional regression equations between these variables and fluid-like biovolume (Wiebe et al., 1975; Wiebe, 1988):

$$\text{Log}(Bv) = 0.139 + 1.003 * \text{Log}(WW) \quad \text{Eq. (4.1)}$$

where  $Bv$  is the fluid-like mean biovolume (in  $\text{cm}^3 \cdot \text{m}^{-3}$ ) in the epipelagic layer.

- (v) the integrated macrozooplankton biomass of the epipelagic community per elementary sampling unit was then estimated by multiplying their mean density by  $Z_{VEEC}$ .

---

The total acoustic biomass (in  $\text{g.m}^{-2}$ ) was estimated as the weighted mean of the biomass from the three ecological domains. We used the areas of shelf, slope and offshore domains as weightings values to estimate the weighted mean biomass.

To compare acoustic with net sampling we also converted net sampling zooplankton biovolume into wet-weight by applying the Equation 4.1.

- *Statistical analyses*

For each diel period, broad patterns of macrozooplankton distribution according to the ecological domain, distance to the shelf break (every 10 km interval) and latitude were represented using box-plot. When exploring the latitudinal pattern of macrozooplankton distribution, box-plots were first constructed according to latitudinal position only. Then to dismiss a possible overrepresentation of any ecological domain in the broad pattern of macrozooplankton latitudinal distribution, additional latitudinal box-plots for each ecological domain were constructed.

We used box-plot as a tool to explore data behaviour. Box-plot is a graphical method for displaying the median, the upper and lower quartiles, and the minimum and maximum data values. The area between the upper and lower quartiles is known as the inter-quartile range and gives the extension of the middle 50% of the data. Since the inter-quartile range is not affected by outliers or extreme values, it is the most appropriate range for interpretation and gives a less biased visualization of the data spread. The extension of upper whiskers was calculated by summing up the upper quartile with 1.5 times the inter-quartile range, while the extension of the lower whisker was calculated by subtracting 1.5 times the inter-quartile range from the lower quartile. Data values outside of the whisker range were considered outliers.

Box-plots showed that the macrozooplankton biomass data was positively skewed suggesting a non-normal distribution. Therefore we normalized the density and biomass data by applying a cubic root transformation before performing any statistical test. As preliminary exploration of the data showed that biomass and density exhibited very similar patterns, we did not present all densities patterns but provide just one example; the density distribution according to the shelf break. Since the weighted mean biomass and size included only three observations per survey (one mean value per ecological domain) we could not test for significant differences in the weighted mean according to the diel periods, nor within a survey neither between surveys. Instead, we used an ANOVA to test the diel effect within each ecological domain independently. We also applied an ANOVA with further post hoc Turkey test to assess if macrozooplankton biomass significantly differs between domains.

*Table 4.2. Acoustic survey characteristics*

<i>Survey</i>	Pelagic 2005 austral summer	Pelagic 2005 austral spring
<i>Initial End</i>	Feb. 20, 2005 - Apr. 04, 2005	Nov. 25, 2005 - Dec. 24, 2005
<i>Covered area</i>	3°29' S -18° 03' S	05°11'S -13°28' S
<i>Sampled hours</i>	600	840
<i>Echosounder system</i>	Simrad EK500	Simrad EK500
<i>Frequencies</i>	38 and 120 kHz	38 and 120 kHz
<i>Plankton Hansen sampling (nº)</i>	138	96

#### 4.2.3 Mapping the horizontal distribution of macrozooplankton

Patchiness is an ubiquitous property of zooplankton (Levin, 1992). This implies that the abundance of nearby sampling points tend to be similar because they are catching the same patch. If we chose sampling points separated by a small distance and estimate the variance only from those sampling points, low variance estimation would be expected, since all the sampling points might have comparable abundance. Conversely, if a higher distance is chosen, the variance, at that given distance, would tend to be higher as the sampling points might not longer lie in the same patch. To produce a realistic and accurate map of macrozooplankton biomass distribution, it is thus necessary to describe and include the spatial structure of the data on the kriging interpolation method.

The relation between macrozooplankton spatial structure and its variability was explored and modelled by adjusting a variogram (Matheron, 1965). A variogram decomposes the spatial variability of observed variables among distance classes. The structure function plotted as ordinate is called semi-variance ( $y$ ):

$$\gamma(h) = \frac{\sum_{x_i-x_j=h} (z_i - z_j)^2}{2.N(h)} \quad \text{Eq. (4.2)}$$

where  $h$  is the distance class,  $N$  the number of pair observations per distance class and  $(z_i - z_j)$  the difference between two data values that were separated by distance  $h$ .

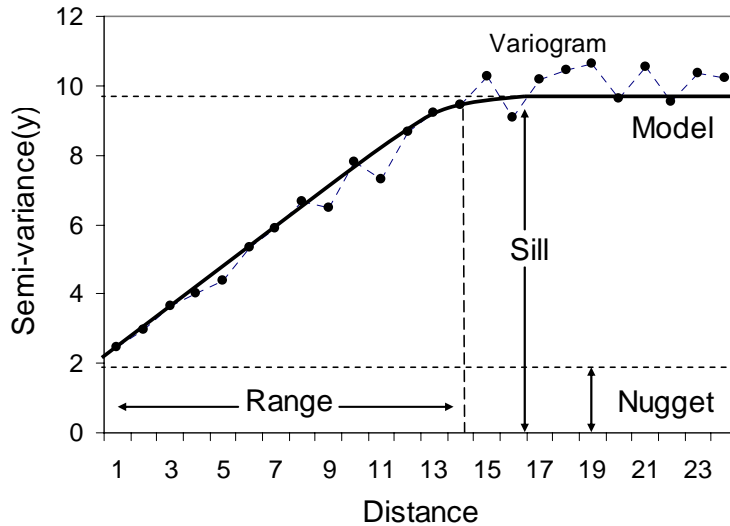


Figure 4.2 Experimental (dash line) and model (solid line) variograms and their main parameters.

The plot of the semi-variance among distance classes is called the experimental semi-variogram (and more concisely variogram). The variance tends to level off at a sill which corresponds to the variance of the variable. The distance at which the sill levels off is called the range. The range indicates the size of the structures. Beyond that distance the data is no more spatially correlated. The intercept is called the nugget effect. It corresponds to the local variation occurring at scales finer than the sampling interval or distance class (Fig. 4.2). These three parameters namely, sill, range and nugget, are the main required parameters to construct a variogram model. A variogram model is a simple mathematical function that models the trend in the experimental variogram. This model provides the variance estimation at any distance, which is required by the kriging method to interpolate and create a map. In this study we fitted a directional variogram to model the spatial structures observed from the acoustic macrozooplankton biomass data and to include this structure in the kriging interpolation method. We used directional variogram because the spatial distribution of macrozooplankton biomass was anisotropic with higher autocorrelation in the along-shore direction than in the across-shore direction. Day and night macrozooplankton biomass maps were then created for the spring and summer surveys of 2005. These maps were then compared with the corresponding plots of zooplankton biomass from net samplings. Zooplankton biomass data from net sampling was not interpolated.

To provide an example of macrozooplankton biomass with its corresponding environmental context, we complement the macrozooplankton distribution during the spring survey with additional environmental data. We created maps of the upper OMZ, water masses, sea surface temperature and chlorophyll conditions during the spring survey. The data of upper limit of the OMZ was obtained according to the method described in chapter 3 and interpolated by kriging to create a map of the Upper OMZ. Water masses were determined according to Swartzman et al. (2008) and the data was plotted along the transect tracks to create the water masses maps. Sea surface temperature and chlorophyll maps were created from available average satellite data

during February of 2005 obtained from Modis and SeaWiFS (<http://oceancolor.gsfc.nasa.gov/>) respectively.

## 4.3 Results

### 4.3.1 Diel variation in macrozooplankton biomass and size

- **Macrozooplankton Biomass**

Total macrozooplankton epipelagic biomass (wet weight) exhibited great variations according to diel cycle but were very similar between surveys (Fig. 4.3). Total nocturnal epipelagic biomass was estimated to be 114.6 and 112.4 g.m<sup>-2</sup> during 2005 austral summer and spring, respectively. These night-time estimates were about four times higher than diurnal biomasses, which were estimated to be 28.6 and 24.3 g.m<sup>-2</sup> during 2005 austral summer and spring, respectively.

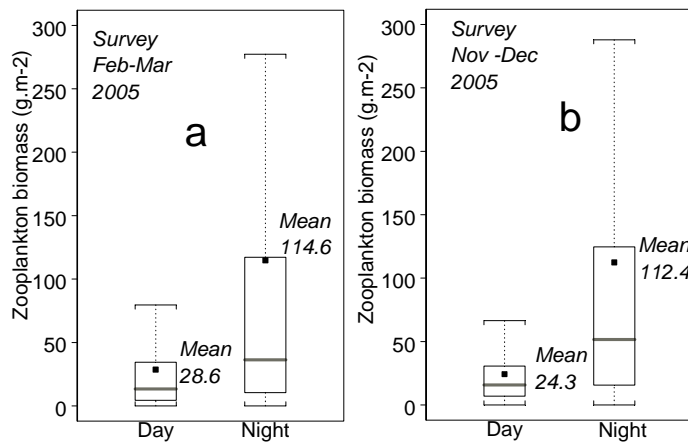


*Figure 4.3 Box plot of day and night epipelagic macrozooplankton biomass (g.m<sup>-2</sup>) during austral summer (a) and spring (b) pelagic surveys 2005. The size of the box is determined by the upper and lower quartiles, median is indicated as a horizontal line inside the box. Weighted mean is represented as a black solid square point. The whiskers indicate the minimum and maximum values without considering outliers.*

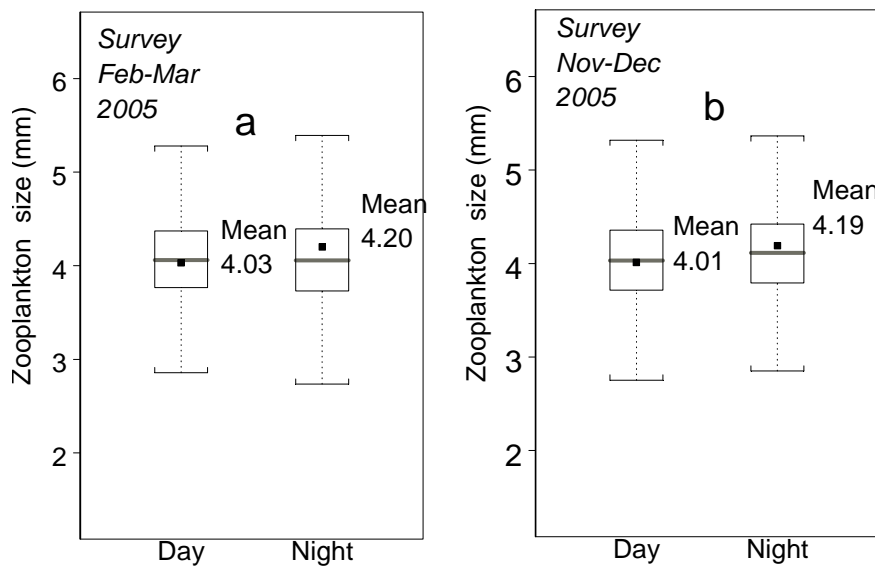


*Figure 4.4 Box plot of day and night epipelagic macrozooplankton equivalent spherical radius (mm) during Austral summer (a) and spring (b) pelagic surveys 2005 (for details on box plot see the caption of Figure 4.3).*

- **Macrozooplankton sizes**

Macrozooplankton size must be understood as the radius of the fluid sphere which is assumed to have the same volume as a “mean zooplankton organism”, it is the equivalent spherical radius or ESR. This ESR can be converted into organisms total length by empirical formulas, e.i. length = (ESR-0.095)/0.134 for euphausiids (Greenlaw, 1977); or length = (ESR-0.018)/0.181 for copepods (Pieper and Holliday, 1984).

Macrozooplankton ESR were slightly different according to diel cycle, but very similar between surveys (Fig. 4.4). In both surveys, the nocturnal macrozooplankton ESR estimate was about 5% larger than the corresponding diurnal macrozooplankton ESR estimation.

#### **4.3.2 Macrozooplankton biomass and size in relation to ecological domains**

- **Macrozooplankton biomass**

Macrozooplankton epipelagic biomass (transformed by cubic root) varied significantly with the ecological domain (Fig. 4.5) during both day (ANOVA:  $F_{[2, 115020]} = 10758.1$ ,  $p=0.0000$  for summer survey and  $F_{[2, 132416]} = 22699.5$ ,  $p=0.0000$  for spring survey) and night (ANOVA:  $F_{[2, 91995]} = 25249.8$ ,  $p=0.0000$  for summer survey and  $F_{[2, 96455]} = 18912.5$ ,  $p=0.0000$  for spring survey). In all cases, post hoc Turkey tests were significant ( $p < 0.05$ ). Macrozooplankton biomass increased across the continental shelf and slope and toward the offshore area (Fig. 4.5), regardless of the survey or the diel period considered (except during the day in Feb.-March 2005 when the biomass was slightly lower in the shelf break compared with the shelf).

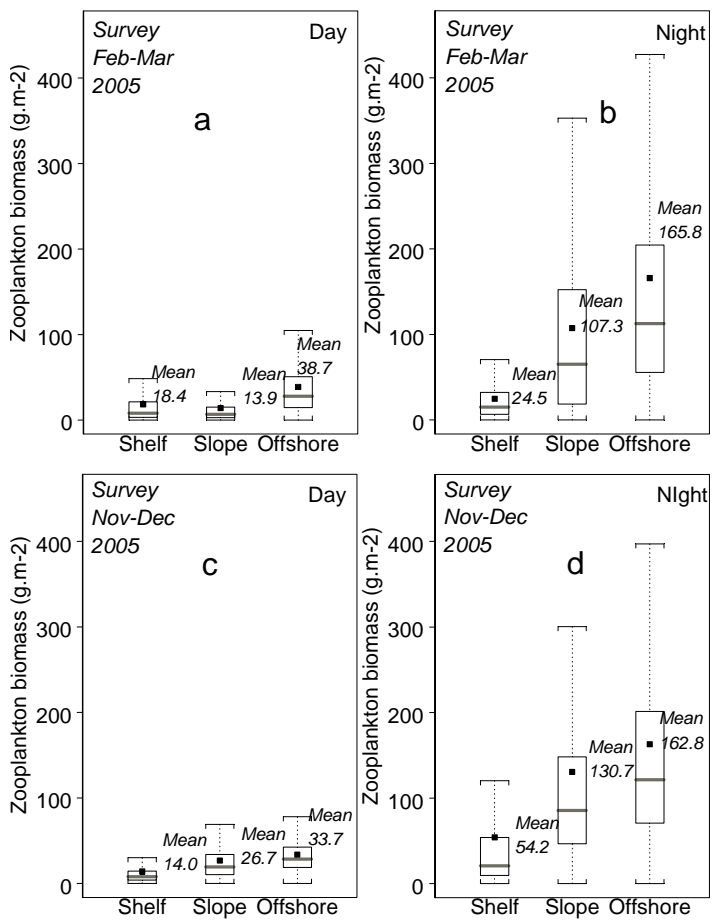


*Figure 4.5 Day and night box plots of epipelagic macrozooplankton biomass (in  $\text{g.m}^{-2}$ ) according to the shelf, slope and the offshore ecological domains for both austral summer (a,b) and spring (c,d) 2005 (for details on box plot see the caption of Figure 4.3).*

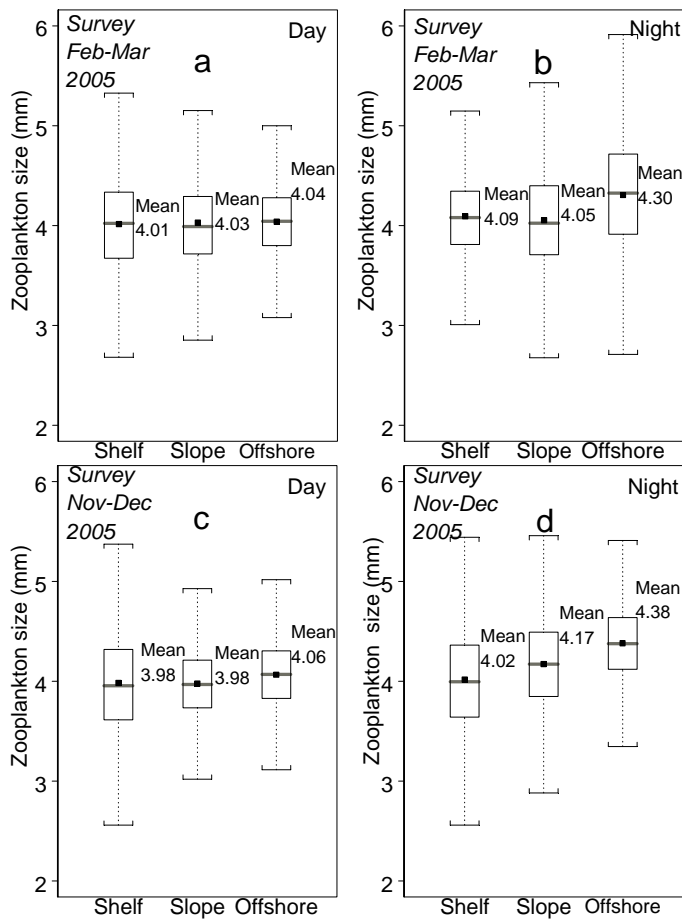


Figure 4.6 Day and night box plots of epipelagic macrozooplankton equivalent spherical radius (in mm) according to the shelf, slope and the offshore ecological domains for both austral summer (a,b) and spring (c,d) 2005 (for details on box plot see the caption of Figure 4.3).

- **Macrozooplankton sizes**

Macrozooplankton sizes across the ecological domains during the day exhibited a relatively flat pattern when compared to the corresponding estimated sizes during the night (Fig 4.6). Whatever the survey or the diel period, macrozooplankton were significantly larger offshore than in the shelf, this pattern being more pronounced during the night (Table 4.3). The size pattern of macrozooplankton distributed in the slope was variable. Compared with the shelf, the size of macrozooplankton distributed over the slope was significantly larger in spring 2005 during the night, significantly smaller in summer 2005 during the night, and not significantly different in the other cases (Fig 4.6, Table 4.3). Finally, in each survey, macrozooplankton size was significantly larger during the night than during the day and this pattern was particularly pronounced offshore (Fig 4.6, Table 4.3).

Table 4.3 Post hoc Turkey multicomparison test of mean macrozooplankton size (in mm) according to survey, diel period and ecological domain. Asterisks indicate significant difference ( $p < 0.05$ ).

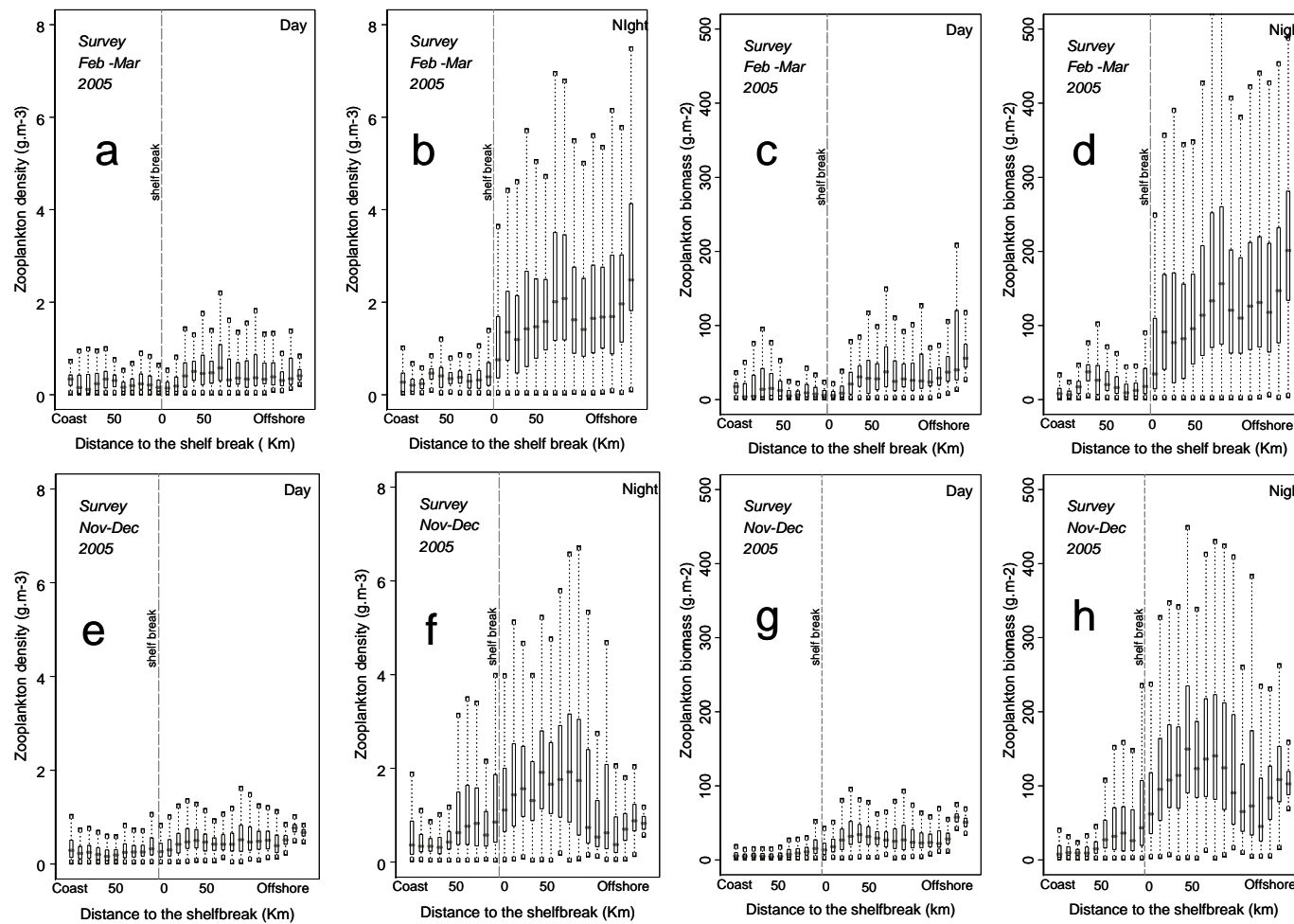
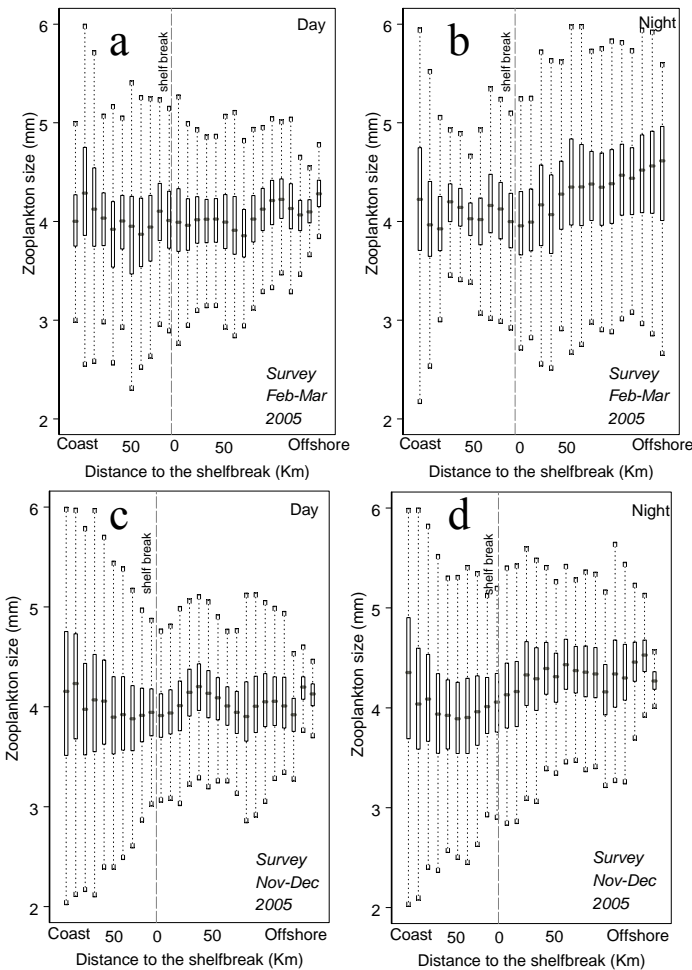


Figure 4.7. Day and night box plots of across-shore macrozooplankton density ( $\text{g.m}^{-3}$ ) and biomass ( $\text{g.m}^{-2}$ ) in relation to the shelf break for both austral summer (a,b,c and d) and spring (e,f,g and h) 2005 (for details on box plot see the caption of Figure 4.3).

### 4.3.3 Across-shore distribution of macrozooplankton density, biomass and size

- **Macrozooplankton density and biomass**

Previous results showed that macrozooplankton biomass increases from the coast toward offshore waters. A more detailed description of the across-shore distribution of macrozooplankton biomass (Fig. 4.7) illustrates the importance of the shelf break as cut-off point with higher biomasses offshore, in particular during the night. Offshore, macrozooplankton density and biomass increase with the distance to the shelf break but with a different pattern according to the survey. In the summer survey, the offshore macrozooplankton density and biomass increased with the distance to the shelf break (Fig. 4.5b, d). In contrast, during the spring survey, macrozooplankton density and biomass exhibited a bell shape pattern with the highest values around 50 km offshore the shelf break and a decreasing trend thereafter (Fig. 4.7f, h).



*Figure 4.8 Day and night box plots of across-shore macrozooplankton equivalent spherical radius (in mm) in relation to the shelf break for both austral summer (a, b) and spring (c, d) 2005. Box plot was made for every 10 km interval (for details on box plot see the caption of Figure 4.3).*

- *Macrozooplankton size*

The broad patterns in across-shore macrozooplankton size distribution presented in Figure 4.6 are described in more detail in Figure 4.8. This figure shows the high variability in macrozooplankton size at any point, probably illustrating the size-diversity of the epipelagic macrozooplankton community. The across-shore trend of increasing macrozooplankton size was clear during the night but not obvious during the day (Fig. 4.8). During the summer survey and at night, the largest sizes were observed in the furthest offshore area. During the spring survey this night-time size estimates increased until around 50 km offshore and then stabilized. Large macrozooplankton also occurred in the closest coastal areas whatever the survey and the diel period (Fig. 4.8).

#### **4.3.4 Along-shore macrozooplankton biomass distribution**

- *Macrozooplankton biomass*

Patterns of along-shore macrozooplankton biomass distribution varied according to the diel period and the survey. During the day, low macrozooplankton biomass dominated in all latitudes without exhibiting any clear along-shore pattern. During the night, higher macrozooplankton biomasses were observed in the northern and southern areas, coinciding with the area where the continental shelf was narrower (Fig. 4.9b, d). This pattern, however, was no longer held when separating the macrozooplankton data according to the shelf, slope and offshore (Appendix A, B). This revealed that the apparent along-shore pattern was an artefact of the sampling method, which did not sample the ecological domains with the same intensity (Figs. 4.11 and 4.12). As seen in these figures, because of a wider shelf in the central area off Peru, the offshore domain in this section was poorly sampled in comparison to the corresponding offshore domain of the northern and southern sections

- *Macrozooplankton sizes*

Similar along-shore distribution patterns were observed between macrozooplankton biomass and sizes, with larger sizes coinciding with high biomass and vice versa (Figs. 4.9 and 4.10).

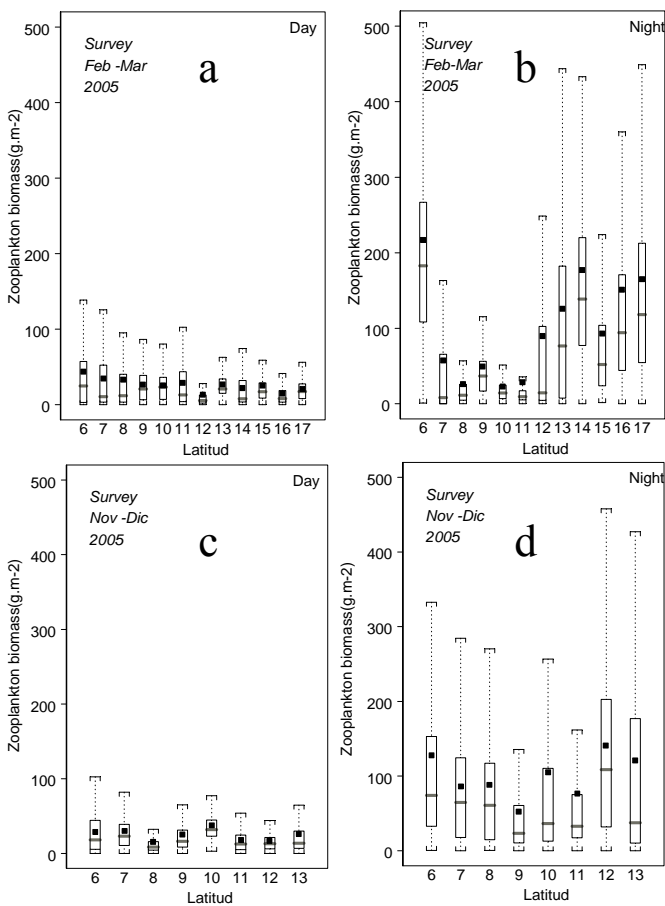
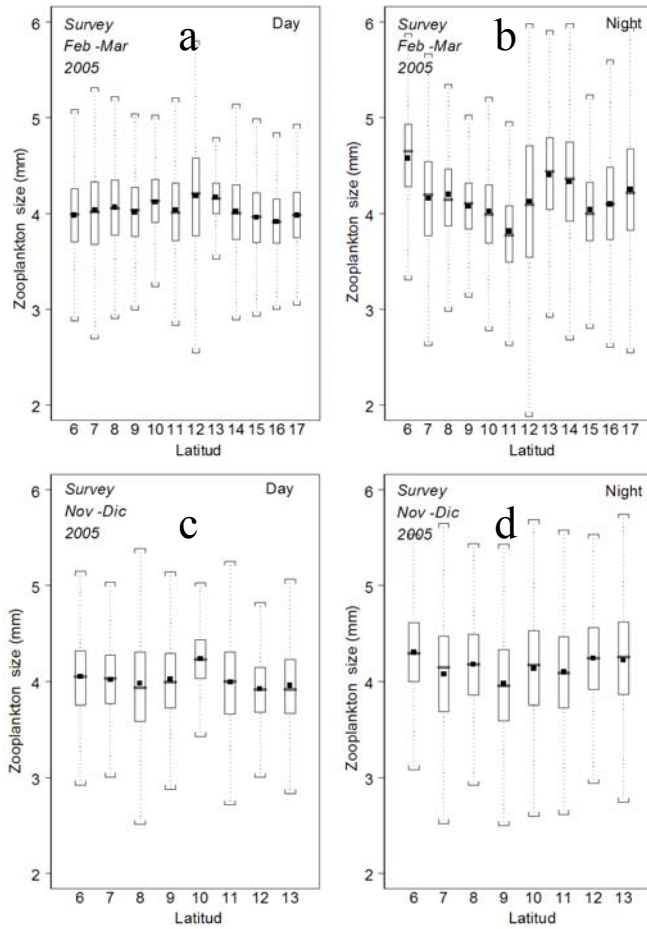


Figure 4.9 Day and night box plots of along-shore macrozooplankton biomass distribution ( $\text{g.m}^{-2}$ ) for both austral summer (a,b) and spring (c,d) pelagic surveys of 2005. Box plot were constructed by intervals of one degree of latitude (for details on box plot see the caption of Figure 4.3).



*Figure 4.10 Day and night box plots of along-shore macrozooplankton equivalent spherical radius distribution (mm) for both austral summer (a,b) and spring (c,d) pelagic surveys of 2005. Box plot were constructed by intervals of one degree of latitude (for details on box plot see the caption of Figure 4.3).*

#### 4.3.5 Macrozooplankton horizontal distribution

The maps of horizontal macrozooplankton biomass distribution constructed from acoustic and Hansen net sampling data (Figs. 4.11 and 4.12) exhibited overall similar spatial patterns. Especially the increase in zooplankton biomass toward offshore was evidenced in both data sources. This pattern was particularly noticeable during the night but also observable during the day. However, macrozooplankton from acoustics had a higher day-night biomass difference when compared to the one from net sampling, in particular in the offshore area. Also some hot spots (e.g. extreme north in austral summer 2005 and offshore at  $\sim 13^{\circ}$ S in austral spring 2005) were detected by both acoustic and net data. Since there is about three orders of magnitude more acoustic data than net-sampled data, the interpolated maps of macrozooplankton biomass from acoustics also provided far more details on macrozooplankton patchiness which could not be detected from net data. Interesting patterns emerged when comparing the 2005 summer distribution of macrozooplankton (Fig.4.11) with the corresponding distribution of the depth of the upper OMZ, the water masses, the chlorophyll-a concentration and the SST (Fig. 4.13). For instance, a jet filament in the offshore area

between 12° and 14°S that advected cold coastal water and mixed coastal water toward offshore (Fig. 4.13b) and affected the upper OMZ depth (Fig. 4.13a), chlorophyll-a concentration (Fig. 4.13c) and sea surface temperature (Fig. 4.13d), seems to also have affected macrozooplankton biomass. Low biomass was observed within the filament, while a large macrozooplankton patch was observed on the southern side of the filament (Fig. 4.11).

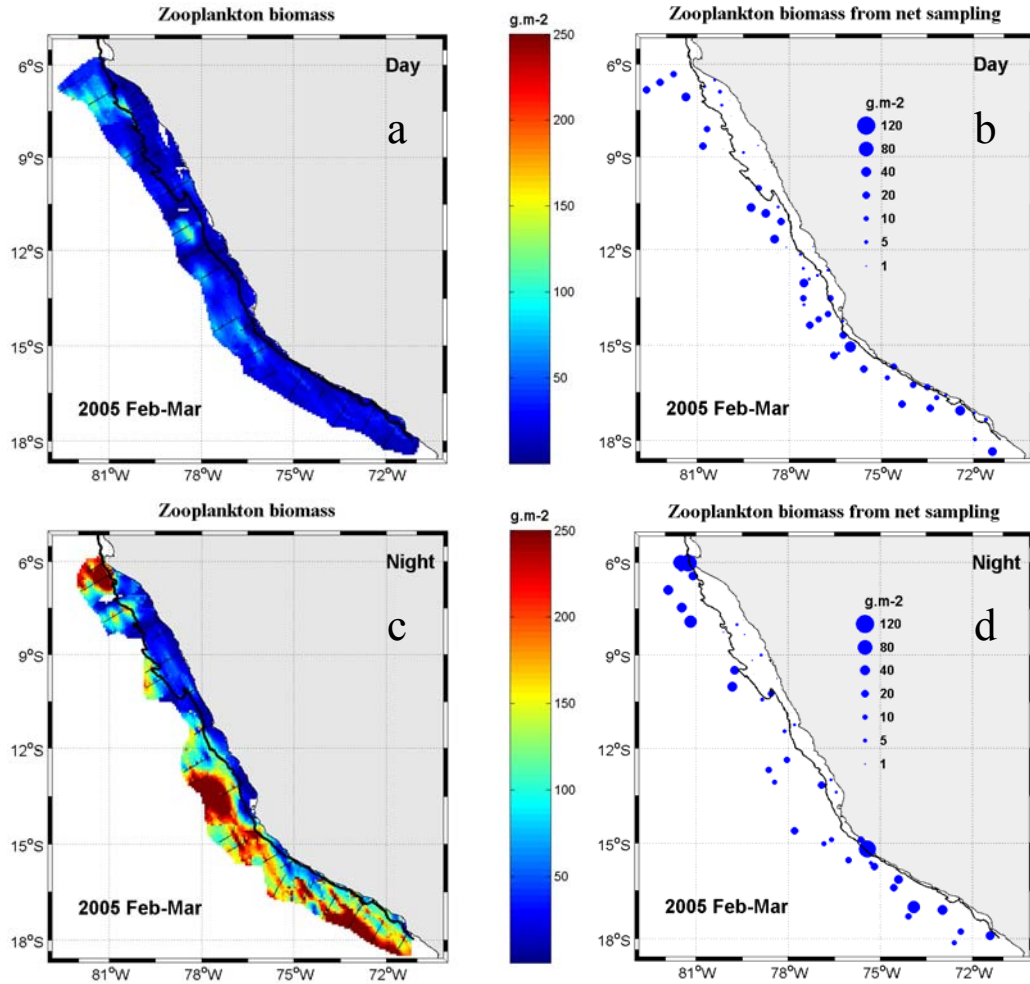


*Figure 4.11 Horizontal zooplankton biomass ( $\text{g.m}^{-2}$ ) distribution during austral summer 2005. Acoustic macrozooplankton biomass during day (a) and night (c). Zooplankton biomass from Hansen nets towed vertically from 50 m to the surface during day (b) and during night (d). The black line shows the (continental shelf limit, 200 m bottom depth).*

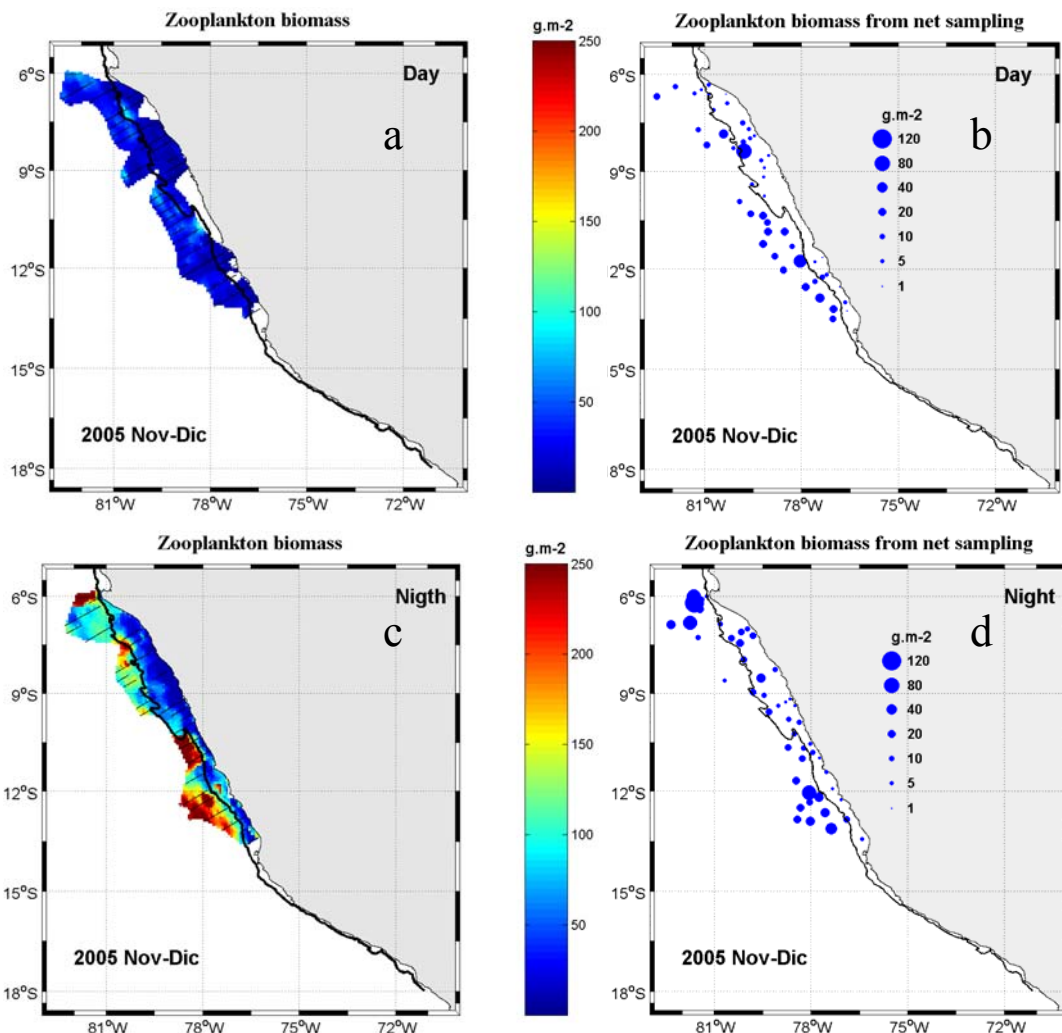
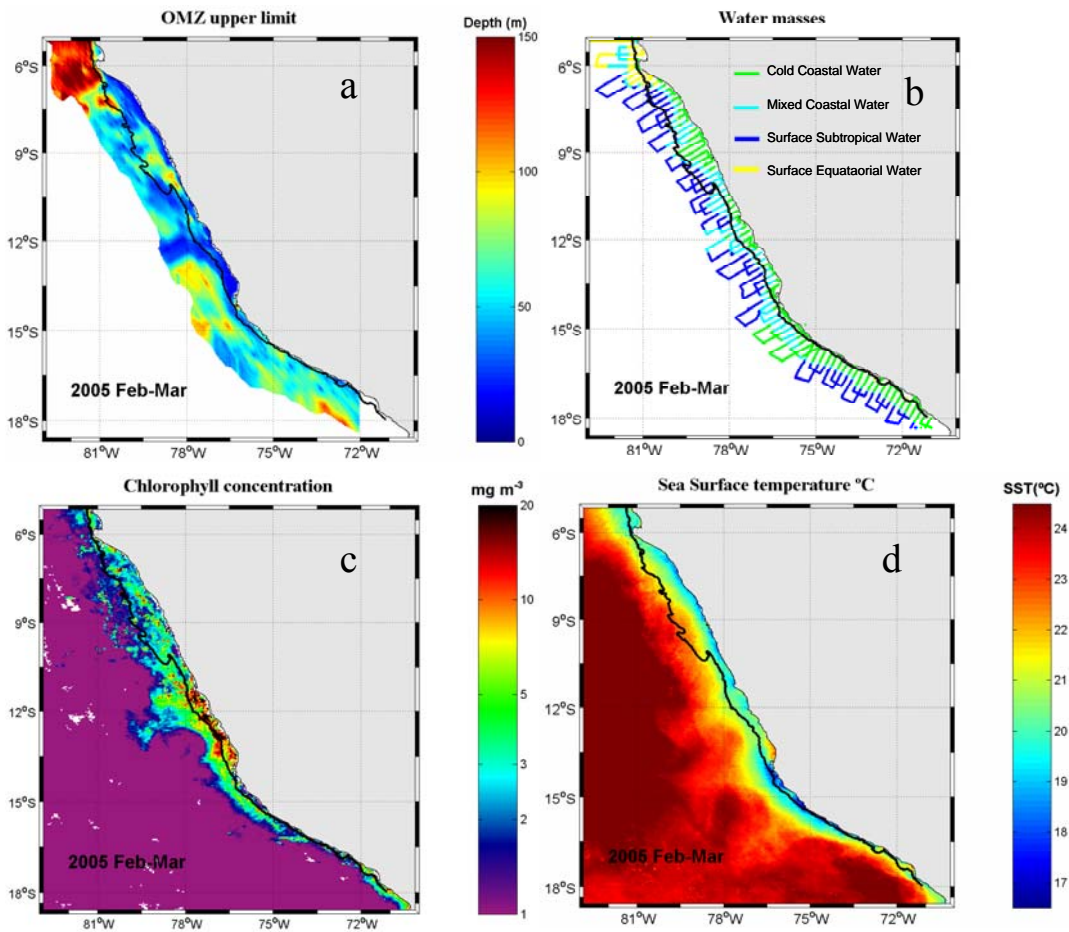


Figure 4.12 Horizontal macrozooplankton biomass ( $\text{g.m}^{-2}$ ) distribution during austral spring 2005. Acoustic macrozooplankton biomass during day (a) and night (c). Zooplankton biomass from Hansen nets towed vertically from 50 m to the surface during day (b) and during night (d). The black line shows the continental shelf limit (200 m bottom depth).



*Figure 4.13 Environmental conditions during the summer survey 2005. (a) Depth of the upper limit of the OMZ. (b) Water masses. (c) Satellite chlorophyll concentration. (d) Satellite sea surface temperature. The black line shows the continental shelf limit (200 m bottom depth).*

#### 4.4 Discussion

This study provides the first direct estimation of macrozooplankton biomass in the NHCS. In a previous chapter (2) it was hypothesised that euphausiids were the main responsible organisms of the observed acoustic distribution pattern, but based on limited data and covering a small area. Here we will first discuss if this hypothesis can be reinforced while assessing a much larger area (the whole NHCS) and different time periods (austral summer and spring). We will then compare our macrozooplankton biomass estimates with other estimates from the same and other systems. Finally, we will discuss how these new findings allow for a better understanding of the high fish productivity in the NHCS.

#### **4.4.1. What are the main responsible organisms for the observed macrozooplankton acoustic pattern?**

- ***Day-night difference***

The high day-night difference in the estimated epipelagic macrozooplankton biomass illustrates the fact that the bulk of the nocturnal epipelagic biomass is composed by migratory fluid-like macrozooplankton. By definition, migratory organisms were not included within the epipelagic biomass during the day. The direct biomass estimation of these organisms is not possible by day because they migrate deeper than the actual acoustic range of the Simrad EK500 at 120 kHz which we used in this study (150 m). It is worth mentioning that data acquired during the ‘Filamentos 2008’ survey with the Simrad EK60 at 120 kHz (allowing work down to 300 m) showed that most of the migrating macrozooplankton community formed a layer at about 200 m during the day (see Fig. 2.9 in Chapter 2). We can provide an estimate of the biomass of migrating macrozooplankton by subtracting the diurnal estimate from the nocturnal, which encompasses both migrating and non-migrating communities. We obtained that ~77% of the macrozooplankton observed during the night performed vertical migration. This result is similar to the estimates provided by Escrivano et al. (2009) in the Southern HCS (75%) and Postel et al. (2007) in the Northern Benguela system (71%). In the Southern HCS, Escrivano et al. (2009) also found that the main constituent of the biomass of this migratory community was composed by large zooplankton, mainly euphausiids, but also large *Eucalanus* copepods. In this study, we have found that macrozooplankton size increased about 5% during the night. This suggests that the migratory fluid-like macrozooplankton not only attained a much higher biomass than the non-migrating community but is also composed by larger individuals.

- ***The across and along-shore distribution of macrozooplankton***

In this study, migratory macrozooplankton made up of relatively large organisms were more abundant over the slope and offshore. This pattern was also observed in the along-shore macrozooplankton distribution. Lower biomass and smaller size were estimated in the latitudes with a relatively wider continental shelf; in contrast, higher biomass and larger size were estimated in the latitudes with a narrower continental shelf (Ayón et al., 2008a). The high biomass of this migratory macrozooplankton was apparently delimited by the shelf break. The shelf break is known to play an important role in transporting and retaining macrozooplankton (Bakun, 1996; Genin, 2004; Zhu et al., 2009). Shelf break upwelling can result from the interaction between subsurface currents and the shelf break (Hill and Johnson, 1975; Lill, 1979; Bakun, 1996). To counteract the upslope upwelling transport toward the surface, it has been suggested that euphausiids swim downward against upwelling during day which allows them to maintain a preferred depth (Genin, 2004). This would result in a retention and accumulation of euphausiids along the shelf break (Genin, 2004). Thus very high concentrations of euphausiids usually occur where the deep flow is convergent and the upwelling is the strongest (Simard and Mackas, 1989; Mackas et al., 1997). An ecological advantage of this counter-upwelling swimming behaviour of euphausiids would be the ability to stay near the shelf break upwelling and exploit the enhanced phytoplankton productivity and biomass during the night migration to the surface (Lu et al., 2003). In the NHCS, there is a lack of knowledge on euphausiid distribution (Ayón et al., 2008a), information from other upwelling regions, however, has shown that euphausiid distribution is strongly

affected by the shelf break (Barange and Pillar, 1992; Swartzman et al., 2005). In the California Current system, euphausiid patches are more frequently observed along the shelf break over the slope area (Swartzman et al., 2005). In the Benguela system, the shelf break seems to effectively separate inshore and offshore euphausiid populations which complete their life cycles within each area (Barange and Pillar, 1992). In the Canary system, there is also evidence of higher euphausiid abundance after the shelf break in the slope area (Blackburn, 1979). Thus, the observed across-shore pattern of macrozooplankton in this study, together with the evidence of high euphausiid densities over the slope and offshore area (Vinogradov and Shushkina, 1978), suggested that the shelf break might also be important for retaining and accumulating macrozooplankton over the slope and offshore areas of the HCS.

- ***Matching the acoustic patterns to specific macrozooplankton taxa***

Despite the lack of ground-trust catch data to effectively allocate this high nocturnal biomass to zooplankton taxa (multinet data were only available during the surveys ‘Cardumenes 2004’ and ‘Filamentos 2008’, see Chapter 2, and Hansen zooplankton data are available as global biovolume and not discriminated by taxonomic group), only few zooplankton organisms could reach such a high biomass and/or fit the patterns described above: munida, salps, large copepods and euphausiids. Munida have been separated from other fluid-like based on a threshold Sv value. Munida echoes with low Sv could have been misclassified as macrozooplankton, which would lead to an overestimation of its biomass. This species, however, is vertically constrained within the epipelagic zone and does not perform large vertical migrations. In addition, Gutiérrez et al. (2008) showed that munida distribution is restricted to the coldest (coastal) part of the cold coastal water. Thus munida is mainly confined to the shelf area, an area in which macrozooplankton biomass was very low. Although munida larvae can not be distinguished as an independent fluid-like group (Chapter 2), their high abundance could only have contributed to the macrozooplankton biomass from near coastal areas (Fagetti and Campodonico, 1971). Salps can reach high biomass and are capable to migrate vertically (Pakhomov, 2004). However, these organisms are mainly distributed in equatorial and tropical waters that are restricted to the northern part of the NHCS (Ayón et al., 2008a), an area that was excluded from this study. We can thus assume that salps account only for a small part of the estimated macrozooplankton biomass.

Large copepods, in particular *Eucalanus inermis*, are relatively abundant in the system (Ayón et al., 2008a) and are the second most important food item of anchovy and sardine (Espinoza and Bertrand, 2008; Espinoza et al., 2009). *E. inermis* also perform large diel vertical migration between the epipelagic layer and the OMZ (Ayón et al., 2008a; Escribano et al., 2009). These large copepods, however, need to occur at a very high density to be properly detected and quantified by the used acoustic frequencies (Murase et al., 2009) even if the +MVBS method should improve the acoustic power of detection thanks to a better separation (Lebourges-Dhaussy and Fernandes, submitted). *E. inermis* is considered a typical zooplankton of the cold coastal water and used as indicator for the presence of this water mass (Ayón et al., 2008a). Thus, high densities of *Eucalanus spp.* are more likely to occur and contribute to the macrozooplankton biomass from the shelf area rather than from further offshore areas.

Finally, euphausiids, particularly the endemic species (Brinton, 1962) *Euphausia mucronata*, which constitute up to 50% of the total system zooplankton biomass (Antezana, 2002), present a similar distribution pattern to the one described from acoustics. Euphausiid species have adapted to the OMZ and can stand very low dissolved oxygen concentrations (Antezana 2002, 2010; Escribano et al., 2009). They perform extensive diel vertical migration from the photic zone, where they forage during the night, to the OMZ, where they take refuge during the day (Escribano et al., 2009). Adults are usually distributed offshore where they can reach very high biomass (Vinogradov and Shushkina, 1978; Escribano et al., 2009), while juvenile and larvae stages are usually distributed in the shelf area (Arones et al., 2009). Also, the presence of high biomass of euphausiids is indirectly confirmed by anchovy, sardine and jack mackerel diets (Konchina, 1981, 1983, 1991; Espinoza and Bertrand, 2008; Espinoza et al., 2009). The contribution of euphausiids in anchovy diet is particularly high offshore during the night (P. Espinoza, IMARPE, unpublished data). The similarities between the night pattern of size and biomass macrozooplankton distribution from this study (Chapters 2 and 4) and the known pattern of euphausiids, in particular *E. mucronata*, suggest that euphausiids might be the main constituent of the acoustic macrozooplankton biomass estimated during the night.

In this study, we have also found large fluid-like organisms with relatively low biomass near the coastal areas. Near-coastal areas usually contain a distinct zooplankton community among which meroplanktonic larvae of benthic invertebrates (e.g. decapoda, cirripedia, mollusca, polychaeta) constitute an important fraction (Ciales-Hernández et al., 2008). Also the large larvae of munida, the most abundant and largest macrozooplankton within the cold coastal water (Gutiérrez et al., 2008), may be quite abundant near the coast (Fagetti and Campodonico, 1971). This highly diverse near-coastal zooplankton community is more likely to have relatively larger organisms than the inner shelf community, composed mainly by copepods (Ayón et al., 2008a), and could explain the observed large fluid-like size in the near coastal areas.

In summary our macrozooplankton biomass estimation potentially includes a variety of fluid-like organisms such as misclassified adult munida, juveniles munida, salps, large copepods, meroplanktonic crustacean larvae and euphausiids. However, when contrasting organism behaviour and habitat preference with the observed day-night difference in fluid-like biomass and size, along with the across- and along-shore fluid-like distribution, euphausiids are probably the main constituent of the fluid-like group observed by acoustics, even if other fluid-like scatters, particularly *Euclanus spp.*, probably account for a significant part of the fluid-like group.

#### **4.4.2 Macrozooplankton biomass in the NHCS: higher than assumed**

This study provides the first direct high-resolution large-scale estimation of macrozooplankton in the NHCS and it is to our knowledge the first one among the main upwelling systems. The total estimated biomass, i.e., the biomass estimated during the night when both migrating and non-migrating macrozooplankton communities are in the epipelagic layer ( $\sim 112 \text{ g.m}^{-2}$ ), was more than 5 times higher than their corresponding net sampling of total zooplankton biomass ( $\sim 20 \text{ g.m}^{-2}$ ). This high difference is not surprising since macrozooplankton usually avoid nets (Fleminger and Clutter, 1965; Debby et al., 2004), which results in an underestimation of global zooplankton biomass by net sampling when compared to acoustics (Lawson et al., 2008). However, there is

still concern about the accuracy of the acoustic method: is this a realistic estimation of the macrozooplankton biomass of the NHCS?

The ideal situation would be to compare our results with validated acoustic estimates from the same system and from other comparable upwelling systems. However, most of the studies that provided biomass acoustic estimates have been performed in the Antarctic area, where acoustics is used as a standard tool to estimate krill biomass (Watkins and Brierley, 2002). Acoustic has seldom been used in eastern boundary upwelling systems (EBUS) to estimate zooplankton biomass (Ressler et al., 2005; Postel et al., 2007). When employed, acoustics was calibrated to match the biomass levels obtained by net sampling (Ressler et al., 2005; Postel et al., 2007) and was not used to provide independent biomass estimates. In EBUS, only net sampling and trophic model estimates are therefore available to compare our results. To facilitate the comparison and the discussion, we synthesised the published zooplankton biomass estimates in EBUS, Antarctic and eastern Canada (Table 4.4). These estimates were obtained from different nets and mesh sizes taken over various vertical ranges, from trophic models and from acoustics (Table 4.4). Thus, each individual estimate corresponds to a set of different conditions and must be taken with caution when used as reference value for the purpose of comparison.

- ***Comparing with in situ data (net and acoustic)***

Compared with all biomass estimates considered in Table 4.4, our estimates are among the highest and generally more than twice as high as others estimates. Comparable or higher biomass estimates were encountered only in some specific measurements in the southern HCS (Escribano et al., 2009, from only 4 net samples), the Northern Benguela during the 1960s (Cushing, 1971), Canada (Cotté and Simard, 2005) and Antarctic (Table 4.4).

The only work that compared zooplankton biomass (from net samples) between upwelling systems is a synthesis from Cushing (1971). According to Cushing (1971) zooplankton biomass was about  $40\text{-}50 \text{ g.m}^{-2}$  in all EBUS. Lower biomasses were observed in southern California ( $21 \text{ g.m}^{-2}$ ) and Southern Humboldt ( $\sim 33 \text{ g.m}^{-2}$ ) while higher biomasses were observed in northern Canary ( $21^\circ\text{N}\text{-}28^\circ\text{N}, 80 \text{ g.m}^{-2}$ ) and northern Benguela ( $23^\circ\text{S}\text{-}29^\circ\text{S}, 114 \text{ g.m}^{-2}$ ). Our estimation ranges among the highest values proposed by Cushing (1971) but is more than twice higher than most other cases. Cushing estimates come from different sources and net types that can partly limit the comparison. Also Cushing (1971) assumed that the zooplankton biovolumes were mainly composed by crustacean zooplankton and converted this biovolume into biomass without excluding or correcting tunicates (salps) contribution, which could have overestimated this biomass (Lavaniegos and Ohman, 2007).

- ***Compared with trophic models and what we know about trophodynamics***

Macrozooplankton abundance and/or their turn-over rates can be indirectly determined by trophic models. These models estimate the amount of prey biomass required to balance its predator consumption. The availability of diet information is crucial when building trophic models and any misevaluation of a predator's diet would definitely affect prey biomass estimates, particularly if the predators attain very high biomass, as in the case of anchovy. So far, trophic models constructed in the NHCS have considered

that anchovy mainly forage on phytoplankton, rather than on macrozooplankton (e.g. Jarre-Teichmann, 1992; Tam et al., 2008). Since we now know that it is not the case, these trophic models probably underestimated macrozooplankton biomass. When increasing macrozooplankton contribution in the anchovy diet (Guénette et al., 2008), higher biomass levels of macrozooplankton are needed to balance the model. For instance, when changing macrozooplankton contribution to the anchovy diet from 19% to 60%, macrozooplankton biomass had to be increased from 16 to 50 g.m<sup>-2</sup> to meet anchovy consumption (Guénette et al., 2008). However, (i) according to Espinoza and Bertrand (2008) macrozooplankton account for more than 80% of anchovy diet, and (ii) Guénette et al. (2008) also strongly underestimated the importance of macrozooplankton in the diet of other main predators such as mackerel, horse mackerel and sardine (Konchina 1981, 1991; Espinoza et al., 2009), whose biomass were relatively high during the model period (1983-1992) and together with anchovy was estimated to be ~110 g.m<sup>-2</sup> (anchovy account for 75 g.m<sup>-2</sup>).

In addition to diet information, a trophic model needs to be documented on how fast a prey population produces its own biomass in a given time. In other words, it requires the prey production/biomass ratio (P/B). Since predators' consumption can be balanced by combining low prey biomass with high P/B ratios, or vice versa, it is advisable to look at the assumed P/B ratios. To build trophic models of the NHCS, Tam et al. (2008) and Guénette et al. (2008) used a P/B of 20 for the macrozooplankton (euphausiids). The P/B ratio of euphausiids from similar environments usually ranges between 9 and 15 (Taki, 2006). Thus the apparent high ratio assumed by the trophic models in NHCS also leads to an underestimation of macrozooplankton biomass.

It is important to note that in the SHCS, Neira et al. (2004) constructed a trophic model with euphausiids as the main prey of pelagic fish (assuming a P/B ratio of 2.9) and estimated the biomass of macrozooplankton to 73-106 g.m<sup>-2</sup>, values that are much more similar to our estimation.

In the NHCS, anchovy biomass has been estimated to 83 g.m<sup>-2</sup> (period 1995-96, Tam et al., 2008). This biomass is 27% lower than our macrozooplankton biomass estimate (112 g.m<sup>-2</sup>). The comparison of these predator and prey biomasses recalled the main question of this study: is this prey biomass enough to feed the anchovy population? To provide an answer we needed to determine if, when using our macrozooplankton biomass estimation (112 g.m<sup>-2</sup>), appropriate P/B ratio (from 9 to 15; Taki, 2006), predator diets (Espinoza and Bertrand, 2008, Espinoza et al., 2009) and predator consumption ratios (Guénette et al., 2008), macrozooplankton production could fit with the predation from anchovy and other main predators (Tam et al., 2008). We found that along with our macrozooplankton biomass (112 g.m<sup>-2</sup>), a P/B ratio of ~10 had to be assumed to produce enough macrozooplankton production to feed anchovy (83 g.m<sup>-2</sup>) and other predators (~27.6) such as sardine, mackerel and horse mackerel (Tam et al., 2008). Unlike previous macrozooplankton P/B ratios used in trophic models of the NHCS (Guénette et al., 2008; Tam et al., 2008), the assumed P/B ratio in this study lay within the expected P/B ratio of euphausiids from environments similar to the NHCS (Taki, 2006). This indicates that our high macrozooplankton biomass is coherent with both euphausiid life-history parameters and predators' trophic ecology. Moreover, this strongly suggests that the NHCS has a high macrozooplankton biomass to feed the also high abundance population of anchovy. Finally, it is important to keep in mind that the anchovy population is restricted to the coastal area and occupies less than 154 000 km<sup>2</sup>.

(Gutiérrez, 2000; Simmonds et al., 2009), while the distribution of euphausiids and other main macrozooplanktonic species occupy a much larger area (Brinton, 1962; see also Fig.1.7). The total biomass of macrozooplankton we estimated in the study area ( $112 \text{ t.km}^{-2} * 263\,000 \text{ km}^2$ ) is actually 2.3 times that of anchovy ( $83 \text{ t.km}^{-2} * 154\,000 \text{ km}^2$ ), which probably helps compensating the grazing effect in areas of overlap between fish and zooplankton.

In summary, our estimate of macrozooplankton biomass seems coherent because (i) it is about 5 times higher than the estimates from traditional net sampling (Ayón et al., 2004) that is known to underestimate macrozooplankton biomass (Fleminger and Clutter, 1965; Debby et al., 2004), (ii) lies within the range of published macrozooplankton biomass in EBUS and other productive marine ecosystems and is lower than local biomass estimates from high abundance hot spots (Table 4.4), (iii) is comparable with other estimates performed in systems with high euphausiid abundance (e.g., Cotté and Simard, 2005 for St. Laurent Estuary in Canada), (iv) it is higher than macrozooplankton biomass from trophic models of the NHCS which have strongly underestimated the importance of macrozooplankton in the diet of anchovy and other main predators and have overestimated the P/B ratio of macrozooplankton by at least 25% and (v) is coherent with both euphausiid life-history parameters and predators' trophic ecology.

#### **4.4.3 What could be the reasons for such a high secondary production?**

The assumption that the high fish production of the HCS directly depends on primary production (Ryther, 1969) had lead scientists to search for the unique properties of this system (Hutching, 1992; Bakun and Weeks, 2008; Chavez and Messie, 2009). Since the primary production of the HCS is not higher than other EBUS (Carr, 2002; Patti et al., 2008; Demarcq, 2009), high primary production has been dismissed as an explaining factor for the system high fish production (Bakun and Weeks, 2008; Chavez and Messie, 2009).

- ***Intermediate Upwelling***

In an upwelling system, there are optimal conditions at which the physical energy can be transformed by primary producers and efficiently transferred to higher trophic levels to enhance secondary (Ayón et al., 2008a) and tertiary productions (Cury and Roy, 1989; Cury et al., 1998). These optimal conditions arise from a balance between the positive effect of high wind speed, which enhance nutrients supply and promote high primary production, and its associated turbulence that, if too strong, could hamper feeding efficiency on early life stages of higher trophic level organism (Cury and Roy, 1989). Thus optimal conditions for high fish recruitment occur at intermediate level of upwelling intensity (Cury and Roy, 1989). This dome-shaped relation has also been observed for zooplankton production and used to explain the intra and interannual zooplankton production variability (Ayón et al., 2008a). Finally, high primary production and optimal conditions for fish growth, reproduction and egg and larval retention are suggested to results from the intermediate upwelling-favourable winds of the HCS (Cury et al., 1998; Bakun and Weeks, 2008; Chavez and Messié, 2009).

- ***Near equator location***

According to Bakun and Weeks (2008) the low latitude situation of the NHCS permits a strong upwelling-based nutrient enrichment with low wind-induced turbulence generation. Additionally, the residence times (time within the Ekman layer) within this favourable near-coastal habitat dramatically increases at near equatorial latitude (Bakun and Weeks, 2008). Thus anchovy larvae and larval food can remain longer in a wide rich upwelling zone from which loss due to advection would be minimal (Bakun and Weeks, 2008). These favourable conditions for recruitment, together with anchovy preference to prey directly on phytoplankton have been suggested as main factors to explain the high fish production of the HCS (Bakun and Weeks, 2008). In addition, the near-coastal upwelling zone is also the main habitat of mesozooplankton and larvae and juveniles of macrozooplankton (Ayón et al., 2008a). A longer residence time in a less turbulent and high food concentrated habitat may also increase both food availability and zooplankton recruitment success and thus prompt a high biomass of zooplankton. Since small (zooplankton larvae, nauplius, etc.) and large (large copepods and euphausiids) zooplankton are the main preys of anchovy larvae (van der Linen et al., 2009), and juveniles and adults (Espinoza and Bertrand, 2008; P. Espinoza, unpublished data), respectively; the high macrozooplankton biomass found in this study suggest that the NHCS may provide a higher offer of food to anchovy, when compared to other upwelling systems.

- ***El Niño***

It has been hypothesized that El Niño keeps the NHCS system in a '*r*' state, favouring fast growing fish like anchoveta (Chavez, 1987) and preventing long lived ocean dwelling predators from getting established (Bakun and Weeks, 2008). In this sense, zooplankton species presenting *r* strategies and plastic ecology (e.g. can distribute more or less offshore according to the condition) such as euphausiids, could be little impacted by the climatic variability. Brinton (1967) observed that euphausiids latitudinal distribution as well as abundance did not change much during El Niño 1958. Although, the strong 1997-98 El Niño led to drastic changes in species zooplankton composition, there was not apparent effect on the abundance of euphausiids larvae (Arones et al., 2009). During the 1997-98 El Niño there was an increase in juveniles and euphausiids larvae in the Southern HCS and the biomass of adult euphausiids was as high as during normal periods (Fernandez et al., 2002). This suggests that El Niño does not seem to have a detrimental effect on euphausiids, which could explain why in several cases it was observed a fast recover of anchovy, likely due to high food availability.

In summary our high biomass estimation of macrozooplankton complements and gives support to the current hypotheses proposed to explain the high fish production of the NHCS because (i) when compared with other EBUS this system presents an intermediate upwelling intensity (Cury et al., 1998; Bakun and Weeks, 2008; Chavez and Messié, 2009), which favour zooplankton production (Ayón et al., 2008a), (ii) zooplankton production also benefits from the near equator location of the NHCS as the high primary production combined with low wind-induce turbulence increases zooplankton feeding efficiency, (iii) the near equator location of the NHCS also increases the residence time within this high productive and less turbulent water minimizing zooplankton loss due to advection and increasing zooplankton recruitment, (iii) El Niño events do not seem to have any strong detrimental effect on euphausiids,

the main constituent of the zooplankton biomass and finally, (iv) according to anchovy feeding ecology a high biomass of euphausiids is needed to support the high biomass of anchovy.

Chapter 4 Is there enough zooplankton to feed the anchovy population?

*Table 4.4. Synthesis of biomass estimations (in g.m<sup>-2</sup>) of meso- and macrozooplankton in main upwelling systems, Antarctic and eastern Canada.*

Region	Sampling method	Depth sampled (m)	Sampling date	Meso zooplankton	Macro zooplankton	Time	Reference and comments	
Humboldt Northern 6° -18°S	Acoustic, this study	$Z_{VEEP}$	Feb.-Mar. 2005		28.6	Day	This study	
	Acoustic, this study		Nov.-Dic. 2005		114.6 24.3 112.4	Night Day Night	This study This study This study	
Humboldt Northern 4°-18°S	Hansen net 300 µm / 0.33 m <sup>2</sup>	Upper 50	Feb.-Mar. 2005	11 20.6* 12.6 19.4*		Day Night Day Night	P. Ayón personal communication. Conversion from biovolume to wet weight. Factor from Wiebe et al. (1975, 1988)	
	Hansen net 300 µm / 0.33 m <sup>2</sup>	Upper 50	Nov.-Dic. 2005					
Humboldt Northern 4°-18°S	Hansen net 300 µm / 0.33 m <sup>2</sup>	Upper 50	Austral summer 1960s					
	Hansen net 300 µm / 0.33 m <sup>2</sup>	Upper 50	Austral summer 1970s					
	Hansen net 300 µm / 0.33 m <sup>2</sup>	Upper 50	Austral summer 1980s					
	Hansen net 300 µm / 0.33 m <sup>2</sup>	Upper 50	Austral summer 1990s					
Humboldt Northern 4°-10°S	Diverse	Upper 300	1960s	51.5*			Cushing (1971). Conversion from gC.m <sup>-2</sup> to wet mass g.m <sup>-2</sup> from Hunt et al. (1981)	
Humboldt Northern 10°- 18°S	Diverse	Upper 300	1960s	45.5*			Cushing (1971). Conversion from gC.m <sup>-2</sup> to wet mass g.m <sup>-2</sup> from Hunt et al. (1981)	
Humboldt Northern 4°-16°S	Trophic model		1995-1996	31.2	21.1		Tam et al. (2008). Macrozooplankton P/B ratio assumed to be 20. Period 1997 - 1998 correspond to a very strong El Niño. Area within 60 nm from the coast	
	Trophic model		1997-1998	17	34.8			
Humboldt Northern 4°-14°S	Trophic model		1953-1984		50		Guénette et al. (2008). Macrozooplankton P/B ratio assumed to be 20. Area within 40 nm from the coast. Anchovy diet 0.3 diatom and 0.6 macrozooplankton	
Humboldt Southern 33°-39°S	Trophic model		1992	48.9	73.6		Neira et al. (2004). Only to meet the energy demand of the comertial fish sp. Low P/B ratio for macrozooplankton (2.6).	
			1998	70.8	106.3			
Humboldt Sourthern 20°S	Tucker trawl net 300 µm / 1 m <sup>2</sup>	Upper 60	Mar. 2000		64.1 355.9	Day Night	Escribano et al. (2009). Epipelagic layer offshore area from 4 stations.	
Humboldt Sourthern 36°30'S	Tucker trawl net 200 µm 1 m <sup>2</sup>	Upper 80	Aug. 2002 to Dec. 2005	46.6		Day	Escribano et al. (2007). One coastal station over time for 3 years 2002 -2005. Conversion from mgC.m <sup>-2</sup> to wet mass g.m <sup>-2</sup> from Hunt et al. (1981)	
Humboldt Sourthern 23°-35°S	Diverse	Upper 300	1960s	34.2*			Cushing (1971). Conversion from gC.m <sup>-2</sup> to wet mass g.m <sup>-2</sup> from Hunt et al. (1981)	

Chapter 4 Is there enough zooplankton to feed the anchovy population?

Humboldt Southern 35°- 45°S	Diverse	Upper 300	1960s	33.2*			Cushing (1971). Conversion from C.m <sup>-2</sup> to wet mass g.m <sup>-2</sup> from Hunt et al. (1981)
California Central 35°-38°N	Double oblique tows using ring (1 m diameter) and bongo net (0.71 m diameter) ~0.5 mm mesh size	Upper 140-210	1951-2005	6.7	3	Night	Lavaniegos and Ohman (2007). Converted from organic carbon to wet weight from Hunt et al. (1981)
California Southern 31°-34°N	Double oblique tows using ring (1 m diameter) and bongo net (0.71 m diameter) ~0.5 mm mesh size	Upper 140-210	1951-2005	5.9	1.4	Night	Lavaniegos and Ohman (2007). Converted from organic carbon to wet weight from Hunt et al. (1981)
California Southern 31°-34°N	Diverse	Upper 140	1960s	21.2			Cushing (1971). Conversion from C.m <sup>-2</sup> to wet mass g.m <sup>-2</sup> from Hunt et al. (1981)
California Central 34°-40°N	Diverse	Upper 140	1960s	43.5			Cushing, 1971. Conversion from C.m <sup>-2</sup> to wet mass g.m <sup>-2</sup> from Hunt et al. (1981)
California Northern 40°-48°N	Diverse	Upper 140	1960s	53			Cushing (1971). Conversion from C.m <sup>-2</sup> to wet mass g.m <sup>-2</sup> from Hunt et al. (1981)
Benguela Northern 9°-20°19'S	L-ADCP calibrated by multinet	Upper 200	Sept. 2000	39.8*		Night	Postel et al. (2007). Converted from ash free dry mass to dry mass by factor 0.8 <sup>-1</sup> ( Postel et al., 2000) and from dry mass to wet mass by factor 0.1 <sup>-1</sup> Hutching et al. (1991)
				11.5*		Day	
Benguela Northern 15°-29°S	Trophic model			11.7	8.2		Heymans and Baird (2000). Converted from organic carbon to wet weight from Hunt et al. (1981)
Benguela Northern 17°30-26°S	Bongo net 300 and 500 µm mesh size	Upper 50	Sept. and Nov. 1982 Jan.-Mar., Sept. and Nov. 1983 Jan. and Mar. 1984		32.8	Night	Barange and Stuart (1991). Only biomass of <i>Nyctiphanes capensis</i> (94%) and <i>Euphausia hansenii</i> (6%). Converted from dry mass to wet mass by factor 0.1 <sup>-1</sup> from Hutching et al. (1991)
Benguela Southern South of 29°S	Trophic model		1980s 1990s	8.0 8.7	13.3 14.6		Shannon et al. (2003). Biomass required to sustain the other components of the system. Macrozooplankton P/B ratio was assumed to be 13 (from Hutching et al., 1991)
Benguela Northern 17°-23°S		Upper 200	1960s	56.9			Cushing (1971). Conversion from C.m <sup>-2</sup> to wet mass g.m <sup>-2</sup> from Hunt et al. (1981)
Benguela Northern 23°-29°S		Upper 200	1960s	113.8			Cushing (1971). Conversion from C.m <sup>-2</sup> to wet mass g.m <sup>-2</sup> from Hunt et al. (1981)

Chapter 4 Is there enough zooplankton to feed the anchovy population?

Benguela Southern 29°-34°S		Upper 200	1960s	48.5			Cushing, 1971. Conversion from C.m <sup>-2</sup> to wet mass g.m <sup>-2</sup> from Hunt et al. (1981)
Canary Current along a line at 21°40'N,	Bongo net 102 µm mess size	Upper 200	Mar, Apr, May 1974	3.5*, 10.5* and 76.2*	16 - 208	Night	Blackburn (1979). Biomass from the inner shelf, outer shelf and slope respectively. Macrozooplankton biomass made up 77% of the slope biomass (76.2)
Canary Current 8°-14°N		Upper 200	1960s	56.9			Cushing (1971). Conversion from C.m <sup>-2</sup> to wet mass g.m <sup>-2</sup> from Hunt et al. (1981)
Canary Current 14°-21°N		Upper 200	1960s	40.2			Cushing, 1971. Conversion from C.m <sup>-2</sup> to wet mass g.m <sup>-2</sup> from Hunt et al. (1981)
Canary Current 21°-28°N		Upper 200	1960s	80.4			Cushing (1971). Conversion from C.m <sup>-2</sup> to wet mass g.m <sup>-2</sup> from Hunt et al. (1981)
Canary Current 28°-33°N		Upper 200	1960s	43.3			Cushing, 1971. Conversion from C.m <sup>-2</sup> to wet mass g.m <sup>-2</sup> from Hunt et al. (1981)
South Channel of Lawrence estuary Canada	Acoustics, 2 frequencies 38 and 120 kHz (Simrad Ek 60). Net sampling for sizes and species identification.		Jul. 2002		85.6 - 235	Day	Cotté and Simard (2005). Scatter layers of <i>Euphausia superba</i> in the estuary. Area 25 km <sup>2</sup> , survey time 3 days. Biomass estimated using target strength of individual weight
Elephant Island	Acoustics, one frequency 50, 120 or 150 kHz. Sizes from net samples		1981-1993 range  mean		2.5-134.5  53.2		Hewitt and Demer (1994), <i>Euphausia superba</i>
South Georgia	Acoustics 2 frequencies 125 and 300 kHz		2002-2005 Winter  2002-2005 Summer		19.2  112.6		Saunders et al. (2007). From two moorings systems at 200 m. <i>Euphausia superba</i> biomass estimated using target strength.
Scotia Sea	Acoustics, 3 frequencies 38, 120 and 200 kHz (Simrad EK500)		Jan.-Feb. 2000		21.4		Hewitt et al. (2004). <i>Euphausia superba</i> biomass estimated using target strength.

\* Macrozooplankton were not excluded but assumed of being highly underestimated by the net sampling.

#### ***4.4.4 Conclusion***

We performed the first high resolution, large-scale acoustic macrozooplankton biomass estimation in an EBUS and provided a comprehensible view of the horizontal patterns of distribution of epipelagic macrozooplankton biomass according to the diel cycle.

This new independent high biomass estimation gives support to the current hypotheses (intermediate wind intensity, near equator location and El Niño) explaining the NHCS high fish production and it is in agreement with the new finding in trophic ecology indicating that forage fish consume mainly macrozooplankton. The availability of continuous high-resolution (one data per second) information on zooplankton is a noticeable advantage of this acoustic zooplankton biomass estimation when compared to one from net sampling. This method allows a more precise sampling of large areas of macrozooplankton distribution with a much lower cost than classic methods. However net sampling (or alternative devices for zooplankton identification such as LOKI) will always be necessary to identify the observed organisms. We are able to evidence that mesoscale physical structures were associated to zooplankton patches that could not be evidenced from net sampling. This method opens many perspectives to study, at multiple scales, the bottom-up physical forcing on zooplankton biomass and its further effect on zooplankton predators, which is the subject of the next chapter 5.

## Chapter 5

### *Effects of meso- and submesoscale physical forcing on the distribution of macrozooplankton and its further impact on the distribution of forage fish*

#### 5.1 Introduction

As indicated by Bertrand et al. (2008b) in marine ecosystems there is a series of evidences for a bottom-up transfer of behaviours and spatial structuring (Frontier, 1987; Russel et al., 1992): physics structures the ocean landscape and drives the distribution of particles and passive organisms (plankton); then, because living organisms have to find their prey, they tend to track their distribution (e.g. Frontier et al., 2004) and by the succession of predator-prey relationships, the spatial structuring originally driven by physical forcing tends to be transmitted along the trophic levels of the ecosystem (Fig. 5.1).

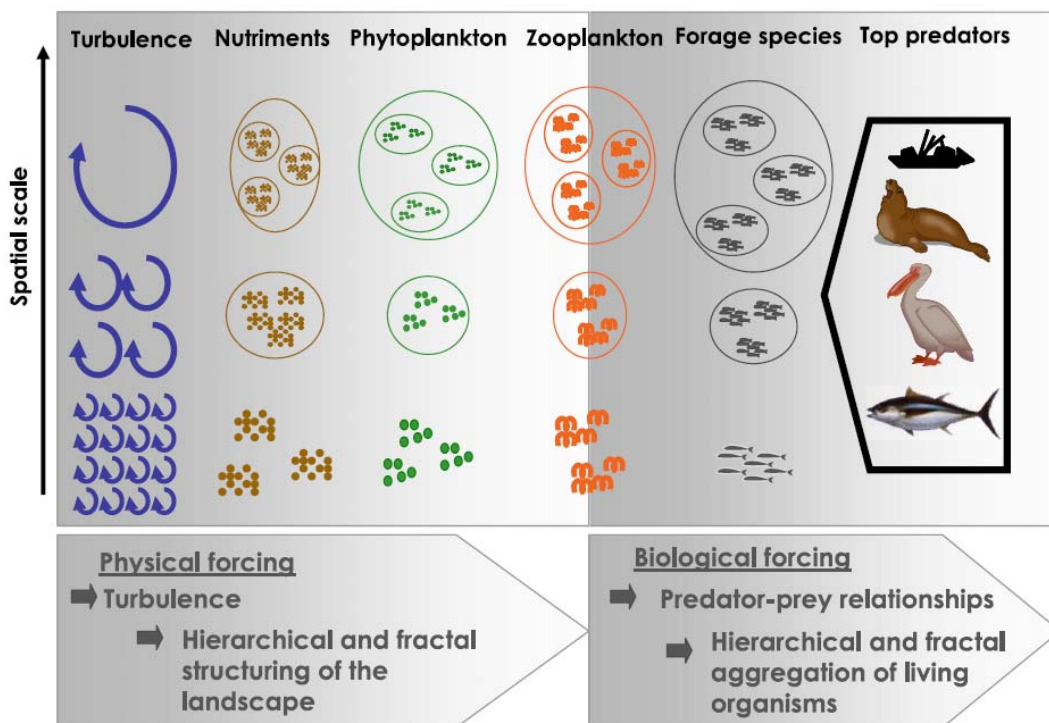


Figure 5.1 Schematic representation of the concept of bottom-up transfer of behaviours and spatial structuring. The physical forcing structures the pelagic landscape by introducing turbulence in the water mass. The dissipation of this turbulence is fractal by nature and generates a hierarchical structuring of the water mass. The inert particles (nutrients) and part of living organisms (phytoplankton and most of the zooplankton) are passively organized in space by this physical forcing. Then, biological interactions such as predator-prey relationships transmit to a certain extent this spatial structuring along the trophic chain. Source: Bertrand et al. (2008b).

The ocean landscape is fundamentally structured by gradients and discontinuities at a variety of spatial and temporal scales (Steele, 1989). Upwelling ecosystems are highly heterogeneous on small scales of time and space scales (Lavaniegos et al., 2002; Carr and Kearns, 2003; Bertrand et al., 2004b; Gutiérrez et al., 2007; Chaigneau et al., 2008; Swartzman et al., 2008). This is because there is intense mesoscale (10s km) and submesoscale (100s m to km) activity that generates sharp fronts between coastal rich and oceanic poor waters (Chaigneau and Pizarro, 2005a), filaments (Thomas, 1999), eddies (Hormazabal et al., 2004; Chaigneau and Pizarro, 2005b) and internal waves (Bertrand et al., 2008a).

Mesoscale physical features (filaments, eddies) can increase productivity, structure zooplankton and, through a succession of predator-prey relationships, structure higher trophic levels (Bertrand et al., 2008b). At mesoscale in the NHCS physical processes are more stable and less intense than in other eastern boundary upwelling systems (EBUS) (Chaigneau et al., 2009). This may be important for increasing the transfer efficiency from primary production through the food web to fish (Chavez and Messie, 2009). Also submesoscale physical processes can enhance productivity (Klein and Lapeyre, 2009) and structure zooplankton and higher trophic levels (Bertrand et al., 2008a). The study of submesoscale processes, however, has been elusive because of the lack of high-resolution data (Capet et al., 2008; Klein and Lapeyre, 2009).

Zooplankton distribution tends to be extrinsically driven on scales ranging from 100s m to kms, which corresponded to physical submeso- and mesoscale structures, and intrinsically driven on a fine scale (metres; swimming) (Levin, 1992). Because of its swimming behaviour, zooplankton can exhibit even more fine-scale variation than phytoplankton (Levin, 1992). Zooplankton therefore present a patchy distribution along a continuum of scales (e.g. Wiebe, 1970; Steele, 1976; Haury et al., 1978; Mackas and Boyd, 1979; Mackas et al., 1985; Frontier, 1987; Russel et al., 1992), which is why its distribution cannot be explained by a single mechanism on all scales (Levin, 1992). Since multiscale physical and biological external and internal drivers act simultaneously on zooplankton, it is usually difficult to discern which mechanisms are responsible for a given zooplankton pattern, particularly if the data have been obtained at a very fine scale (as in this study). Despite this difficulty, high-resolution data enable us to choose a specific scale from a wide range of possible scales (i.e. to focus on submesoscale to mesoscale processes), something which would be impossible with lower resolution data. Thus, by applying the appropriate filter (i.e changing the scale description and/or removing large trends) to high-resolution data, it is possible to focus on a particular scale and extract and abstract the features that are relevant to the phenomena observed on other scales (Levin, 1992).

To explore the impact of meso- and submesoscale physical features on macrozooplankton and higher trophic levels, based on the knowledge currently available in the literature we first formed hypotheses on the expected impact of meso- and submesoscale structures on organisms' patterns of distribution (Fig. 5.2).

Mesoscale anticyclonic eddies are convergence features that transport water and plankton toward their centre and deepen the pycnocline/oxycline (Bakun, 1996; Siegel et al., 1999). These structures are therefore expected to accumulate zooplankton at the centre (Yebra et al., 2005) and become attractive to zooplankton predators. Mesoscale cyclonic eddies, on

the other hand, are divergent features that pump water from deeper layers towards the surface and make the pycnocline/oxycline shallow (Bakun, 1996; Siegel et al., 1999). Thus zooplankton is expected to be advected from the center of the structure since the new upwelled water, with relatively low abundance of zooplankton, displaces water from the surface toward the eddy borders. Because of the low zooplankton abundance in these structures, a low abundance of zooplankton predators is also expected.

Similar submesoscale structures, such as internal wave or small eddies, can be both convergent and divergent features with effects on zooplankton distribution that are similar to the patterns described for mesoscale structures. Convergent submesoscale structures are expected to deepen the pycnocline/oxycline and accumulate plankton at the centre (Lennert-Cody and Frank, 1999; Rinke et al., 2007), making them attractive features for predators (Bertrand et al., 2008a). In contrast, divergent submesoscale structures upwell water and shallow the pycnocline/oxycline, dispersing zooplankton as the new upwelled water displaces surface water toward the borders of the structure. Since the correlation between the depth of the pycnocline and oxycline is highly significant ( $p < 0.0001$ ) and positive (Alexis Chaigneau, IRD, unpublished data), we assume that both meso- and submesoscale structures would be equally perceived from the oxycline and the pycnocline. We therefore use  $Z_{VEEC}$  as a proxy to discriminate the meso- and submesoscale physical structures.

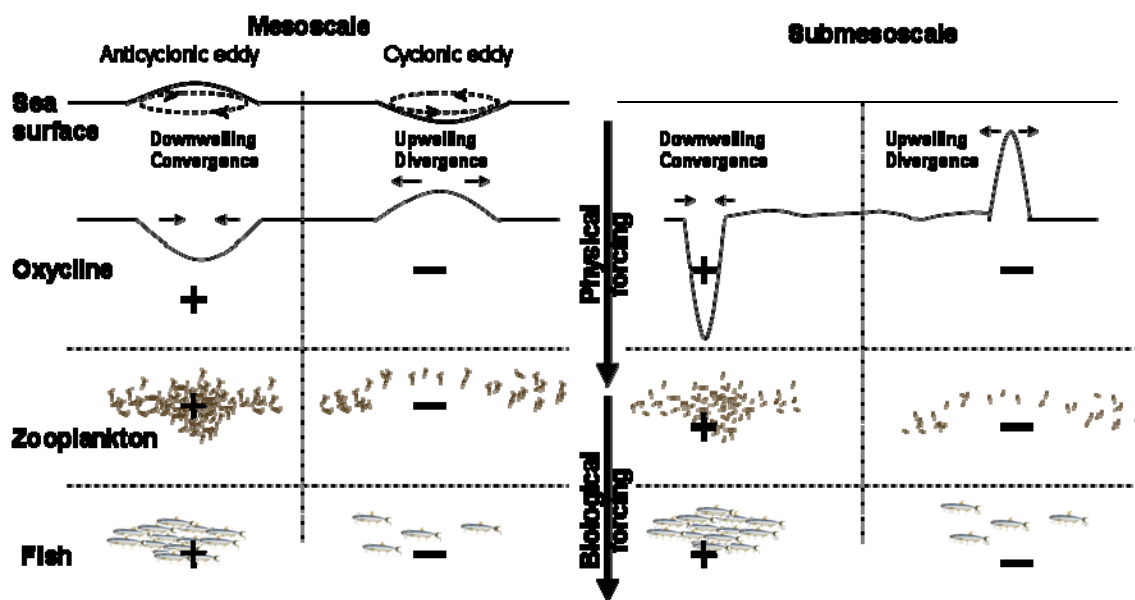


*Figure 5.2 Schematic representation of the meso- and submesoscale physical structuring and their expected impacts on organism distribution. A convergence/divergence structure leads to a locally deeper/shallower oxycline that should concentrate/disperse zooplankton at the center of the structure. It is thus assumed that any positive or negative deviation of the oxycline, regardless of its origin (e.g. eddies, ocean fronts), have a corresponding positive or negative effect on zooplankton. Then fish should concentrate where zooplankton are concentrated since predator-relationship transmits to a certain extent this spatial structuring to fish. This figure was constructed from, Frontier (1987), Russel et al.(1992), Bakun (1996), Siegel et al. (1999), Lennert-Cody and Frank, 1999 and Bertrand et al. (2008a, 2008b).*

The main objectives of this Chapter are (i) to test the impact of meso- and submesoscale physical features on macrozooplankton distribution, and (ii) to infer the further indirect impacts that these structures have on fish distribution (e.g. predators attracted by a highly dense, physically driven patch of zooplankton) by examining the relationship between zooplankton and its predators, fish in our case. To do this, we exploit the high-resolution physical and biological data collected according to the methods described in Chapters 2 and 3.

## **5.2 Materials and Method**

### **5.2.1 Data**

Acoustic data were obtained from the pelagic survey carried out during austral summer 2005 (see Chapter 4). Mean values of epipelagic macrozooplankton biomass and density per 3 pings long elementary sampling unit (ESU) were estimated according to the procedure described in Chapters 2 and 4. Mean values of epipelagic acoustic fish biomass (in nautical area scattering coefficient; NASC) per ESU were estimated according to the procedure described in Chapter 2. The vertical extension of the epipelagic community ( $Z_{VEEC}$ ) was obtained according to the method described in Chapter 3 and used as a proxy of the upper limit of the oxygen minimum zone (OMZ) in each ESU. Sea surface temperature (SST) and chlorophyll maps were created from available satellite data during February 2005 obtained from Modis and SeaWiFS (<http://oceancolor.gsfc.nasa.gov/>), respectively. Water masses were determined according to Swartzman et al. (2008).

### **5.2.2 Scale of description and sample unit**

In fisheries acoustics, it is a common practice to average the acoustic measurements at a given unit length of cruise track to give one sample (Simmonds and MacLennan, 2005). This sample is called the elementary sample distance unit (ESDU), ESU in our case. The size of this sampling unit is decided on the base of the size of the main spatial structure of the population. It must be small enough to capture the main spatial structure (macrostructure) but not too small to make successive samples dominated by local variability (microstructure) (Laloë, 1985; Simmonds and MacLennan, 2005).

The patterns of zooplankton spatial distribution (at scales > metres) are assumed to be imposed by physical drivers (Levin, 1992). According to the literature in the HCS and elsewhere we defined two scales based on the size of known physical spatial structures: i) the submesoscale (100s m to kms) to account for physical structures such as internal waves or frontogenesis (Lennert-Cody and Franks, 1999; Rinke et al., 2007; Bertrand et al., 2008a) and ii) the mesoscale (10s km) to account for larger physical processes such as cyclonic and anticyclonic eddies (Chaigneau et al., 2008 ) or upwelling filaments (Keister et al., 2009). To work at these two scales, two ESU values were defined: a 200 m ESU and a 2 km ESU for the mesoscale and submesoscale analysis, respectively (see section 5.2.4 for more details)

To be able to work at these scales with the same data, only transects longer than 100 km were selected. By doing this, we ensured that there were enough independent samples of

both meso- and submesoscale zooplankton structures to make statistical inferences. In total 17 transects were selected, 8 during day and 9 during night.

First, we will focus on selected large mesoscale structures. Then, at both meso- and submesoscale, we will examine the relationships of physics-macrozooplankton and macrozooplankton-fish.

### **5.2.3 Exploratory analysis**

To describe the main spatial patterns at a transect-scale of  $Z_{VEEC}$  and macrozooplankton biomass in relation to mesoscale structures, transect tracks were superimposed on satellite maps of chlorophyll and sea surface temperature. For this purpose we chose a specific area where mesoscale activity, as observed in satellite chlorophyll and SST data, was clear (presence of upwelling filaments and sea fronts; see also Fig. 5.3c from Chapter 3). Several transects were located across these mesoscale physical structures. To properly observe the along-transect pattern of the upper OMZ and macrozooplankton biomass, we fitted a smoothing spline on the series. The degree of smoothness was changed until the residuals of the fit were normally distributed and the oscillations over the space (along-transect) did not exhibit any long-term trend. The along-transects patterns of  $Z_{VEEC}$  and macrozooplankton biomass were then compared to the main physical structures, water masses and the distance to the shelf breaks at the transect scale.

### **5.2.4 Using $Z_{VEEC}$ to reveal small-scale physical structures**

Although large-scale physical structures can be observed on satellite maps of sea surface altitude, sea surface temperature or chlorophyll, small physical structures are more difficult to observe, since they require a higher resolution, which is not yet available from current satellite databases (Capet et al., 2008). In Chapter 3 we showed that  $Z_{VEEC}$  estimated from acoustic data is a robust proxy of the depth of the lower oxycline corresponding to the upper limit of the OMZ. Similarly to the altimetry data, which are used to observe and study the effect of large-scale physical structures like cyclonic or anticyclonic eddies on the zooplankton community (Le Cann et al., 2005; Capet et al., 2008),  $Z_{VEEC}$  was used as a proxy to detect the mesoscale and submesoscale physical structures and to study their effect on macrozooplankton.

#### ***Focusing on meso- and submesoscale processes***

The upper limit of the OMZ not only oscillates according to the presence of small-scale physical forces but also according to larger scale physical drivers. The depth of the upper limit of the OMZ is known to present an overall across-shelf increasing trend (Fuenzalida et al., 2009). As our aim is not to focus on such large-scale processes, but on meso- and submesoscale activity, we removed this trend by applying a least trimmed square regression (LTS) on the along-transect  $Z_{VEEC}$  before analysing the pattern at the meso- or submeso scales (Fig. 5.3). With this regression method the effect of the outliers on the overall linear tendency was minimized because only a given percent of the data with the lower residuals (90 % in this study) is used, excluding the remaining data with the largest residuals (10 % outliers).

To work at mesoscale we used the residuals of the LTS regression and aggregated the data by 2 km long elementary samples (Figs. 5.3 and 5.4). At this scale the effect of mesoscale physical activity was better observed while the effect of the high frequency physical structures (e.g. internal waves, small eddies) was minimized.

To work at the submesoscale we removed the mesoscale patterns from the residuals of the LTS regression (Fig. 5.3). For that we fitted a smoothing spline on the data. The degree of smoothness was changed until the residuals of the fit were normally distributed and the oscillations over the space (along-transect) did not exhibit any long-term trend. Then we aggregated the data by 200 m long elementary samples (Figs. 5.3 and 5.4).

The same methodology was applied to the series of macrozooplankton biomass, density and fish abundance but in this case the large-scale trend present in ZVEEC was not present and therefore not removed. Macrozooplankton biomass and density series were transformed by applying a cubic root, while fish abundance was transformed by taking its logarithm.

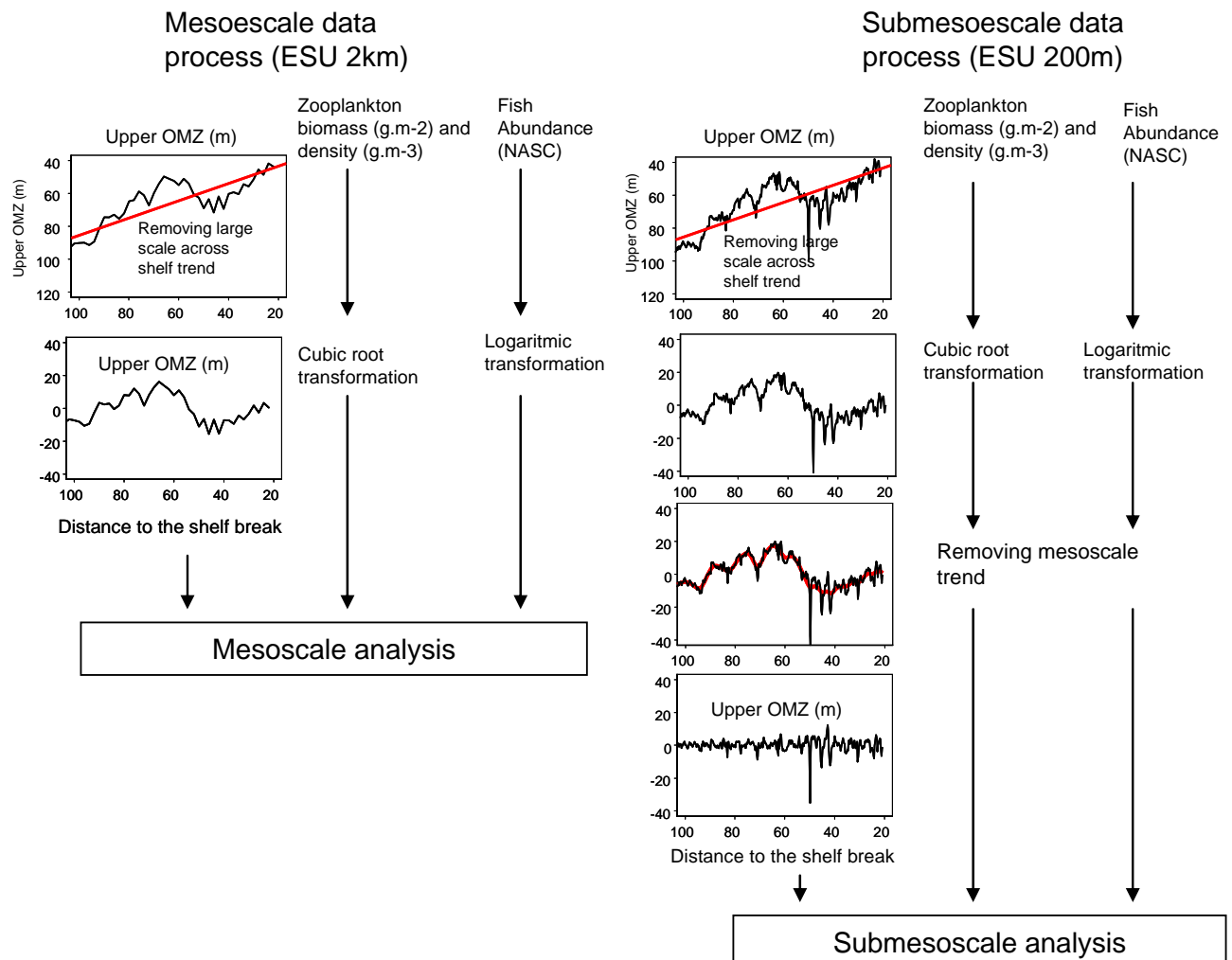


Figure 5.3 Synthesis of data process at meso- and submesoscale.

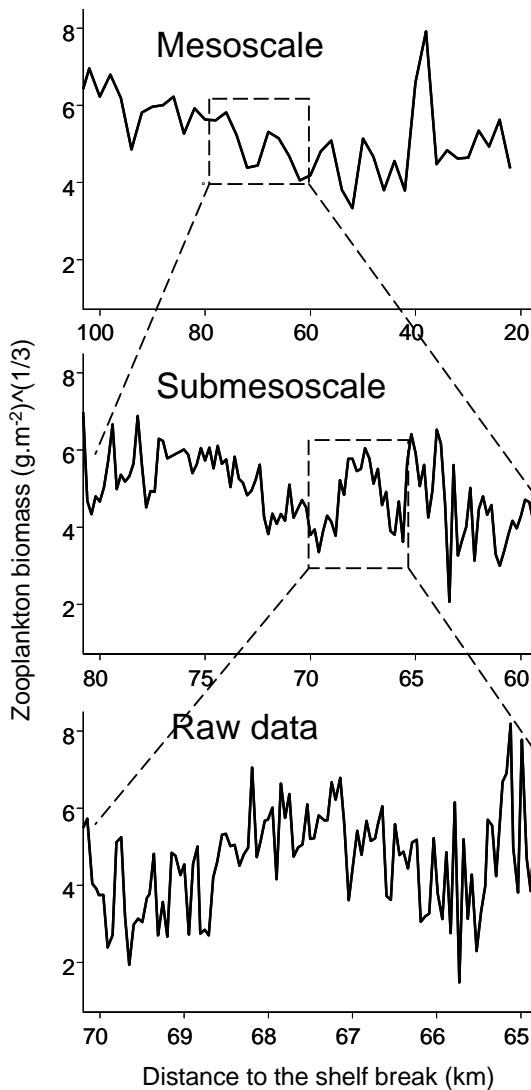


Figure 5.4 Example of macrozooplankton biomass variability at three scales; meso- and submesoscale and from raw data.

### 5.2.5 Statistical analysis

#### 5.2.5.1 Dealing with autocorrelation

To verify our hypothesis we need to test for the correlation between physics ( $Z_{\text{VEEC}}$ ) and macrozooplankton at both meso- and submesoscales. We further need to test the correlation between macrozooplankton and its predator. However, before making any correlation we first need to test if spatial autocorrelation, which could affect the significance of our results, was present in our physical and biological series. Indeed, marine resources usually present a patchy distribution (e.g. Wiebe, 1970; Steele, 1976; Haury et al., 1978; Mackas and Boyd, 1979; Mackas et al., 1985; Frontier, 1987; Russel et al., 1992). Patchiness implies that nearby observations of species abundance tend to be similar or that individual conspecific organisms are more narrowly spaced than by random chance (Wagner and Fortin, 2005). This can be caused either by the positive spatial

autocorrelation among the locations of individual organisms due to ecological spatial processes (e.g., species dispersal, competition for space and resources) or by spatial dependence due to (positive or negative) species responses to underlying environmental conditions (Wagner and Fortin, 2005). Spatial autocorrelation is a strong limitation for parametric statistical inference (e.g. linear correlation) because autocorrelated data violate the assumption of independence of most standard statistical procedures (Legendre, 1993). When the presence of spatial autocorrelation has been demonstrated at least four techniques could be used to deal with this limitation.

The first alternative is to randomly remove observations until spatial independence is attained. This solution is not recommended because it entails a net loss of information often obtained at a great cost (Legendre and Legendre, 1998).

The second alternative is to group the observations until new larger independent units are attained. This method also implies the loss of expensive and valuable information.

A third alternative is based on the fact that autocorrelation is like repeating the same observation many times in the sample, thus in order to counteract this effect, the sample size must be modified in the statistical test according to the degree and kind of autocorrelation of the series and its residuals (Dale and Fortin, 2009). According to Dale and Fortin (2009) it is safe to correct the degree of freedom of a statistic test (e.g. linear correlation) when the product of autocorrelation of the variables does not have a regular cycle or when this has a slow decrease. In general, the product of the autocorrelations is "well-behaved" when declining with lag distance or with amplitude of cycles declining rapidly with distance (Dale and Fortin, 2009).

A fourth alternative consists in simulating several realizations of a stochastic spatial process based on the same spatial structure as the one observed in each dependent and independent variables (e.g. macrozooplankton biomass and  $Z_{VEEC}$ ). Then, for each realization, the correlation between the variables can be calculated and used to generate the correlation density distribution. This distribution can be used to test for the significance of the correlation coefficient calculated from the original series (Fortin and Dale, 2005). However, it is a time-consuming process, especially if many samples (e.g. transects) have to be analysed.

Since an exploratory analysis revealed the presence of spatial autocorrelation in the data we applied the first three methods for correcting the autocorrelation for a linear correlation:

Method 1: We performed a random sampling of  $x$  pairs of data (keeping the spatial structure) until we obtained series that were no longer autocorrelated. The new  $n$  (number of data),  $n'$  was then very small and similar to the corrected degrees of freedom calculated from method 3.

Method 2: We increased the size of our elementary sample units so that each sampled unit was independent (i.e. mean values per ESU are not longer autocorrelated). The remaining number of sampling units was also similar to  $n'$  as calculated from method 3.

Method 3: Following the recommendations of Dale and Fortin (2009), we performed a visual inspection of the product of autocorrelation between two variables (e.g. the normalized series - by applying a cubic root - of macrozooplankton biomass and  $Z_{VEEC}$ ). As the product of autocorrelation of both series exhibited a rapid decline with distance (Fig. 5.5), we corrected the degrees of freedom according to Clifford et al. (1989, see below) and used this corrected value when testing the significance of the linear correlation (see description bellow). Since the series exhibited a high level of autocorrelation, the degree of correction was also high, decreasing the degree of freedom up to 11% of its initial value.

**Clifford et al. (1989) correction:**

If  $s_x^2$  and  $s_y^2$  are the sample variances of the two variables, x and y, and  $s_{xy}$  is the sample covariance (derived from the corrected sums of squares and products,  $S_{xx}$ ,  $S_{yy}$ , and  $S_{xy}$ ), then the correlation coefficient is calculated in the usual way

$$r_{xy} = \frac{s_{xy}}{s_x s_y} = \frac{S_{xy}}{\sqrt{S_{xx} S_{yy}}}, \quad \text{Eq. (5.1)}$$

and its significance is tested by comparing

$$t_r = \frac{r \sqrt{n-2}}{\sqrt{1-r^2}}, \quad \text{Eq. (5.2)}$$

with the t distribution with  $n-2$  degrees of freedom.

With spatial autocorrelation in the data, however,  $n$  must be replaced with an effective sample size that accounts for the autocorrelation. According to Clifford et al. (1989), this sample size ( $n'$ ) can be calculated as:

$$n'_r = 1 + s_r^{-2} \quad \text{Eq. (5.3)}$$

where  $s_r^{-2}$  is the variance of the correlation coefficient, which can be estimated based on the autocorrelations of x ( $r_x$ ) and y ( $r_y$ ). Using the autocorrelations at lag  $k$ ,  $r_x(k)$  and  $r_y(k)$ , with  $n(k)$  being the number of pairs in distance class  $k$  (here  $n-k$ ), the effective sample size can be calculated as:

$$n'_r = 1 + n \frac{1}{1 + \frac{2}{n} \sum_{k=1}^{n-1} n(k) r_x(k) r_y(k)} \quad \text{Eq. (5.4)}$$

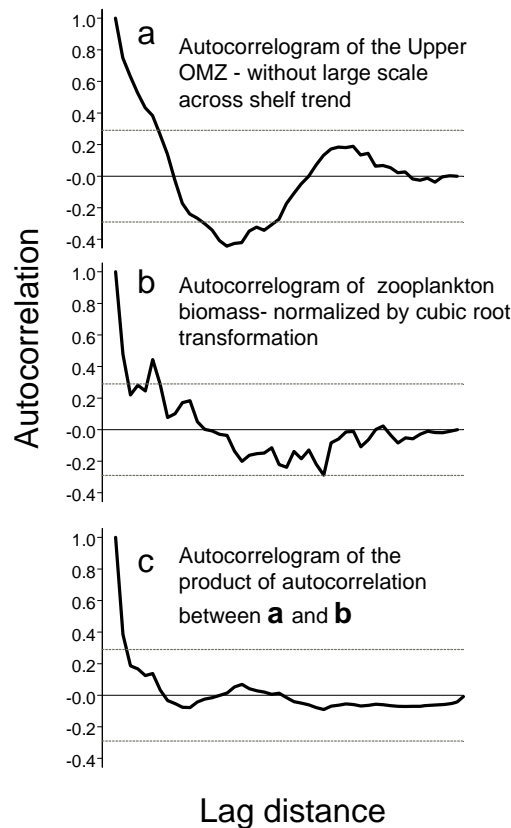


*Figure 5.5 Example of autocorrelograms from the detrended  $Z_{VEEC}$  (a), the normalized macrozooplankton biomass (b), and their autocorrelation product (c). Values within dotted lines are not significantly correlated. Each data point corresponds to a 2 km elementary sample unit.*

After contacting Dr. Fortin, it was suggested that we use the PASSaGE software ([www.passagesoftware.net](http://www.passagesoftware.net)) to apply the correction proposed by Dutilleul (1993). Similarly to the one described above, the Dutilleul (1993) method corrects the degree of freedom to account for the autocorrelation. Dutilleul (1993) provides a method to estimate  $n'$  based on a mathematical derivation for a finite number of locations. Clifford et al. (1989) and Dutilleul (1993) corrections do converge with an increasing number of observations, but more or less quickly depending on conditions (Dale and Fortin, 2009). As we did not find any difference in the test of significance when comparing the results from both methods, we used Clifford et al. (1989) correction because it was easier to compute. We finally selected this method (Method 3) because it does not eliminate data or the structures (eddies, internal wave), in the way that occurs when a small random sample is selected (Method 1) or when the size elementary sample units is increased excessively (Method 2).

### **5.2.5.2 The effect of physical structuring on macrozooplankton distribution**

In Chapter 2 we showed that macrozooplankton biomass significantly differed according to the ecological domain. Before performing the correlations between  $Z_{VEEC}$  and macrozooplankton biomass and density at submesoscale, we used an ANOVA to test for any effect of the ecological domain transect by transect. Results (Table 5.1) indicated significant differences (except in two daytime transects - note that results were similar when testing the effect on density instead of biomass and are not shown) so we performed the correlation in the shelf and offshore independently (the offshore section also included the slope domain since this section was too short - less than 10 km - to be analysed separately). Such tests were not performed on the mesoscale series since mesoscale structures extend beyond the considered ecological domains.

A scatter plot exploration showed that the relationship between  $Z_{VEEC}$  and macrozooplankton biomass (and density) was linear. Thus, we applied a linear correlation and corrected the degree of freedom according to the procedure previously described.

*Table 5.1. ANOVA test between shelf and offshore macrozooplankton biomass from diurnal and nocturnal transects.*

Day	$F_{[1, 8235]} = 600.7$	$p = 0.0000$
	$F_{[1, 4641]} = 1626.4$	$p = 0.0000$
	$F_{[1, 5323]} = 651.9$	$p = 0.0000$
	$F_{[1, 4582]} = 1887.9$	$p = 0.0000$
	$F_{[1, 4802]} = 1.5$	$p = 0.2252$
	$F_{[1, 5267]} = 1.2$	$p = 0.2743$
Night	$F_{[1, 8235]} = 477.7$	$p = 0.0000$
	$F_{[1, 4641]} = 7297.3$	$p = 0.0000$
	$F_{[1, 5323]} = 3862.0$	$p = 0.0000$
	$F_{[1, 4582]} = 1056.2$	$p = 0.0000$
	$F_{[1, 4802]} = 1661.0$	$p = 0.0000$
	$F_{[1, 5267]} = 425.4$	$p = 0.0000$

### **5.2.5.3 Predator-prey relationships: fish vs. macrozooplankton**

Depending on the scale of description, fish and prey can have a negative, positive or null relationship (Rose and Legett, 1990; Bertrand et al., 2004a). At a small scale, negative relationships may occur due to the grazing effect of fish on zooplankton or because of prey avoidance (mainly when the prey is part of the nekton), while at a larger scale a positive relationship might emerge as fish biomass would be higher where there is higher prey abundance (Rose and Legett, 1990; Bertrand et al., 2004a).

Fish acoustic data (e.g. Fish NASC per ESU) are characterised by a very high proportion of zeros, which limits the use of most statistical methods. To overcome this problem we worked in two steps for both scales.

First, we worked with presence-absence data for fish. In this case we used Generalized Additive Modelling (GAM, Hastie and Tibshirani, 1990); a technique that can detect non-linear and multivariate relationships between variables. GAM was used to model fish presence-absence as a function of macrozooplankton biomass/density. These models were constructed using the binomial distribution.

Second, we used the data where fish were present (NASC+) only. In this case we made a preliminary scatter plot exploration between fish NASC+ and macrozooplankton biomass/density. Since the trend was linear, we applied a linear correlation. Because we worked with discontinued spatial series, it was not possible to apply the correction from Clifford et al. (1989) to account for potential autocorrelation. To counterbalance a potential autocorrelation effect, we used a confidence level of 0.99 when testing for statistical significance of the correlations.

### 5.3 Results

#### 5.3.1 *The impact of satellite-resolved mesoscale structures on macrozooplankton distribution and Z<sub>VEEC</sub>*

Chlorophyll and SST maps showed the presence of an upwelling filament characterised by a strong geostrophic current located at about 12°S during the survey (Fig. 5.6). This filament was present for around two weeks, advecting offshore the coastal waters and enhancing the offshore primary production. Additionally, a sharp oceanic front was located south of the filament and remained stable (at the map scale) for about seven days. These hydrographic structures clearly affected both Z<sub>VEEC</sub> and the macrozooplankton biomass. Along the core of the filament, Z<sub>VEEC</sub> and the biomass of macrozooplankton were minimal (Fig. 5.6 transect 2). On the sides of the filament, regardless of the diel period, Z<sub>VEEC</sub> was also shallow (Fig. 5.4 transects 1, 3) in comparison to Z<sub>VEEC</sub> from areas outside the filament (Fig. 5.6 transects 4 and 5). Macrozooplankton biomass on the sides of the filament was much higher than along the core of the filament, regardless of the diel period. South of the filament and during the day, a relatively steady ocean front coincided with an offshore deepening of the Z<sub>VEEC</sub> and a rapid increase in macrozooplankton biomass (Fig. 5.6 transect 4). In the southern part of the selected area and during the night, both the Z<sub>VEEC</sub> and macrozooplankton biomass rapidly increased after the shelf break, toward offshore. (Fig. 5.6 transect 5).

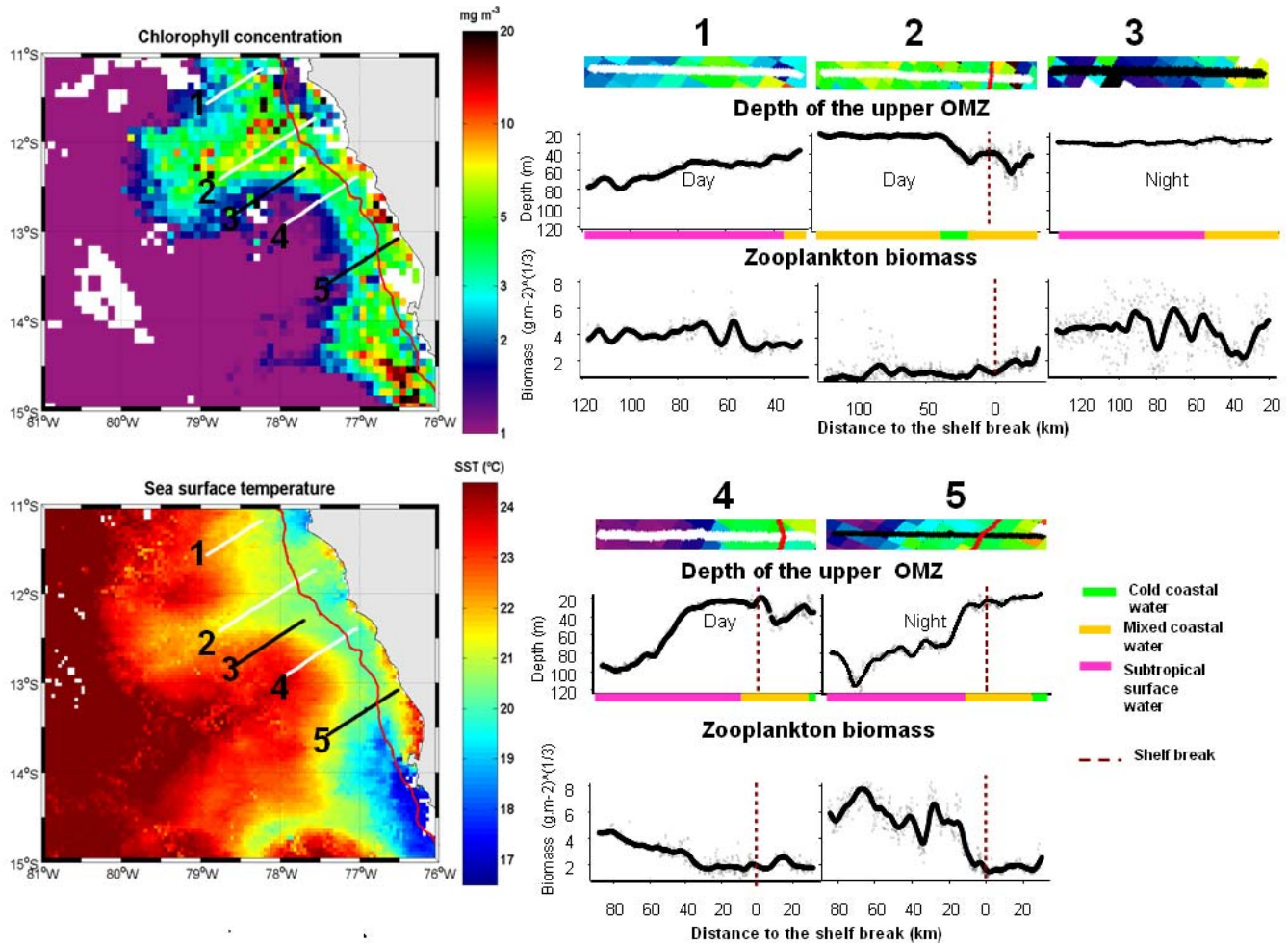


Figure 5.6 Macrozooplankton biomass (in g.m<sup>-2</sup> normalized by cubic root) distribution and Z<sub>VEEC</sub> (in m) along five selected transects in relation to chlorophyll, sea surface temperature and water masses. Satellite maps (left panels) correspond to the average chlorophyll and sea surface temperature conditions during 14 -18 March and 16 -18 Mar 2005, respectively. Water masses are represented as horizontal colour bar on the x-axis of Z<sub>VEEC</sub> panels. Transects were carried out during the period 13 -19 Mar 2005 and are represented as black (night) and white (day) lines on the satellite maps. X-axis of the macrozooplankton biomass panels represent the distance to the shelf break (indicated as vertical red dotted lines).

### 5.3.2 Mesoscale analysis

#### 5.3.2.1 The impact of mesoscale physical structures on macrozooplankton

Considering all transects together, macrozooplankton biomass and Z<sub>VEEC</sub> were slightly positively and significantly correlated during both day and night even if the correlation was rather weak (Fig. 5.7, Appendix C). At the transect scale and regardless of the diel cycle, macrozooplankton biomass was not significantly correlated to the upper depth of the OMZ except one positive correlation during day and one negative during the night.

However it is worth mentioning that all the correlations were positive (except one out of nine during the day and two out of ten during the night). Note that most of the non-significant correlations observed at the transect scale had a steeper slope than the significant correlation obtained considering all transects together. This remark is valid for most analyses described below performed by transect. Regardless of the diel period, macrozooplankton density was not significantly correlated to the Z<sub>VEEC</sub>, neither when considering all transects together, nor at the transect scale (except one negative correlation during the night) (Fig. 5.7, Appendix D)

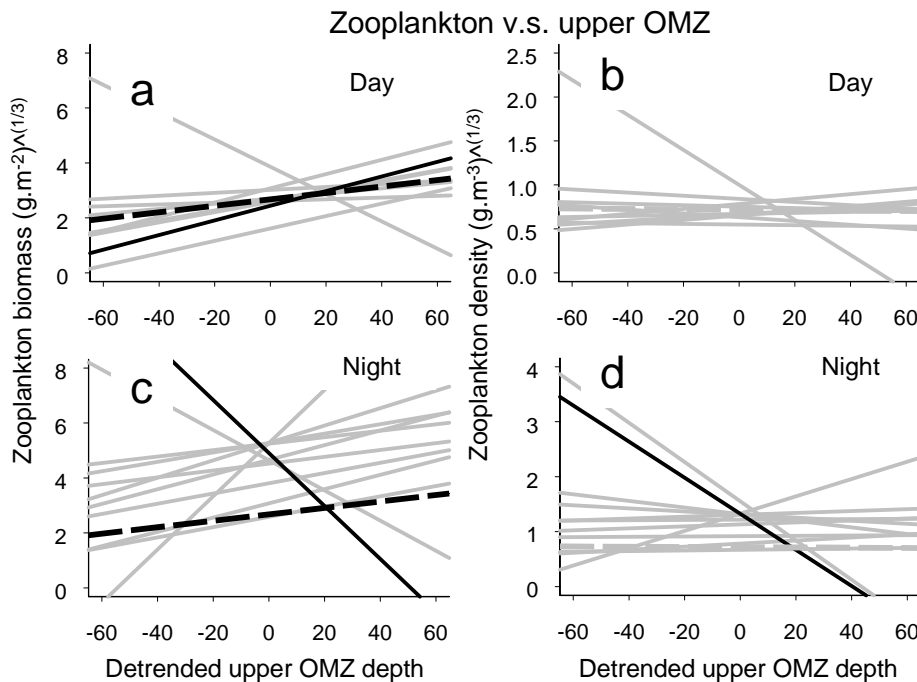


*Figure 5.7 Linear relation, at mesoscale, between macrozooplankton biomass (a, c) and density (b, d) normalized by cubic root and the detrended Z<sub>VEEC</sub> during the day (a, b) and during the night (c, d). Each solid line corresponds to one transect. The dotted line corresponds to the linear correlation considering all transects together. Black and grey colors indicate significant and not significant linear correlation, respectively.*

### 5.3.2.2 Mesoscale predator-prey relationships

- *Generalized additive models of fish presence-absence vs. macrozooplankton biomass and density*

GAM was used to model the probability of fish presence in an ESU as a function of macrozooplankton biomass or density. All models suggested a positive linear-like relationship between fish presence and macrozooplankton biomass and density (Fig. 5.8). However, the only significant relationship ( $p < 0.01$ ) was observed during the night when macrozooplankton biomass was considered (Fig. 5.8c). A gap in macrozooplankton data near the origin, however, affected the smoothed process artificially, creating a v-shaped trend near the origin. Note that both models constructed with daytime data would be significant if a 10% significance level were chosen.

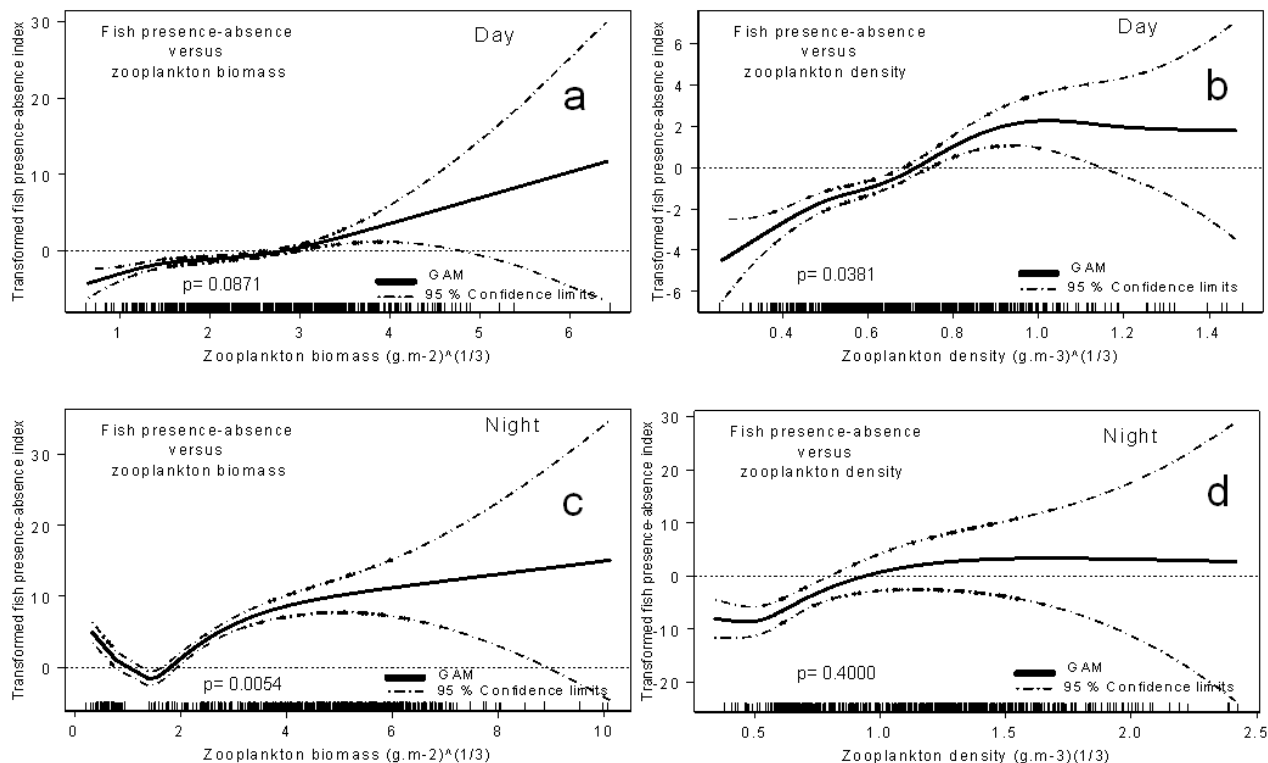


*Figure 5.8 Cubic spline fits (solid lines) of GAMs based on fish presence-absence at mesoscale according to: macrozooplankton biomass (a, c) and density (b, d) during the day (a, b) and during the night (c, d). The transformed fish presence index is in relative scale and corresponds to the spline smoother that was fitted on the data so that a y-value of zero is the mean effect of the x variable on the transformed fish presence index. Positive and negative y-values indicate positive and negative effect on the transformed fish presence index. The dotted lines show the 95% confidence limits of GAMs.*

#### • Fish NASC+ versus macrozooplankton biomass/density

When considering all transect together, fish NASC+ and macrozooplankton biomass were not significantly correlated during the day (Fig. 5.9a, Appendix E) but positively and significantly correlated during the night (Fig. 5.9c, Appendix E). At the transect scale, day-time fish abundance was significantly correlated (positive correlation) to macrozooplankton biomass in only one transect even if 7 out of 9 relationships were positive (Fig. 5.9a). During the night significant positive correlation was observed in 6 out of 9 transects.

Looking at all transects together, fish NASC+ and macrozooplankton density were significantly and positively correlated regardless of the diel period. At the transect scale, daytime fish abundance was not significantly correlated to macrozooplankton density but 7 out of 9 relationships were positive (Fig. 5.9b, Appendix F). During the night, fish abundance and macrozooplankton density were significantly positive correlated in 4 out of 9 transects (Fig. 5.9d, Appendix F).

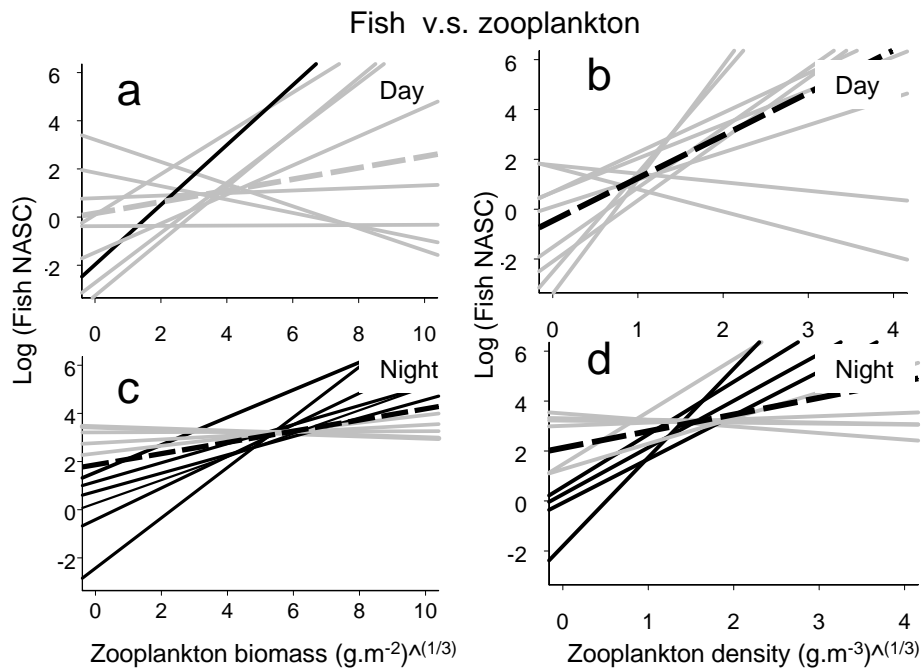


*Figure 5.9 Linear correlation, at mesoscale, between log-transformed fish acoustic nautical area scattering coefficient (NASC+) and macrozooplankton biomass (a, c) and density (b, d) normalized by cubic root, during the day (a,b) and during the night (c, d). Each solid line correspond to one transect. The dotted line corresponds to the linear correlation considering all transects together. Black and grey colors indicate significant and not significant linear correlation, respectively.*

### 5.3.3 Submesoscale analysis

#### 5.3.3.1 The impact of submesoscale physical structures on macrozooplankton

- *Shelf domain*

Over the shelf at the submesoscale, macrozooplankton biomass from all transects together was significantly and positively correlated to  $Z_{VEEC}$ , regardless of the diel period (Fig. 5.10a,c; Appendix G). At the transect scale positive and significant correlations were obtained in 4 out of 7 transects during the day (Fig. 5.10a, Appendix G). During the night, only two significant correlations (one positive and one negative) were observed out of 4 transects (Fig. 5.10c, Appendix G).

Macrozooplankton density from all transects together was not significantly correlated to  $Z_{VEEC}$ , regardless of the diel period (Fig. 5.10b,d; Appendix H). Similar results were observed at the transect scale with no significant correlations except one day-time transect which presented a significant negative correlation (Fig. 5.10b, Appendix H).

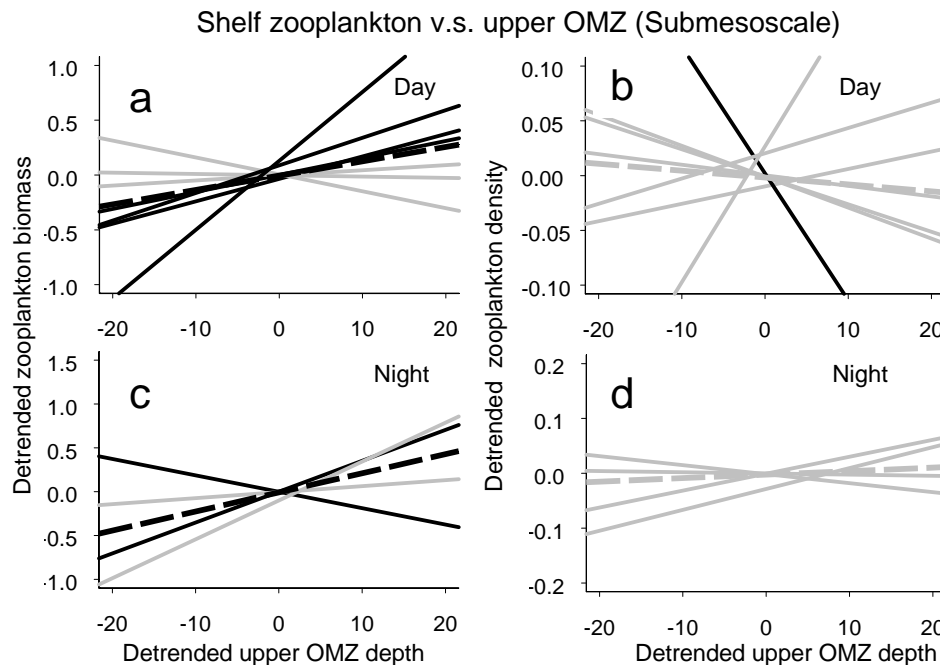


*Figure 5.10 Linear correlations, at submesoscale, between detrended shelf macrozooplankton biomass (a, c) and density (b, d) normalized by cubic root and the detrended  $Z_{VEEC}$  during the day (a,b) and during the night (c, d). Each solid line correspond to one transect. The dotted line corresponds to the linear correlation considering all transects together. Black and grey colors indicate significant and not significant linear correlation, respectively.*

- *Offshore domain*

Offshore at the submesoscale, when considering all transects together macrozooplankton biomass and  $Z_{VEEC}$  were significantly and positively correlated during the day (Fig. 5.11a, Appendix G). During the night the correlation was also significant but negative (Fig. 5.11c, Appendix G). The trends were similar at the transect scale with 5 out of 9 positive significant correlations during the day (Fig. 5.11a) and 4 out of 10 negative significant correlation during the night (Fig. 5.11c).

Macrozooplankton density from all transects together, was not significantly correlated to  $Z_{VEEC}$  (Fig. 5.11b, Appendix H) during the day, but significantly and negatively correlated during the night (Fig. 5.11d). At the transect scale, the correlations were not significant during the day (except one transect with a negative correlation) while a negative significant correlation was observed in 5 out of 10 transects during the night (Fig. 5.11b,d; Appendix H).

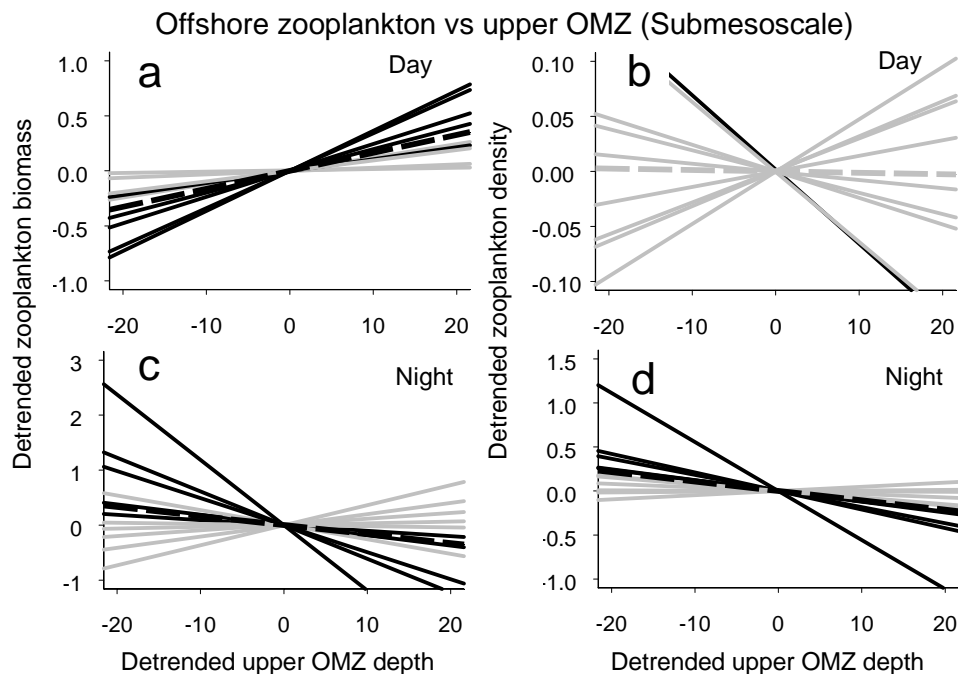


*Figure 5.11- Linear correlations, at submesoscale, between detrended offshore macrozooplankton biomass (a, c) and density (b, d) normalized by cubic root and the detrended  $Z_{VEEC}$  during the day (a,b) and during the night (c, d). Each solid line correspond to one transect. The dotted line corresponds to the linear correlation considering all transects together. Black and grey colors indicate significant and not significant linear correlation, respectively.*

### 5.3.3.2. Predator-prey relationships at submesoscale

- *GAM model of fish presence-absence vs. macrozooplankton biomass and density*

At the submesoscale, all GAM models showed that the fish presence index was significantly and positively related to macrozooplankton biomass and density ( $p<0.0001$ ), regardless of the diel period (Fig. 5.12).

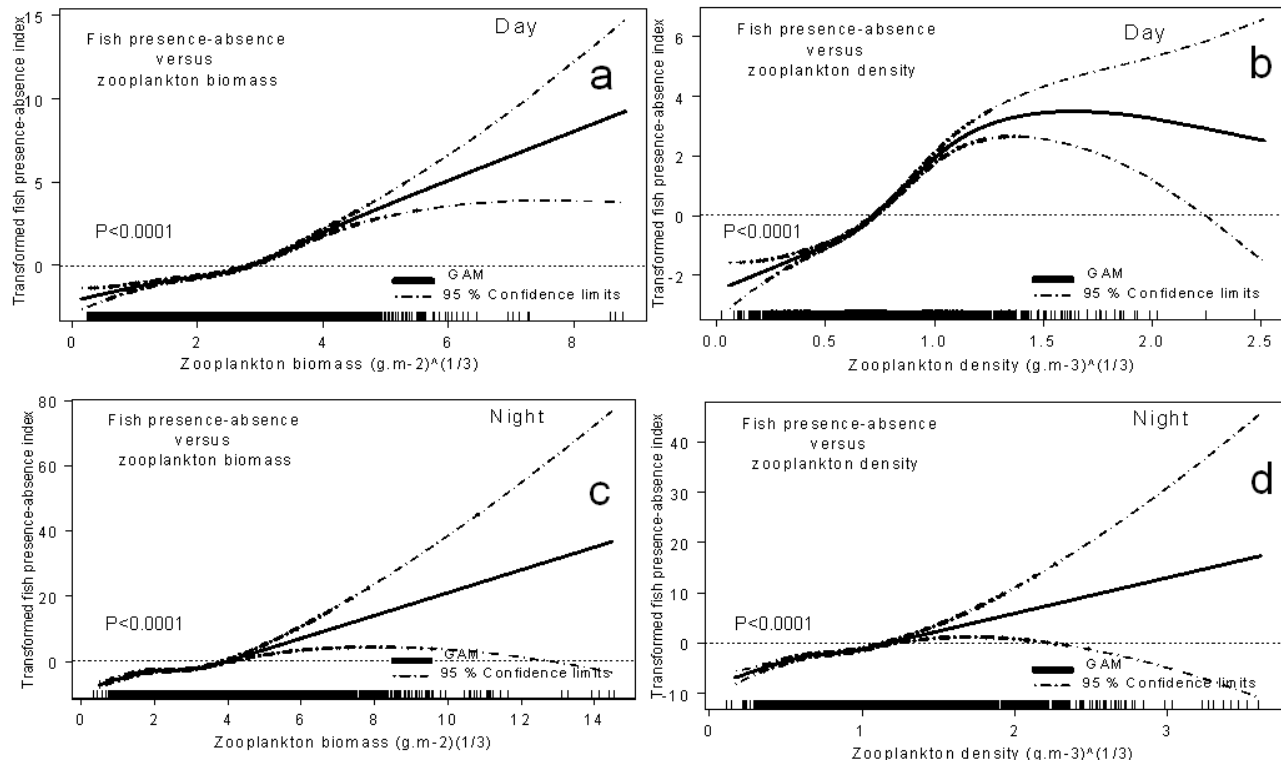


*Figure 5.12* Cubic spline fits (solid lines) of GAMs based on fish presence-absence at submesoscale according to: zooplankton biomass (a, c) and density (b, d) during the day (a, b) and during the night (c, d). The transformed fish presence index is in relative scale and corresponds to the spline smoother that was fitted on the data so that a y-value of zero is the mean effect of the x variable on the transformed fish presence index. Positive and negative y-values indicate positive and negative effect on the transformed fish presence index. The dotted lines show the 95% confidence limits of GAMs.

- **Fish NASC+ vs. macrozooplankton biomass**

#### **Shelf domain**

Over the shelf, regardless of the diel period and considering all transects together, fish NASC+ was significantly and positively correlated to macrozooplankton biomass and density (Fig. 5.13, Appendix I). At the transect scale, the correlations between fish NASC+ and macrozooplankton biomass were significant and positive in 2 out of 6 transects during the day (Fig. 5.13a, Appendix I), and in 2 out of 4 transects during the night (Fig. 5.13c, Appendix I). Similarly, the correlations between fish NASC+ and macrozooplankton density were significant and positive in 5 out of 7 transects during the day (Fig. 5.13b, Appendix J) and in 2 out of 4 transects during the night (Fig. 5.13b,

Appendix J). A significant negative correlation between fish NASC+ and macrozooplankton density was also observed in one transect during the night.

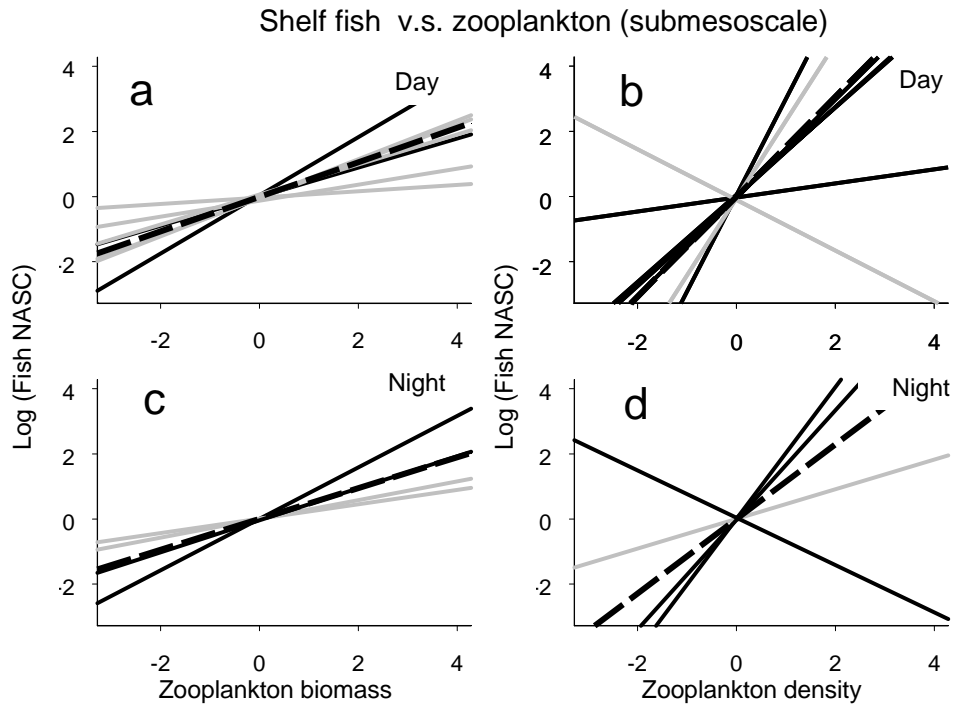


*Figure 5.13 Linear correlation, at submesoscale, between detrended log-transformed shelf fish acoustic nautical area scattering coefficient (NASC+) and macrozooplankton biomass (a, c) and density (b, d) normalized by cubic root, during the day (a,b) and during the night (c, d). Each solid line correspond to one transect. The dotted line corresponds to the linear correlation considering all transects together. Black and grey colors indicate significant and not significant linear correlation, respectively.*

#### *Offshore domain*

Similar to the correlation patterns observed in the shelf area, offshore fish NASC+ from all transects together was significantly and positively correlated to macrozooplankton biomass/density, regardless of the diel period (Fig. 5.14, Appendix I-J). Also at the transect scale and regardless of the diel period, all significant correlations between fish NASC+ and macrozooplankton biomass/density were positive (Fig. 5.14, Appendix I-J).

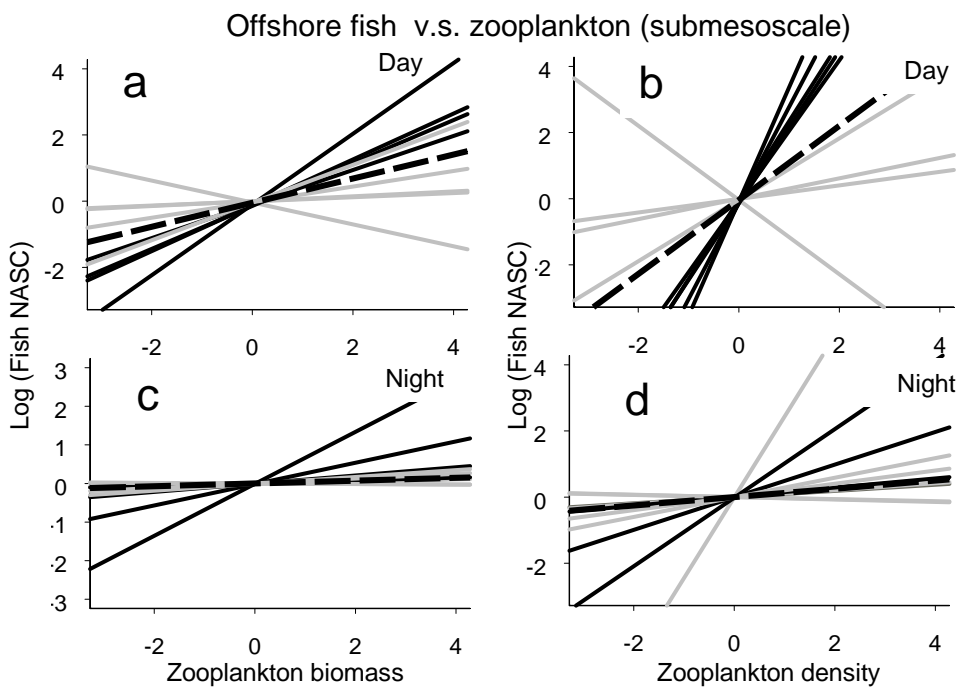


Figure 5.14 Linear correlation, at submesoscale, between detrended log-transformed offshore fish acoustic nautical area scattering coefficient ( $NASC+$ ) and macrozooplankton biomass (a, c) and density (b, d) normalized by cubic root, during the day (a,b) and during the night (c, d). Each solid line correspond to one transect. The dotted line corresponds to the linear correlation considering all transects together. Black and grey colors indicate significant and not significant linear correlation, respectively.

## 5.4 Discussion

In this Chapter we used the high-resolution data on  $Z_{VEEC}$ , macrozooplankton biomass and density, and fish biomass to test for the impact on physical mesoscale and submesoscale structures on organism distribution. We provide some evidence of the bottom-up spatial structuring of macrozooplankton at these two scales. We further provide evidence that the spatial structuring driven by physical forcing was transmitted to higher trophic levels. There is, however, a complexity of physical and biological factors as well as methodological assumptions that could have affected or increased the uncertainty about the expected patterns. Here we will discuss whether our results agreed with the expected patterns with regard to the various factors affecting both the spatial distribution of macrozooplankton and the spatial distribution of its predators at the meso- and submesoscales.

### 5.4.1 The impact of satellite-resolved mesoscale structures on macrozooplankton distribution and $Z_{VEEC}$

Our results showed that the presence of an upwelling filament (Fig. 5.6) was characterised by the advection of rich cold coastal mixed water and corresponded to a raising of  $Z_{VEEC}$ . The biomass along the core of the filament, however, was the lowest in the area. Such results were expected since our method allows detecting mainly macrozooplankton and strongly underestimates small zooplankton. Upwelling filaments can consistently expand the across-shelf regions and spread the biomass of cold coastal zooplankton from the shelf into the offshore (Keister et al., 2009). The abundance of small non-vertically migrant zooplankton from cold coastal water is therefore usually higher within a filament than outside, in the warm ocean (Keister et al., 2009). The abundance of large migratory zooplankton such as euphausiids, however, seems to be higher outside a filament (Huntley et al., 1995) as they may decouple their horizontal movement from the circulation of the filament (Keister et al., 2009).

Outside the filament,  $Z_{VEEC}$  exhibited the characteristic OMZ downward trend toward offshore (Fuenzalida et al., 2009) with a rapid decline at the site of the ocean front. In Chapter 4 we showed that the overall macrozooplankton biomass was higher offshore than over the shelf, with a shift over the slope. When taking a closer look in this chapter, it appears that a rapid increase in macrozooplankton biomass coincided with the frontal area more than with the position of the slope. Therefore, even if the shelf break probably plays a role, its effect may be overridden by processes related more to the water column (e.g. fronts), at least in those transects we studied in more detail. Ocean fronts constitute areas of active energy and matter exchanges, and harbour specific ecosystems (Sournia et al., 1990 *in* Anderson et al., 2004). Zooplankton behaviour associated with frontal circulation leads to a strong cross-frontal gradient in species composition, depth distribution, and zooplankton biomass (Olson et al., 1994). Major aggregations of euphausiids have been reported in association with frontal areas (Nishikawa et al., 1995; Molinero et al., 2008). In the NHCS, there is also evidence of large concentrations of euphausiids in fronts (Vinogradov and Shushkina, 1978). We suggest that zooplankton behaviour associated with the frontal circulation might be responsible for the observed offshore accumulation of macrozooplankton.

### ***5.4.2 The impact of mesoscale physical structures on macrozooplankton***

Our results showed that whatever the diel period, the overall impact of the mesoscale structures on the distribution of macrozooplankton biomass agreed with the expected theoretical patterns. Indeed, the areas with local lower/higher  $Z_{VEEC}$ , that are assumed to correspond to convergent/divergent mesoscale structures, were characterised by higher/lower macrozooplankton biomass. A different methodological approach, with the same data set, has also produced similar results (Grados, 2010). The author applied cross-variogram and principal coordinate of neighbourhood matrix and found that the  $Z_{VEEC}$  and macrozooplankton biomass were positively spatially associated on scales ranging from 1 to 60 km. However, contrary to the apparent agreement between the hypothesized and the observed impacts of the mesoscale physics on macrozooplankton biomass, no impact was observed on macrozooplankton density.

The weak correlation/association between  $Z_{VEEC}$  and macrozooplankton biomass and the apparent lack of correlation between mesoscale physics and macrozooplankton density reflect the complexity of the factors driving the mesoscale spatial distribution of macrozooplankton. Mesoscale variability of the  $Z_{VEEC}$  must reflect young and intensifying or old and decaying physical structures which may have a different effect on zooplankton (Goldthwait and Stainberg, 2008). Additionally, mesoscale deviance of  $Z_{VEEC}$  does not necessarily indicate transport in the assumed direction. For instance, there are evidence of accumulation of large zooplankton on the periphery of cyclonic eddies, possibly as a result of eddie-eddie interactions (Goldthwait and Stainberg, 2008). Even in the presence of active mesoscale structure, the convergence/divergence must be strong enough to directly affect zooplankton distribution. Some bias could have also resulted from the method applied. Due to the lack of available processed historical data -climatology - (when processing the data) on dissolved oxygen vertical structures; when determining the across-shore trend of the upper OMZ depth along a specific transect, we assumed that the trend was linear, and we thus removed it accordingly. This could have created artificial structures of convergence/divergence and thus increased variability and diluted the real mesoscale structuring signal. It is also possible that in some mesoscale ESUs (data aggregated over a distance of 2 km) the effect of high-frequency physical structures was still important. All these factors (and maybe others) could explain the weak relationship between the  $Z_{VEEC}$  and macrozooplankton biomass found in this study. Also they could be partially responsible for the lack of correlation between mesoscale physics and macrozooplankton density. However, it is more likely that zooplankton density responds to the mesoscale physics, in a different way than zooplankton biomass. Besides all the abovementioned factors, our results provide evidence of a bottom-up mesoscale spatial structuring of macrozooplankton biomass in accordance with our hypothesis.

### ***5.4.3 The impact of submesoscale physical structures on macrozooplankton***

At submesoscale, the overall impacts of physical structures on macrozooplankton biomass/density varied according to the ecological domain. While the overall shelf-macrozooplankton biomass was significantly accumulating on the convergence structures (positive deviance) and vice versa, during both, day and night, offshore-macrozooplankton biomass was higher in convergence structures during the day and in divergence structures during the night. Results from the corresponding cross-variograms and principal coordinate of neighbourhood matrix showed that submesoscale spatial structures of the

overall macrozooplankton biomass were positively associated to spatial structure in  $Z_{VEEC}$ , regardless of the diel period (although day-time associations were stronger) (Grados, 2010). However, when applying wavelet analysis at each transect, the author showed that submesoscale macrozooplankton biomass structures were sometimes positively and sometimes negatively related to the corresponding structures in the  $Z_{VEEC}$ , particularly during the night. Although the impacts of the submesoscale physics on macrozooplankton biomass agreed to a certain extent (depending on diel period and ecological domain) with our proposed hypothesis, macrozooplankton density was almost invariant to this effect and the only significant effect (in the offshore area during the night) was opposite to what was proposed.

The weak and sometimes opposite correlations and spatial association between macrozooplankton biomass and the  $Z_{VEEC}$  as well as the apparent lack of effect of physics on the distribution of macrozooplankton density reflects the complexity of the factors driving the submesoscale spatial distribution of zooplankton. As observed by Baukus (2008), not all submesoscale structures affect zooplankton distribution. Besides, since there is a limitation of instrumental sampling and computational resolution (Carpet et al., 2008), many unknown submesoscale physical processes could have affected macrozooplankton distribution in ways distinct from our proposed hypothesis. Methodological bias could have also been introduced. In addition to one described at mesoscale (see below), some bias could have been produced when fitting a smoothing trend to remove mesoscale signal from the submesoscale one. Additional bias is likely to occur when estimating macrozooplankton biomass in the presence of large fish aggregations. Large fish aggregations could have hidden most of macrozooplankton echoes (Chapter 4), thus locally increasing the uncertainty of macrozooplankton biomass/density estimation because of the few remaining data. Besides the possible methodological bias, some physics-zooplankton interaction can result in patterns different from the one we hypothesized (Lenner-Cody and Franks, 1999; Helfrich and Pineda, 2003). While relatively passive zooplankton should be concentrated by convergent physical flow, continuous upward swimming at speeds greater than the convergent flow would result in a net migration of organisms to the surface, concentrating zooplankton over the crest rather than at trough of the submesoscale structure (Lenner-Cody and Franks, 1999). This latter pattern has been observed with strong macrozooplankton swimmers, in particular euphausiids (Stevick et al., 2008). Results from Chapter 4 have shown that while relatively small macrozooplankton, and likely weak swimmers, dominate over the shelf domain (Chapter 4), high nocturnal biomass of large migratory macrozooplankton was found on the offshore domain. Euphausiids was probably the main constituent here. Thus the different correlations according to ecological domain may be also explained by the interactions between submesoscale physical structures and the distinct swimming capabilities of the shelf and offshore macrozooplankton communities. Our results may suggest that submesoscale physics structures macrozooplankton biomass according to our hypothesis only where relatively small macrozooplankton, and likely weak swimmers, dominated. Additionally, and as suggested for the mesoscale physics, it is more likely that macrozooplankton density responds to the submesoscale physics in a different way than macrozooplankton biomass and thus our approach failed to capture this effect. For instance, zooplankton aggregation could be higher or lower depending on the species, size or reproduction state (Ambler, 2002). Also, the interaction between topographic features and zooplankton swimming behaviour can result in higher or lower zooplankton aggregation (Greene et al., 1994).

Because of the limitations of our method and the number of potential factors that can affect our results, further studies are needed before arriving at any conclusion. But how about the next assumption: Was the predator distribution determined by the prey distribution?

#### **5.4.4 Biological forcing - fish vs macrozooplankton**

Our results indicate that it is more likely to find fish where macrozooplankton biomass/density is high. When both predators and prey are present, our results also indicate that a higher biomass/density of macrozooplankton attracts higher abundance of fish. This pattern was observed during the night at mesoscale and during day and night at submesoscale. Our results confirm those from Bertrand et al. (2008a), who observed that fish clusters were aggregated in macrozooplankton patches during the night. At this time most macrozooplankton are distributed at the surface (Chapter 4) and become available as food. Fish schools get dispersed (Bertrand et al., 2008a), which enhances individual feeding ability (e.g. Fréon et al., 1996; Cardinale et al., 2003).

During the day, our results indicate that fish are still aggregated in submesoscale structures that concentrate macrozoolankton, which suggests an active diurnal feeding behaviour. At this point, it is worth recalling that our ‘fish’ group included a variety of fish species with different feeding and vertical behaviours. The two most abundant fish are the mesopelagic (particularly *Vinciguerria lucetia* and myctophiids) and anchovy. Since mesopelagic fish perform large diel vertical migration, they are not distributed in the epipelagic layer during the day. We can thus assume that most of day-time fish observations were anchovy. This species is known to adapt its feeding period to prey availability (Espinoza and Bertrand, 2008). Therefore, if prey patches are available during the day, anchovy would presumably look for these aggregations and adapt their spatial distribution accordingly.

In most transects and regardless of the scale, we also found that when fish biomass was significantly correlated to macrozooplankton biomass, it was also significantly correlated to macrozooplankton density. This is an interesting result. Fish distribution seems structured by macrozooplankton aggregations that fulfil two characteristics: high density and high biomass. On the other hand, we evidenced an effect of physical features on the spatial patterns of macrozooplankton biomass, but not on macrozooplankton density. Although we have some evidence that physics structure zooplankton into high or low biomass patches, further studies are therefore needed to unveil the additional physical processes that make some patches denser, and apparently more attractive to fish, than others. Besides this, our results agree with the classic concept of higher fish abundance in rich prey areas (Bertrand et al., 2002), and highlight the importance of concentrated zooplankton aggregation for the predator feeding behaviour (Stevich et al., 2008). Regardless of how macrozooplankton was structured, our results at both scales indicate that macrozooplankton biomass/density exert bottom-up structuring on its predators.



## *General conclusions*

In this dissertation, an original acoustic method was developed and applied in the Northern Humboldt Current system (NHCS) in order to (i) extract valuable information on the main ecosystem compartments, particularly on the poorly known macrozooplankton, (ii) determine the vertical extension of their epipelagic habitat constrained by the presence of an oxygen minimum zone (OMZ), (iii) provide an acoustic estimation of the macrozooplankton biomass and its across and along-shore distribution according to the diel cycle, and (iv) investigate at submeso- and mesoscale the impact of physics on macrozooplankton distribution and its further effect on forage fish.

The acoustic method was designed to exploit bi-frequency acoustic databases obtained from routine acoustic surveys. It included a recently developed methodology based on the sum of backscattering strength from two or more frequencies, which significantly improved organism separation (Lebourges-Dhaussy and Fernandes, submitted). The method was applied to the most productive (in terms of fish production) eastern boundary upwelling system, the NHCS, and enabled us to extract quantitative and qualitative data on the biomass and the patterns of distribution of macrozooplankton, munida, fish and other (blue noise) marine compartments. Although more frequencies would ensure a higher accuracy in organism recognition as well as in size and biomass estimation (Napp et al., 1993; Holliday and Pieper, 1995), the strength of this method lies in its applicability to historical bi-frequency acoustic databases which have not yet been fully exploited. Indeed, valuable information about the features of the physical environment and marine organisms under different climatic conditions is ‘hidden’ in historical databases, and may be revisited with this method. Furthermore, when historical data are available (e.g. from IMARPE), intra- and interannual temporal dynamics could be studied. A shortcoming of the method remains in the validation of the acoustic biomasses, particularly for macrozooplankton. Indeed, the only independent available data on macrozooplankton biomass come from net sampling, which is characterized by a low efficacy when capturing macrozooplankton.

Our acoustic method also exploits the constraining effect of the OMZ on the spatial distribution of the epipelagic organisms, which are confined to the upper oxygenated layer (Diaz et al., 2008; Prince and Goodyear, 2006). This effect was observable in the acoustic records and was used to reveal, at a very high spatiotemporal resolution, the depth of the vertical extension of the epipelagic community ( $Z_{VEEC}$ ). Having defined  $Z_{VEEC}$ , it was possible to estimate the biomass of its main constituents as well as the biomass contribution of large nocturnal migratory organisms. By crossing the high-resolution data of  $Z_{VEEC}$  with anchovy horizontal distribution as determined from water masses (Swartzman et al., 2008) it was also possible to estimate its volume of habitat. Furthermore, we demonstrated that  $Z_{VEEC}$  coincided with the upper limit of the OMZ. We used this property to perform a high-resolution spatial monitoring of the upper limit of the OMZ (corresponding to the lower part of the oxycline), a parameter that is especially relevant for physical, biogeochemical and biological processes and interactions. Also we are in capacity to revisit historical acoustic data for the reconstruction of spatiotemporal dynamics of the epipelagic habitat and the upper limit of the OMZ that shallows in the context of climate change (Stramma et al., 2008). This methodology can also be applied to other ecosystems where OMZs or oceanic dead zones are present. This method should be applied not only in areas already known to encompass an OMZ (e.g. Eastern tropical

North Pacific, Arabian Sea) but also, before fish kills are noted, in systems where hypoxia/anoxia has clearly been increasing and affecting organisms (e.g. Oregon, Chan et al., 2008). This method, however, can only be applied when the present marine organisms are large and abundant enough to be detected by the frequencies used.

By applying our methodology we could perform the first direct estimation of the macrozooplankton biomass in the NHCS (Chapter 4) and studied its patterns of distribution. The estimated biomass was about 4 times higher than previously reported (net sampling; Ayón et al., 2004) or assumed (trophic models; Tam et al., 2008). The large-scale patterns of macrozooplankton distribution highlighted the importance of the shelf break for retaining and accumulating macrozooplankton over the slope and offshore areas of the NHCS. Furthermore, this pattern emphasizes euphausiids as the main constituent of the macrozooplankton biomass. The high biomass estimated is in agreement with the new finding in trophic ecology (Espinoza and Bertrand, 2008; Espinoza et al., 2009) indicating that forage fish consume mainly macrozooplankton and gives support to the current hypotheses (intermediate wind intensity, near-equator location and El Niño) explaining the NHCS high fish production (Bakun and Weeks, 2008; Chavez et al., 2008).

Lastly, the high-resolution biological (macrozooplankton and fish biomass) and physical (ZVEEC) data, allowed us to study the impacts of submeso- and mesoscale physical structures on macrozooplankton distribution and their further effects on their main predator, the forage fish (Chapter 5). Even if preliminary, the results provided evidence of the bottom-up physical effect on the spatial distribution of macrozooplankton biomass at these two scales. Additionally, we found further evidence of the bottom-up effect that macrozooplankton exert on forage fish distribution. Yet it was not clear how physical processes make some macrozooplankton patches denser, and apparently more attractive to fish, than others.

The application of the method we developed opens a series of scientific perspectives.

We are able to revisit present-day and historical acoustic databases and extract high-resolution data of macrozooplankton, a key ecological compartment of the ecosystem. Since zooplankton is the link between the physically driven primary producers and the biologically driven tertiary consumers, this information is essential to achieve a mechanistic understanding of the system, from physics to top predators. This high-resolution zooplankton information can be used to validate biogeochemical models, adjust trophic models and, more generally, to provide the “to” in end to end models (Mitra and Davis, 2010) of the NHCS. Furthermore, since the OMZ also affects biogeochemical and biological processes, these models would be highly benefit from the more realistic and high-resolution spatial representation of the upper limit of the OMZ. This would certainly further our understanding of how the NHCS functions on an ecosystem level (note that the results of this study will soon be used to calibrate the OSMOSE and SEAPODYM models, Shin and Cury, 2001; Lehodey et al., 2008). Depending on the availability of complementary net samples and oceanographic data, the high-resolution biological and physical data obtained in this study places us in a position to perform integrated multiscale ecological studies of the NHCS. Such integrated approaches are crucial to implement the ecosystem approach to fisheries (Pikitch et al., 2004). It allow us, for instance, to focus research effort on assessing the bottom-up physical effects of specific structures such as internal waves, filaments, ocean fronts or shallow epipelagic areas, on the patterns of distribution and abundance of the main compartment of the ecosystem. When a physical

structure has an apparent insignificant effect on the organism distribution, this high resolution data may also allow us to focus on biological processes and assess if the distribution patterns of organism are better explained by inter-species competition (e.g. munida and anchovy) or predator-prey relationships. Thus this study represents a step toward the implementation of an EBFM.



## References

- Alamo A. & Espinoza P. (1998) Variaciones alimentarias en *Engraulis ringens* y otros recursos pelágicos durante invierno-primavera de 1997. Informe Instituto del Mar del Perú 130: 45-52 (in Spanish, with abstract in English).
- Alamo A. (1989) Stomach contents of anchoveta (*Engraulis ringens*), 1974-1982. In: Pauly, D., Muck, P., Mendo, J., Tsukayama, I. (Eds.), The Peruvian upwelling ecosystem: dynamics and interactions. ICLARM Conference Proceedings, vol. 18, pp. 105-108.
- Alamo A., Espinoza P., Zubiate P. & Navarro I. (1997a) Comportamiento alimentario de la anchoveta peruana *Engraulis ringens*, durante el invierno de 1996. Crucero BIC Humboldt 9608-09. Informe Instituto del Mar del Perú 123: 38-46 (in Spanish, with abstract in English).
- Alamo A., Espinoza P., Zubiate P. & Navarro I. (1997b) Comportamiento alimentario de los principales recursos pelágicos peruanos en verano y comienzos de otoño 1997.
- Alamo A., Navarro I., Espinoza P. & Zubiate P. (1996a) Espectro alimentario y ración de alimentación de *Engraulis ringens* y de *Sardinops sagax sagax*, y mortalidad de huevos de la anchoveta peruana por predación. Informe Instituto del Mar del Perú 119: 34-42 (in Spanish, with abstract in English).
- Alamo A., Navarro I., Espinoza P. & Zubiate P. (1996b) Relaciones tróficas, espectro alimentario y ración de alimentación de las principales especies pelágicas en el verano 1996. Informe Instituto del Mar del Perú 122: 36-46 (in Spanish, with abstract in English).
- Alheit J. & Niquen M. (2004) Regime shifts in the Humboldt Current ecosystem. Progress in Oceanography 60: 201-222.
- Ambler J. W. (2002) Zooplankton swarms: characteristics, proximal cues and proposed advantages. Hydrobiologia 480: 155-164.
- Andersen V., Devey C., Gubanova A., Picheral M., Melnikov2 V., Tsarin2 S. & Prieur L. (2004) Vertical distributions of zooplankton across the Almeria-Oran frontal zone (Mediterranean Sea). Journal of Plankton Research 26: 275-293.
- Antezana T. (2002) Adaptative behaviour of *Euphausia mucronata* in relation to the oxygen minimum layer of the Humboldt Current. In: Färber, Jaime (Ed.), Oceanography of the Eastern Pacific II. Centro de Investigación Científica y de Educación Superior de Ensenada CICESE, México: 29-40.
- Antezana T. (2010) *Euphausia mucronata*: A keystone herbivore and prey in the Humboldt Current System. Deep Sea Research II doi:10.1016/j.dsr2.2009.10.014.
- Arntz W. E. & Fahrbach E. (1996) El Niño: experimento climático de la naturaleza. Fondo de cultura económica, Mexico.
- Aronés K., Ayón P., Hirche H.-J. & Schwamborn R. (2009) Hydrographic structure and zooplankton abundance and diversity off Paita, northern Peru (1994 to 2004) - ENSO effects, trends and changes. Journal of Marine Systems 78: 582-598.
- Ayón P., Criales-Hernandez M. I., Schwamborn R. & Hirche H.-J. (2008a) Zooplankton research off Peru: A review. Progress in Oceanography 79: 238-255.
- Ayón P., Purca S. & Guevara-Carrasco R. (2004) Zooplankton volume trends off Peru between 1964 and 2001. ICES Journal of Marine Science 61: 478-484.

- Ayón P., Swartzman G., Bertrand A., Gutiérrez M. & Bertrand S. (2008b) Zooplankton and forage fish species off Peru: large-scale bottom-up forcing and local-scale depletion. *Progress in Oceanography* 79: 208-214.
- Bakun A. & Mendelsohn R. (1989) Along shore wind stress 1953-82: correction, reconciliation and update through 1986. In: Pauly, D., Muck, P., Mendo, J., Tsukayama, I. (Eds.), *The Peruvian Upwelling Ecosystem: Dynamics and Interactions*. International Center for Living Aquatic Resources Management (ICLARM), Manila, Philippines, pp. 77-81.
- Bakun A. & Weeks S. J. (2008) The marine ecosystem off Peru: What are the secrets of its fishery productivity and what might its future hold? *Progress in Oceanography* 79: 290-299.
- Bakun A. (1996) Patterns in the ocean: ocean processes and marine population dynamics. University of California Sea Grant, San Diego, California, USA, in cooperation with Centro de Investigaciones Biológicas de Noroeste, La Paz, Baja California Sur, Mexico,: 323 pp.
- Ballón M., Wosnitza-Mendo C., Guevara-Carrasco R. & Bertrand A. (2008) The impact of overfishing and El Niño on the condition factor and reproductive success of Peruvian hake, *Merluccius gayi peruanus*. *Progress in Oceanography* 79: 300-307.
- Ballón, M. (2005) Comparative analysis of the community structure and trophic relations of the Peruvian hake *Merluccius gayi peruanus* and its by-catch of the years 1985 and 2001. Masters Thesis, University of Bremen, Bremen, Germany, unpublished.
- Barange M. & Pillar S. (1992) Cross-shelf circulation, zonation and maintenance mechanisms of *Nyctiphanes capensis* and *Euphausia hansenii* (Euphausiacea) in the northern Benguela upwelling system. *Continental Shelf Research* 12: 1027-1042.
- Barange M. & Stuart V. (1991) Distribution patterns, abundance and population dynamics of the euphausiids *Nyctiphanes capensis* and *Euphausia hansenii* in the northern Benguela upwelling system. *Marine Biology* 109: 93-101.
- Barber R. T. & Chavez F. P. (1983) Biological consequences of El Niño. *Science* 222: 1203-1210.
- Baukus A. J. (2008) Importance of Internal Waves for the Distribution, Density and Trophic Dynamics of Euphausiids on a Small Offshore Bank. Thesis - University of Southern Maine, Biology Dept. Aquatic Systems Group.
- Bertrand A., Barbieri M. A., Cordova J., Hernandez C., Gomez F. & Leiva F. (2004a) Diel vertical behaviour, predatoreprey relationships, and occupation of space by jack mackerel (*Trachurus murphyi*) off Chile. *ICES Journal of Marine Science* 61: 1105-1112.
- Bertrand A., Bard F.-X. & Josse E. (2002) Tuna food habits related to the micronekton distribution in French Polynesia. *Marine Biology* 140: 1023-1037.
- Bertrand A., Gerlotto F., Bertrand S., Gutierrez M., Alza L., Diaz E., Espinoza P., Ledesma J., Quesquén R., Peralta S. & Chavez F. (2008a) Contribution of schooling behaviour and environmental forcing in the patterns of fish 3d distribution across scales: the case for anchoveta. *Progress in Oceanography* 79: 264-277
- Bertrand A., Josse E., Bach P. & Dagorn L. (2003) Acoustics for ecosystem research: lessons and perspectives from a scientific programme focusing on tuna-environment relationships. *Aquatic Living Resources* 16: 197-203.
- Bertrand A., Segura M., Gutiérrez M. & Vasquez L. (2004b) From small-scale habitat loopholes to decadal cycles: a habitat-based hypothesis explaining fluctuation in pelagic fish populations off Peru. *Fish and Fisheries* 5: 296-316.

- Bertrand S., Dewitte B., Tam J., Díaz E. & Bertrand A. (2008b) Impacts of Kelvin wave forcing in the Peru Humboldt Current system: Scenarios of spatial reorganizations from physics to fishers. *Progress in Oceanography* 79: 278-289.
- Blackburn M. (1979) Zooplankton in an upwelling area off northwest Africa: composition, distribution and ecology. *Deep Sea Research I* 24A: 41-56.
- Brewer PG, Peltzer ET (2009) Limits to marine life. *Science* 324: 347-348.
- Brinton E. (1962) The distribution of Pacific euphausiids. *Bulletin of the Scripps Institution of Oceanography* 8: 51-270.
- Brinton E. (1967) Vertical migration and avoidance capability of euphausiids in the California current. *Bulletin of the Scripps Institution of Oceanography* 12: 451-483.
- Buitrón B. & Perea A. (2000) Aspectos reproductivos de la anchoveta peruana durante el período 1992-2000. *Boletín del Instituto del Mar del Perú* 19: 45-54.
- Capet X., Mc Williams J. C., Molemaker M. J. & Shchepetkina F. (2008) Mesoscale to Submesoscale Transition in the California Current System. Part I: Flow Structure, Eddy Flux, and Observational Tests. *Journal of Physical Oceanography* 38: 29-43.
- Cardinale M., Casini M., Arrhenius F. & Håkansson N. (2003) Diel spatial distribution and feeding activity of herring (*Clupea harengus*) and sprat (*Sprattus sprattus*) in the Baltic Sea. *Aquatic Living Resources* 16: 283-292.
- Carlotti F. & Poggiale J. C. (2010) Towards methodological approaches to implement the zooplankton component in "end to end" food-web models. *Progress in Oceanography* 84: 20-38.
- Carr M.-E. & Kearns E. J. (2003) Production regimes in four Eastern Boundary Current systems. *Deep Sea Research Part II: Topical Studies in Oceanography* 50: 3199-3221.
- Carr M.-E. (2002) Estimation of potential productivity in Eastern Boundary Currents using remote sensing. *Deep Sea Research Part II* 49: 59-80.
- Carritt DE, Carpenter JH (1966) Comparison and evaluation of currently employed modifications of the Winkler method for determining dissolved oxygen in seawater; a NASCD report. *Journal of Marine Research* 24: 286-318.
- Castillo R., Antezana T. & Ayón P. (2007) The influence of El Niño 1997-98 on pelagic ostracods in the Humboldt Current Ecosystem off Peru. *Hydrobiologia* 585: 29-41.
- Chaigneau A. & Pizarro O. (2005a) Surface circulation and fronts of the South Pacific Ocean, east of 120W. *Geophysical Research Letters* 32, L08605. doi:10.1029/2004GL022070.
- Chaigneau A. & Pizarro O. (2005b) Mean surface circulation and mesoscale turbulent flow characteristics in the eastern South Pacific from satellite tracked drifters. *Journal of Geophysical Research* 110, C05014, doi:10.1029/2004JC002628.
- Chaigneau A., Eldin G. & Dewitte B. (2009) Eddy activity in the four major upwelling systems from satellite altimetry. *Progress in Oceanography* 83: 117-123
- Chaigneau A., Gizolme A. & Grados C. (2008) Mesoscale eddies off Peru in altimeter records: Identification algorithms and eddy spatio-temporal patterns. *Progress in Oceanography* 79: 106-119.
- Chan F, Barth JA, Lubchenco J, Kirincich A, Weeks H, et al. (2008) Emergence of anoxia in the California Current large marine ecosystem. *Science* 319: 920.
- Chavez F. P. & Messié M. (2009) A comparison of Eastern Boundary Upwelling Ecosystems. *Progress in Oceanography* 83: 80-96

- Chavez F. P. (1987) El Niño y la Oscilacion del Sur. Investigacion y Ciencia (Spanish edition of Scientific American) 128: 46-55.
- Chavez F. P., Pennington J. T., Castro C. G., Ryan J. P., Michisaki R. P., Schlining B., Walz P., Buck K. R., McFadyen A. & Collins C. A. (2002) Biological and chemical consequences of the 1997-1998 El Niño in central California waters. Progress in Oceanography 54: 205-232.
- Chavez F. P., Ryan J., Lluch-Cota S. E. & Niquen M. (2003) From anchovies to sardines and back: multidecadal change in the Pacific Ocean. Science 299: 217-221.
- Chavez F., Bertrand A., Guevara-Carrasco R., Soler P. & Csirke J. (2008) The northern Humboldt Current System: Brief history, present status and a view towards the future. Progress in Oceanography 79: 95-105.
- Chiappa-Carrara X. & Gallardo-Cabello M. (1993) Estudio del régimen y hábitos alimentarios de la anchoveta *Engraulis mordax* Girard (Pises: Engraulidae), en Baja California, Mexico. Ciencias Marinas 19 285-305.
- Chu D. & Wiebe P. H. (2005) Measurements of sound-speed and density contrasts of zooplankton in Antarctic waters. ICES Journal of Marine Science 62: 818-831.
- Clifford P., Richardson S. & Hémon D. (1989) Assessing the significance of correlation between two spatial processes. Biometrics 45: 123-134.
- Colombo G. A., Mianzan H. & Madriolas A. (2003) Acoustic characterization of gelatinous plankton aggregations: four case studies from the Argentine continental shelf. ICES Journal of Marine Science 60: 650-657.
- Cotté C. & Simard Y. (2005) Formation of dense krill patches under tidal forcing at whale feeding hot spots in the St. Lawrence Estuary. Marine Ecology Progress Series 288: 199-210.
- Cressie N., Hawkins M. (1980) Robust Estimation of the Variogram: I. Mathematical Geology 12: 115-125.
- Criales-Hernández M., Schwamborn R., Graco M., Ayón P., Hirche H. J. & Wolff M. (2008) Zooplankton vertical distribution and migration off Central Peru in relation to the oxygen minimum layer. Helgoland Marine Research 62: 85-100.
- Cury P. & Roy C. (1989) Optimal environmental window and pelagic fish recruitment success in upwelling areas. Canadian Journal of Fisheries and Aquatic Sciences 46: 670-680.
- Cury P., Roy C. & Faure V. (1998) Environmental constraints and pelagic fisheries in upwelling areas: the Peruvian puzzle. South African Journal of Marine Science 19: 159-167.
- Cushing D. H. (1971) Upwelling and the production of fish. Advances in Marine Biology 9.
- Dale M. R. T. & Fortin M.-J. (2009) Spatial autocorrelation and statistical test: some solutions. Journal of Agricultural, Biological, and Environmental Statistics 14: 188-206.
- Debby L., Jackson G. A., Angel M. V., Lampitt R. S. & Burd A. B. (2004) Effect of net avoidance on estimates of diel vertical migration. Limnology and Oceanography 46: 2297-2303.
- Demarcq H. (2009) Trends in primary production, sea surface temperature and wind in upwelling systems (1998-2007). Progress in Oceanography 83: 376-385.
- Diaz RJ, Rosenberg R (2008) Spreading dead zones and consequences for marine ecosystems. Science 321: 926-929.

- Dutilleul P., Clifford P., Richardson S. & Hemon D. (1993) Modifying the t test for assessing the correlation between two spatial processes. *Biometrics* 49: 305-314.
- Echevin V., Aumont O., Ledesma J. & Flores G. (2008) The seasonal cycle of surface chlorophyll in the Peruvian upwelling system: A modelling study. *Progress in Oceanography* 79: 167-176.
- Ekau, W, Auel, H, Pörtner, HO, Gilbert, D. (2010) Impacts of hypoxia on the structure and processes in the pelagic community (zooplankton, macro-invertebrates and fish). *Biogeosciences*, vol. 7: 1669-1699.
- Escribano R., Hidalgo P. & Krautz C. (2009) Zooplankton associated with the oxygen minimum zone system in the northern upwelling region of Chile during March 2000. *Deep Sea Research Part II: Topical Studies in Oceanography* 56: 1083-1094.
- Escribano R., Hidalgo P., González H., Giesecke R., Riquelme-Bugueño R. & Manríquez K. (2007) Seasonal and inter-annual variation of mesozooplankton in the coastal upwelling zone off central-southern Chile. *Progress in Oceanography* 75: 470-485.
- Espinosa P. & Bertrand A. (2008) Revisiting Peruvian anchovy (*Engraulis ringens*) trophodynamics provides a new vision of the Humboldt Current system. *Progress in Oceanography* 79: 215-227.
- Espinosa P. (2001) Alimentación de la merluza peruana y sus fluctuaciones en el tiempo. In: M. Espino, M. Samamé, and R. Castillo (eds). *La merluza peruana (Merluccius gayi peruanus): Biología y Pesquería*. IMARPE. Documento de trabajo: 50-54.
- Espinosa P., Bertrand A., Van der Lingen C. D., Garrido S. & Rojas de Mendiola B. (2009) Diet of sardine (*Sardinops sagax*) in the northern Humboldt Current system and comparison with the diets of clupeoids in this and other eastern boundary upwelling systems. *Progress in Oceanography* 83: 242-250.
- Espinosa P., Blaskovic' V. & Navarro I. (1998b) Comportamiento alimentario de *Engraulis ringens*, a finales del invierno 1998. Crucero de evaluación hidroacústica de recursos pelágicos 9808-09 Informe Instituto del Mar del Perú 141: 67-71 (in Spanish, with abstract in English).
- Espinosa P., Blaskovic' V., Torriani F. & Navarro I. (1999) Dieta de la anchoveta *Engraulis ringens* según intervalos de talla. Crucero BIC José Olaya Balandra y BIC Humboldt 9906 Informe Instituto del Mar del Perú 149: 41-48 (in Spanish, with abstract in English).
- Espinosa P., Navarro I. & Torriani F. (1998a) Variaciones en el espectro alimentario de los principales recursos pelágicos durante otoño 1998. Crucero BIC Humboldt 9803-05 de Tumbes a Tacna. Informe Instituto del Mar del Perú 135: 134-142 (in Spanish, with abstract in English).
- Espinosa P., Navarro I. & Torriani F. (2000) Variaciones espaciales en la dieta de la anchoveta a finales de la primavera 1999. Crucero BICs José Olaya Balandra y SNP-2 9911-12. Informe Instituto del Mar del Perú 157 72-76 (in Spanish, with abstract in English).
- Fagetti E. & Campodonico I. (1971) Larval development of the red crab *Pleuroncodes monodon* (Decapoda Anomura: Galatheidae) under laboratory conditions. *Marine Biology* 8.
- Farías L, Paulmier A, Gallegos M (2007) Nitrous oxide and N-nutrient cycling in the oxygen minimum zone off northern Chile. *Deep Sea Research II* 54: 164-180.
- Feely RA, Sabine CL, Hernandez-Ayon M, Ianson D, Hales B (2008) Evidence for upwelling of corrosive "acidified" water onto the continental shelf. *Science* 320: 1490-1492.

- Fernandes P. G. (2009) Classification trees for species identification of fish-school echotrances. ICES Journal of Marine Science 66: 1073-1080.
- Fernandes, P. G., Korneliussen, R. J., Lebourges-Dhaussy, A., Masse, J., Iglesias, M., Diner, N., Ona, E., et al. 2006. The SIMFAMI Project: Species Identification Methods from Acoustic Multifrequency Information. Final Report to the EC, Q5RS-2001-02054.
- Fernández D., Escribano R. & Hidalgo P. (2002) Distribución de eufáusidos en el sistema de surgencia frente a la península de Mejillones (23°S) asociada a condiciones previas y durante El Niño 1997-98. Investigaciones Marinas 30: 25-43.
- Fernandez-Alamo A. & Färber-Lorda J. (2006) Zooplankton and the oceanography of the eastern tropical Pacific: A review Progress in Oceanography 69: 318-359.
- Fleminger A. & Clutter R. I. (1965) Avoidance of Towed Nets by Zooplankton. Limnology and Oceanography 10: 96-104.
- Foote K. & Stanton T. (2000) Acoustical Methods, in ICES Zooplankton Methodology Manual, edited by R. Harris, P. Wiebe, J. Lenz, H. Skjoldal, and M. Huntley (Academic, London), Chap. 6: 223-258.
- Foote K. G. (1980) Importance of the swimbladder in acoustic scattering by fish: A comparison of gadoid and mackerel target strengths. The Journal of the Acoustical Society of America. 67: 2084-2089.
- Foote K. G. (1983) Linearity of fisheries acoustics, with addition theorems. The Journal of the Acoustical Society of America 73: 1932-1940.
- Foote K. G. (1990) Spheres for calibrating an eleven-frequency acoustic measurement system. ICES Journal of Marine Science 46: 284-286.
- Foote K. G., Knudsen H. P. & Vestnes G. (1987) Calibration of acoustic instruments for fish density estimation: a practical guide. ICES Cooperative Research Report 144.
- Fortin M. J. & Dale M. R. T. (2005) Spatial Analysis: A Guide for Ecologists, Cambridge: Cambridge University Press.
- Forward R. B. (1988) Diel vertical migration: zooplankton photobiology and behaviour. Oceanography and Marine Biology: an Annual Review 26: 361-393.
- Fréon P., Barange M. & Arístegui J. (2009) Eastern boundary upwelling ecosystems: integrative and comparative approaches. Progress in Oceanography 83: 1-14.
- Fréon P., Bouchon M., Mullon C., García C. & Ñiquen M. (2008) Interdecadal variability of anchoveta abundance and overcapacity of the fishery in Peru. Progress in Oceanography 79: 401-412.
- Fréon P., Gerlotto F. & Soria M. (1996) Diel variability of school structure with special reference to transition periods. ICES Journal of Marine Science 53: 459-464.
- Frontier S. (1987) Applications of fractal theory to ecology. In Developments in Numerical Ecology: pp. 335- 378. Ed. by P. Legendre, and L. Legendre. Springer, Berlin. NATOASI Series, 314.
- Frontier S., Pichod-Viale D., Leprêtre A., Davoult D. & Luczak C. (2004) Ecosystèmes. Dunod, Paris. 550 p.
- Fuenzalida R., Schneider W., Garceés-Vargas J. & Bravo L. (2008) Satellite altimetry data reveals jet-like dynamics of the Humboldt Current. J. Geophys. Res. 113, C07043, doi: 10.1029/2007JC004684.
- Fuenzalida R., Schneider W., Garcés-Vargas J., Bravo L. & Lange C. (2009) Vertical and horizontal extension of the oxygen minimum zone in the eastern South Pacific Ocean Deep Sea Research II 56: 992-1003.

- Garcia HE, Locarnini RA, Boyer TP, Antonov JI (2006) World Ocean Atlas 2005, Vol. 3: Dissolved Oxygen, Apparent Oxygen Utilization, and Oxygen Saturation. Levitus S, editions. NOAA Atlas National Environmental Satellite, Data, and Information Service 63, Washington DC 342 p.
- Genin A. (2004) Bio-physical coupling in the formation of zooplankton and fish aggregations over abrupt topographies. *Journal of Marine Systems* 50: 3-20.
- Gerlotto F., Bertrand S., Bez N. & Gutierrez M. (2006) Waves of agitation inside anchovy schools observed with multibeam sonar: a way to transmit information in response to predation. *ICES Journal of Marine Science* 63 1405-1417.
- Goldthwait S. A. & Steinberg D. K. (2008) Elevated biomass of mesozooplankton and enhanced fecal pellet flux in cyclonic and mode-water eddies in the Sargasso Sea *Deep Sea Research II* 55: 1360-1377.
- González H. E., Daneri G., Iriarte J. L., Yannicelli B., Menschel E., Barría C., Pantoja S. & Lizárraga L. (2009) Carbon fluxes within the epipelagic zone of the Humboldt Current System off Chile: The significance of euphausiids and diatoms as key functional groups for the biological pump. *Progress in Oceanography* 83: 217-227.
- Grados D. (2010) Identificación de estructuras y relaciones espaciales en los componentes del sistema de la corriente de Humboldt: una comparación de métodos estadísticos. Tesis de Ingeniero estadístico, Universidad Nacional de Ingeniería, Lima, Perú, no publicada.
- Graham W. M., Pages F. & Hamner W. M. (2001) A physical context for gelatinous zooplankton aggregations: a review. *Hydrobiologia* 451: 199-212.
- Greene C. H., Wiebe P. H. & Zamon J. E. (1994) Acoustic dynamics visualization of patch in ocean ecosystems. *Oceanography* 7: 4-12.
- Greene C. H., Wiebe P. H., Burczynski J. & Youngbluth M. J. (1988) Acoustical detection of high-density krill demersal layers in the submarine canyons off Georges Bank. *Science* 241: 359-361.
- Greenlaw C. & Johnson R. (1982) Physical and acoustical properties of zooplankton. *The Journal of the Acoustical Society of America* 72: 1706-1710.
- Greenlaw C. (1979) Acoustical estimation of zooplankton populations. *Limnology and Oceanography* 24(2): 226-242.
- Greenlaw C. F. (1977) Backscattering spectra of preserved zooplankton. *The Journal of the Acoustical Society of America* 62: 44-52.
- Guénette S., Christensen V. & Pauly D. (2008) Trophic modelling of the Peruvian upwelling ecosystem: Towards reconciliation of multiple datasets. *Progress in Oceanography* 79: 326-335.
- Guevara-Carrasco R. & Lleonart J. (2008) Dynamics and Fishery of the Peruvian hake: between the nature and the man. *Journal of Marine Systems* 71: 249-259.
- Guevara-Carrasco R. (2004) Peruvian hake overfishing: misunderstood lessons. *Boletín Instituto del Mar Perú* 21: 27-32.
- Gutiérrez D., Arónés K., Chang F., Quipuzcoa L. & Villanueva P. (2005) Impacto de la variación oceanográfica estacional e interanual sobre los ensambles de Microfitoplancton, mesozoopláncton, ictioplancton y macrozoobentos de dos áreas costeras del norte del Perú entre 1994 y 2002. *Boletín Instituto del Mar del Perú* 22: 1-60.

- Gutiérrez D., Enríquez E., Purca S., Quipúzcoa L., Marquina R., Flores G. & Graco M. (2008) Oxygenation episodes on the continental shelf of central Peru: Remote forcing and benthic ecosystem response. *Progress in Oceanography* 79: 177-189.
- Gutiérrez D., Sifeddine A., Field D. B., Ortlieb L., Vargas G., Chávez F., Velazco F., Ferreira V., Tapia P., Salvatucci R., Boucher H., Morales M. C., Valdés J., Reyss J.-L., Campusano A., Boussafir M., Mandeng-Yogo M., García M. & Baumgartner T. (2009) Rapid reorganization in ocean biogeochemistry off Peru towards the end of the Little Ice Age. *Biogeosciences Discussions* 5: 3919-3943.
- Gutiérrez M, Herrera N, Marin D (1999) Distribución y abundancia de anchoveta y otras especies pelágicas entre los eventos El Niño 1982-83 y 1997-98. *Boletín Instituto del Mar del Perú* 18: 77-88.
- Gutiérrez M. (2000) Estimados de biomasa hidroacústica de los cuatro principales recursos pelágicos en el mar peruano durante 1983-2000. *Boletín Instituto del Mar del Perú* 19: 139-156.
- Gutiérrez M., Ramirez A., Bertrand S., Mórón O. & Bertrand A. (2008) Ecological niches and areas of overlap of the squat lobster ‘munida’ (*Pleuroncodes monodon*) and anchoveta (*Engraulis ringens*) off Peru. *Progress in Oceanography* 79: 256-263.
- Gutiérrez M., Swartzman G., Bertrand A. & Bertrand S. (2007) Anchovy (*Engraulis ringens*) and sardine (*Sardinops sagax*) spatial dynamics and aggregation patterns in the Humboldt Current ecosystem, Peru, from 1983-2003. *Fisheries Oceanography* 16: 155-168.
- Hastie T. & Tibshirani R. (1990) Generalized Additive Models. Chapman and Hall, London.
- Haury L. R., McGowan J. A. & Wiebe P. H. (1978) Patterns and processes in the time-space scales of plankton distributions. In: Spatial pattern in plankton communities pp. 277-327, Plenum, New York, USA.
- Hazen HL, Craig JK, Good CP, Crowder LB (2009) Vertical distribution of fish biomass in hypoxic waters on the Gulf of Mexico shelf. *Mar Ecol Prog Ser* 375: 195-207.
- Helfrich K. R. & Pineda J. (2003) Accumulation of particles in propagating fronts. *Limnology and Oceanography* 48: 1509-1520.
- Helly JJ, Levin LA (2004) Global distribution of naturally occurring marine hypoxia on continental margins. *Deep Sea Research I* 51: 1159-1168.
- Hewitt R. P. & Demer D. A. (1994) Acoustic estimated of krill biomass in the Elephant Island area: 1981 - 1993 CCAMLR Science, Vol. 1: 1-5.
- Hewitt R., Watkins J., Naganobu M., Sushin V., Brierley A. S., Demer D. A., Kasatkina S., Takao Y., Goss C., Malyshko A., Brandon M., Kawaguchi S., Siegel V., Trathan P., Emery J., Everson I. & Miller D. (2004) Biomass of Antarctic krill in the Scotia Sea in January/February 2000 and its use in revising an estimate of precautionary yield. *Deep Sea Research II* 51: 1215-1236.
- Heymans J. J. & Baird D. (2000) A carbon flow model and network analysis of the northern Benguela upwelling system, Namibia. *Ecological Modelling* 126: 9-32.
- Heywood K. (1996) Diel vertical migration of zooplankton in the Northeast Atlantic. *Journal of Plankton Research* 18: 163-184.
- Hill R. B. & Johnson J. A. (1975) A theory of upwelling over the shelf break. *Journal of Physical Oceanography* 4: 19-26.
- Holliday D. V. & Pieper R. E. (1995) Bioacoustical oceanography at high frequencies. *ICES Journal of Marine Science* 52: 279-296.

- Holliday D. V., Pieper, R. E., and Kleppel, G. S. (1989) Determination of zooplankton size and distribution with multi-frequency acoustic technology. *Journal du Conseil International pour L'Exploration de la Mer* 46: 52-61.
- Hormazabal S., Shaffer G. & Leth O. (2004) Coastal transition zone off Chile. *Journal of Geophysical Research - Oceans* (109), C01021 doi:10.1029/2003JC00195.
- Huggett J., Verheyen H., Escribano R. & Fairweather T. (2009) Copepod biomass, size composition and production in the Southern Benguela: Spatio-temporal patterns of variation and comparison with other eastern boundary upwelling systems. *Progress in Oceanography* 83: 197-207.
- Hunt G. L. J., Burgeson B. & Sanger G. A. (1981) Feeding ecology of seabirds of the eastern Bering Sea. In: *The Eastern Bering Sea Shelf: Oceanography and Resources*. Edited by D. W. C. Hood, J.A., NOAA, Univ. of Washington Press, Seattle, Washington 2: 629-647.
- Huntley M., Zhou M. & Nordhausen W. (1995) Mesoscale distribution of zooplankton in the California Current in late spring, observed by Optical Plankton Counter. *Journal of Marine Research* 53: 647-674.
- Hutchings L. (1992) Fish harvesting in a variable productive environment -searching for rules or searching for exceptions? *South African Journal of Marine Science* 12: 297-318.
- Hutchings L., Pillar S. & Verheyen H. M. (1991) Estimates of standing stock, production and consumption of meso- and macrozooplankton in the Benguela ecosystem *South African Journal of Marine Science* 11: 499-512.
- Hutchins D. A., Hare C. E., Weaver R. S., Zhang Y., Firme G. F., DiTullio G. R., Alm M. B., Riseman S. F., Maucher J. M., Geesey M. E., Trick C. G., Smith G. J., Rue E. L., Conn J. & Bruland K. W. (2002) Phytoplankton iron limitation in the Humboldt Current and Peru Upwelling. *Limnol. Oceanogr.* 47(4): 997-1011.
- Huyer A., Smith R. L. & Paluszakiewicz T. (1987) Coastal upwelling off Peru during normal and El Niño times *Journal of Geophysical Research* 92 14, 297-214, 307.
- Hyslop E. J. (1980) Stomach contents analysis - a review of methods and their application. *Journal of Fish Biology* 17: 411-429.
- ICES (2007) Collection of acoustic data from fishing vessels. ICES Cooperative Research Reports No. 287.
- Informe Instituto del Mar del Perú 127 82-89 (in Spanish, with abstract in English).
- Jahncke J., Checkley D. M. J. & Hunt Jr. G. L. (2004) Trends in carbon flux to seabirds in the Peruvian upwelling system: effects of wind and fisheries on population regulation. *Fisheries Oceanography* 13: 208-223.
- James A. G. & Chiappa-Carrara X. (1990) A comparison of field based studies on the trophic ecology of *Engraulis capensis* and *E. mordax*. In: Barnes, M., Gibson, R.N. (Eds.), *Trophic relationships in the marine environment*. Aberdeen University Press: pp. 208-221.
- James A. G. (1987) Feeding ecology, diet and field-based studies on feeding selectivity of the Cape anchovy *Engraulis capensis* Gilchrist. In: Payne, A.I.L., Gulland, J.A., Brink K.H. (Eds.). *The Benguela and Comparable Ecosystems* South African *Journal of Marine Science* 5 673-692.
- Jarre-Teichmann A. (1992) Steady-state modelling of the Peruvian upwelling ecosystem. Vorgelegt dem Fachbereich 2 (Biologie) der Universität Bremen als dissertation zur Erlangung des grades eines Doktors der Naturwissenschaften: 133.

- John E. H., Batten S. D., Harris R. P. & Hays G. C. (2001) Comparison between zooplankton data collected by the Continuous Plankton Recorder survey in the English Channel and by WP-2 nets at station L4, Plymouth (UK). Journal of Sea Research 46: 223-232.
- John M. A. S., Ruiz J., Monfray P., Grigorov I. & Hannah C. G. (2010) Introduction to the Cadiz Symposium on marine ecosystem model parameterisation: Examining the state of our art. Progress in Oceanography 84: 1-5.
- Johnson R. (1977) Sound scattering from a fluid sphere revisited. Journal of the Acoustical Society of America 61: 375-377.
- Kang M., Furusawa M. & Miyashita K. (2002) Effective and accurate use of difference in mean volume backscattering strength to identify fish and plankton. ICES Journal of Marine Science 59: 794-804.
- Karstensen J., Stramma L., Visbeck M. (2008) Oxygen minimum zones in the eastern tropical Atlantic and Pacific oceans. Progress in Oceanography 77: 331-350.
- Keister J. E., Cowles T. J., Peterson W. T. & Morgan C. A. (2009) Do upwelling filaments result in predictable biological distributions in coastal upwelling ecosystems? Progress in Oceanography 83: 303-313.
- Keister J. E., Houde E. D., Breitburg D. L. (2000) Effects of bottom-layer hypoxia on abundances and depth distributions of organisms in Patuxent River, Chesapeake Bay. Marine Ecology Progress Series 205: 43-59.
- Klein P. & Lapeyre G. (2009) The Oceanic Vertical Pump Induced by Mesoscale and Submesoscale Turbulence. Annual Review of Marine Science 1: 351-375.
- Kloser R. J., Ryan T., Sakov P., Williams A. & Koslow J. A. (2002) Species identification in deep water using multiple acoustic frequencies. Canadian Journal of Fisheries and Aquatic Sciences 59: 1065-1077.
- Knight M. D. (1984) Variation in larval morphogenesis within the southern California bight population of *Euphausia pacifica* from winter through summer, 1977-1978 CalCOFI Rep. 25.
- Konchina Y. V. & Pavlov Y. P. (1995) On methods of determining the trophic status of species in ichthyocenes. Journal of Ichthyology 35: 150-166.
- Konchina Y. V. (1981) The Peruvian jack mackerel, *Trachurus symmetricus murphyi*, a facultative predator in the coastal upwelling ecosystem. Journal of Ichthyology 21: 46-59.
- Konchina Y. V. (1983) The feeding Niche of Hake, *Merluccius gayi* (Merlucciidae), and Jack Mackerel, *Trachurus symmetricus* (Carangidae), in the Trophic System of the Peruvian Coastal Upwelling. Journal of Ichthyology 23: 87-98.
- Konchina Y. V. (1991) Trophic status of the Peruvian anchovy and sardine. Journal of Ichthyology 31: 59-72.
- Korneliussen R. J. & Ona E. (2003) Synthetic echograms generated from the relative frequency response. ICES Journal of Marine Science 60: 636-640.
- Koslow J. A. (1981) Feeding selectivity of schools of northern anchovy, *Engraulis mordax*, in the southern California. Fishery Bulletin 79: 131-142.
- Kramer D., Kalin M. J., Stevens E. G., Threlkeld J. R. & Zweifel J. R. (1972) Collecting and processing data on fish eggs and larvae in the California Current region. NOAA Technical Report NMFS Circ-370.
- Laloë F. (1985) Contribution à l'étude de la variance d'estimateurs de biomasse de poisson par échointégration. Océanographie Tropicale 20: 161-169.

- Lampert W. (1989) The adaptive significance of diel vertical migration of zooplankton. *Functional Ecology* 3: 21-27.
- Lau K-M, Weng H-Y (1995) Climate signal detection using wavelet transform: How to make a time series sing. *Bulletin of the American Meteorological Society* 76: 61-78.
- Lavanegos B. E. & Ohman M. D. (2007) Coherence of long-term variations of zooplankton in two sectors of the California Current System. *Progress in Oceanography* 75: 42-69.
- Lavanegos B. E., Jiménez-Pérez L. C. & Gaxiola-Castro G. (2002) Plankton response to El Niño 1997-1998 and La Niña 1999 in the southern region of the California Current. *Progress in Oceanography* 54: 33-58.
- Lavery A., Wiebe P. H., Stanton T. K., Lawson G. L., Benfield M. C. & Copley N. (2007) Determining dominant scatterers of sound in mixed zooplankton populations. *The Journal of the Acoustical Society of America* 122: 3304-3326.
- Lavoie D., Simard Y. & Saucier F. J. (2000) Aggregation and dispersión of krill at channel heads and shelf edges: the dynamics in the Saguenay-St. Lawrence Marine Park. *Canadian Journal of Fisheries and Aquatic Sciences* 57: 1853-1869.
- Lawson G. L., Wiebe P. H., Ashjian C. J. & Stanton T. K. (2008) Euphausiid distribution along the Western Antarctic Peninsula - Part B: Distribution of euphausiid aggregations and biomass, and associations with environmental features. *Deep Sea Research Part II: Topical Studies in Oceanography* 55: 432-454.
- Lawson G., L., Wiebe P., H., Ashjian C., J., Chu D. & Stanton T., K. (2006) Improved parametrization of Antarctic krill target strength models. *The Journal of the Acoustical Society of America* 119: 232-242.
- Le Cann B., Assenbaum M., Gascard J.-C. & Reverdin G. (2005) Observed mean and mesoscale upper ocean circulation in the midlatitude northeast Atlantic. *Journal of Geophysical Research* 110, C07S05, doi:10.1029/2004JC002768.
- Lebourges-Dhaussy A. & Fernandes P. G. (submitted) Multifrequency thresholding: simple algorithms for discriminating echotraces of fish from other scatterers ICES Journal of Marine Science.
- Legendre P. & Legendre L. (1998) Numerical ecology. Second English edition. Elsevier Science BV, Amsterdam, The Netherlands.
- Legendre P. (1993) Spatial autocorrelation: Trouble or New Paradigma? *Ecology* 74: 1659-1673.
- Lehodey, P., Senina, I., and Murtugudde, R. (2008). A spatial ecosystem and populations dynamics model (seapodym) - modeling of tuna and tuna-like populations. *Progress in Oceanography*, 78(4):304-318.
- Lennert-Cody C. E. & Franks P. J. S. (1999) Plankton patchiness in high-frequency internal waves. *Marine Ecology Progress Series* 186: 59-66.
- Levin L. A. (2003) Oxygen minimum zone benthos: adaptation and community response to hypoxia. *Oceanography And Marine Biology* 41: 1-45.
- Levin S. A. (1992) The problem of pattern and scale in ecology: The Robert H. Mac Arthur Award lecture. *Ecology* 73: 1943-1967.
- Lill C. C. (1979) Upwelling over the Shelf Break. *Journal of Physical Oceanography* 9.
- Link J. S. (2002) What does ecosystem-based fisheries management mean? *Fisheries* 27: 18-21.
- Liu Y, Liang XS, Weisberg RH (2007) Rectification of the bias in the wavelet power spectrum. *Journal of Atmospheric and Oceanic Technology* 24: 2093-2102.

- Logerwell E. A. & Wilson C. (2004) Species discrimination of fish using frequency-dependent acoustic backscatter. ICES Journal of Marine Science 61: 1004-1013.
- Lu B., Mackas D. L. & Moore D. F. (2003) Cross-shore separation of adult and juvenile euphausiids in a shelf-break alongshore current. Progress in Oceanography 57: 381-404.
- MacIsaac J. J., Dugdale R. C., Barber R. T., Blasco D. & Packard T. T. (1985) Primary production cycle in an upwelling center. Deep Sea Research Part A. Oceanographic Research Papers 32: 503-529.
- Mackas D. L. & Beaugrand G. (2009) Comparisons of zooplankton time series. Journal of Marine Systems 79: 286-304.
- Mackas D. L. & Boyd C. M. (1979) Spectral analysis of zooplankton spatial heterogeneity. Science 204: 62-64.
- Mackas D. L., Denman K. L. & Abbott M. R. (1985) Plankton patchiness: Biology in the physical vernacular. Bulletin of Marine Science 37: 652-674.
- Mackas D. L., Kieser R., Saunders M., Yelland D. R., Brown R. M. & Moore D. F. (1997) Aggregation of euphausiids and Pacific hake (*Merluccius productus*) along the outer continental shelf off Vancouver Island. Canadian Journal of Fisheries and Aquatic Sciences 54: 2080-2096.
- MacLennan D. N., Fernandes P. G. & Dalen J. (2002) A consistent approach to definitions and symbols in fisheries acoustics. ICES Journal of Marine Science 59: 365-369.
- Madureira L. S. P., Ward P. & Atkinson A. (1993) Differences in backscattering strength determined at 120 and 38 kHz for three species of Antarctic macroplankton. Marine Ecology Progress Series 93: 17-24.
- Manriquez K., Escribano R., Hidalgo P. (2009) The influence of coastal upwelling on the mesozooplankton community structure in the coastal zone off Central/Southern Chile as assessed by automated image analysis. Journal of Plankton Research 31: 1075-1088.
- Mantua N. J., Hare S. R., Zhang Y., Wallace J. M. & Francis R. C. (1997) A Pacific interdecadal oscillation with impacts on salmon production. Bulletin of the American Meteorological Society 78: 1069-1079.
- Matheron G. (1965) Les variables rigionalisées et leur estimation (Masson, Paris).
- Mathisen O. A. & Macaulay M. C. (1983) The morphological features of a superswarm of Krill, *Euphausia superba*. Memoirs of National Institute of Polar Research. Special Issue 27, National Institute of Polar Research, Tokyo, pp: 153-164.
- Mathisen O. L. (1989) Adaptation of the anchoveta (*Engraulis ringens*) to the Peruvian Upwelling System. In: The Peruvian upwelling ecosystem: Dynamics and interactions. 220-234. Ed by D. Pauly, P. Muck, J. Mendo, and I. Tsukayama. ICLARM Conference Proceedings 18, 438 p.
- McWilliams JC, Colas F, Molemaker MJ (2009) Cold filamentary intensification and oceanic surface convergence lines. Geophysical Research Letters 36: L18602, doi:10.1029/2009GL039402.
- Mitra A. & Davis C. (2010) Defining the "to" in end-to-end models. Progress in Oceanography 84: 39-42.
- Mitson R. B., Simard Y. & Goss C. (1996) Use of a two-frequency algorithm to determine size and abundance of plankton in three widely spaced locations. ICES Journal of Marine Science 53: 209-215.

- Molinero J. C., Ibanez F., Souissi S., Bosc E. & Nival P. (2007) Surface patterns of zooplankton spatial variability detected by high frequency sampling in the NW Mediterranean. Role of density fronts. *Journal of Marine Systems*.
- Morales C., Braun M., Reyes H., Blanco J. L. & Davies A. G. (1996) Anchovy larval distribution in the coastal zone off northern Chile: the effect to flow dissolved oxygen concentration and of a cold-warm sequence (1990-1995). *Investigaciones Pesqueras(Chile)* 24: 77-96.
- Mosteiro A., Fernandes P. G., Armstrong F. & S.P.R. G. (2004) A dual frequency algorithm for the identification of sandeel school echotrades pp. 13 pp.
- Muck P. (1989) Anchoveta consumption of Peruvian hake: a distribution and feeding model. In D. Pauly, P. Muck, J. Mendo & I. Tsukayama (Eds.) *The Peruvian upwelling ecosystem: dynamics and interactions* (pp. 306-320). ICLARM Conference Proceedings 18.
- Murase H., Ichihara M., Yasuma H., Watanabe H., Yonezaki S., Nagashima H., Kawahara S. & Miyashita K. (2009) Acoustic characterization of biological backscatterings in the Kuroshio-Oyashio inter-frontal zone and subarctic waters of the western North Pacific in spring. *Fisheries Oceanography* 18: 386-401.
- Napp J. M., Ortner P. B., Pieper R. E. & Holliday D. V. (1993) Biovolume-size spectra of epipelagic zooplankton using a multi-frequency acoustic profiling system (MAPS). *Deep Sea Research Part I: Oceanographic Research Papers* 40: 445-459.
- Naqvi SWA, Jayakumar DA, Narvekar PV, Naik H, Sarma VVSS, et al. (2000) Increased marine production of N<sub>2</sub>O due to intensifying anoxia on the Indian continental shelf. *Nature* 408: 346-349.
- Neira S., Arancibia H. & Cubillos L. (2004) Comparative analysis of trophic structure of commercial fishery species off central Chile in 1992 and 1998. *Ecological Modelling* 172: 233-248.
- Neivison CD, Lueker T J, Weiss RF (2004) Quantifying the Nitrous Oxide Source from Coastal Upwelling. *Global Biogeochemical Cycles* 18: GB1018.
- Nicol S. (2006) Krill, Currents, and Sea Ice: *Euphausia superba* and Its Changing Environment. *BioScience* 56: 111-120.
- Nishikawa J., Tsuda A., Ishigaki T. & Terazaki M. (1995) Distribution of euphausiids in the Kuroshio front and warm water tongue with special reference to the surface aggregation of *Euphausia pacifica*. *Journal of Plankton Research*. 17: 611-629.
- Olson D. B., Hitchcock G. L., Mariano A. J., Ashian C. J., Peng G., Nero R. W. & Podesta G. P. (1994) Life on the edge: Marine life and fronts. *Oceanography* 7: 52-60.
- Orr JC, Fabry VJ, Aumont O, Bopp L, Doney SC, et al. (2005) Anthropogenic ocean acidification over the twenty-first century and its impact on calcifying organisms. *Nature* 437: 681-686.
- Oschlies A., Schulz KG, Riebesell U, Schmittner A (2008) Simulated 21st century's increase in oceanic suboxia by CO<sub>2</sub>-enhanced biotic carbon export. *Global Biogeochemical Cycles* 22: GB4008, doi:10.1029/2007GB003147.
- Pakhomov E. A. (2004) Salp/krill interactions in the eastern Atlantic sector of the Southern Ocean. *Deep Sea Research II* 51: 2645-2660.
- Patti B., Guisande C., Vergara A. R., Riveiro I., Maneiro I., Barreiro A., Bonanno A., Buscaino G., Cuttitta A., Basilone G. & Mazzola S. (2008) Factors responsible for the differences in satellite-based chlorophyll a concentration between the major global upwelling areas. *Estuarine, Coastal and Shelf Science* 76: 775-786.

- Paulmier A, Ruiz-Pino D (2009) Oxygen minimum zones (OMZs) in the modern ocean. *Progress in Oceanography* 80, 113-128.
- Paulmier A, Ruiz-Pino D, Garçon V, Farías L (2006) Maintaining of the Eastern South Pacific Oxygen Minimum Zone (OMZ) off Chile. *Geophysical Research Letters* 33: L20601, doi:10.1029/2006GL026801.
- Pauly D., Jarre A., Luna S., V. S. J., Rojas de Mendiola B. & Alamo A. (1989) On the quantity and types of food ingested by Peruvian anchoveta, 1953-1982. In: Pauly, D., Muck, P., Mendo, J., Tsukayama, I. (Eds.), *The Peruvian upwelling ecosystem: dynamics and interactions*. ICLARM Conference Proceedings, vol. 18, pp. 109-124.
- Pieper R. E. & Holliday D. V. (1984) Acoustic measurements of zooplankton distributions in the sea. *Journal du Conseil International pour l'Exploration de la Mer* 226-238
- Pikitch E. K., Santora C., Babcock E. A., Bakun A., Bonfil R., Conover D. O., Dayton P., Doukakis P., Fluharty D., Heneman B., Houde E. D., Link J., Livingston P. A., Mangel M., McAllister M. K., Pope J. & Sainsbury K. J. (2004) Ecosystem-Based Fishery Management. *Science* 305: 346-347.
- Pizarro O., Clarke A. J. & Van Gorder S. (2001) El Niño sea level and currents along the South American coast: comparison of observations with theory. *Journal of Physical Oceanography* 31: 1891-1903.
- Pizarro O., Shaffer G., Dewitte B. & Ramos M. (2002) Dynamics of seasonal and interannual variability of the Peru-Chile Undercurrent. *Geophysical Research Letters* 29 (12)
- Postel L., da Silva A. J., Mohrholz V. & Lass H.-U. (2007) Zooplankton biomass variability off Angola and Namibia investigated by a lowered ADCP and net sampling. *Journal of Marine Systems* 68: 143-166.
- Postel, L., Fock, H., Hagen, W. 2000. Biomass and abundance. In:Harris, R., Wiebe, P., Lenz, J., Skjoldal, H.R., Huntley, M. (Eds.). *Zooplankton Methodology Manual*. Academic Press, San Diego, pp. 83-192
- Prather MR, Derwent D, Ehhalt P, Fraser E et al. (1995) Chapter 2.2: Radiative Forcing of Climate Change, in Climate Change. In Houghton JT et al. editions. *The Science of Climate Change*, Intergovernmental Panel on Climate Change. Cambridge U Press, pp. 86-103.
- Prince ED, Goodyear P (2006) Hypoxia-based habitat compression of tropical pelagic fishes. *Fisheries Oceanography* 15: 451-464.
- Ressler P. H., Brodeur R. D., Peterson W. T., Pierce S. D., Vance P. M., Røstad A. & Barth J. A. (2005) The spatial distribution of euphausiid aggregations in the Northern California Current during August 2000. *Deep Sea Research II* 52: 89-108.
- Rinke K., Hubner I., Petzoldt T., Rolinski S., König-Rinke M., Post J., Lorke A. & Benndorf J. (2007) How internal waves influence the vertical distribution of zooplankton. *Freshwater Biology* 52: 137-144.
- Rojas B. (1953) Estudios preliminares del contenido estomacal de las anchovetas. *Boletín de la Compañía Administradora del Guano* 1: 33-42.
- Rojas de Mendiola B. (1969) The food of the Peruvian anchovy. *Journal du Conseil International pour l'Exploration de la Mer* 32: 433-434.
- Rojas de Mendiola, B. (1989) Stomach contents of anchoveta (*Engraulis ringens*), 1953-1974. In: Pauly, D., Muck, P., Mendo, J., Tsukayama, I. (Eds.) *The Peruvian upwelling ecosystem: dynamics and interactions*. ICLARM Conference Proceedings, vol. 18, pp. 97-104.

- Rose G. A. & Leggett W. C. (1990) The importance of scale to predator-prey spatial correlation: an example of Atlantic Fishes. *Ecology* 71: 33-43.
- Russel R. W., Hunt G. L., O'Coyle K. & Cooney R. T. (1992) Foraging in a fractal environment: spatial patterns in a marine predator-prey system. *Landscape Ecology* 7: 195-209.
- Ryther J. H. (1969) Photosynthesis and fish production in the sea. *Science* 166: 72-76.
- Sameoto D. (1981) Horizontal and vertical distributions of zooplankton numbers and biomass off the coast of Peru. *Boletín Instituto del Mar del Perú Volumen Extraordinario*.
- Sanchez S. (2000) Variación estacional e interanual de la biomasa fitoplantónica y concentración de clorofila A frente a la costa peruana durante 1976-2000. *Boletín Instituto del Mar del Perú* 19: 29-43.
- Santander H. & De Castillo O. (1973) Estudio de las primeras etapas de vida de anchoveta. *Informe Inst. Mar Perú-Callao* (41): 30 p.
- Santander H. (1981) The zooplankton in an upwelling area off Peru. In: Richards, F.A. (Ed.), *Coastal Upwelling Coastal and Estuarine Sciences*, vol. 1. American Geophysical Union, Washington, DC, pp: 411-416.
- Santander H., Carrasco S. & Luyo G. (1981) El zooplancton del área norte del Perú. *Boletín Instituto del Mar del Perú Volumen Extraordinario*
- Saunders R. A., Brierley A. S., Watkins J. L., Reid K., Murphy E. J., Enderlein P. & Bone D. G. (2007) Intra-annual variability in the density of Antarctic krill (*Euphausia superba*) at South Georgia, 2002-2005: within-year variation provides a new framework for interpreting previous 'annual' estimates of krill density. *CCAMLR Science* 1: 1-5.
- Shannon L., Moloney C., Jarre A. & Field J. (2003) Trophic flows in the southern Benguela during the 1980s and 1990s. *Journal of Marine Systems* 39: 83-116.
- Shin, Y.J. & Cury, P. 2001. Exploring fish community dynamics through size-dependent trophic interactions using a spatialized individual-based model. *Aquatic Living Resources* 14, 65-80.
- Siegel D., McGillicuddy D. & Fields E. (1999) Mesoscale eddies, satellite altimetry, and new production in the Sargasso Sea. *Journal of Geophysical Research* 104: 13 359-13379.
- Sifeddine A., Gutiérrez D., Ortlieb L., Boucher H., Velazco F., Field D., Vargas G., Boussafir M., Salvatteci R., Ferreira V., García M., Valdes J., Caquineau S., Mandeng Yogo M., Cetin F., Solis J., Soler P. & Baumgartner T. (2008) Laminated sediments from the central Peruvian continental slope: a 500 year record of upwelling system productivity, terrestrial runoff and redox conditions. *Progress in Oceanography* 79: 190-197.
- Simard Y. & Mackas D. L. (1989) Mesoscale aggregations of euphausiid sound scattering layers on the continental shelf of Vancouver Island. *Canadian Journal of Fisheries and Aquatic Sciences* 46: 1238-1249.
- Simmonds E. J., Gutiérrez M., Chipollini A., Gerlotto F., Woillez M. & Bertrand A. (2009) Optimizing the design of acoustic surveys of Peruvian anchoveta. *ICES Journal of Marine Science* 66: 1341-1348.
- Simmonds J. & MacLennan D. (2005) *Fisheries Acoustics. Theory and practices* 2nd Ed. Chapman & Hall: 325 p.

- Smith A. D. M., Fulton E. J., Hobday A. J., Smith D. C. & Shoulder P. (2007) Scientific tools to support the practical implementation of ecosystem-based fisheries management. ICES Journal of Marine Science 64: 633-639.
- Stanton T. & Chu D. (2000) Review and recommendations for the modelling of acoustic scattering by flui-like elongated zooplankton: euphausiids and copepods. ICES Journal of Marine Science 57: 793-807.
- Stanton T. K., Chu D. & Wiebe P. H. (1996) Acoustic scattering characteristics of several zooplankton groups. ICES Journal of Marine Science 53: 289-295.
- Stanton T. K., Nash R. D. M., Eastwood R. L. & Nero R. W. (1987) A field examination of acoustical scattering from marine organisms at 70 kHz. IEEE Journal of Oceanic Engineering: OE-12: 339-348.
- Steele J. H. (1976) Patchiness. In The ecology of the seas, Cushing D.H. & Walsh J.J. (ed.), Blackwell, London, pp 98-115.
- Steele J. H. (1989) The ocean 'landscape'. Landscape Ecology 3: 185-192.
- Stevick P. T., Incze L. S., Kraus S. D., Rosen S., Wolff N. & Baukus A. (2008) Trophic relationships and oceanography on and around a small offshore bank. Marine Ecology Progress Series 363: 15-28.
- Stramma L., Johnson G. C., Sprintall J. & Mohrholz V. (2008) Expanding Oxygen-Minimum Zones in the Tropical Oceans. Science 320: 655-658.
- Strub P. T., Mesias J. M., Montecino V., Rutllant J. & Salinas S. (1998) Coastal ocean circulation off western South America, in The Sea, vol. 11, edited by A. R. Robinson and K. H. Brink, pp. 273- 314, John Wiley, Hoboken, N. J.
- Swartzman G., Bertrand A., Gutiérrez M., Bertrand S. & Vasquez L. (2008) The relationship of anchovy and sardine to water masses in the Peruvian Humboldt Current System from 1983 to 2005. Progress in Oceanography 79: 228-237.
- Swartzman G., Hickey B., Kosro M. & Wilson C. (2005) Poleward and equatorward currents in the Pacific Eastern Boundary Current in summer 1995 and 1998 and their relationship to the distribution of euphausiids. Deep Sea Research II 52 73-88.
- Taki K. (2006) Biomass and production of the euphausiid *Euphausia pacifica* along the coastal waters off north-eastern Japan. Fisheries Science 72: 221-232.
- Tam J., Taylor M., Blaskovic V., Espinoza P., Ballón M., Díaz E., Wosnitza-Mendo C., Argüelles J., Purca S., Ayón P., Quipuzcoa L., Gutiérrez D., Goya E., Ochoa N. & Wolff M. (2008) Trophic modeling of the Northern Humboldt Current Ecosystem, Part I: Comparing trophic linkages under La Niña and El Niño conditions. Progress in Oceanography 79: 352-365.
- Taylor J.C., Rand P. S. (2003) Spatial overlap and distribution of anchovies (*Anchoa* spp.) and copepods in a shallow stratified estuary. Aquatic Living Resources 16: 191-196.
- Thiel M., Macaya E. C., Acuña E. & Lancellotti D. A. e. a. (2007) The Humboldt Current System of northern and central Chile: oceanographic processes, ecological interactions and socioeconomic feedback. Oceanography and Marine Biology: an Annual Review 45: 195-344.
- Thomas A. (1999) Seasonal distributions of satellite-measured phytoplankton pigment concentration along the Chilean coast Journal of Geophysical Research - Oceans 104 (C11) doi:10.1029/1999JC900171.
- Thomas A. C., Carr M. E. & Strub P. T. (2001) Chlorophyll variability in eastern boundary currents. Geophysical Research Letters 28 18 3421-3424.

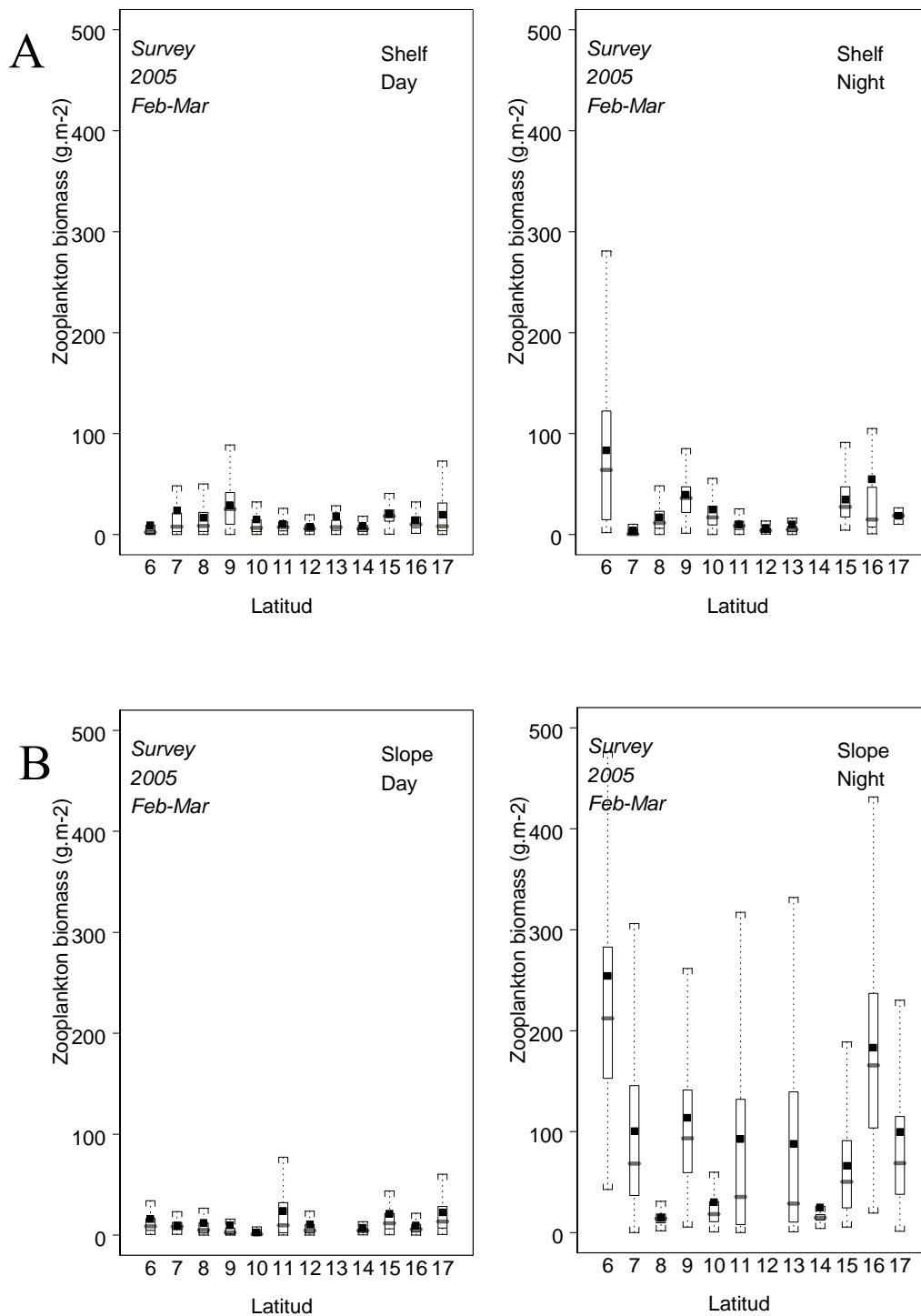
- Thomas LN, Tandon A, Mahadevan A (2008) Eddy Resolving Ocean Modeling. Hecht M, Hasumi H, editors. Amer Geophys Union, Washington DC.
- Torrence C, Compo GP (1998) A practical guide to wavelet analysis. Bulletin of the American Meteorological Soci 79: 61-78.
- Trevorrorow M. V., Mackas D. L. & Benfield M. C. (2005) Comparison of multifrequency acoustic and in situ measurements of zooplankton abundances in Knight Inlet, British Columbia. The Journal of the Acoustical Society of America 117: 3574-3588.
- Urick R. J. (1975) Principles of Underwater Sound for Engineers, 2nd edn. McGraw Hill, New York, 384 pp.
- Valdés J., Ortlieb L., Gutiérrez D., Marinovic L., Vargas G. & Sifeddine A. (2008) 250 years of sardine and anchovy scale deposition record in Mejillones Bay, Northern Chile. Progress in Oceanography 79: 198-207.
- van der Lingen C. D., Bertrand A., Bode A., Brodeur R., Cubillos L., Espinoza P., Friedland K., Garrido S., Irigoien X., Möllmann C., Rodriguez-Sanchez R., Tanaka H. & Temming A. (2009) Trophic dynamics of small pelagic fish. In: Checkley Jr., D.M., Roy, C., Alheit, J., Oozeki, Y. (Eds.), Climate Change and Small Pelagic Fish. Cambridge University Press, pp. 112-157 (Chapter 7).
- van der Lingen C., Hutchings L. & Field J. (2006) Comparative trophodynamics of anchovy *Engraulis encrasicolus* and sardine *Sardinops sagax* in the southern Benguela: are species alternations between small pelagic fish trophodynamically mediated? African Journal of Marine Science 28 (3-4): 465-477.
- Vaquer-Sunyer R, Duarte CM (2008) Thresholds of hypoxia for marine biodiversity. Proceedings of the National Academy of Sciences U S A 105: 15452-15457.
- Vinogradov M. E. & Shushkina E. A. (1978) Some Development Patterns of Plankton Communities in the Upwelling Areas of the Pacific Ocean. Marine Biology 48: 357-366.
- Wagner H. H. & Fortin M.-J. (2005) Spatial analysis of landscapes: concepts and statistics Ecology 86: 1975-1987.
- Walsh DA, Zaikova E, Howes CG, Song YC, Wright JJ, et al. (2009) Metagenome of a versatile Chemolithoautotroph from expanding oceanic dead zones. Science 326: 578-582.
- Watkins J. L. & Brierley A. S. (2002) Verification of the acoustic techniques used to identify Antarctic krill. ICES Journal of Marine Science 59: 1326-1336.
- Wiebe P. H. (1970) Small-scale spatial distribution in oceanic zooplankton Limnology and Oceanography 15: 205-217.
- Wiebe P. H. (1988) Functional regression equations for zooplankton displacement volume, wet weight, dry weight and carbon: a correction. Fishery Bulletin 86: 833-835.
- Wiebe P. H., Boyd S. H. & Cox J. L. (1975) Relationships between zooplankton displacement volume, wet weight, dry weight, and carbon. Fishery Bulletin U.S. 73: 777-786.
- Wishner K. F., Ashjian J., Gelfman C., Gowing, M.M., et al. (1995) Pelagic and benthic ecology of the lower interface of the Eastern Tropical Pacific oxygen minimum zone. Deep Sea Research I 42: 93-115.
- Wyrtki K. (1963) The horizontal and vertical field of motion in the Peru Current. Bulletin of the Scripps Institution of Oceanography 8: 313-344.

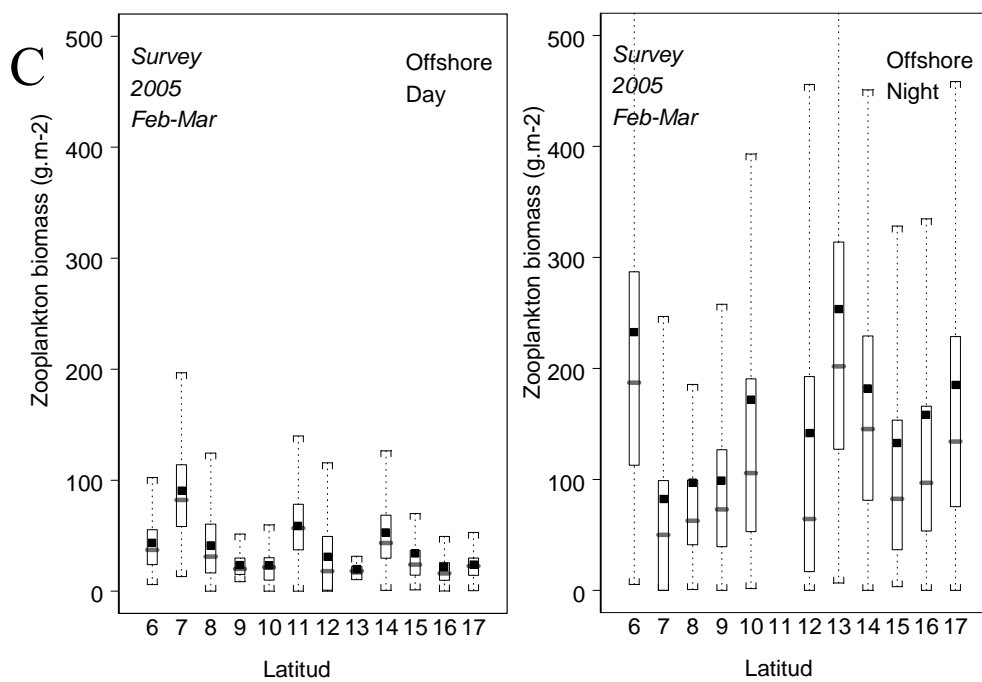
Yebra L., Almeida C. & Hernandez-Leon S. (2005) Vertical distribution of zooplankton and active flux across an anticyclonic eddy in the Canary Island waters. Deep Sea Research I 52: 69-83.

Zhu Y., Tande K. & Zhou M. (2009) Mesoscale physical processes and zooplankton transport-retention in the northern Norwegian shelf region. Deep Sea Research Part II, doi:10.1016/j.dsr2.2008.11.019.

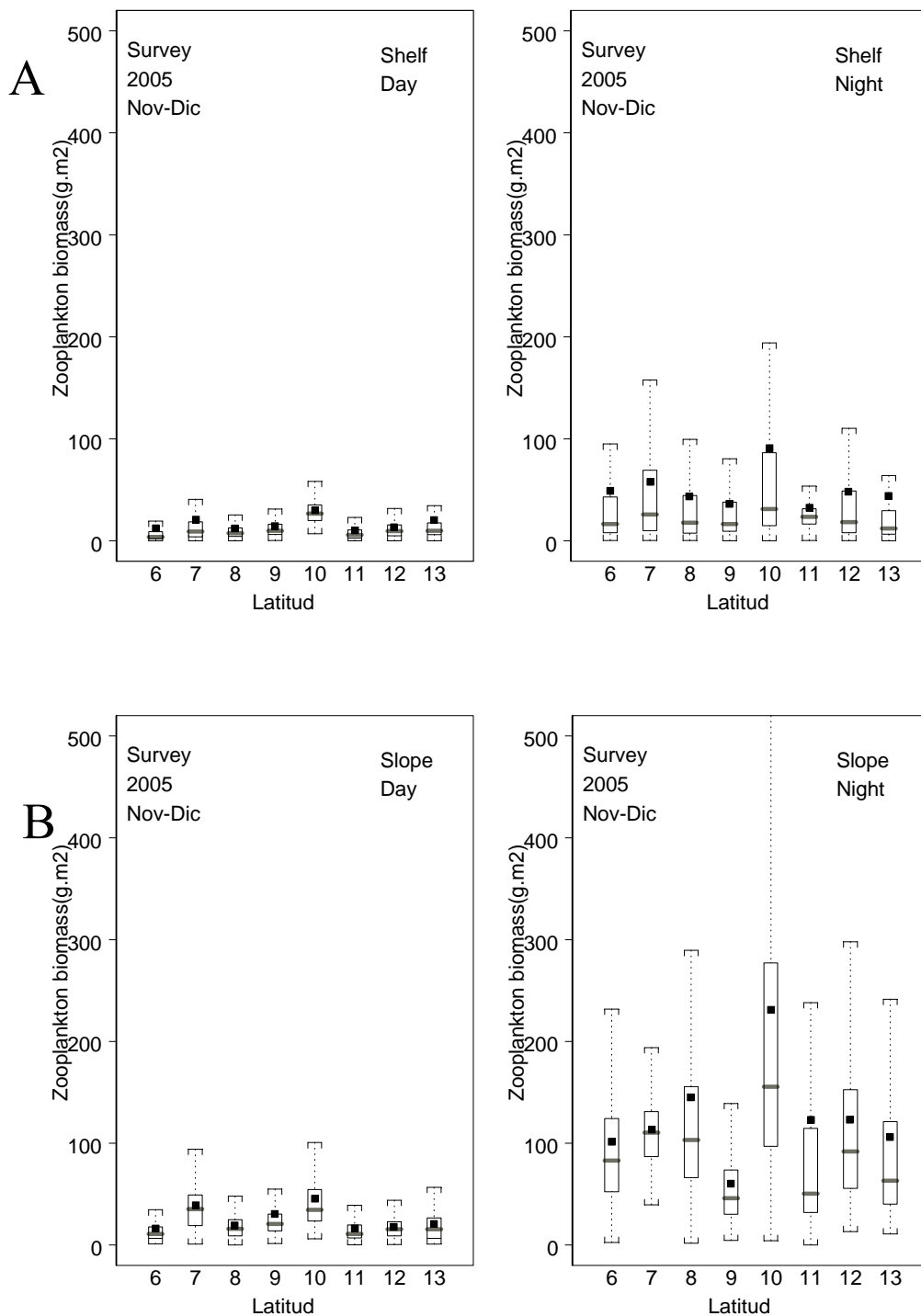
*Appendices*

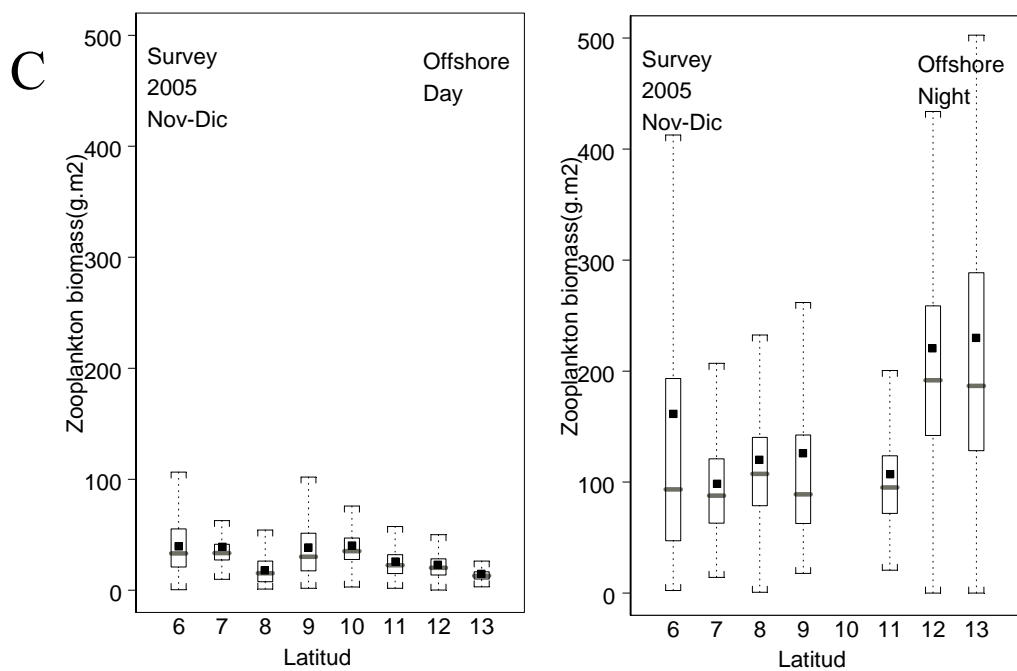
*Appendix A. Day and night box plots of along-shore macrozooplankton biomass distribution ( $\text{g.m}^{-2}$ ) for the shelf (A) slope (B) and offshore(C) ecological domain. Data from austral summer pelagic survey of 2005.*





*Appendix B. Day and night box plots of along-shore macrozooplankton biomass distribution ( $\text{g.m}^{-2}$ ) for the shelf (A) slope (B) and offshore(C) ecological domain. Data from austral spring pelagic survey of 2005.*





*Appendix C. Statistical characteristics of linear correlation, at mesoscale, between macrozooplankton biomass, normalized by cubic root, and the detrended ZVEEC during day and night.*

Diel period	Transects	Significance	R <sup>2</sup> (0.05)	Slope	n	n'
Day	36	NS	0.0402	0.0054	69	11
	42	NS	0.1142	-0.0497	45	16
	46	NS	0.0728	0.0226	78	25
	50	NS	0.0326	0.0093	61	7
	64	NS	0.1980	0.0259	64	12
	72	NS	0.0066	0.0031	65	43
	80	NS	0.1210	0.0182	65	25
	84	NS	0.0379	0.0187	49	25
	88	***	0.3227	0.0267	57	15
	Total	NS	0.0364	0.0117	553	179
Night	26	NS	0.1656	0.0127	59	23
	32	NS	0.1283	0.0186	68	11
	48	NS	0.0088	-0.0549	56	30
	54	NS	0.0049	0.0124	58	23
	70	NS	0.1275	0.0267	66	22
	74	NS	0.2493	0.0968	42	14
	78	NS	0.0636	0.0316	50	26
	82	NS	0.0135	0.0117	57	19
	86	NS	0.0277	0.0171	46	15
	90	***	0.4284	-0.0963	35	12
Total		***	0.0238	0.0192	537	194

*Appendix D. Statistical characteristics of linear correlation, at mesoscale, between macrozooplankton density, normalized by cubic rood, and the detrended  $Z_{VEEC}$  during day and night.*

Diel period	Transects	Significance	$R^2_{(0.05)}$	Slope	n	n'
Day	36	NS	0.0581	-0.0018	69	32
	42	NS	0.2634	-0.0199	45	14
	46	NS	0.0002	-0.0004	78	24
	50	NS	0.0122	-0.0008	61	11
	64	NS	0.0561	0.0028	64	17
	72	NS	0.0503	-0.0022	65	30
	80	NS	0.0227	0.0018	65	28
	84	NS	0.0006	0.0006	49	26
	88	NS	0.0620	0.0026	57	20
	Total	NS	0.0003	-0.0002	553	202
Night	26	NS	0.0024	-0.0003	59	29
	32	NS	0.0006	0.0003	68	10
	48	NS	0.0337	-0.0357	56	30
	54	NS	0.0031	0.0018	58	23
	70	NS	0.0002	0.0002	66	23
	74	NS	0.1549	0.0157	42	18
	78	NS	0.0031	0.0017	50	35
	82	NS	0.0689	-0.0060	57	34
	86	NS	0.0154	-0.0028	46	24
	90	***	<b>0.5955</b>	-0.0328	35	11
	Total	NS	0.0000	0.0000	537	238

*Appendix E. Statistical characteristics of linear correlation, at mesoscale, between log-transformed fish acoustic nautical area scattering coefficient (NASC+) and macrozooplankton biomass, normalized by cubic root, during the day and during the night.*

Diel period	Transects	Significance	R <sup>2</sup> (0.01)	Slope	n
Day	42	NS	0.090	-0.4596	43
	50	NS	0.001	0.0529	52
	64	NS	0.030	-0.2781	60
	46	NS	0.073	0.8461	54
	36	***	0.255	1.2423	67
	72	NS	0.055	1.0369	49
	80	NS	0.000	0.0054	51
	84	NS	0.157	1.1315	32
	88	NS	0.120	0.6032	34
	Total	NS	0.012	0.2364	458
Night	26	***	0.124	0.5710	57
	32	NS	0.007	-0.0454	66
	48	***	0.275	0.6558	54
	54	***	0.386	0.3953	54
	70	***	0.524	1.0447	64
	74	***	0.280	0.3807	40
	78	NS	0.001	0.0046	48
	82	NS	0.057	0.1592	55
	86	NS	0.085	0.0756	44
	90	***	0.349	0.4826	33
Total		***	0.131	0.2324	533

*Appendix F. Statistical characteristics of linear correlation, at mesoscale, between log-transformed fish acoustic nautical area scattering coefficient (NASC+) and macrozooplankton density normalized by cubic root, during the day and during the night.*

Diel period	Transects	Significance	R <sup>2</sup> (0.01)	Slope	n
Day	42	NS	0.003	-0.3412	43
	50	NS	0.007	1.0926	52
	64	NS	0.013	-0.8929	60
	46	NS	0.022	1.5883	54
	36	NS	0.024	1.3596	67
	72	NS	0.054	3.9664	49
	80	NS	0.034	2.4542	51
	84	NS	0.175	4.5818	32
	88	NS	0.094	2.3897	34
	Total	***	0.033	1.7099	458
Night	26	NS	0.070	2.1020	57
	32	NS	0.013	-0.2612	66
	48	***	0.216	1.7523	54
	54	***	0.352	2.1073	54
	70	***	0.432	3.5540	64
	74	***	0.289	1.8729	40
	78	NS	0.006	-0.0586	48
	82	NS	0.002	0.1299	55
	86	NS	0.001	-0.0402	44
	90	NS	0.131	1.0241	33
Total		***	0.064	0.6691	533

*Appendix G. Statistical characteristics of linear correlation, at submesoscale, between macrozooplankton biomass, normalized by cubic root, and the detrended Z<sub>VEEC</sub> during the day and during the night.*

Diel period	Domain	Transect	Significance	R <sup>2</sup> (0.05)	Slope	n	n'
Day	Shelf	42			0.0155	149	75
		50	***	0.205	-0.0154	96	44
		64	NS	0.026	0.0205	152	32
		46	***	0.344	0.0047	400	140
		36	NS	0.003	-0.0012	27	16
		72	NS	0.002	0.0628	16	7
		80	***	0.586			
		84					
	Offshore	88	***	0.249	0.0252	19	19
		Total	***	0.013	0.0539	553	333
		42	***	0.055	0.0549	442	224
		50	NS	0.010	0.0105	437	192
		64	***	0.033	0.0331	526	195
		46	NS	0.000	0.0002	578	443
		36	NS	0.000	0.0001	275	174
Night	Shelf	72	***	0.049	0.0491	615	197
		80	***	0.017	0.0167	627	234
		84	***	0.052	0.0517	482	197
		88	NS	0.015	0.0153	538	182
		Total	***	0.018	0.0163	4520	2039
		26	***	0.197	0.0187	321	160
		32	NS	0.022	0.0068	324	121
		48					
	Offshore	54	***	0.160	0.0352	194	57
		70					
		74					
		78					
		82	NS	0.116	0.0444	59	27
		86					
		90					
	Offshore	Total	***	0.088	0.0218	553	366
		26	***	0.148	0.0098	129	46
		32	NS	0.010	0.0105	216	75
		48	***	0.024	-0.1187	561	402
		54	NS	0.012	0.0204	372	209
		70	***	0.012	-0.0188	599	322
		74	NS	0.000	0.0032	406	198
		78	***	0.036	-0.0612	491	160
		82	NS	0.014	-0.0265	489	232
		86	***	0.040	-0.0492	452	215
		90	NS	0.000	-0.0021	330	174
		Total	***	0.004	-0.0164	4045	2033

*Appendix H. Statistical characteristics of linear correlation, at submesoscale, between macrozooplankton density, normalized by cubic root, and the detrended Z<sub>VEEC</sub> during the day and during the night.*

Diel period	Domain	Transect	Significance	R <sup>2</sup> (0.05)	Slope	n	n'
Day	Shelf	42					
		50	NS	0.011	-0.0010	149	88
		64	***	0.118	-0.0116	96	43
		46	NS	0.038	0.0016	152	88
		36	NS	0.007	-0.0025	400	149
		72	NS	0.165	-0.0028	27	12
		80	NS	0.497	0.0124	16	7
		84					
		88	NS	0.049	0.0023	19	18
	Offshore	Total	NS	0.001	-6E-04	553	406
		42	NS	0.007	0.0032	442	268
		50	NS	0.004	-0.0024	437	228
		64	NS	0.010	0.0048	526	205
		46	NS	0.005	-0.0064	578	460
		36	***	0.024	-0.0067	275	181
		72	NS	0.013	0.0029	615	213
		80	NS	0.001	-0.0007	627	282
		84	NS	0.004	0.0014	482	214
		88	NS	0.008	-0.0019	538	180
Night	Shelf	Total	NS	0.000	-1E-04	4520	2230
		26	NS	0.000	0.0002	321	160
		32	NS	0.022	-0.0016	324	130
		48					
		54	NS	0.012	0.0031	194	69
		70					
		74					
		78					
		82	NS	0.013	0.0038	59	31
	Offshore	86					
		90					
		total	NS	0.001	0.0006	553	391
		26	NS	0.015	-0.0007	129	54
		32	NS	0.020	-0.0038	216	73
		48	***	0.048	-0.0556	561	394
		54	NS	0.000	-0.0004	372	206
		70	***	0.069	-0.0123	599	287
		74	NS	0.007	-0.0076	406	207
		78	***	0.067	-0.0211	491	158
		82	***	0.045	-0.0118	489	192
		86	***	0.082	-0.0183	452	207
		90	NS	0.018	-0.0083	330	165
		total	***	0.024	-0.0107	4045	1941

*Appendix I. Statistical characteristics of linear correlation, at submesoscale, between log-transformed fish acoustic nautical area scattering coefficient (NASC+) and macrozooplankton biomass normalized by cubic root, during the day and during the night.*

Diel period	Domain	Transect	Significance	R <sup>2</sup> (0.01)	Slope	n
Day	Shelf	36	***	0.024	0.447	371
		42				
		46	***	0.111	0.893	147
		50	NS	0.001	0.097	124
		64	NS	0.049	0.592	63
		72	NS	0.016	0.461	19
		80	NS	0.000	-0.026	16
		84				
		88	NS	0.005	0.246	19
		Total	***	0.034	0.530	759
Night	Offshore	36	NS	0.000	0.000	428
		42	***	0.055	0.055	202
		46	NS	0.000	0.000	196
		50	NS	0.010	0.010	170
		64	***	0.033	0.033	325
		72	***	0.049	0.049	195
		80	***	0.017	0.017	175
		84	***	0.052	0.052	169
		88	NS	0.015	0.015	156
		Total	***	0.026	0.364	2016
Night	Shelf	26	***	0.050	0.790	321
		32	NS	0.009	0.287	324
		48				
		54	NS	0.003	0.221	140
		70				
		74				
		78				
		82	***	0.158	0.492	59
		86				
		90				
Night	Offshore	Total	***	0.038	0.473	844
		26	***	0.056	0.673	128
		32	***	0.054	0.277	209
		48	NS	0.002	0.078	533
		54	***	0.051	0.106	372
		70	NS	0.011	0.089	566
		74	NS	0.004	0.026	395
		78	NS	0.006	-0.007	491
		82	***	0.017	0.034	489
		86	NS	0.003	-0.006	452
		90	NS	0.013	0.061	330
		Total	***	0.006	0.036	3965

*Appendix J. Statistical characteristics of linear correlation, at submesoscale, between log-transformed fish acoustic nautical area scattering coefficient (NASC+) and macrozooplankton density normalized by cubic root, during the day and during the night.*

Diel period	Domain	Transect	Significance	R <sup>2</sup> (0.01)	Slope	n
Day	Shelf	36	***	0.023	1.375	371
		42				
		46	***	0.066	2.961	147
		50	***	0.000	0.214	124
		64	***	0.043	1.506	63
		72	***	0.010	1.338	19
		80	NS	0.001	2.371	16
		84				
		88	NS	0.002	-0.777	19
		Total	***	0.026	1.535	759
Offshore	Shelf	36	NS	0.001	0.205	428
		42	NS	0.003	0.308	202
		46	NS	0.022	-1.122	196
		50	***	0.070	3.450	170
		64	***	0.104	2.135	325
		72	***	0.052	2.905	195
		80	***	0.143	2.123	175
		84	***	0.043	2.387	169
		88	NS	0.014	0.929	156
		Total	***	0.019	1.121	2016
Night	Offshore	26	***	0.023	2.021	321
		32	NS	0.001	0.455	324
		48				
		54	***	0.004	-0.727	140
		70				
		74				
		78				
		82	***	0.126	1.683	59
		86				
		90				
Offshore	Shelf	Total	***	0.016	1.145	844
		26	NS	0.040	2.441	128
		32	***	0.050	1.036	209
		48	NS	0.003	0.083	533
		54	***	0.061	0.493	372
		70	NS	0.009	0.296	566
		74	NS	0.004	0.104	395
		78	NS	0.010	-0.036	491
		82	***	0.017	0.138	489
		86	NS	0.005	-0.031	452
Total	Offshore	90	NS	0.010	0.200	330
		Total	***	0.005	0.126	3965